Pliocene-Pleistocene variability of upwelling activity, productivity and nutrient cycle in the Benguela Upwelling System and the Eastern Equatorial Pacific

Monographische Dissertation

zur Erlangung des Doktorgrades
der Mathematisch-Naturwissenschaftlichen Fakultät
der Christian-Universität zu Kiel

Vorgelegt von

Johan Etourneau

Kiel 2009

Referent: Prof. Dr. Ralph Schneider
Koreferent: Dr. Dirk Nürnberg
Tag der Disputation: 13.07.2009
Zum Druck genehmigt: 15.07.2009
Der Dekan: Prof. Dr. Lutz Kipp

EIDESSTATTLICHE ERKLÄRUNG

Hiermit erkläre ich an Eides statt, dass die vorliegende Dissertation mit dem Titel 'Pliocene-Pleistocene variability of upwelling activity, productivity and nutrient cycle in the Benguela Upwelling System and the Eastern Equatorial Pacific', abgesehen von der Beratung durch meine akademischen Lehrer, in Inhalt und Form meine eigene Arbeit darstellt. Ferner habe ich weder diese noch eine ähnliche Arbeit an einer anderen Hochschule im Rahmen eines Prüfungsverfahrens vorgelegt.

Kiel, den 28.05.2009

J. Etourneau

Contents

Chapter III. Age models

Chapter IV. Pliocene-Pleistocene variability of upwelling activity, productivity, and nutrient cycling in the Benguela region

Chapter V. Links between biological production and iron supply in the Eastern Equatorial Pacific since the Pliocene

Chapter VI. Pliocene-Pleistocene high-resolution sea surface temperature records from the Benguela Upwelling System and the Eastern Equatorial Pacific

Chapter VII. General conclusions

Chapter VIII. Perspectives

Acknowledgements

First of all, I would like to thank my primary advisor Prof. Dr. Ralph Schneider, for guidance, direction, and expertise on paleoceanography. I truly appreciate his support during my entire PhD program, his open mind, and the trust and independence he gave me all along this time passed in Kiel. I truly thank you Ralph, for all your encouragements.

I also wish to thank Philippe Martinez, my co-supervisor, who considerably contributed to this thesis by stimulating vigorous and productive discussions, and by helping a lot for writing articles. I particularly appreciate his scientific mind and vision of science, always pushing me in the right direction and asking the good questions. A person I really like very much for his character.

Thanks also to all the group of Kiel. A particular thanks to Thomas Blanz and Sylvia Koch, with whom I started this PhD and fighted sometimes for improving my german. However, they finally gave up when they saw more and more foreigners joining the group, especially french speaking people. Thanks to them, I learned a lot. For the lab work, I wish also to thank Isabelle Billy and Karine Charlier, the equal of Sylvia in Bordeaux, who also helped me, particularly for understanding the sensitive machine that is the mass spec, a very sensitive machine.

Even if she came later than me to Kiel, Birgit Schneider has always been free for me whatever I asked for. Yiming, Stephanie, and Bettina, also contributed to make my life better in Kiel. Finally, I realize that I asked a lot to all of them. Actually I asked many things to everybody. So, thank you.

Rüdiger. Hard to define! An alien in our group. Somebody on whom you can account for everything, anytime. Always free to offer his help, especially in the complexities of the german administration, but also just for talking about life and sailing boat, of course. A lot. I shared very important times of my thesis with him, even if he tried to kill me several times. He failed!

I also thank the hiwis, especially Agatha, Nathalie and Frederike who helped a lot for sampling, washing, drying and cleaning the samples. A considerable help.

Veronica. Unfortunately we did not have so much time spent together to know each other better. But just for this last month, you already helped me and I am really grateful. I wish you good luck for your thesis.

I also wish to really thank the Bremerhaven´s team of Ralf Tiedemann, particularly Daniel and Frank with whom I spent a lot of time for discussions on science, improved my papers and shared very good times.

The "French mafia". Sorry, the following part is censored and in french. Merci, vous aussi vous m´avez beaucoup aidé. Comme je disais, j´ai sans doute demandé pas mal de choses à beaucoup de monde mais je sais que j´ai pu particulièrement compter sur vous dans les moments importants. Merci à vous deux, Guillaume et Elfi. Désolé Guillaume si j´ai pas pu venir faire ma lessive chez toi hier soir.

Nabil et Tim. Après pratiquement trois ans passés ensemble à Kiel, après avoir partagé de grands moments de nos vies privées, je vous remercie en tout cas pour ces moments mémorables et de franches rigolades passés tous les trois.

Enfin la famille. Eh bien oui, je pense à vous qui m´avez soutenu pendant toutes ces longues années. Sans doute que je n´en serais pas là. Ou du moins, je ne me poserais sans doute pas la question. En tout cas, merci mille fois pour votre soutien.

Et puis finalement, je remercie mes deux amours. Celles qui ont dû vivre séparées de moi pendant plus de trois ans. Des moments difficiles mais des moments qui renforcent aussi. En tout cas, des épreuves qui ne peuvent qu´aider à surmonter les prochaines.

Vielen Dank !

Summary

Over the last ~4.5 Ma, the Earth's climate transitioned from a warm and relative stable state towards cold conditions marked by amplified glacial/interglacial cycles and widespread ice-sheets in the Northern Hemisphere. The causes and consequences of this global cooling are still uncertain, albeit likely tied to the interaction of several mechanisms, including oceanic and atmospheric circulation, tectonic activity, greenhouse gases, and marine productivity. In this PhD thesis, the long term variability of coastal and open ocean upwelling systems has been explored by reconstructing for the last ~3.5 Ma, sea surface temperature (SST), primary productivity and nutrient cycling in the Benguela Upwelling System (BUS) and the Eastern Equatorial Pacific (EEP), two areas particularly sensible and influential to climate change. For the last ~3.5 Ma, the new records provide evidence for profound changes in both regions:

In the BUS, the coastal upwelling activity mainly intensified ~2.4-2.0 Ma ago in response to stronger trade winds, strengthened by Southern Ocean cooling. The combined effects of upwelling intensification and reduction of silica import to the Benguela region probably resulted in the termination of the Matuyama Diatom Maximum, characterized by very high abundance of mats-forming and Antarctic type diatoms, which was replaced by diatom species indicative of strong coastal upwelling. The reduction of silica export from the Southern Ocean to the Benguela was probably linked to the development of a modern-like polar frontal system, increased silica utilization in the Southern Ocean by local diatom productivity and formation of subantarctic mode waters. The equatorward advection of the latter nitrate-rich water-mass may have altered the global available nitrogen pool, by increasing carbonate productivity in the low-latitude coastal upwelling regions, and global denitrification rate, the main nitrogen loss.

In the EEP, different interactions were found. Unlike the Benguela region where oceanic reorganization associated with changes in nutrient supply probably controlled the regional productivity over the last ~3.5 Ma, in the EEP, other factors regulated periods of high productivity. Indeed, biological production evolved independently of warm or cold conditions. Instead, phytoplankton productivity varied outstandingly in phase with changes in nutrient supply, especially iron. Pulses in iron input, mainly supplied by eastward subsurface water currents from the western equatorial Pacific and terrestrial transport (aeolian and/or riverine origins) from South America, probably triggered the two highest productive periods between ~3.2-2.8 and ~1.9-1.4 Ma occurring

in this region over the past 5 Ma. However, in this study, no clear relationship has been established between variations of EEP productivity and Plio-Pleistocene climate. This suggests that changes in EEP biological production probably had only a minor impact on Plio-Pleistocene transition.

In addition to the biogeochemical processes that may have had an influence on climate change since the Mid-Pliocene, physical mechanisms, especially atmospheric circulation, could also have played a great role on the Plio-Pleistocene transition. Oceanic conditions in the two upwelling regions are directly tied to trade winds, the EEP being connected to zonal (or Walker) atmospheric convective cells and the Benguela region to meridional (or Hadley) ones. The west-to-east SST gradient across the equatorial Pacific synchronously increased with the meridional SST gradient across the Benguela from ~2.4-2.0 to 0.5 Ma, implying a parallel development of both atmospheric patterns. The establishment of Hadley circulation was probably regulated by the increasing pole to equator temperature gradient during the Plio-Pleistocene, thus resulting in stronger trade winds, and, enhanced coastal and open ocean upwelling in the low latitudes. The strengthening of the equatorial upwelling might have caused the EEP cooling around ~2.2 Ma, increased the zonal SST asymmetry along the equatorial Pacific and hence promoted the intensification of WC. While the development of both atmospheric circulations probably affected environmental conditions in the tropical and subtropical regions by regulating heat and moisture distribution, the link with the high latitudes climate remains not clear. It is therefore questionable whether changes in low latitudes atmospheric circulation may have participated to the Plio-Pleistocene cooling, since both WC and HC intensified much later (~2.4-2.0 Ma ago) than the onset of widespread ice sheets in the Northern Hemisphere (~3.0 Ma ago).

Zusammenfassung

Im Laufe der vergangenen ~4.5 Mio. Jahre durchlief das globale Klima eine Veränderung von warmen und relativ stabilen Bedingungen im Pliozän hin zu kühleren Verhältnissen im Pleistozän. Charakteristisch waren dabei ausgeprägte Glazial/Interglazial-Zyklen sowie ausgedehnte Eisdecken in der Nordhemisphäre. Wenngleich die Ursachen und Folgen dieser globalen Abkühlung bislang nicht vollständig verstanden sind, so besteht doch ein Zusammenhang zu verschiedenen Mechanismen, und deren Wechselwirkungen – darunter ozeanische und atmosphärische Zirkulation, tektonische Aktivität, Treibhausgase und marine Produktivität. Im Rahmen dieser Dissertation wurde die Langzeitvariabilität küstennaher und ozeanischer Auftriebsgebiete untersucht, indem für die letzten ~3.5 Mio. Jahre die oberflächennahe Wassertemperatur (sea surface temperature, SST), die Primärproduktion sowie die Nährstoffkreisläufe in der Benguela Region (Benguela Upwelling System, BUS) und im östlichen äquatorialen Pazifik (Eastern Equatorial Pacific, EEP) rekonstruiert wurden. Die genannten Untersuchungsregionen reagieren besonders sensibel auf klimatische Veränderungen. Diese neuen Datensätze belegen deutliche paläohydrographischeVeränderungen in beiden Regionen.

Im BUS, intensivierte sich der küstennahe Auftrieb vor Namibia vorwiegend vor ~2.4-2.0 Mio. Jahren als Reaktion auf stärkere Passatwinde und verstärkt durch eine Abkühlung des Antarktischen Ozeans. Das Zusammenwirken der Auftriebsintensivierung mit einer Reduktion des Silikatimports in die Benguela Region führte wahrscheinlich zum Ende des Matuyama Diatomeen Ablagerungsmaximum. Hierbei wurden die für dieses Ereignis charakteristischen hohen Gehalte von mattenbildenden, antarktischen Diatomeen durch Arten ersetzt, welche als typisch für Auftriebsgebiete gelten. Die Reduktion des Silikatexports aus der Antarktis in die Benguela Region hing vermutlich mit der Ausbildung einer polaren Front ähnlich der heutigen, mit erhöhtem Silikatverbrauch durch verstärkte lokale Diatomeenproduktivität, und der Ausbildung subantarktischen Zwischenwassers zusammen. Die Advektion des nitratreichen Zwischenwassers in Richtung Äquator könnte den globalen Stickstoffpool verändert haben, und zwar einerseits durch eine Steigerung der Karbonatproduktivität in den äquatornahen Auftriebssystemen und andererseits durch eine Erhöhung der globalen Denitrifikationsrate, dem Hauptmechanismus des Stickstoffentzugs aus dem Ozean. Diese Veränderung könnte ihrerseits den pliozän-pleistozänen Klimawandel beeinflusst haben.

Im EEP hingegen finden sich Hinweise auf andere Steuermechanismen als im BUS, wo eine Reorganisation der ozeanischen Verhältnisse mit dadurch veränderten Nährstoffeinträgen die Produktivität über die letzten 3.5 Mio. Jahre steuerte. Die biologische Produktivität entwickelte sich nicht in Abhängigkeit von warmen oder kalten Phasen, sondern variierte synchron mit Veränderungen in den Mikronährstoffkonzentrationen, insbesondere Eisen. Schubartige Eiseneinträge lösten vermutlich die beiden höchsten Produktivitätsperioden der vergangenen 5 Mio. Jahre in dieser Region (zwischen ~3.2-2.8 und ~1.9-1.4 Mio. Jahren) aus. Eisen wurde dabei vermutlich vorwiegend über ostwärts gerichtete Tiefenwasserströmungen aus dem westlichen äquatorialen Pazifik sowie über aeolischen und/oder flussgebundenen Eintrag aus terrestrischen Quellen in Südamerika importiert. Allerdings konnte in dieser Studie keine eindeutige Beziehung zwischen den Variationen der Produktivität und dem Plio-Pleistozänen Klima im EEP festgestellt werden. Daher ist zu vermuten, dass Veränderungen in der biologischen Produktivität im EEP nur unwesentliche Einflüsse auf den klimatischen Übergang von Plio- zum Pleistozän hatte.

Neben den biogeochemischen Prozessen spielten vermutlich auch physikalische Mechanismen, insbesondere die atmosphärische Zirkulation, eine wichtige Rolle beim Übergang von pliozänen zu pleistozänen Klimabedingungen. Die Verhältnisse in den Stromsystemen der beiden Untersuchungsregionen hängen direkt mit den Passatwinden zusammen, wobei der EEP mit den zonalen atmosphärischen Konvektionszellen (auch Walker-Zellen), und das BUS mit den meridionalen Konvektionszellen (auch Hadley-Zellen) verknüpft war. In der Zeit von ~2.4-2.0 bis 0.5 Mio Jahre, verstärkte sich der West-Ost Temperaturgradient entlang des äquatorialen Pazifiks zeitgleich mit dem meridionalen SST Gradienten im BUS. Dies impliziert eine parallele Verstärkung der beiden atmosphärischen Zirkulationszellen. Die Entwicklung der Hadley-Zirkulation wurde vermutlich durch den verstärkten Pol Äquator Temperaturgradient während des Plio-Pleistozän gesteuert. Dies führte zu intensivierten Passatwinden und erhöhtem Auftrieb sowohl in der Küstenregion als auch auf dem offenen Ozean in niedrigen Breiten. Die Verstärkung des äquatorialen Auftriebes vor 2.2 Mio Jahre könnte zu einer Abkühlung des EEPs geführt haben, welche wiederum die zonale Temperaturasymmetrie entlang des äquatorialen Pazifiks verstärkte und somit eine Intensivierung der Walkerzirkulation zur Folge hatte. Obwohl die Entwicklung der atmosphärischen Zirkulationsmuster sicherlich durch Regulierung der Wärme und Feuchtigkeitsverteilung die Umweltbedingungen in tropischen und subtropischen Regionen beeinflusste, ist die Verbindung zum Klima der hohen Breiten nicht eindeutig. Es ist bisher ungeklärt ob die Veränderungen der atmosphärischen Zirkulation in niedrigen Breiten an der plio-pleistozänen Abkühlung beteiligt waren, da sowohl die Walker- und Hadleyzirkulation nach dem

Aufbau der ausgedehnten nordhemisphärischen Eisschilde zwischen 2.4 und 2.0 Mio Jahre intensiviert wurden.

Chapter I

Introduction

1.1. The Pliocene-Pleistocene climate transition

Since ~4.5 Ma, Earth's climate has experienced a transition from a state marked by warm temperatures, high sea level, high atmospheric CO_2 concentration, and ice sheets restricted to Antarctica (Ravelo et al., 2004; Ravelo and Andreasen, 2000; Raymo et al., 2006, 1996; Shackleton et al., 1984), towards conditions characterized by widespread development of ice sheets in the Northern Hemisphere, and pronounced glacial/interglacial cycles reaching their maximum amplitude during the last 800 kyrs (Bartoli et al., 2005; Jansen et al., 2000; Lisiecki and Raymo, 2005) (Fig.1).

The most pronounced Pliocene-Pleistocene climate cooling associated to continental ice sheet formation in the Northern Hemisphere occurred ~3.0 Ma ago and has been hypothesized to result from the finale closure of the Panama Gateway (Driscoll and Haug, 1998; Haug and Tiedemann, 1998; Keigwin et al., 1982). The cessation of water exchange between the Equatorial Pacific and Atlantic Ocean favored the development and the strengthening of the Gulf Stream transporting warm and saline surface water masses to the North Atlantic. Enhanced warm water export into the high latitudes probably induced increased moisture transport over Eurasia, thus promoting river runoff and additional fresh water into the Arctic Ocean. Lower density waters in the Arctic Ocean may have in turn short-circuited the global thermohaline circulation and hence contributed to shift Northern Hemisphere climate to a colder state. However, this mechanism which may explain the initiation of the Northern Hemisphere cooling has been recently dismissed by several studies demonstrating that the closure of Panama likely caused changes in North Atlantic circulation some ~4.5 Ma ago (Haug and Tiedemann, 1998; Ravelo et al., 2004), well before the inception of intense ice sheets expansion in the northern high latitudes ~3.0 Ma ago.

More recent studies argued that major NHG resulted instead of drastic changes in the high-latitudes, especially within the polar oceans (Haug et al., 2005; Sigman et al., 2004). The Pliocene cooling would have led to North Pacific stratification which, combined with favorable temperature conditions (extension of the summer warming into the autumn), would have contributed to ice sheet development in the Northern high latitudes by increasing the permanent continental snow cover (Haug et al., 2005). Other studies proposed that the synchronous stratification of both North Pacific and Southern Ocean diminished the CO_2 release from the deep ocean to the atmosphere (Haug et al., 1999; Sigman et al., 2004), thus causing atmospheric CO_2 drawdown. The later assumption is further corroborated by model experiments which stated that lowering of atmospheric

CO_2 could have substantially contributed to ice sheet formation in the Northern Hemisphere, especially over Greenland (Lunt et al., 2008).

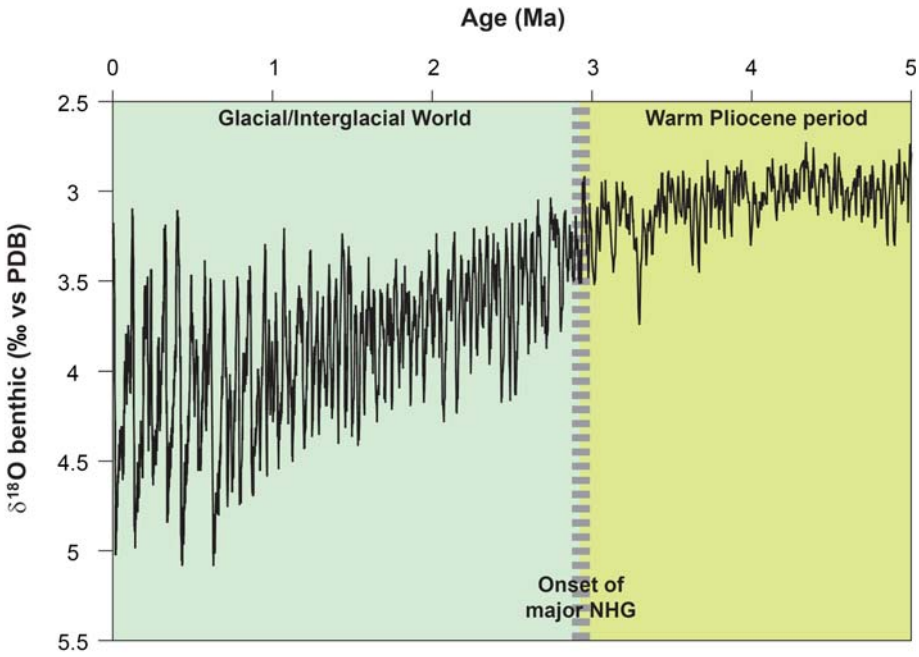

Figure 1.1 Plio-Pleistocene cooling trend over the last 5.0 Ma as shown by increasing oxygen isotope ratios ($\delta^{18}O$) in benthic foraminifera (Lisiecki and Raymo, 2005).

While reorganization of the polar oceans probably played a great role on the Pliocene cooling, changes in climatic and oceanic conditions in the subtropical and tropical regions may also have contributed to amplify this major climate transition. For instance, atmospheric conditions in the equatorial Pacific likely switched from a permanent El Niño-like state (weak Walker circulation), a dominant feature characterizing the warm Pliocene period, towards a perennial La Nina-like pattern (strong Walker circulation) during the late Pliocene/Pleistocene (Wara et al., 2005; Ravelo et al., 2004). Although this shift in atmospheric circulation pattern may have substantially modulated heat and moisture transfer from low-to-high latitudes and promoted ice accumulation over North America (Barreiro et al., 2005; Philander and Fedorov, 2006), its contribution to significant NHG is still controversial (Haywood et al., 2007).

Change in zonal atmospheric circulation along the equatorial Pacific over the last ~ 3.0 Ma was probably related to the occurrence of a cold tongue in the Eastern Equatorial Pacific (EEP), and

enhanced east-to-west sea surface temperature and pressure gradients. The EEP cooling may have responded to changes of the thermocline structure, tied either to a shoaling of the thermocline depth in response to the cooling of deep waters for instance (Fedorov et al., 2006) or to changes in the source of upwelled waters (Dekens et al., 2007). The latter hypothesis has been supported by a recent study which asserted that the concomitant narrowing of the Indonesian Gateway may have modified the origin of water masses entering the EEP, from North Pacific Intermediate Waters during the Early Pliocene to dominant Subantarctic waters after ~3.0 Ma ago (Karas et al., 2009). The constriction of the Indonesia Gateway may have also cooled the thermocline waters, supposed to precondition the surface water cooling in coastal upwelling regions, e.g. off Namibia (Karas et al., 2009).

While the physical processes, e.g., stratification of the polar oceans, contributing to the hypothesized atmospheric CO_2 drawdown have been described as the most plausible causes responsible of the Pliocene cooling, the mechanisms involving the biogeochemical processes, in particularly tied to the marine biological pump efficiency, are still poorly known. Changes in phytoplankton productivity are thought to play a major role in the global carbon cycle and thus could have also had a strong influence as an important internal climate feedback mechanism causing cooling by drawdown of atmospheric carbon dioxide levels. It has been widely documented that global primary productivity is mainly regulated by changes in nutrient supply into the euphotic zone for the modern as well as for the last glacial/interglacial cycles. However, few studies at a million-year time scale focused on the reconstruction of past changes in the distribution of nutrients between ocean basins and changes in the supply of nutrients to certain areas of high productivity, e.g., the Antarctic ocean, and the eastern boundary upwelling areas in the Pacific, Atlantic, or in the Arabian Sea. Such information is urgently needed to unravel whether Pliocene-Pleistocene climate change triggered reorganisation of ocean circulation and subsequently caused redistribution of nutrients and changes in marine productivity, affecting in turn global climate.

One of the outstanding examples that changing nutrient availability in surface waters on past primary productivity probably was an important feedback mechanism through the Plio-Pleistocene was reported for the high-latitude oceans (Haug et al. 1999, Sigman et al. 2004, Haug et al. 2005). According to the authors the diatom production in the North Pacific ceased at about ~2.7 Ma because surface water stratification hampered the upwelling of nitrate- and silicate-rich subsurface waters, strongly increasing nitrate utilisation, while in the Southern Ocean this increase in stratification did not change the balance between nitrate supply and utilisation very much. This

would imply that changes in marine productivity depending on varying nutrient supply cannot have initiated the Plio-Pleistocene cooling as a whole but may have amplified certain phases of cooling in strength or duration as a positive feedback mechanism via an increase in atmospheric carbon sequestration. In contrast, they may have terminated cooling trends as a negative feedback by an increase in wind driven upwelling of CO_2 rich subsurface waters. However, the relationship of Plio-Pleistocene changes in nutrient cycling to productivity, upwelling or circulation changes in areas of high marine productivity in low latitudes is not as clear as for the high-latitude ocean at 2.7 Ma (Ettwein et al. 2001) and necessitate further investigations.

1.2. Aims and objectives of the thesis

In order to address some of the remaining uncertainties in our understanding of Pliocene to Pleistocene cooling, the major aims of this study are:

- to generate high-resolution records of alkenone-based sea surface temperature (SST), and paleoproductivity by using alkenone concentration, nitrogen, organic carbon, biogenic opal contents, from deep sea sediments of the Benguela Upwelling System (BUS) and the Eastern Equatorial Pacific (EEP).

- to put special emphasis on the use of the $\delta^{15}N$ signal of organic matter by:

  - reconstructing changes in nutrient content of surface waters in low-latitude upwelling areas and deciphering their temporal relationship with prominent climate shifts during the last 3.5 Ma.

  - comparing the different $\delta^{15}N$ patterns and absolute $\delta^{15}N$ values over the last 3.5 Ma between the low-latitudes upwelling systems of the BUS, the EEP and the California margin.

  - unravelling if the $\delta^{15}N$ signal shows a pattern of correspondence for the Plio-Pleistocene climate cooling similar to that for the Late Pleistocene glacial/interglacial periods.

- to reconstruct and discuss the Plio-Pleistocene variability of coastal and open ocean upwelling activity, productivity, and nutrient cycling in the BUS and EEP over the last 3.5 Ma.

- to examine potential links between different upwelling systems in low latitudes in response to the Plio-Pleistocene cooling as well as the probable consequences of such changes on global climate.

This study will address the above cited points in seven distinct chapters as follows:

Chapter I contains a general introduction into the Pliocene-Pleistocene cooling and the possible causes of this global climate transition, as well as the oceanographic context of the concerned areas in the Southeast Atlantic and EEP, and the setting of location of the sites off Namibia and Ecuador. In addition, it is presented the different proxies used in this study to reconstruct paleoclimatic conditions.

Chapters II and **III** give detailed information on the materials and methods applied in this study, and the age models used at each studied sites.

Chapter IV presents the first manuscript (accepted in GEOLOGY) focusing on the reconstruction of the upwelling activity, productivity and nutrient cycle within the BUS over the past ~3.5 Ma. The manuscript was developed and written primarily by me, and I was responsible for the establishment of an improved age model for Site 1082. I also managed sampling work, and I carried out, with technical assistance, especially thanks to Dr. Thomas Blanz, all the analyses presented in the manuscript. I also actively participated to the elaboration of ideas and assumptions addressed in the manuscript with the support of my two supervisors, Prof. Dr. Ralph Schneider and Dr. Philippe Martinez.

Chapter V corresponds to the second manuscript (in review Nature Geoscience), which discusses the factors having controlled the phytoplankton productivity, including oceanic circulation and nutrient supply, in the EEP over the past ~3.0 Ma. As described for the former manuscript, I have written most of the manuscript and developed most of the hypotheses presented in this work with the support of my co-supervisors, and the team of Prof. Dr. Ralf Tiedemann, Dr. Frank Lamy, Daniel Rincon-Martinez and Cornelia Saukel. The age model at Site 1239 was mostly established

by me, and improved for the most recent the oldest part by Prof. Dr. Ralf Tiedemann. I also managed the sampling strategy and most of the data presented in the manuscript were performed by me, with technical assistance, except the iron data provided by Daniel Rincon-Martinez and the group of Prof. Dr. Ralf Tiedemann at AWI Bremerhaven.

Chapter VI gives attempts to compare past changes in atmospheric circulation affecting zonal and meridional sea surface temperature gradients of the subtropical and tropical regions throughout the Pliocene-Pleistocene climate transition, which corresponds to a manuscript under review at Geophysical Research Letters. The manuscript mainly lies on my own initiatives, ideas and assumptions developed during the PhD thesis, and improved by my two supervisors. The few data presented in the manuscript, added to the results presented in the two preceding manuscript, were performed by me, with technical assistance.

Finally, the conclusions and the perspectives originating from the individual manuscripts are presented at the end of this manuscript in **Chapters VII** and **VIII**.

1.3. Oceanographic settings and site selection

1.3.1 The Benguela Upwelling System (BUS)

The Benguela Current contains the most productive upwelling setting among the four major eastern boundary currents (California, Peru, Mauritania, and Benguela) (Carr et al., 2002). It flows equatorward along the South African coast and separates in two distinct segments at 28°S: the Benguela Ocean Current (BOC) and the Benguela Coastal Current (BCC) (Fig. 1.2). The Benguela Current is mainly fed by both surface advection and wind-driven upwelling of deep waters. The advected waters are mainly sourced by northward surface water transport derived from the South Atlantic Current and the Agulhas Current. The upwelled waters are made up of South Atlantic Central Water (SACW) and subtropical subsurface waters of the poleward flowing Benguela Undercurrent (BUC) (Gordon et al., 1995). SACW originates in the Subtropical Convergence Zone from subtropical and Subantarctic Mode Water (SAMW) that sinks and spreads northward (Shannon et al., 1985), while subsurface waters flowing in the BUC arise from the Angola gyre and extend until 30°S (Gordon et al., 1995).

The intensity of the coastal upwelling off Southwest Africa depends on the variation of the southeastern trade winds strength. The trade winds are driven by the seasonal position of the South Atlantic High pressure cell (SAH) which migrates northward during the austral winter and southward during the summer. At wintertime, the SAH is closer to the low pressure system over the continent, thus increasing the high-to-low pressure gradient. This leads to the strengthening of trade winds and hence to strong seasonal upwelling. This seasonality is mainly marked in the upwelling cells of the northern upwelling region, while in the central part of the BUS, strong offshore trade winds blow almost year-round and upwelling cells are permanently active (Summerhayes et al., 1995).

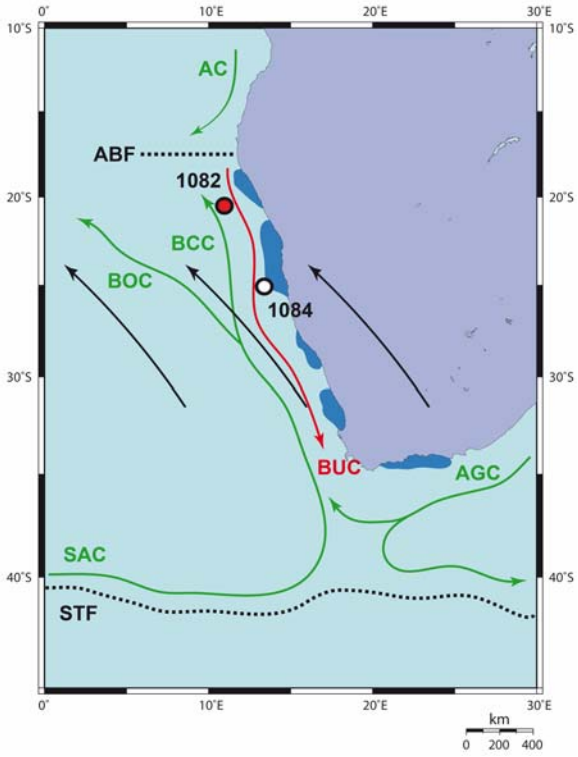

Figure 1.2 Modern surface oceanic circulation in the BUS and the locations of the study Site 1082 (red dot) and the Site 1084 (white dot). AC – Angola Current, AGC – Agulhas Current, BCC – Benguela Coastal Current, BOC – Benguela Ocean Current, BUC – Benguela Undercurrent, SAC – South Atlantic Current. ABF – Angola Benguela Front, and STF – Subtropical Front (dashed lines). The coastal upwelling cells are shaded in dark blue. Black arrows indicate the dominant wind forcing

In the BUS, nutrients are mainly carried to the surface layers through upwelling of nutrient-rich waters essentially arising from SAMW, but also, to a lesser extent, from the poleward undercurrent. In contrast, nutrient supply from the Indian Ocean remains relatively poor. Advected waters from the Agulhas Current are only sporadically spread into the Benguela region as filaments, and therefore only have a limited influence on Benguela Current surface waters. In consequence, phytoplankton primary productivity mainly responds to enhanced upwelling activity, when the nutrient supply rate feeding the surface waters is high (Fig. 1.3).

In order to reconstruct changes in upwelling intensity, nutrient supply and phytoplankton productivity in the BUS during the Plio-Pleistocene climate cooling, the Ocean Drilling Program (ODP) Site 1082 (21°06'S, 11°49'E, 1279 m water depth) has been selected and compared to the nearby Site 1084 (25°30'S, 13°1E, 1991 m water depth) studied by Marlow et al. (2000) (Fig. 1.2, 1.3). The Site 1082 is located in the north of the Cape basin, on the Walvis Ridge, where the upwelling activity is seasonally quite intense, while Site 1084 is located in the central part of the BUS, beneath the Lüderitz upwelling cell, which is the most active and perennial upwelling cells of the BUS (Shannon, 1985). The comparison of the two sites allows to scrutinize past Benguela upwelling activity as well as the influences of changes in the incoming waters.

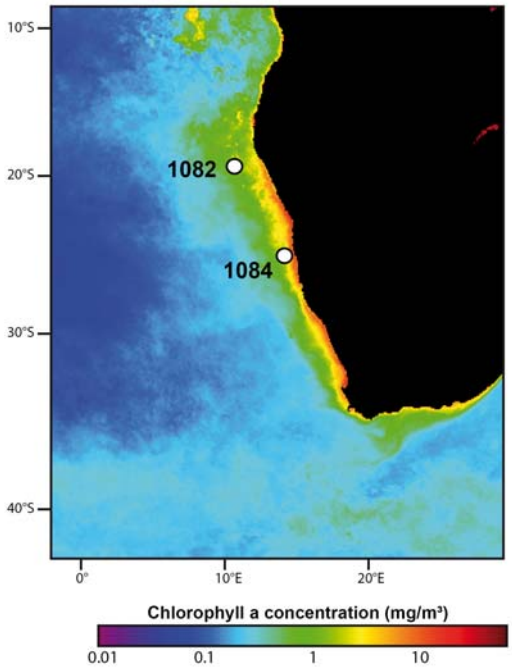

Figure 1.3 Modern chlorophyll *a* concentration, as indicator of phytoplankton productivity in the Benguela, from SeaWifs during the year 2005 (http://oceancolor.gsfc.nasa.gov/).

1.3.2 The Eastern Equatorial Pacific (EEP)

The EEP surface waters are mainly influenced by three ocean currents: the South Equatorial Current (SEC), the North Equatorial Countercurrent (NECC), and the Equatorial Undercurrent (EUC) (Fig. 1.4). The SEC flows westward and is mainly the continuation of the Peru-Chile Current (PCC) (Kessler et al., 2005). The latter comprises the coastal upwelling system off Peru where subsurface waters of the Gunther Undercurrent (GUC) upwell. The GUC corresponds to the lower branch of the EUC. The EUC circulate either into the GUC or seasonally upwells along the equator when convergent trade winds force the thermocline to shoal. The waters feeding the EUC have a minor northern hemisphere source and a more dominant (50-70%) southern hemisphere source (Dugdale et al., 2002; Rodgers et al., 2003). The southern hemisphere contribution is mainly derived from SAMW and Antarctic Intermediate Waters (AAIW) formed in the Subtropical and Subantarctic Convergence Zones, respectively.

In the modern EEP, the convergent trade winds from both northern and southern hemispheres cause divergent upwelling along the equator which is accompanied by the rising of cold water from below the thermocline to the surface. The shallow thermocline in the EEP mainly result from the zonal gradients in sea level pressure and SST across the equatorial Pacific, which strengthen the trade winds, and hence the upwelling in the EEP. In contrast, the thermocline in the western equatorial Pacific (WEP) is deep and warm water from above the thermocline upwells when trade wind strengthen. The east-to-west SST asymmetry between the warm WEP and the cold EEP leads to a zonal atmospheric circulation pattern, referred to as Walker circulation (Cane, 1986). The Walker circulation is further strengthened as far as the EEP cooling and the west-to-east SST gradient increase. In addition to the equatorial upwelling, the EEP surface water cooling can be further accentuated by the upwelling off Peru, seasonally controlled by strong offshore trade winds, which leads to a strongly developed cold tongue, starting from the Peru margin and extending towards 110°W, and therefore to an enhanced Walker circulation. Inversely, when both equatorial and coastal upwelling in the eastern tropical Pacific (EEP and Peru) weaken, the EEP surface water warms, the zonal SST gradient along the equatorial Pacific decreases and the Walker circulation weaken.

When the thermocline is shallow and the upwelling intense, the biological production in the EEP increases (Fig. 1.5). However, contrary to the coastal BUS where macronutrients (e.g. nitrate) are thought to be limiting, the open ocean EEP upwelling region is a High Nutrient Low

Chlorophyll (HLNC) area (Bruland et al., 2005; Pennington et al. 2005). Despite high nutrient supply from the upwelling of nutrient-rich waters, for which the EUC is the main contributor, biological production is limited by micronutrients such as iron (Murray et al., 1994). High iron input from terrestrial (fluvial and aeolian) sources mainly fertilizes surface waters along the South American coastline, but is relatively weak in open ocean upwelling areas. In open ocean waters, iron is mainly carried to the euphotic zone as dissolved fraction through the EUC and PCC (Murray et al., 1994; Schroth et al., 2009; Ziegler et al., 2008). Because of its low concentration, the phytoplankton growth is limited (Pennington et al., 2006).

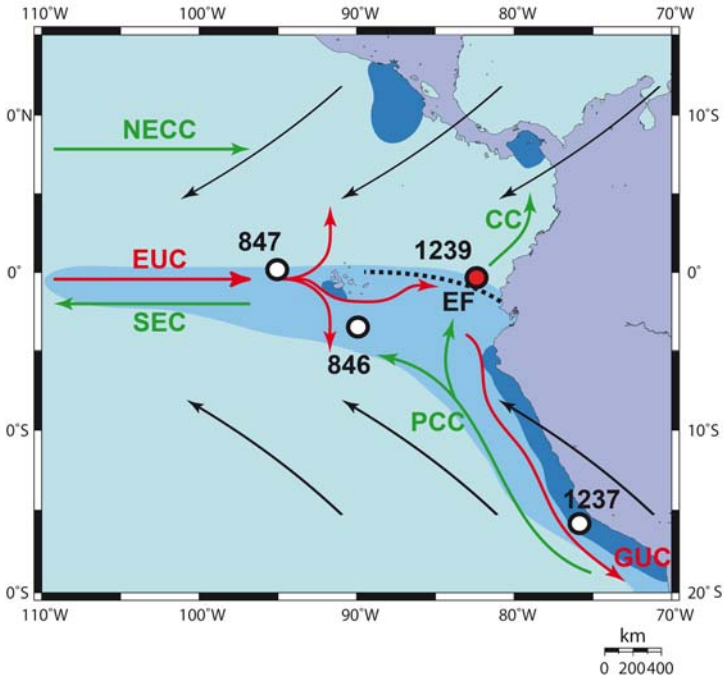

Figure 1.4 Modern surface and subsurface oceanic circulation in the EEP and the locations of the study Site 1239 (red dot) and the Sites 1237, 847 and 846 (white dots). CC – Coastal Current, EUC – Equatorial Undercurrent, GUC – Gunther Undercurrent, NEC – North Equatorial Current, PCC – Peru-Chile Current. EF – Equatorial Front (dashed line). The open ocean and coastal upwelling cells are shaded in dark blue, and the cold tongue in lighter blue. Black arrows indicate the dominant wind forcing.

To reconstruct Plio-Pleistocene changes in surface oceanic circulation, nutrient supply and primary production, the EEP Site 1239 (0°40.32'S, 82°4.86'W, 1414 m water depth) has been selected. Site 1239 is located 120 km off the Ecuador coast, under the eastern reaches of the

equatorial cold tongue, affected by open ocean equatorial upwelling. The site is close to the equatorial front that separates cold water masses, south of equator, from the warm water masses of the Panama Basin (Strub et al., 1998). This site is compared to the Sites 1237 (16°S, 76°23'W, 3334 m water depth) and 847 (0°12'N, 95°19'W, 1165 m water depth) studied by Dekens et al. (2008), and Site 846 (3°'S, 90°49'W, 3295 m water depth) studied by Lawrence et al. (2006). This comparison enables to document further the overall mechanisms involved in the reorganization of EEP surface circulation, together with past changes in primary productivity as well as changes in nutrient supply since the warm Pliocene period.

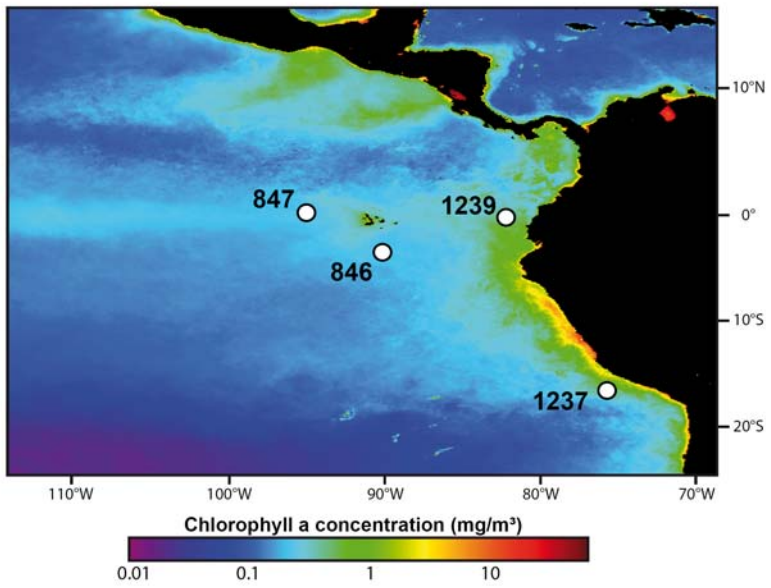

Figure 1.5 Modern chlorophyll *a* concentration, as indicator of phytoplankton productivity in the EEP, from SeaWifs during the year 2005 (http://oceancolor.gsfc.nasa.gov/).

Contrary to the BUS Site 1082, the EEP Site 1239 is situated in a region of strong tectonic activity which may partly account for the reconstructed changes in past oceanic circulation, productivity and nutrient supply when considering past relocation of this site. Over the last 4 Ma, the tectonic backtrack path of the Nazca plate displaces Site 1239 westward by 200 km, slightly to the south relative to a fixed South America (Gripp and Gordon 1990; Pisias et al., 1995; Mix et al., 2003). Therefore, Site 1239 remained along an equatorial transect and the paleoposition of Site

1239 unlikely altered the signal of past changes in the equatorial upwelling, nutrient cycling and the associated primary productivity.

1.4. Paleoclimatic proxies

1.4.1 Sea surface temperature

Past sea surface temperatures (SST) since the warm Pliocene period at both Benguela Site 1082 and EEP Site 1239 were reconstructed by using the alkenone unsaturation index ($U^{K'}_{37}$). The $U^{K'}_{37}$ index (Eq. (1)) has a strong correlation with annual average SST in the modern ocean (Conte and Eglinton, 1993; Prahl and Wakeham, 1987; Sicre et al., 2002; Ternois et al., 1997) and has been extensively calibrated from surface sediments throughout the world ocean (Conte et al., 2006; Müller et al., 1998; Pelejero and Grimalt, 1997; Prahl et al., 1987, 1988; Sikes et al., 1991; Sonzogni et al., 1997).

$$(1)\ U^{K'}_{37} = \frac{C_{37:2}}{C_{37:2} + C_{37:3}}$$

The $U^{K'}_{37}$ index utilizes long-chain ($C_{37:2}$ and $C_{37:3}$, fig. 1.6) ketones (Brassell et al., 1986; Prahl and Wakeham, 1987) synthesized by certain species of phytoplankton (coccolithophorid algae), living mainly in the upper layer (0-20 m) of the euphotic zone (Conte et al., 2001; Prahl et al., 2005). Among the different coccolithophorids species, only a few unicellular haptophytes, mostly *Emiliana huxleyi* (*E. huxleyi*) and *Gephyrocapsa oceanica* (*G. oceanica*) (Marlowe et al., 1990; Conte et al., 1995; Volkman et al., 1995), produce alkenones in the modern ocean.

The first evolutionary appearance of *E. huxleyi*, the main alkenone synthesizer in the modern, is dated at about ~0.27 Ma, and ~1.7 Ma for *G. oceanica* (Emeis et al., 1995; Müller et al., 1998; Thierstein et al., 1977; Raffi et al., 2006). The application of the different calibrations, global or specific to one species and commonly used for the late Pleistocene (Conte et al., 2006; Müller et al., 1998; Pelejero and Grimalt, 1997; Prahl et al., 1987, 1988; Sikes et al., 1991; Sonzogni et al., 1997), could be problematic when applied to the Early Pleistocene and the Pliocene sediments.

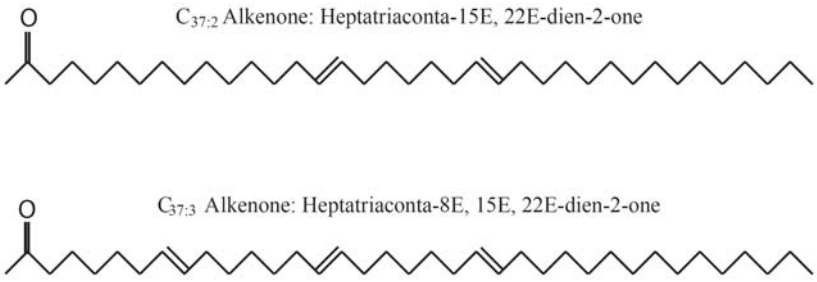

Figure 1.6 Chemical structure of the long-chain ketones ($C_{37:2}$ and $C_{37:3}$). $C_{37:4}$ alkenone (Heptatriaconta-8E, 15E, 22E, 29E-tetraen-2-one) can be present, only in the high latitude sediments, but in insignificant proportion compared to $C_{37:2}$ and $C_{37:3}$ in the low latitudes sediments such as in the Benguela and EEP regions, and generally are not considered in most of the calibrations.

The co-occurrence of alkenones and ancestral family of *E. huxleyi* and *G. oceanica* in marine sediments since the Eocene (Marlowe et al., 1990) implies that the alkenone synthesis was likely performed in a similar manner than today by ancient haptophytes. Second, considering that the alkenone production during the Early Pleistocene and Pliocene probably had the same biological function than today, regulator of membrane fluidity (Brassell et al., 1986), metabolic storage lipids (Epstein et al., 2001), or buoyancy controllers (Sawada and Shiraiwa, 2004), it is reasonable to assume that application of alkenones as a paleothermometer for the Late Pleistocene can also be extended to older periods (Pliocene). Third, it has been shown that the relationship between the $U^{K'}_{37}$ index and the index of the C_{38} methyl ketones for Pliocene and Miocene sediments is similar to that established for late Pleistocene age samples (Herbert et al., 1998). This observation has been used as an argument to suggest that the alkenone unsaturation response remained identical during the Plio-Pleistocene. Fourth, if alkenone-SST calibrations for ambient conditions applied for the Pliocene would yield arbitrary temperature estimates, discrepancies between different SST proxy reconstructions (e.g. alkenone-SST versus Mg/Ca-SST) should be detected. However, SST interproxy comparison in the equatorial Pacific showed outstanding similarities in term of trends and values since ~5 Ma (Dekens et al., 2008; Medina-Elizalde et al., 2008; **Chapter VI**). Each of those arguments taken together reinforce therefore the idea that the use of modern ocean

calibrations for converting Pliocene $U^{K'}_{37}$ values into SST is reasonable for the studied time interval, while some precaution is needed when discussing the absolute values.

1.4.2 Paleoproductivity

In this study, to monitor past changes in primary productivity in the Benguela and EEP regions for the past ~3.5 Ma, alkenone concentration, total nitrogen, organic carbon and biogenic opal contents were determined at the Sites 1082 and 1239. To avoid effects of dilution or concentration of biogenic components by changing proportions of terrigenous constituents in the sediment, the MAR of the biogenic component were calculated at both sites according to Eq. (2).

(2) Component MAR (g/cm^2ka) = LSR (cm/ka) x DBD (g/cm^3) x component percentage/100

in which LSR is linear sedimentation rates; DBD is dry bulk density. The LSR is determined from the age model (see ***Chapter III****), while the DBD is given by shipboard measurements during Leg 175for Site 1082 and 202 for Site 1239 (Wefer et al., 1998; Mix et al., 2003).*

The alkenone MAR is commonly used to reflect past changes in coccolithophorid productivity export from surface to sediments, which roughly gives an estimate of coccolithophorid production rate produced in the euphotic zone. The reconstruction of such productivity is of particular interest in the upwelling regions (e.g. Benguela) where coccolithophores seasonally bloom with nutrient-rich water supply through enhanced upwelling activity, and reach extremely high production rates. In the upwelling regions, a significant proportion of this high production is exported into the deep ocean. However, during its downward transport, water-column and sediment degradation may substantially affect this phytoplankton productivity export. It has been shown that only ~1% of the total coccolithophorids production in the photic zones reaches the sediment (Conte et al., 1992; Prahl et al., 2000; Wakeham et al., 1997). Thus, we assume that the alkenone MAR only gives an assessment of the magnitude of change in burial but not a precise quantification of surface productivity. The coccolithophores are one of the main calcium carbonate producers in the open ocean. Assessing past changes in coccolithophorid production via alkenone MAR may thus help to estimate the role played by this group of organisms on the carbonate cycle, and ultimately on the global carbon cycle and atmospheric CO_2 concentrations (Archer et al., 2000), the drawdown of the latter being hypothesized to be one of the major cause of the Plio-Pleistocene cooling (Lunt et al., 2008).

Total nitrogen (TN) and organic carbon (C_{org}) MARs preserved in the sediments are also considered to reflect past changes in productivity, but, unlike to alkenone concentration MAR, the two proxies record past changes in the overall biological production and not exclusively that related to coccolithophorid productivity. Thus, the TN and C_{org} MARs give an overview of the total phytoplankton productivity which developed in the subsurface and surface waters. However, the ammonium (NH_4) can be often bound in clays and can significantly contribute to TN, thus biasing the use of TN MAR as paleoproductivity proxy. It is assumed here that sediments in the BUS do not contain so much terrigenous clay because they were mainly constituted of carbonate, biogenic opal and organic carbon as found in most of the upwelling regions. Therefore, TN is almost all nitrogen coming from organic tissues assimilated to organic nitrogen. The C_{org}/TN ratio can be used to assess the origin of the organic matter buried in the sediments, either of terrestrial or marine origin, and enable to assess the nature of the dominant productivity exported to and preserved in the sediments. The C_{org}/TN ratio has been widely applied to determine the provenance of the sedimentary organic matter (Martinez et al., 2000; Meyers et al., 1997; Pichevin et al., 2005; Twichell et al., 2002). Marine algae C_{org}/TN ratios range between 4 and 10, whereas terrestrial C_{org}/TN ratios show values up to 20 (Meyers et al., 1997).

While the alkenone MAR is an indicator of past changes in coccolithophorid productivity, TN and C_{org} MAR, of the overall phytoplankton productivity, changes in silicate productivity can be assessed by determining the biogenic opal MAR. Biogenic silica, or opal, is produced by diatoms, radiolarian, sponges and silicoflagellates. However, diatoms are frequently the dominant component of the underlying sediments and hence of opal accumulation. The biogenic opal MAR is an essential proxy for reconstructing past diatom production, especially in upwelling regions where phytoplankton productivity over long periods was dominated by extremely high diatom abundance in the BUS such as during the Late Pliocene cooling. Moreover, diatom productivity is believed to have significantly contributed to atmospheric CO_2 sequestration into the deep ocean for the last glacial/interglacial cycles (Sigman and Boyle, 2000). The reconstruction of biogenic opal MAR in upwelling systems across the Plio-Pleistocene may therefore reveal an eventual close relationship between variations in siliceous productivity, as efficient biological pump, and climate cooling.

1.4.3 Marine nitrogen cycle

The primary productivity (e.g. diatoms, coccolithophores) is overall limited in the ocean by nutrients such as nitrogen (Dugdale and Goering, 1967). Phytoplankton productivity is generally high when fixed (or soluble) Nitrogen (N) concentrations are elevated and low when they are depleted. N gain in the ocean is mainly sourced by N fixation, by atmospheric deposition and river runoff (Fig. 1.7) (Wada and Hattori, 1990). N loss is mostly caused by microbial denitrification, and to lesser extent by burial in the sediments and export from the ocean to the continent (Fig. 1.7) (Codispoti and Christensen, 1985). The balance between both denitrification and nitrogen fixation processes is supposed to control the global oceanic fixed N inventory (Tyrell et al., 1999; Deutsch et al., 2004, 2007). However, the balance between both mechanisms in the modern ocean is still uncertain. Some authors asserted that the rate of marine denitrification significantly exceeds that of nitrogen fixation (Codispoti et al., 2001; Brandes and Devol, 2002), which lead to the suggestion that, if true, the ocean would become increasingly depleted of fixed N which does not seem to be the case. Thus, to balance the N loss due to denitrification, a subsequent source of N is needed (Deutsch et al., 2004; Gruber et al., 2004). Other studies indicate that nitrogen fixation rates may have been largely underestimated (Gruber and Sarmiento, 1997; Karl et al., 1997, 2002), and may have compensated to a large extent the loss tied to the denitrification process. This implies that N fixation could play a greater role than expected on the modern N cycling and hence the biological pump. This assumption was also suggested for the past glacial/interglacial cycles (Ganeshram et al., 2002; Ren et al., 2009; Sachs and Repeta, 1999), but remains unknown for warm Pliocene conditions.

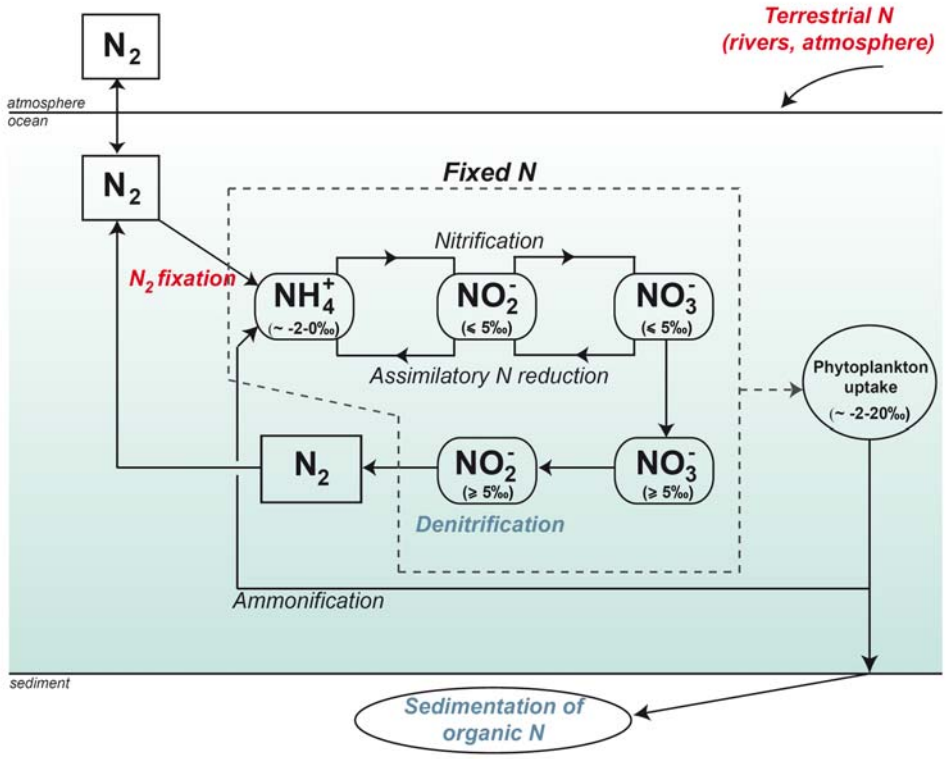

Figure 1.7 Simplified representation of the marine N cycle (modified after Karl et al. (2002)). Dotted lines define the bioavailable N. Arrows indicate the different N conversion through physical-chemical processes. The small numbers refer to average $\delta^{15}N$ values. The N sources are indicated in red and the N sinks in blue.

1.4.3.1 Nitrogen isotopes

Nitrogen exists naturally as two stable isotopes, ^{14}N (~99.63 % of the total nitrogen) and ^{15}N (0.36 %) (Karl et al., 2002). The nitrogen isotopic ratio is reported to that of a reference standard and reported in delta notation (Eq. (3)) in units of per mil (‰), and used to reflect past nutrient (mostly nitrate) cycle, especially in high productive regions such as in the Benguela and EEP regions.

$$(3) \qquad \delta^{15}N\ (‰\ \text{vs Air}) = \left(\frac{^{15}N/^{14}N_{sample}}{^{15}N/^{14}N_{standard}} - 1\right) \times 10^3$$

in which atmospheric N_2 is the reference standard (with a $\delta^{15}N$ = 0‰ (Mariotti, 1983)).

The $\delta^{15}N$ signal in deep-sea sediments records primarily the degree of fixed N (mostly nitrates, NO_3^-) utilization by the phytoplankton, which corresponds to the fraction of the bioavailable N supply taken up by the primary producers during the photosynthesis. The lighter ^{14}N isotope is preferentially incorporated into phytoplankton, thus leaving the ambient seawater enriched in the heavier ^{15}N isotope. The degree of depletion thus determines the magnitude of isotopic signature, following Rayleigh fractionation kinetics (Fig. 1.8). The relative utilization of nitrate by phytoplankton can be estimated according to Eq. (4) (Altabet and Francois, 1994). However, the $\delta^{15}N$ of organic matter buried in the sediment also depends on the isotopic character of the regional N pool, the latter being mainly controlled by two bacterial processes, fixation of atmospheric N_2 and the denitrification of dissolved nitrate.

$$(4) \qquad \delta^{15}\text{Nsed (‰)} = \delta^{15}\,\text{NO}_{3\ \text{initial}\ (f=1)}^{-} + \frac{f}{(1-f)}\ \text{x}\ \varepsilon\ \text{x}\ \ln(f)$$

in which f is the fraction of the initial nitrate pool remaining ($[NO_3^-]_{obs}/[NO_3^-]_{initial}$), ε, the fractionation factor.

Nitrogen fixation is the main source of bioavailable N in the modern ocean. This process involves N_2-fixing microorganisms (*Bacteria*, *Archea* and *Cyanobacteria*) (Karl et al., 2002) which, under warm and stratified water conditions, convert the atmospheric N_2 in fixed N (Fig. 2.3a). This fixed N can also be consumed by some nitrifying bacteria converting it in nitrite (NO_2^-) and nitrates (NO_3^-). The N fixation hardly discriminates ^{15}N versus ^{14}N, resulting in light $\delta^{15}N$ values of the organic N buried in the sediment similar to those of the atmospheric ones (~0 ‰) (Brandes and Devol, 2002).

In contrast to the N fixation, the denitrification process occurs under suboxic water column conditions (<2-5 μM O_2) (Codispoti et al., 2005) and corresponds to bacteria-mediated reduction reaction that convert nitrates (NO_3^-) to nitrite (NO_2^-) to nitrous oxide (N_2O) to nitrogen gas (N_2) (Fig. 2.3a). Changes in water column denitrification could be driven by the interplay between variations in local productivity leading to a change in remineralisation rates and oxygen drawdown, and changes in ocean circulation and ocean temperature resulting in variations of the physical supply of dissolved oxygen. While several studies emphasize the importance of variations in biological productivity (Altabet et al. 1995, Altabet et al. 2002, Ganeshram et al. 2000), other

highlight the role of variable oxygen supply due to changes in upper ocean ventilation (e.g., Behl and Kennett, 1996; Galbraith et al. 2004). Contrary to N fixation and nitrate uptake, the denitrification leads to isotopically heavy residual nitrate resulting in typical heavy sedimentary $\delta^{15}N$ values (from 5 to 30 ‰), denitrification occurring with a broad isotopic fractionation, while on the other hand producing isotopically light N_2 and N_2O mainly lost to the atmosphere (Fig. 1.8) (Cline and Kaplan, 1975; Liu and Kaplan, 1989).

During sinking through the water column and the burial of the organic matter in sediments, the $\delta^{15}N$ could be also altered by bacterial degradation which may shift values up to +4‰ (Altabet and François, 1994; Sachs and Repeta, 1999), an effect that can be superior to the isotopic variations in the surface waters. This could be due to the preferential remineralization of the ^{14}N during the oxidation of the organic matter, releasing light $\delta^{15}N$ and increasing the $\delta^{15}N$ of the organic N fraction, later buried in the sediments. This process seems of greatest importance under oxygen-rich deep waters and organic-poor deep-sea sediment conditions. Thus, comparison of the bulk-sediment $\delta^{15}N$ signal with paleoproductivity-related proxies (e.g. Corg) and surface water conditions has to be considered when attempting to reconstruct past N cycle changes.

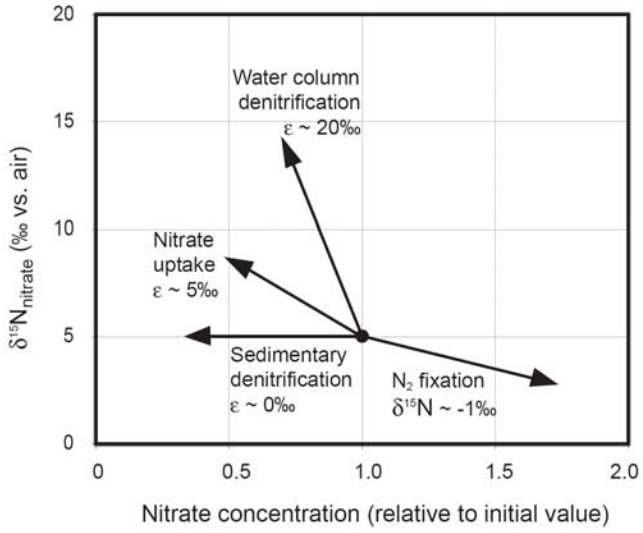

Figure 1.8 Schematic view of the fractionation process of the nitrogen isotopes ratio in both water column and sediments from an initial N pool with a $\delta^{15}N$ of 5 ‰ (after Galbraith et al., 1996; Sigman et al, 2000).

The sedimentary $\delta^{15}N$ signal can also record terrestrial organic matter signal which has a different N composition and low $\delta^{15}N$ values (McKay et al., 2004). Thus, the origin of the organic matter, either marine or continental, has to be determined. To characterize the origin of the organic matter, the sedimentary carbon isotopes ($\delta^{13}C_{org}$) as well as the C/N ratio can be used (see 1.4.2). The continental organic matter typically exhibits light δ^{13}Corg values (<-26‰), while marine algae indicate high $\delta^{13}C_{org}$ values (~22-20‰) (Twichell et al., 2002).

1.4.3.2 Nitrogen cycling in the modern BUS

In the modern Benguela, denitrification associated to oxygen minimum zones (OMZ) is restricted to the most active upwelling cells (e.g. Lüderitz) on the Namibian inner shelf. The occurrence of denitrification is attributed to phytoplankton blooms during enhanced seasonal upwelling off Namibia which almost fully utilized nitrate and oxygen from the oxygenated-poor subsurface waters of the poleward undercurrent, thus resulting in very high sedimentary $\delta^{15}N$ values (Pichevin et al., 2005). It is, however, unlikely that the high $\delta^{15}N$ values of the shelf sediments are tied to an isotopic signal sourced by the Angola Basin, where low oxygenated water conditions develop (Fig. 1.9), because of the reconstructed patchy distribution of high $\delta^{15}N$ in the BUS (Pichevin et al., 2005) (Fig. 1.9). Besides, it is not certain that strong denitrification occurs in the Angola Basin, except on the shelf, because the oxygen concentrations in the subsurface waters are not low enough in this area for promoting nitrate reduction (< 2 ml/l) (Holmes et al., 1996).

In contrast to the inner shelf, the sedimentary $\delta^{15}N$ values found on the continental slope mainly reflect changes in nutrient utilization tied to the nutrient-rich and well-oxygenated waters supplied by upwelling. However, it may also mirror global changes in mid-depth nitrate $\delta^{15}N$ as demonstrated for the recent past (Pichevin et al., 2005). Indeed, some studies based on deep cores revealed that during the last glacial/interglacial periods, the $\delta^{15}N$ signal varied in phase with denitrification variations in the far Arabian Sea (Pichevin et al., 2005). This has been interpreted as the result of past changes in the nutricline $\delta^{15}N$ signal transmitted by subsurface waters circulation, from the western Indian to the southeastern Atlantic Ocean via the Agulhas Current. Site 1082 is not located today in a denitrifying zone, but at relatively the same water depth as the core of the previous study which stated that global changes in $\delta^{15}N$ of the nutricline might affect the sedimentary $\delta^{15}N$ values in this area. Thus, the $\delta^{15}N$ values at Site 1082 could reflect (1) changes in nitrate utilization relative to the source of nutrients, and (2) global ocean changes in mid-depth nitrate $\delta^{15}N$.

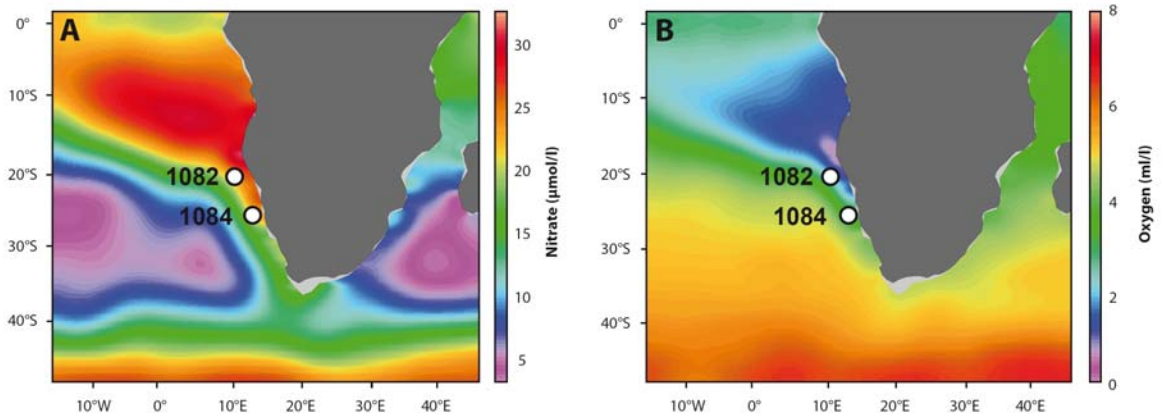

Figure 1.9 Modern conditions for dissolved nitrate (A) and oxygen (B) concentration in 200 m in the BUS. Data source WOA 2001 (Conkright et al., 2002), plots generated with Ocean Data View software (Schlitzer, 2005).

1.4.3.3 Nitrogen cycling in the modern EEP

The most active zones of denitrification in the eastern Pacific are mainly situated along the coastline of western South America (Cline and Kaplan, 1975; Liu, 1979) particularly along the Peruvian and Chilean margins (Liu, 1979; Martinez et al., 2006). This is illustrated by extremely low oxygen concentrations observed at 200 m water depth in these areas (Fig. 2.0). Along the western North and South America coasts, strong upwelling seasonally strengthens, and nutrient-rich waters reach the surface. Stimulated by strong iron supply, mainly from aeolian inputs, phytoplankton blooms and utilizes most of the nitrate contained in the upwelled waters. However, these upwelled waters rising in these regions originate from poorly oxygenated intermediate waters from, both, northern and southern high-latitudes. The high biological production therefore consumes most of the oxygen during strong upwelling seasons, beyond the critical threshold (< 2 ml/l) required for promoting denitrification. As a result, the sedimentary $\delta^{15}N$ signal recording the denitrification process along the Peru-Chile coasts for instance can reach extremely high values up to 14 ‰ (Martinez et al., 2006; Hebbeln et al., 2000a). While nitrate-depleted waters from the eastern tropical North Pacific do not influence so much surface waters in the EEP, those from the Peru-Chile coast can alter the nitrate availability in the EEP surface waters by advection through the equatorward and westward cold tongue.

However, in the EEP, the open ocean equatorial upwelling ventilates surface waters by a supply of new subsurface waters transported by the EUC. Besides, unlike to eastern Pacific coasts, the EEP primary productivity is limited by iron fertilization (Bruland et al., 2005; Murray et al., 1994). Thus, the EEP, known as high nutrient, low productivity region, is not a zone of denitrification despite the low oxygenated water upwelling to the surface. The sedimentary $\delta^{15}N$ signal mainly records past changes in nutrient utilization, rather than reflecting any changes in denitrification rate (Farrell et al., 1995).

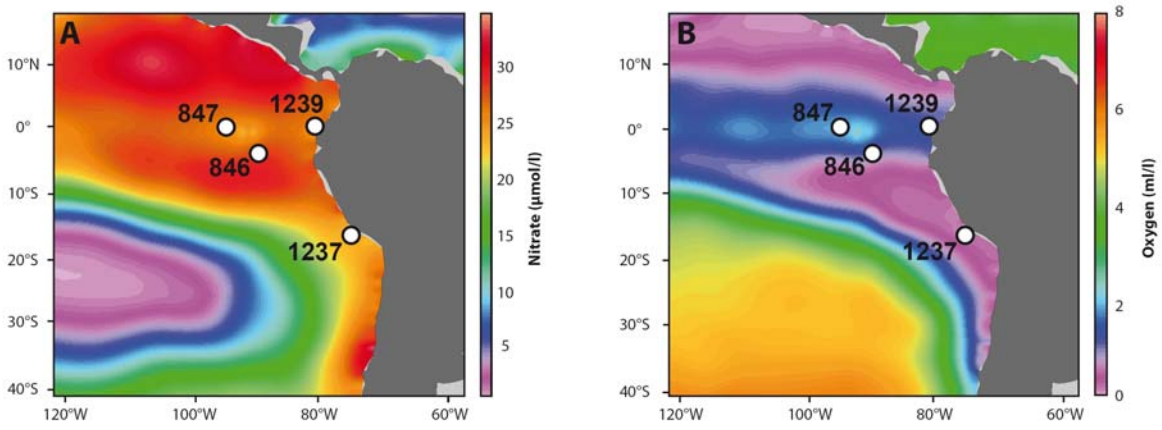

Figure 1.10 Modern conditions for dissolved nitrate (A) and oxygen (B) concentration in 200 m in the EEP. Data source WOA 2001 (Conkright et al., 2002), plots generated with Ocean Data View software (Schlitzer, 2005).

Chapter II

Materials and Methods

2.1 Sampling strategy

In order to cover the Plio-Pleistocene climate transition at a 2-5 ka resolution, the alkenones at Site 1082 were measured on 420 sediment samples taken every ~50 cm from the Hole A (3.48-1.28 Ma) and every ~20-40 cm from the Hole C (1.95-1.46 Ma), added to the 256 previously measured at Hole A by Jahn et al. (unpublished data) for the younger part (1.28-0.17 Ma). At Site 1239, 746 samples taken every ~20 cm from the Hole A were measured to span the period ~3.2-0.5 Ma.

Biogenic opal data was selectively determined from 113 samples at the Benguela Site 1082 Hole A for the period ~3.0-2.0 Ma. Organic carbon was measured at low resolution on 41 samples taken every ~60-70 cm at Site 1239 Hole A in order to cover the period ~3.2-0.5 Ma.

The $\delta^{15}N$ and nitrogen content measurements from the bulk sediment were performed at a 4-6 kyr resolution on 603 samples taken every ~50 cm at the Benguela Site 1082 Hole A for the period ~3.48-0.37 Ma. Keeping similar resolution, 376 samples taken every ~40 cm at the EEP Site 1239 Hole A were measured for the period ~3.16-0.51 Ma.

All Sites 1082 and 1239 data are presented in Appendix A and B, respectively, at the end of this manuscript.

2.2 Analysis of alkenones

2.2.1 Analytical technique

Alkenones were extracted at the CAU (Christian Albrecht University of Kiel) from a sample vial containing the freeze-dried and homogenized sediment (~1 g dried weighted) after addition of 1 cm layer of silicagel, 1 µg of cholestane ($C_{27}H_{48}$) and 0.5 µg of hexatriacontane ($C_{36}H_{74}$) as internal standards, and modified Diatomeenerde (Isolute HM-N, extraction grade) to increase the sample volume to 11 ml, the size of the extraction cell. Each sample was extracted twice by an accelerated solvent extraction with a Dionex ASE 200 for 10 min using 25 ml dichloromethane at a temperature of 75°C with 80 bar nitrogen gas pressure. After heating, the extract was flushed from the sample cell into a standard collection vial and cooled down in a freezer (-20°C). The resulting extract is concentrated to 50 µl with a rotary evaporator bath at 300 mbar, 20-22°C. Afterward, it

was transferred into glass vials and dried over nitrogen. After drying, the residues were taken up in 100 µl hexane.

The resulting sample was analyzed with multidimensional, double column gas chromatography (MDGC) using two Agilent 6890 gas chromatographs (GC1 and GC2) equipped with two independent ovens and two flame ionization detectors (FID), connected by a transfer line. MDGC combines the separation efficiency of two capillary columns with different polarities, each in a separate temperature-controlled oven arranged in series, and the sensitivity of two FID for quantifying the specific compounds eluting. In the oven 1, the eluate is transported by hydrogen flux under constant pressure through a fused silica precolumn (or Guard column) (~1.0-2.0 m length x 0.32 mm ID x 0.5 µm df), and then through a RTX-1 fused silica column (10 m length x 0.32 mm ID x 0.25 µm df). In the oven 2, the selected fraction is carried by hydrogen flux under constant pressure through a RTX-200 fused silica chromatographic column (30 m length x 0.32 mm ID x 0.25 µm df) (Fig. 2.1). GC1 and GC 2 have two different temperature programmed. In the GC 1 temperature oven was initially of 100°C, then after 3 min, increased from 100°C to 330°C by 15°C/min, where the temperature is maintained at 330°C during 6 min before cooling down to 260°C for 18.10 min. In the GC 2, the oven temperature stepwise increases was initially of 100 °C, then after 3 min, increased to 210°C by 15°C/min, hold during 9.83 min, increased again to 290°C by 5°C/min, before a second isothermal holding step during 5 min, and warmed again until 330°C where it hold for 3.30 min.

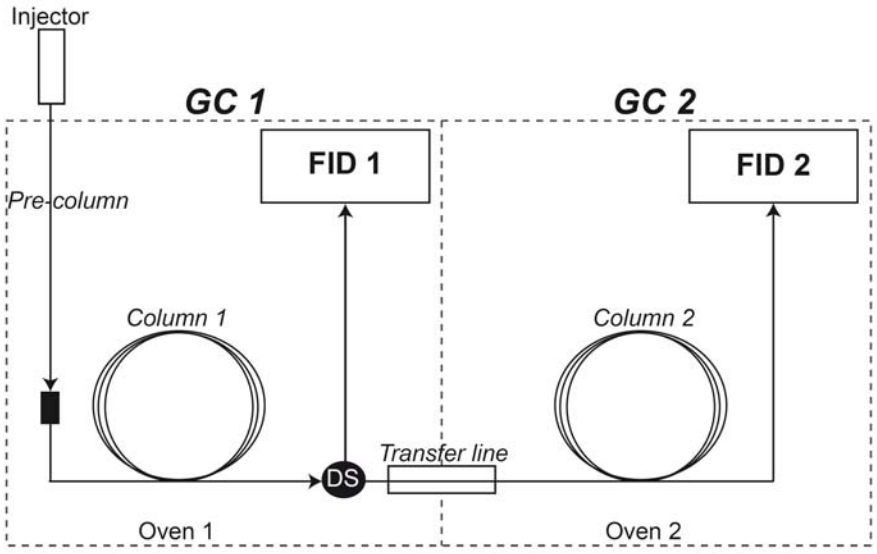

Figure 2.1 Schematic view of the double column MDGC. GC, Gas Chromatograph; DS, Dean Switch; FID, Flame Ionization Detector. Arrows indicate the direction of the molecules flow.

The eluate of the first column passed either through the monitor detector or switched through a deanswitch system to the second column and the main detector. In the latter mode, a preselected small fraction was cut from the eluate of the first column and transferred via a transfer line to the second column after ~17 min, the predefined cut time. The usual FID chromatogram (FID 1) is recorded by the monitor detector, only interrupted during the cut time. The chromatogram recorded by the main FID (FID 2) shows only a few peaks depending on the components (alkenones) included in that cut (Fig. 2.2). The main detector has a much higher sensitivity than the monitor detector, because of the reduced memory effect and reduced level of contamination by coeluates, as it receives small selected fractions from the first column through the heart cut.

From the main detector chromatogram, the areas of the $C_{37:2}$ and $C_{37:3}$ alkenones are obtained. The $U^{K'}_{37}$ index (Eq. (5)) is then calculated as the ratio between the different $C_{37:2}$ and $C_{37:3}$ areas.

$$(5) \qquad U^{K'}_{37} = \frac{AreaC_{37:2}}{AreaC_{37:2} + AreaC_{37:3}}$$

The results are thereafter compared to those obtained from an in-house standard (Skagerrak). Skagerrak samples, previously calibrated (Rosell-Melé et al., 2001), and enable to control the stability of the MDGC and to adjust values if necessary. The C_{36} standard peak, appearing in the chromatogram sequence just before the C_{37} group, is used to precisely define the cut time, the time from which the C_{37} group signal is transferred into the second GC, as well as for the calculation of the alkenone concentration (see 2.2). This relatively new technique, with two running parallel GC, allows to obtain an accurate chromatography signal, even for low alkenone concentration (> 1 ng/g). According to sample and numerous internal standard replicates, the $U^{K'}_{37}$ precision is about ± 0.05 units.

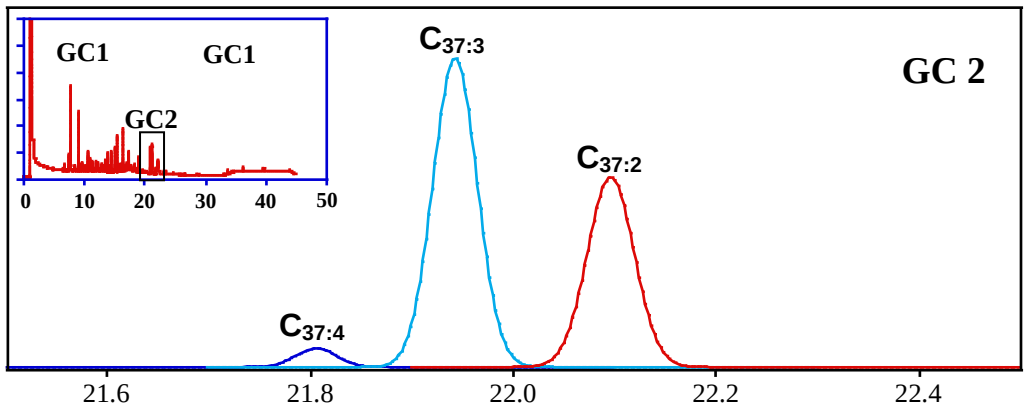

Figure 2.2 Typical alkenone chromatogram recorded by the main detector in the GC 2. In the left small panel is shown the complete sequence obtained from both detectors in the GC 1 and GC 2. Note that the black rectangle below GC 2, in the small panel, indicates the period during which the selected eluate containing the specific compounds, here the alkenones, passed during ~6 minutes to the GC 2.

2.2.2 Alkenone-SST calibration

In this study, the global core-top calibration of Müller et al. (1998) (Eq. (6)) was used. While several calibrations could have been applied in this study, most of the existing calibrations agreed on an almost linear relationship between the unsaturation index variations and temperatures changes for SST colder than 24-26°C (Conte et al., 2006; Sonzogni et al., 1997). During the Plio-Pleistocene, the Benguela SST values mainly ranged below 24°C whereas in the EEP, SST oscillated between 28-22°C. On one hand, the calibration of Müller et al., (1998) has been based on numerous core top samples from the Benguela region and therefore seems of relevance when applying it to this region over the last million years, as previously reported (Marlow et al., 2000). In the EEP, recent SST studies (Dekens et al., 2007; Lawrence et al., 2006) converted the unsaturation index into SST by using the Müller et al. (1998) calibration and revealed good correlation with other SST proxy (Dekens et al., 2008). This calibration seems therefore of relevance in the EEP too, especially when comparisons are made with other paleoSST records in the same region. However, future studies should address the recurrent problem of quantification of the impact that may have the application of different calibrations on long term SST reconstructions,

as recently pointed out along the equatorial Pacific (Medina-Elizalde et al., 2008). By applying this calibration, is assumed that the alkenone-derived SST estimation was not significantly affected by nutrient availability, production depth, production season, or by coccolithophorid extinction or speciation events. Besides, it is thought that the high abundance of alkenones in the sediment at both sites (see **Chapters IV-VI**) significantly reduced the bias tied to the microbial alteration through diagenetic processes in the water column and the sediments.

$$(6) \qquad SST = \frac{U^{K'}_{37} - 0.044}{0.033}$$

The standard error of estimate using this calibration is ± 0.050 $U^{K'}_{37}$ units or ± 1.5 °C. It has been demonstrated that, from interlaboratories comparison using different methodologies, this equation (6) was relatively similar to annual mean calibration, and therefore attests of the robustness of this calibration for converting $U^{K'}_{37}$ into paleotemperatures.

2.3 Analysis of productivity-related proxies

When analyzing $U^{K'}_{37}$, it is possible to also determine the alkenone concentration. As commonly applied in the Plio-Pleistocene studies (Dekens et al., 2007; Herbert et al., 1997; Lawrence et al., 2006; Liu et al., 2008), the Mass Accumulation Rate (MAR) of the total alkenone content (the sum of the $C_{37:2}$ and $C_{37:3}$ concentrations) can be roughly used as proxy for coccolith paleoproductivity. The concentration of both long-chain ketones is determined according to Eq. (7).

$$(7)\ (C_{37}) = \frac{(\text{Area } C_{37}) \times [C_{36}] \times (\text{dilution})}{(\text{Injected vol}) / (\text{Area } C_{36} \times \text{Sample weight})}$$

in which (C_{37}) is the respective concentration in either $C_{37:2}$ or $C_{37:3}$ in ng/g; (C_{36}), the hexatriacontane standard concentration (ng/µl); (dilution), the dilution of the sample for the GC in µl; (injected vol), the volume of the extract injected into the GC in µl and the weight of the sample in gram.

The MAR of total nitrogen (TN) and organic carbon (C_{org}) contents were used to estimate the relative changes in overall paleoproductivity in the Benguela region and EEP. TN determinations were made at the University of Bordeaux 1 with a Carlo-Erba CN elemental analyzer 2500, the same device attached to a MICROMASS-ISOPRIME mass-spectrometer for nitrogen isotopes

measurements (see 2.3.2). C_{org} was measured at the University of Bordeaux 1 by the total combustion of homogenized sediment samples using a LECO C-S 125 analyser after treatment of the sediment with 1N hydrochloric acid to remove calcium carbonate. Precision of both nitrogen content and organic carbon measurements from standards and samples replicates was better than ± 0.5 %.

To detect past variations of the biogenic opal production associated to siliceous phytoplankton productivity (mostly diatoms), the MAR biogenic opal in the Benguela was measured at IFM-GEOMAR by using an automated extraction method and wet chemical leaching as described in Müller and Schneider (1993). For the spanning period, from ~3.0 to 2.7 Ma, biogenic opal MAR was higher than 5 wt%, and the precision of measurements applying this method is considered to be better than ± 4 % (Müller and Schneider, 1993). This new data completes the existing record of biogenic opal MAR at Site 1082 (Lange et al., 1999; Perez et al., 2004; Robinson et al., 2002), thereby providing a continuous and long high resolution biogenic opal MAR record in the Benguela region from ~3.5 to 1.3 Ma. Similar biogenic opal measurements, based on the same technique, were also carried out at Site 1239 by the team of Prof. Ralf Tiedemann at AWI Bremerhaven.

2.4 Determination of nitrogen isotopes

The $\delta^{15}N$ values at Sites 1082 and 1239 were determined at the University of Bordeaux 1 (UMR CNRS 5805 EPOC) on dried, ground bulk sediment, except on Site 1090 where sediments were decarbonated prior to analyses by using 1N hydrochloric acid. About ~15-20 mg of sediments at Site 1082, ~30-40 mg at Site 1239 and ~50-80 mg at Site 1090 were encapsulated in tin and then injected into a Carlo-Erba CN elemental analyzer 2500 (Fig. 2.3). Each sample was first oxidized under high temperatures conditions (~1040°C) by cobalt and chrome oxides, then reduced in a second column by copper. The resulting gas, in particularly N2, was afterward transferred to the MICROMASS-ISOPRIME mass spectrometer where they were ionized, accelerated under high voltage (400 μA), deflected after their molecular weight and then caught in a collector. $\delta^{15}N$ values from certified and in-house standards (Acetanelide, Casein, Glycine, N1 and sdk) were also measured and used to adjust the sedimentary $\delta^{15}N$ values from each samples. The precision of the isotopic analyses based on standards and samples replicates is better than ± 0.2 ‰.

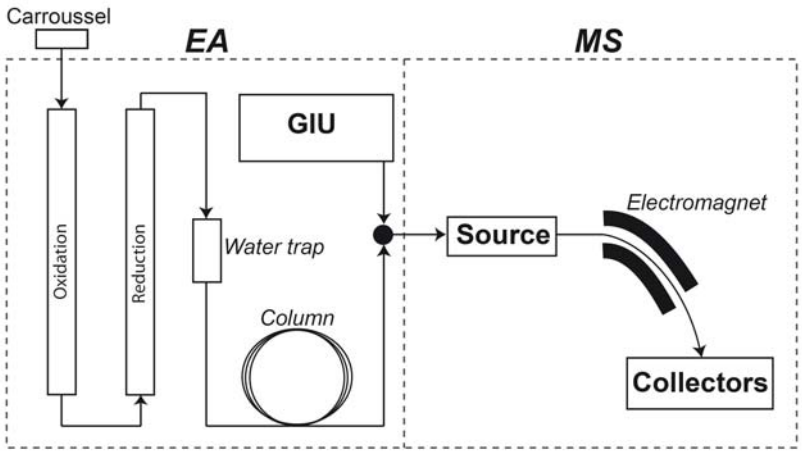

Figure 2.3 Schematic view of the Elemental Analyser (EA) interfaced to a Mass Spectrometer (MS). GIU, Reference Gas Injector (CO_2, He, N_2).

Because the sedimentary $\delta^{15}N$ can also record terrestrial organic matter signal (McKay et al., 2004), the origin of the organic matter, either marine or continental, was determined by measuring the sedimentary carbon isotopic ratio ($\delta^{13}C_{org}$) in the Benguela and the C/N ratio in the EEP. The $\delta^{13}C_{org}$ was measured at a 10 kyr resolution on 248 samples, taken every ~ 100 cm at Site 1082 Hole A. Carbon isotope ratios were obtained from the carbonate-free fraction, after treatment with 1 N hydrolochloric acid solutions, following the same method as for the $\delta^{15}N$ measurements (see above). According to replicates and internal standard, the absolute precision is better than ± 0.1‰. At Site 1239, C/N ratios, the ratio between the organic carbon content measured by a LECO analyser and the total nitrogen content (see 2.2), were determined on 41 samples to infer the primary origin of the organic matter in EEP sediments.

Chapter III

Age models

3.1 The ODP Site 1082

The age model at Site 1082 (Fig. 3.1, 3.2) was initially based on two paleomagnetic boundaries, the Brunhes/Matuyama at ~0.75 Ma and the Matuyama/Gauss at ~2.54 Ma, established by shipboard measurements of natural remanent magnetization (NRM) such as inclination reconstruction (Wefer et al., 1998) (Fig. 3.2A) and then based on oxygen isotope ($\delta^{18}O$) records from planktonic (*Globorotalia inflata*), and benthic (*Cibicoides wuellerstorfi*) foraminifera (Dupont et al., 2005; Jahn et al., 2003) (Fig. 3.1C) tuned against the benthic $\delta^{18}O$ from Site 659 (Tiedemann et al., 1994). Through graphical correlations of peaks obtained from the new alkenone SST record (Fig. 3.1D) and the isotope records with the Analyseries 1.2 software (Paillard et al., 1996) to the LR04 benthic foraminifera oxygen isotope stack (Lisiecki and Raymo, 2005) (Fig. 3.2B), the previous age model was improved for the past 3.5 Ma at Site 1082. The Pleistocene high resolution alkenone record (1.5-0 Ma) clearly revealed the last fifty glacial/interglacial stages. Patterns of change (3.5-2.8 Ma) in $\delta^{18}O$ from benthic foraminifera (Site 1082 and LR04 stack) showed outstanding similarities for the oldest part of the record. For the intermediate period (2.8-1.5 Ma), strong cooling events (Marine Isotopic Stages 58, 78, 82, 96, 100, G6 and G14) were identified in our SST record in agreement with a high resolution alkenone record from the Eastern Equatorial Pacific (Lawrence et al., 2006).

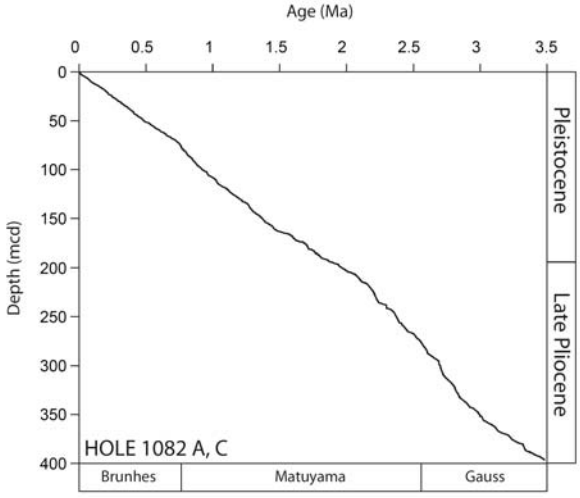

Figure 3.1. Age-depth plot at Hole 1082A and 1082C. Vertical scale indicates the epochs and horizontal scale the magnetostratigraphy.

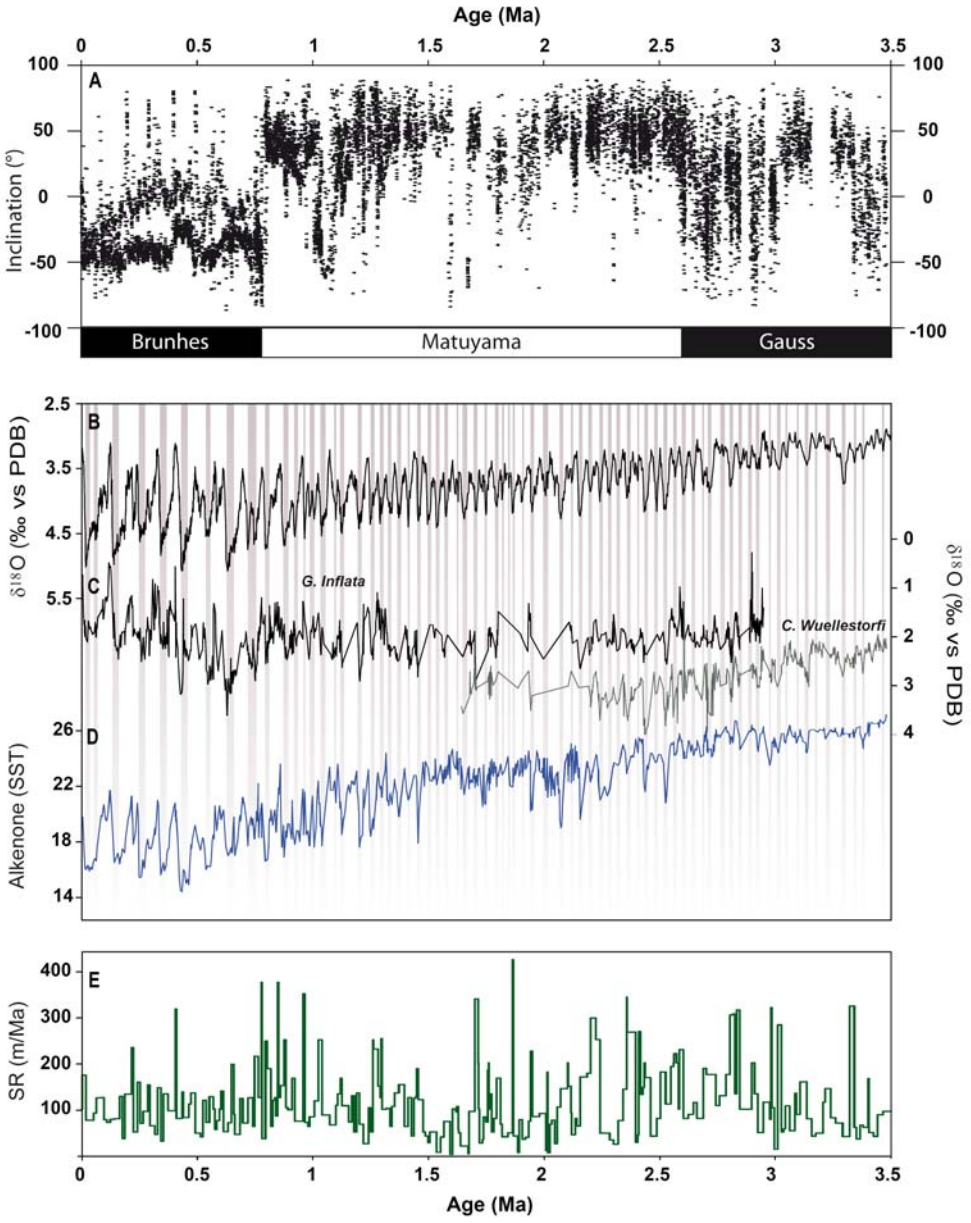

Figure 3.2. Age model at Site 1082. A: Inclination and the magnetostratigraphy in white and black scale (Wefer et al., 1998). B: LR04 benthic foraminiferal oxygen isotopes ($\delta^{18}O$) stack (Lisiecki & Raymo, 2005). C: Planktonic (*G. inflata*) and benthic (*C. wuellerstorfi*) foraminiferal records (Dupont et al., 2005; Jahn et al., 2003). D: alkenone-derived SST record. E, Sedimentation rate (SR).

3.2 The ODP Site 1239

The stratigraphy for EEP Site 1239 between ~3.2 and 0.5 Ma (Fig. 3.3, 3.4) was determined from the correlation of the alkenone-SSTs (Fig. 3.4C) with those performed at the nearby and well-dated Site 846 (Lawrence et al., 2006) (Fig. 3.4B), using Analyseries 1.2 software (Paillard et al., 1996). The striking similarities between both SST records on the long term and at glacial/interglacial cycles scale for the time of 3.2 Ma considered here give relatively high confidence for this age model, especially because the SST record clearly shows most of the cold marine isotopic stages MIS 58, 78, 82, 96, 100 and G6. In addition, the interval ~3.2-2.7 Ma has been tuned by $\delta^{18}O$ and $\delta^{13}C$ measured on benthic foraminifera (Steph et al., submitted), and the Pleistocene part with the precession signal derived from barium content (Tiedemann et al., unpublished data). Also, iron concentration (see **Chapter VI**) measured at Site 1239 shows the same glacial/interglacial variability than the two previously cited proxies, thus supporting the suggested age model.

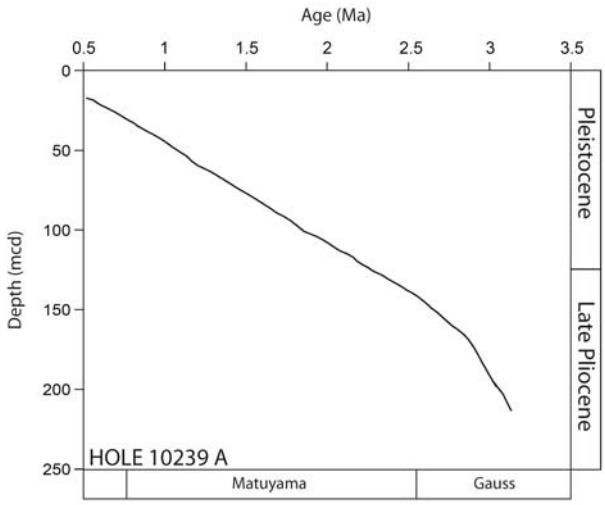

Figure 3.3. Age-depth plot at Hole 1239A. Vertical scale indicates the epochs and horizontal scale the magnetostratigraphy.

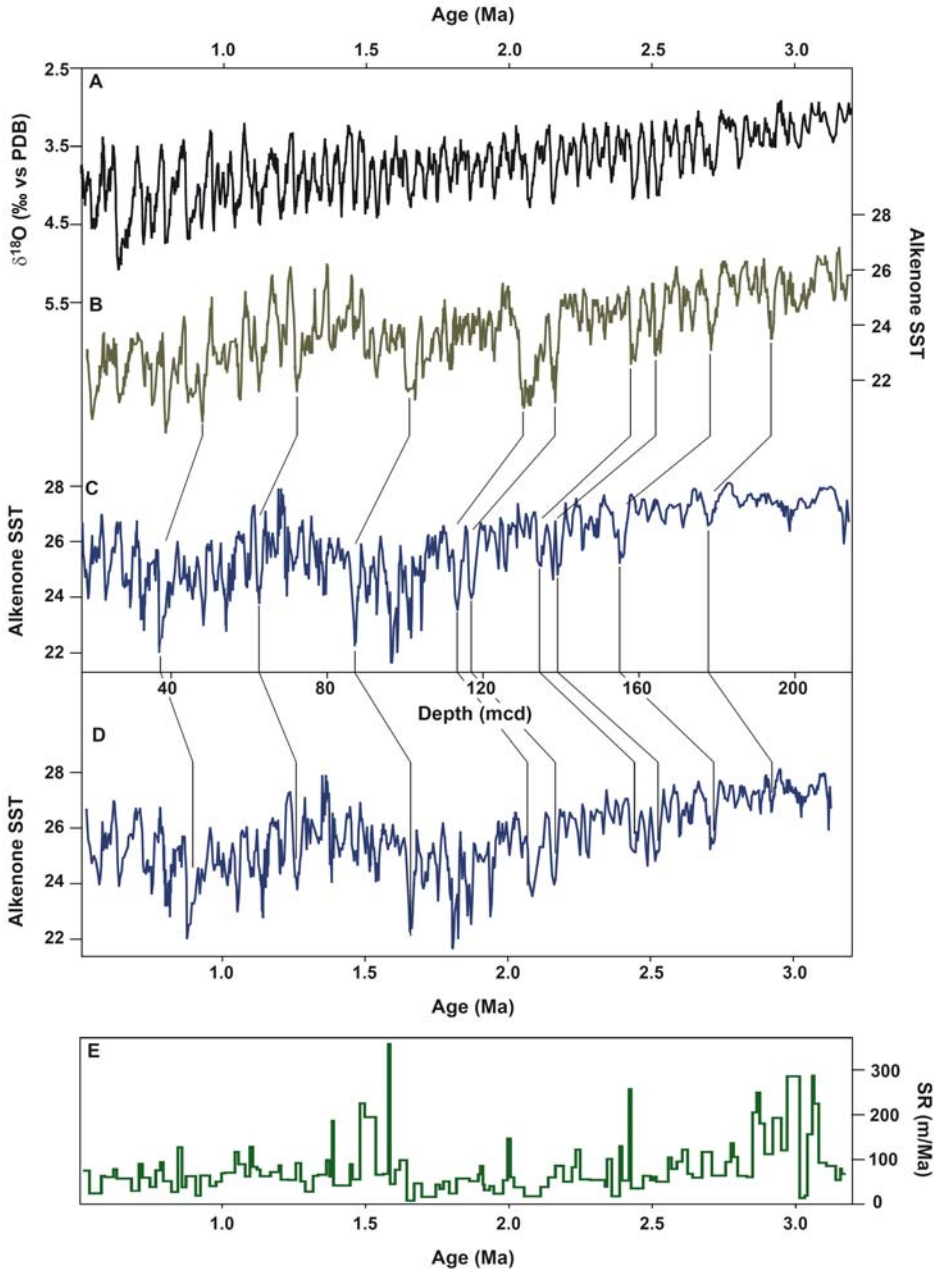

Figure 3.4. Age model at Site 1239. A: LR04 benthic foraminiferal oxygen isotopes ($\delta^{18}O$) stack (Lisiecki & Raymo, 2005). B: alkenone-SST at Site 846 (Lawrence et al., 2006). C: alkenone-SST at Site 1239 vs depth (mcd). D: alkenone-SST at Site 1239 vs age (Ma). E: sedimentation rate (SR).

Chapter IV

Pliocene-Pleistocene variability of upwelling activity, productivity, and nutrient cycling in the Benguela region

---

Johan Etourneau[1], Philippe Martinez[2], Thomas Blanz[1], and Ralph Schneider[1]

[1]Institute for Geosciences, University of Kiel, D-24118 Kiel, Germany

[2]UMR CNRS 5805 EPOC, University of Bordeaux 1, 33405 Talence, France

This chapter corresponds to the Geology article, but include in his following form the supplementary information, giving more details concerning the interpretation of the $\delta^{15}N$ signal, referred to as Data Repository in its published version.

4.1 Abstract

In this study, we present combined high-resolution records of sea surface temperature (SST), phytoplankton productivity, and nutrient cycling in the Benguela Upwelling System (BUS) for the past 3.5 Ma. The SST record provided evidence that upwelling activity off Namibia mainly intensified 2.4-2.0 Ma in response to the cooling of the Southern Ocean and the resultant strengthening of trade winds. As revealed by productivity-related proxies, BUS intensification led to a major transition in regional biological productivity when considering the termination of the Matuyama Diatom Maximum (MDM) (a diatom high-production event). Major oceanic reorganization in the Benguela was accompanied by nutrient source changes as indicated by a new nitrogen isotopic ($\delta^{15}N$) record that revealed a stepwise increase from 2.4 and 1.5 Ma. The change in source region likely resulted from significant changes in intermediate water formation tied to the reorganization of oceanic conditions in the Southern Ocean, which may have in turn mainly controlled the global ocean's N cycle, and therefore the N isotopic composition of nutrients since 3.5 Ma.

4.2 Introduction

Around 3.0 Ma, the Earth underwent a global climatic transition from a warm to a cold state characterized by the development of continental ice sheets in the Northern Hemisphere, and the amplification of glacial-interglacial cycles. The onset of major Northern Hemisphere Glaciation is hypothesized to result from drastic oceanic changes in high latitudes. Recent studies have proposed that Pliocene climate cooling may have increased water-column stratification in the North Pacific; this, associated with longer summer temperature warming and colder winter temperatures, would have initiated the Northern Hemisphere Glaciation (Haug et al., 2005). Contemporaneous water-column stratification for both the Subarctic Pacific and the Southern Ocean would have contributed to reduce significantly CO_2 released from the ocean's interior to the atmosphere by limiting surface and deep water exchanges amplifying global cooling (Haug et al., 1999; Sigman et al., 2004). The latter assumption seems consistent with recent model experiments demonstrating that a substantial decrease in atmospheric CO_2 would have led to or influenced ice formation over Greenland (Lunt

et al., 2008). In this context of global cooling, the role played by the low-latitude oceanic regions is still uncertain.

Global cooling inferred from benthic oxygen isotope records from the Pliocene (Lisiecki and Raymo, 2005) is corroborated for the low-latitudes through a suite of SST records based on the alkenone unsaturation index (Marlow et al., 2000; Lawrence et al., 2006; Dekens et al., 2007). Periods of pronounced Pliocene SST cooling have been detected within major eastern boundary currents such as those off Namibia, Peru, and California (Marlow et al., 2000; Dekens et al., 2007). If such a SST cooling mainly resulted in the intensification of currents and/or upwelling intensity tied, or not tied, to a change in the thermal structure of the upper ocean, it must have influenced the availability of nutrients at the surface and, therefore, productivity. Marine productivity, known to play a major role in the global carbon cycle, could have had a strong influence on Pliocene climatic change as an internal climate feedback mechanism through the modification of atmospheric CO_2 levels. Therefore, high-resolution studies aimed at understanding past SST, productivity, and nutrient supplies in highly productive coastal upwelling areas are needed.

In this study, we examined the most productive coastal upwelling region, the BUS, by combining a complete Pliocene-Pleistocene record of alkenone-derived SSTs with a record of bulk-sediment nitrogen isotopic ratio ($\delta^{15}N$) as a proxy of nitrogen (mainly nitrate) supply. Mass accumulation rates (MAR) of total nitrogen (TN), alkenones, and biogenic opal were also calculated as classic proxies for planktonic production. For the study, we utilized a sediment record from the Ocean Drilling Program (ODP) Site 1082 (21°5'S, 11°49'E, 1280 m water depth) located within the modern BUS (Fig. 4.1).

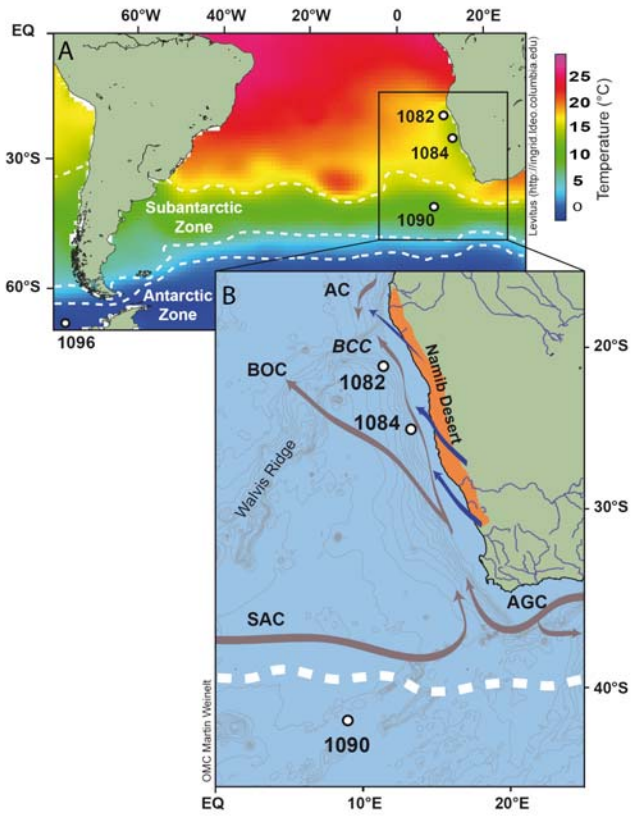

Figure 4.1 A: Modern sea surface temperature in the South Atlantic. B: oceanic and atmospheric settings in the Benguela Upwelling System and trade winds (blue arrows). AC-Angola Current; AGC-Agulhas Current; BCC-Benguela Coastal Current; BOC-Benguela Oceanic Current; and SAC-South Atlantic Current.

4.3 Material and Methods

Alkenone-derived SSTs were measured from sediment samples with a ~2-4 ka resolution taken at Site 1082. Using the commonly accepted ratio $U^{k'}_{37}$ index, SSTs were calculated from global core-top calibrations (Müller et al., 1998), considered here to be extrapolated on a million-year timescale. This type of calibration has been widely used for reconstructing Pliocene alkenone SSTs (Lawrence et al., 2006; Dekens et al., 2007, 2008) and seems relevant according to comparisons with other paleo-SST proxies (Dekens et al., 2008).

Alkenones were extracted from freeze dried samples using Accelerator Solvent Extraction (Dionex ASE) prior to an analysis of the C_{37} group by a double column multi-dimensional gas chromatograph (6890N). According to sample and standard replicates, SST precision was approximately ±0.5 °C. The $\delta^{15}N$ and TN were determined on dried, ground, bulk sediment samples (~15–20 mg aliquots of homogenized bulk sediment except at site 1090, where sediments were decarbonated using hydrochloric acid (1N) prior to isotopic analyses) using a Carlo–Erba CN analyser 2500 interfaced directly to a Micromass-Isoprime mass spectrometer. The precision of the isotopic analyses based on standards replicates was better than 0.2‰.

Based on planktonic and benthic oxygen isotopes ($\delta^{18}O$) and high-resolution alkenone SSTs, tuned to the benthic $\delta^{18}O$ stack and compared to some paleomagnetic boundaries, the Site 1082 age model was found to be well defined (see Chapter III).

4.4 Results and Discussion

At Site 1082, the reconstructed temperature profile resulted in two major cooling periods from 3.0 to 2.0 Ma (-3°C) and 1.5 to 0.5 Ma (-5°C), interrupted by a period of relatively stable SSTs (Fig. 4.2A). Roughly affiliated with the two cooling phases, two periods of high biological productivity between 3.0-2.0 Ma and 1.5-0 Ma occurred as illustrated by a higher MAR in TN, biogenic opal, and alkenones (Fig. 4.2C, 4.2D, and 4.2E). Previously derived similar results for MAR calculations at both Sites 1082 and 1084 (Giraudeau et al., 2002) clearly imply that since the warm Pliocene productivity within the Benguela region responded to the same oceanic or biochemical processes. However, unlike previous reports for the eastern tropical Pacific (Lawrence et al., 2006; Dekens et al., 2007; Liu et al., 2008), SSTs and productivity in the Benguela region seem to be intimately coupled, suggesting a close link between hydrologic conditions and biological production. In addition to strong cooling and high productivity, the BUS also underwent pronounced changes in N cycling as recorded in the bulk $\delta^{15}N$ record at Site 1082 (Fig. 4.2B). The warm Pliocene period was characterized by very low values (0-3‰), and stepwise shifting towards higher values during the cold Pleistocene (3-5‰) at 2.4 and 1.5 Ma.

Our new SST record at Site 1082 shows similarities with the record of Marlow et al. (2000) for Site 1084 (Fig. 4.2A), located 5° southward, enhancing confidence for certain periods of cooling and more stable SST conditions in the Benguela. Despite coeval SST variations, the SST gradient between both sites increased sharply between 2.4 and 2.0 Ma (from ~2 to 4°C) (Fig. 4.2A). During

that time, both sites experienced a cooling trend, less pronounced at Site 1082 than at Site 1084. The SST gradient shift between the two sites can be interpreted as the result of a transition between two different oceanographic regimes, from a short season of strong upwelling cell activity to a modern-like BUS. In modern times, upwelling activity is at a maximum during boreal summer and spring in the north of the Benguela (Site 1082), and active approximately year-round in its central part where Site 1084 is located (Shannon, 1985). The modern upwelling pattern likely started from 2.4-2.0 Ma, whereas before, active upwelling cells were probably restricted to short seasonal periods.

As previously proposed (Giraudeau et al., 2002), the strengthening of the upwelling system off Namibia may have been a direct oceanic response to atmospheric circulation reorganization tied to Southern Ocean cooling. The late Pliocene extension of the Antarctic ice sheet may have gradually modulated the northward movement and development of the polar front system, a dynamic of the subtropical South Atlantic gyre, as well as the southeast Atlantic high pressure cells. When the latter became closer to the low pressure over South Africa it could have seasonally strengthened the southeast trade winds (i.e. stronger Hadley circulation) resulting in a stronger upwelling of deep water to the surface from 2.4-2.0 Ma.

Our findings are consistent with continental climate records. The vegetation in the nearby continental hinterland was directly influenced by humidity transport from the ocean. Because the presence of cool waters at the surface limits evaporation over the oceans and precipitation over the continents, strong upwelling of cold water leads to a coastal drought and the development of the Namib Desert. Pollen records from Site 1082 show an abrupt decrease in grass pollen together with a sharp increase in semi-desert pollen from 2.2 Ma (Dupont, 2006). This fact can be easily explained by less onshore moisture transport, owing to colder SSTs in the Benguela region, a response to stronger perennial wind-driven upwelling activity, as suggested by a contemporaneous SST gradient increase between Sites 1082 and 1084.

Because physical upwelling vertically transports nutrient-rich water from the subsurface, a change in productivity and nutrient cycling must also be observed. Our interpretation of the onset of a modern-like BUS from 2.4-2.0 Ma is supported by diatom assemblage studies at both Benguela sites (Lange et al., 1999). The dominance of diatom mat species between 3.0 and 2.0 Ma, characterizing the Matuyama Diatom Maximum (MDM), is an indicator of quasi-permanent stratified surface conditions over the site with short periods of upwelling (Lange et al., 1999; Marlow et al., 2000). In contrast, the appearance of a different flora, typical of strong upwelling

conditions, since 2.0 Ma, clearly indicates destratified surface waters in an upwelling regime (Lange et al., 1999; Marlow et al., 2000). The end of mass sedimentation in diatom mats known as the "fall dump" model of Kemp et al. (2000), and hence the MDM, would result from a breakdown of stratification initiated from 2.4 Ma as suggested by a progressive decline in TN and opal MARs (Fig. 4.2C and 4.2D), controlled by long seasonal periods of upwelling resumption after 2.0 Ma.

The MDM reflects an intrusion of silica-rich waters, likely arising from the Southern Ocean, to support the local production of diatom mat species, especially *Thalassiothrix antarctica* (Lange et al., 1999; Marlow et al., 2000; Robinson and Meyers, 2002). The redistribution of silicic acid from the Southern Ocean towards the southwestern African coast was directly related to a decrease in silicic acid utilization within the Southern Ocean due to surface water stratification, as indicated by a coeval decrease in opal production in the Antarctic Ocean (Sigman et al., 2004) (Fig. 4.2D) and an increase off Namibia (Pérez et al., 2001). Silicic acid export may have reached the Benguela region through three processes: (1) an enhanced equatorward surface water advection, (2) a gradual shoaling of the thermocline, or (3) a strengthening of coastal upwelling activity. For the third case, we suggested that the upwelling process (even of warm water) off Namibia mainly developed from 2.4-2.0 Ma. In addition, strong upwelling conditions were not favorable for mat-forming diatom growth. In contrast, diatom mats could have grown when nutrients were transported via equatorward advection or flowed below a shallow thermocline, with both mechanisms being consistent with water column stability (seasonal stratification) conditions.

The $\delta^{15}N$ signal recorded in deep-sea sediments primarily depends on isotopic fractionation during nitrate uptake (photosynthesis) that leads to enrichment in the organic product for ^{14}N, with the remaining nitrate pool symmetrically enriched in ^{15}N according to Rayleigh fractionation kinetics. Additionally, the preformed $\delta^{15}N$ signature of dissolved nitrate in water masses feeding surface waters should to be taken into account when reconstructing past nitrate utilization. The sedimentary $\delta^{15}N$ signal can also be influenced by the terrestrial organic matter signal that has a different N composition and lower $\delta^{15}N$ values (Peters et al., 1978). The $\delta^{15}N$ record can also be influenced by water-column denitrification or nitrogen (atmospheric N_2) fixation that account for the main sink and source of bioavailable nitrogen in the ocean, respectively.

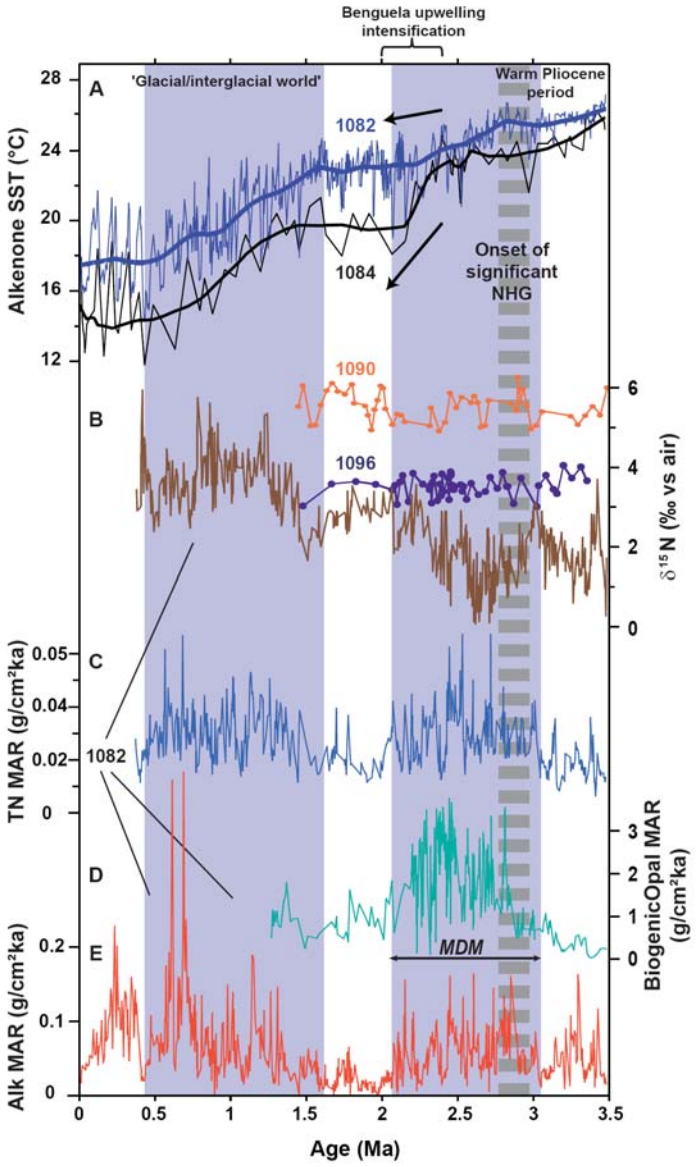

Figure 4.2. A: Alkenone-sea surface temperature (SST), Site 1082 (blue) and Site 1084 (Marlow et al., 2000) (black). B: Sedimentary ^{15}N, Sites 1082 (brown), 1096 (Sigman et al., 2004) (violet), and 1090 (dark orange), ^{15}N (‰ vs air) = {[($^{15}N/^{14}N$sample) /($^{15}N/^{14}N$standard)]-1} x 10^3. C: Site 1082 Total nitrogen (TN) mass accumulation rate (MAR) (g/cm^2/ka). D: Site 1082 Biogenic opal MAR (g/cm^2/ka). E: Site 1082 Alkenone MAR (g/cm^2/ka). MARs were calculated according to Robinson and Meyers (2002). MDM-Matuyama Diatom Maximum; NHG-Northern Hemisphere Glaciation.

Previous studies have shown that hinterland conditions were wetter during the warm Pliocene (Dupont et al., 2006). Therefore, inputs of terrestrial organic matter to the oceanic basin could be responsible for lowering sedimentary $\delta^{15}N$ values at site 1082. We used bulk-sediment $\delta^{13}C_{org}$ from the carbonate-free fraction as an indicator of organic matter origin (continental organic matter exhibiting lighter values (< -26‰) than marine algae (~22-20‰) (Meyers et al., 1997)). At Site 1082, the average $\delta^{13}C_{org}$ remained relatively constant (-23‰ to -20‰) indicating that organic matter since ~3.5 Ma is largely of marine origin (Fig. 4.3).

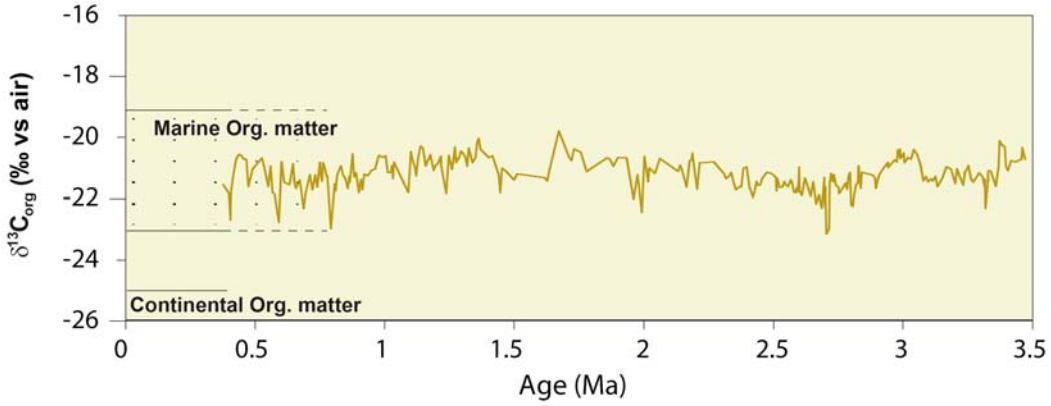

Figure 4.3 The carbonate-free bulk-sediment $^{13}C_{org}$, $^{13}C_{org}$ (‰ vs air) = $\{[(^{13}C/^{12}C\text{sample})/(^{13}C/^{12}C\text{standard})]-1\} \times 10^3$.

At present, the water-column of the BUS is not under denitrifying conditions, with the exception of some near-shore areas influenced by unusual conditions, as indicated both by nutrient profiles and nitrogen isotopic investigations on particles and sediments (Dittmar and Birkicht, 2001; Holmes et al., 1998, 2002; Pichevin et al., 2005). Water column denitrification occurs in the near absence of oxygen during organic matter degradation and leads to isotopically heavy water column nitrates due to large isotopic fractionation between the two isotopes ^{14}N and ^{15}N, and heavy sedimentary $\delta^{15}N$ values (Liu and Kaplan, 1989; Altabet et al., 1995; Ganeshram et al., 1995; Codispoti et al., 2005). $\delta^{15}N$ values recorded at Site 1082 vary in the same range, being even lower especially during the Pliocene than those recorded within particles, surface sediments, and late Quaternary sediments in the BUS (Holmes et al., 1998; Holmes et al., 2002; Pichevin et al., 2005) providing a good indication that regional denitrification did not strongly influence nitrogen cycling in the BUS at least during the last 3.5 Ma.

The N fixation probably had a minor effect on the $\delta^{15}N$ values recorded at Site 1082 since 3.5 Ma, despite extremely low values during the maximum of diatom mats production, which could be interpreted as the result of enhanced regional N fixation. *T. antarctica*, the dominant diatom species characterizing the MDM, is not known for hosting N_2-fixers and *Rhizosolenia spp.*, the species commonly hosting N_2-fixers, was likely only few in numbers (Lange et al., 1999). However, it is still questionable whether the dominant diatom-mats species lived in symbiosis with bacteria-fixing atmospheric N_2 during the MDM. Here we explain the low $\delta^{15}N$ in a more conventional way, as being a result of the nutrient utilization from different nutrients sources and potentially driven by global changes in the N isotopic composition of nutrients as previously suggested.

Changes in nutrient source were cited as the probable interpretation for the $\delta^{15}N$ towards higher values through the Plio-Pleistocene in the Benguela (Robinson and Meyers, 2002). It has been shown that Subantarctic Mode Water (SAMW) was the main contributor of nutrients entering the BUS in the late Pleistocene (Shannon, 1985); previous work has suggested that nutrients were mainly delivered by Antarctic Intermediate Water (AAIW) in the Pliocene (Marlow et al., 2000). If SAMW or AAIW were the main nutrients sources, the $\delta^{15}N$ at Site 1082 should reflect the isotopic signature of preformed nitrate arising from either the Subantarctic or Antarctic zones, plus a small deviation related to the effect of nutrient utilization when nitrate exceeded biological demand (Pichevin et al., 2005).

Therefore, we examined the Pliocene $\delta^{15}N$ signature at Subantarctic Site 1090 and Antarctic Site 1096 (Sigman et al., 2004) (Fig. 4.2B) where SAMW and AAIW form, respectively. At Subantarctic Site 1090, we found no significant $\delta^{15}N$ variations over the interval from 3.5-1.5 Ma, in agreement with previous results from Antarctic Site 1096, but found a constant offset between the two sites, with $\delta^{15}N$ values being ~2‰ higher in the Subantarctic than in the Antarctic area. This shift can be explained by an increase in the $\delta^{15}N$ of nitrate and subsequently of phytoplankton organic matter, due to progressively dissolved nitrate depletion by phytoplankton consumption during northward surface transport of Antarctic water masses. If we assume a Subantarctic origin for nitrate in the BUS, then sediments at Site 1082 should have recorded ^{15}N values similar to those at Site 1090, assuming similar water degradation and diagenesis effects on the $\delta^{15}N$ at both sites.

Until the end of Pliocene cooling, both sites had a $\delta^{15}N$ difference of ~4‰ (of ~2‰ between 2.4 and 1.5 Ma, and ~1‰ after 1.5 Ma). Therefore, the $\delta^{15}N$ offset between Subantarctic and Benguela sites during the MDM rules out a high nitrate contribution from the subantarctic region to the Benguela (contrary to the Pleistocene, when more similar $\delta^{15}N$ values at Sites 1082 and 1090 suggest that SAMW was the main source of nutrients entering the Benguela). Whether the subantarctic zone was not the primary contributor of preformed nutrients during the Pliocene, we can exclude the idea that the surface water advection hypothesis explains the initiation of the MDM. In contrast, low $\delta^{15}N$ gradient between Sites 1082 and 1096 (~0-3‰) suggest that nutrients spreading to low-latitude coastal upwelling areas during the Pliocene mainly originated from AAIW.

From 3.0 Ma, climatic cooling probably led to permanent stratification of surface waters in the Antarctic zone, thereby limiting the utilization of nutrients (Sigman et al., 2004). This pool of nutrients may have been largely redistributed to lower latitudes in the BUS via subsurface cold water masses (Marlow et al., 2000). The intensity of upwelling off Namibia was extremely weak and restricted to short seasons prior to 2.4-2.0 Ma. However, the thermocline depth may have changed significantly during the MDM and carried cold water that sporadically spread to the surface, causing a cooling of SSTs in the Benguela region from 3.0 Ma. Some studies have actually stated that the thermocline shoaled as early as 3.0 Ma in response to deep water cooling (Philander and Fedorov, 2003). A shallower thermocline with nutrient-rich subsurface cold water could have stimulated diatom mat production, since diatom mats have the ability to migrate vertically in the water-column to meet the best conditions for growth.

AAIW as the main nutrient source in the low-latitudes during Pliocene cooling would also explain why opal sinks, a measure of high diatom productivity, directly transferred from the Antarctic to the Benguela regions at 3.0 Ma (as well as for other coastal upwelling systems; Cortese et al., 2004) without an intermediate transition as expected for the subantarctic zone. The development of a modern-like polar front system around 2.1 Ma (Liu et al., 2008) would have contributed to the formation of SAMW and a deeper equatorward AAIW circulation. Associated with the Benguela upwelling intensification, the enhanced utilization of silicic acid in the subantarctic region would have led to the termination of the MDM and pronounced changes in the nutrient supply off Namibia.

4.5 Conclusions and Implications

In this study, we reconstructed SSTs, paleoproductivity, and N cycling in the Benguela region since 3.5 Ma. Our results indicate that strong upwelling activity off Namibia appeared from 2.4-2.0 Ma in response to trade wind strengthening. Preceding this upwelling intensification, the MDM was probably induced by a shallower thermocline and a high supply of nutrients rising from the Southern Ocean through cool AAIW circulation. From 2.4-2.0 Ma, a change in intermediate circulation to low latitudes with the formation of SAMW may have affected global marine productivity and the ocean's N cycle. As previously described for the California upwelling system, denitrification mainly occurred from 2.1 Ma as a result of a shoaling of the thermocline, enhanced low-oxygenated water transported by SAMW, and the development of a modern-like frontal system in the Southern Ocean (Liu et al., 2008). SAMW circulation was probably weak during the Pliocene, and the global denitrification rate may have been weaker, leading to a lower denitrification/N fixation ratio, less bioavailable N loss, and lower $\delta^{15}N$ values in the nutricline. In contrast, a strong contribution of SAMW during the Pleistocene was likely accompanied by a higher denitrification rate, a higher denitrification/N fixation ratio and more bioavailable N loss that, in turn, modified the global isotopic signature of nutrients within the nutricline. This enhanced denitrification/N fixation ratio through the Plio-Pleistocene perhaps explains the increase in $\delta^{15}N$ values at Site 1082.

According to our results and those of studies off California, $\delta^{15}N$ values were lower on average by 2‰ during the Pliocene than today. Considering for modern times that the $\delta^{15}N$ of the global nitrate pool averages ~5‰ (Sigman et al., 1997), our results would suggest that the Pliocene oceanic mean was ~3‰. If true, this would imply that nitrate was probably less limiting in certain oceanic areas during the Pliocene. However, coastal upwelling systems were likely less active and could have contributed to less bioavailable nitrate to the surface. Was therefore the tropical-subtropical biological pump in the coastal upwelling areas more efficient during the Pliocene, and did it contribute significantly to the Pliocene atmospheric CO_2 drawdown? To answer these questions further studies focusing on the marine N cycle and biological productivity within high-productivity oceanic regions spanning the Plio-Pleistocene climate transition are needed.

4.6 Acknowledgements

We acknowledge M. Altabet, G. Leduc, F. Lamy, A. Holbourn, N. Khélifi, J. Xu, and X. Crosta for discussions, and objective criticism; and I. Billy, S. Koch, J. Heinze, and K. Charlier for technical assistance. We also thank the three anonymous reviewers for their helpful comments. This research was supported by the Deutsche Forschungsgemeinschaft through German projects SCHN 621/5-2 and SCHN 621/12-1 (University of Kiel), and the French program CNRS-ECLIPSE to PhM (University of Bordeaux I).

4.7 References

Altabet, M.A., Francois, R., Murray, D.W., & Prell, W.L. Climate related variations in denitrification in the Arabian Sea from sediment 15N/14N ratios. *Nature*, **373**, 506-509 (1995).

Brandes, J.A., & Devol, A.H. A global marine-fixed nitrogen isotopic budget: Implications for Holocene nitrogen cycling. *Global Biogeochemical Cycles*, **16**, 1120 (2002).

Codispoti, L. A., Yoshinari, T., & Devol, A. H. Suboxic respiration in the oceanic water column, in: Respiration in Aquatic Ecosystems, edited by: del Giorgio, P. A. and Williams, P. J. Le B., Oxford University Press, 225–247 (2005).

Cortese, G., Gersonde, R., Hillenbrand, C.-L., & Kuhn, G. Opal sedimentation shifts in the world over the last 15 Myr. *Earth and Planetary Science Letters*, **224**, 509-527 (2004).

Dekens, P.S., Ravelo, A.C., & McCarthy, M.D. Warm upwelling regions in the Pliocene warm period. *Paleoceanography*, **22**, doi: 10.1029/2006PA001394 (2007).

Dekens, P.S., A.C. Ravelo, A.C., M.D. McCarthy, M.D., & Edwards, C.A. A 5 million year comparison of Mg/Ca and alkenone paleothermometers. *Geochemistry, Geophysics, Geosystems*, **9**, doi: 10.1029/2007GC001931 (2008).

Dittmar, T., & Birkicht, M. Regeneration of nutrients in the northern Benguela upwelling and the Angola-Benguela Front areas. *South African Journal of Science*, **97**, 239-246 (2001).

Dupont, L.M. Late Pliocene vegetation and climate in Namibia (southern Africa) derived from palynology of ODP Site 1082. *Geochemistry, Geophysics, Geosystems*, **7**, doi: 10.1029/2005GC001208 (2006).

Ganeshram, R.S., Pedersen, T.F., Calvert, S.E., & Murray, J. Large changes in oceanic nutrient inventories from glacial to interglacial periods. *Nature*, **376**, 755-758 (1995).

Giraudeau, J., Meyers, P.A., & Christensen, B. A. Accumulation of organic and inorganic carbon in Pliocene-Pleistocene sediments along the SW African margin. *Marine Geology*, **180**, 49-69 (2002).

Haug, G.H., Sigman, D.M., Tiedemann, R., Pedersen, T.F., & Sarnthein, M. Onset of permanent stratification in the Subarctic Pacific Ocean. *Nature*, **401**, 779-782 (1999).

Haug, G.H., Ganoposlki, A., Sigman, D.M., Rosell-Melé, A., Swann, G.E.A., Tiedemann, R., Jaccard, S.L., Bollmann, J., Maslin, M., Leng, M.J., & Eglinton, G. North Pacific seasonality and the glaciation of North America 2.7 million years ago. *Nature*, 433, 821- 825 (2005).

Holmes, M.E., Müller, P.J., Schneider, R.R., Segl, M., & Wefer, G. Spatial variations in euphotic zone nitrate utilization based on $\delta^{15}N$ in surface sediments. *Geo-Marine Letters*, **18**, 58-65 (1998).

Holmes, E., Lavik, G., Fischer, G., Segl, M., Ruhland, G., & Wefer, G. Seasonal variability of $\delta^{15}N$ in sinking particles in the Benguela upwelling region. *Deep-Sea Research I*, **49**, 377-394 (2002).

Kemp, A.E.S., Pike, J., Pearce, R.B., & Lange, C.B. The "Fall dump"- a new perspective on the role of "shade flora" in the annual cycle of diatom production and export flux. *Deep-Sea Research II*, **47**, 2129-2154 (2000).

Lange, C.B., Berger, W.H., Lin, H.L., Wefer, G., & Shipboard Scientific Party Leg 175. The early Matuyama Diatom Maximum off SW Africa, Benguela current system (ODP leg 175). *Marine Geology*, **161**, 93-114 (1999).

Lawrence, K.T., Liu, Z., & Herbert, T.D. Evolution of the eastern tropical Pacific through Plio-Pleistocene glaciation. *Science*, **312**, 79-83 (2006).

Lisiecki, L.E., & Raymo, M.E. A Pliocene-Pleistocene stack of 57 globally distributed benthic $\delta^{18}O$ records. *Paleoceanography*, **20**, doi: 10.1029/2004PA001071 (2005).

Liu, Z., Altabet, M.A., & Herbert, T.D. Plio-Pleistocene denitrification in the eastern tropical North Pacific: Intensification at 2.1 Ma. *Geochemistry, Geophysics, Geosystems*, **9**, doi:10.1029/2008GC002044 (2008).

Liu, K.-K., & Kaplan, I.R. The eastern tropical Pacific as a source of ^{15}N-enriched nitrate in seawater off southern California. *Limnology and Oceanography*, **34**, 820–830 (1989).

Lunt, D.J., Foster, G.L., Haywood, A.M., & Stone, E. Late Pliocene Greenland glaciation controlled by a decline in atmospheric CO2 levels. *Nature*, **454**, 1102-1106 (2008).

Marlow, J.R., Lange, C.L., Wefer, G., & Rosell-Melé, A. Upwelling intensification as part of the Pliocene-Pleistocene climate transition. *Science*, **290**, 2288-2291 (2000).

Meyers, P. A. Organic geochemical proxies of paleoceanographic, paleolimnologic, and paleoclimatic processes. *Organic Geochemistry*, **27**, 213-250 (1997).

Müller, P. J., & Schneider, R. An automated leaching method for the determination of opal in sediments and particulate matter. *Deep-Sea Research I*, **40**, 425-444 (1993).

Peters, K.E., Sweeney, R.E., & Kaplan, I.R. Correlation of carbon and nitrogen stable isotope ratios in sedimentary organic matter. *Limnology and Oceanography*, **23**, 598–604 (1978).

Pérez, M.E., Lin, H-L., Lange, C.B., & Schneider, R. Pliocene-Pleistocene opal records off southwest Africa, Sites 1082 and 1084: a comparison of analytical techniques. *Proceedings of the Ocean Drilling Program Scientific Results*, **175**, College Station, Tex (2001).

Philander, S.G., & Fedorov, A.V. Role of tropics in changing the response to Milankovitch forcing some three million years ago. *Paleoceanography*, **18**, 1045 (2003).

Pichevin, L., Martinez, P., Bertrand, P., Schneider, R., & Giraudeau, J. Nitrogen cycling on the Namibian shelf and slope over the last two climatic cycles: Local and global forcings. *Paleoceanography*, **20**, doi: 10.1029/2004PA001001 (2005).

Robinson, R.S., & Meyers, P. Biogeochemical changes within the Benguela Current upwelling system during the Matuyama Diatom Maximum: Nitrogen isotope evidence from Ocean Drilling Program Sites 1082 and 1084. *Paleoceanography*, **17**, doi: 10.1029/2001PA000659 (2002).

Shannon, L.V. The Benguela ecosystem, Evolution of the Benguela physical features and processes: Oceanography and Marine Biology: An Annual Review, edited by M. Barnes, Aberdeen Univ. Press, Aberdeen, UK, 105-182 (1985).

Sigman, D.M., Altabet, M., Michener, R., McCorkle, D.C., Fry, B., & Holmes, R.M. Natural abundance-level measurement of the nitrogen isotopic composition of oceanic nitrate: An adaptation of the ammonia diffusion method. *Marine Chemistry*, **57**, 227–242 (1997).

Sigman, D.M., Jaccard, S.A., & Haug, G.H. Polar ocean stratification in a cold climate. *Nature*, **428**, 59-63 (2004).

Chapter V

Links between biological production and iron supply in the Eastern Equatorial Pacific since the Pliocene

---

Johan Etourneau[1], Daniel Rincon-Martinez[2], Philippe Martinez[3], Frank Lamy[2], Thomas Blanz[1], Cornelia Saukel[2], Ralf Tiedemann[2], and Ralph Schneider[1]

[1]Institute for Geosciences, University of Kiel, 24118 Kiel, Germany

[2]Alfred Wegener Institute, 27568 Bremerhaven, Germany

[3]UMR CNRS 5805 EPOC, University of Bordeaux 1, 33405 Talence, France

This chapter corresponds to the Nature Geoscience letter, but include in his following form the supplementary information, a figure indicating elements contents initially detected during analysis, referred to as Supplementary Information in its submitted version.

5.1 Abstract

The climate switch from a Pliocene warm period into a Pleistocene glacial world is often cited as an analog for future climate prediction. Understanding processes driving to "icehouse" conditions is of primary importance, especially since a significant decline in atmospheric CO_2 level was evocated to explain such global cooling (Lunt et al., 2008). Marine primary productivity, known to remove a part of CO_2 from the atmosphere, may have contributed to the Plio-Pleistocene climate change. Based on a multiproxy approach, we examine different factors capable to control the primary productivity in the Eastern Equatorial Pacific (EEP), one of the most productive areas of the world's oceans, since ~3.5 Ma. Our results show that increases in phytoplankton biomass since the Pliocene in the EEP responded primarily to the nutrients distribution into the photic zone, and particularly to iron (Fe) fertilization. We found that nitrate - an essential nutrient for biological productivity - was likely sufficiently supplied in the EEP surface waters and has supported, not limited, productivity since ~3.5 Ma. In contrast, Fe inputs, currently limited in the modern EEP, have probably served as fertilizer to trigger the most productive periods between ~3.1-2.8 Ma and ~1.9-1.4 Ma occurring in this region for the past 5 Ma.

5.2 Introduction

In order to study past climate to improve future climate prediction, understanding the interactions between oceanic circulation, productivity variations and nutrient distribution in the EEP is of primary importance. This is particularly relevant for the past 3.5 Ma during which Earth's climate switched from a Pliocene warm period (warm temperatures, high atmospheric CO_2, high sea level, ice sheet restrained to Antarctica) (Raymo et al., 1996,2006) to a Pleistocene state characterised by pronounced glacial-interglacial episodes (Lisiecki and Raymo, 2005). In this context, we could expect that profound changes in the EEP primary productivity responding to the reorganization of oceanic circulation and/or overall nutrient distribution, may have influenced as a feedback mechanism the Pliocene climate change by affecting the carbon cycle and hence atmospheric CO_2. However, factors controlling the major past changes in the EEP biological productivity since the last 5 Ma are still poorly known.

In the modern ocean, more than 80% of the primary productivity is concentrated within the open ocean and coastal upwelling systems which represent only 20% of the total surface of the oceans[3]. Marine primary productivity contributes in large extent to increase the CO_2 sequestration from the atmosphere when it sinks into the deep ocean and is buried in the sediments. Conversely, the effects of the biological pump can be counterbalanced by upwelling of dissolved CO_2-enriched waters leading to an inverse CO_2 flux, from the ocean into the atmosphere. Although the upwelling process favours biological production by increasing nutrient supply into the photic zone, the lack of fertilizers such as Fe is generally considered as the main cause of the limited productivity. This is particularly true for the Eastern Equatorial Pacific (EEP), known to be a region of High Nutrient Low Chlorophyll (HNLC) (Bruland et al., 2005). Because of the Fe-limited biological production, both equatorial and coastal upwelling systems in the EEP represent today the most important oceanic source of CO_2 to the atmosphere (Takahashi et al., 1997), the CO_2 flux to the deep ocean via the biological pump uptake being lower than the CO_2 release to the atmosphere from CO_2-rich upwelled waters. While it is well documented for the modern (Kessler, 2006; Pennington et al., 2006), the evolution of both productivity and hydrological conditions at a million-year time scale is still poorly known in this area, especially for the highest productive periods of the EEP (Lawrence et al., 2006).

In this study, we aim to reconstruct the links between productivity changes, nutrient utilization, and surface oceanic conditions since the Pliocene warm period in the EEP. We report a high resolution (~2-4 ka) multi-proxy record from sediment samples of ODP Site 1239, located in the EEP near the equator at 120 km off the coast of Ecuador (Fig. 5.1), spanning the Plio-Pleistocene climate transition (~3.2-0.5 Ma). Our proxies include alkenones for sea surface temperatures (SST), mass accumulation rates (MAR) of alkenone concentration (alk), organic carbon (Corg) and total nitrogen (TN) contents for paleoproductivity, $\delta^{15}N$ for nitrogen (mostly nitrate) cycling, and Fe MAR for iron supply. The age model at Site 1239 is based on SST correlation with the nearby and well-dated Site 846 (Lawrence et al., 2006) (~3.2-0.5 Ma), further fine tuning using the precession signal in the Barium content record for the Pleistocene part, and correlation with the benthic $\delta^{18}O$ and $\delta^{13}C$ for the period ~3.2-2.7 Ma.

Today, Site 1239 is situated under the northeastern reaches of the EEP cold tongue, close to the equatorial front that separates cool (<23°C) and relatively high-salinity surface waters south of the equator from warm (>25°C) and low-salinity waters of the Panama Basin (Strub et al., 1998).

The nutrients mainly originate from local equatorial upwelling, fed by the nutrient-rich waters of the Equatorial Undercurrent (EUC). Despite a high nutrient availability, the surface waters of the EEP are not fully depleted by the phytoplankton assimilation (Fig. 5.1). This bio-limitation results from a limited supply of micronutrients such as Fe, that are today supplied by the EUC (Murray et al., 1994). In addition, terrestrial Fe reaching the surface waters can be partially dissolved and become bio-available for phytoplankton growth (Schroth et al., 2009; Ziegler et al., 2008).

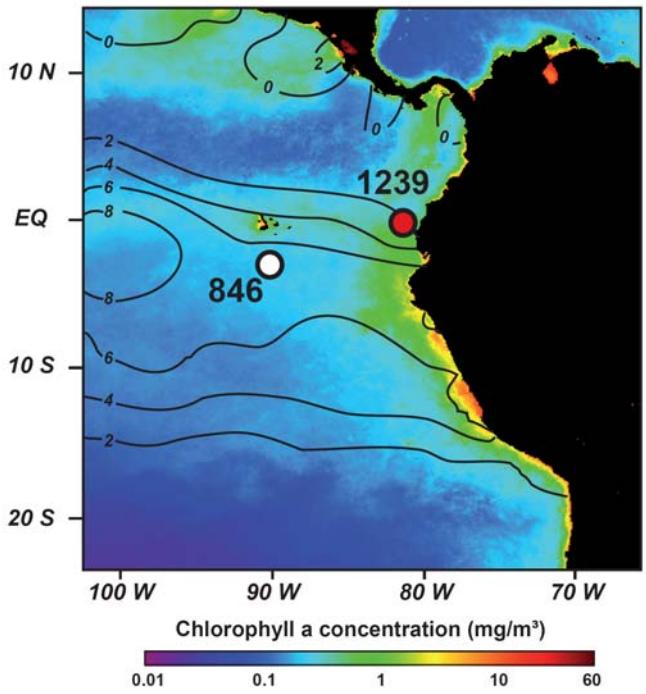

Figure 5.1 Productivity and nutrient distribution in the surface waters of the modern Eastern Equatorial Pacific. Colours represent the mean annual chlorophyll concentrations (primary productivity) and contour lines define the mean annual nitrate concentration at 10m water depth. Shown are the location of our study Site 1239 (0°40.32'S, 82°4.86'W, 1414 m water depth) and close-by reference Site 846 (Lawrence et al., 2006). Note that despite a high nutrient availability, the surface waters of the EEP are not fully depleted by the phytoplankton assimilation due to the lack of iron fertilization.

5.3 Material and Methods

Alkenones were extracted from 747 freeze-dried and homogenized sediment samples (~1 g dry weight for each sample) using an accelerated solvent extractor (Dionex ASE 200) at a resolution of ~2-4 ka. The resulting extract was then concentrated with a rotary evaporator and analyzed within a double column Multidimensional gas chromatograph (MDGC) with two Agilent 6890 gas chromatograph. SSTs were then derived from the commonly used alkenone unsaturation index (Müller et al., 1998). According to sample and internal standard replicates, the SST precision is about ± 0.3°C.

$\delta^{15}N$ and total nitrogen contents (TN, wt %) were determined on dried, ground bulk sediment, using a Carlo–Erba CN analyser 2500 interfaced directly to a Micromass-Isoprime mass spectrometer using ~40–50 mg aliquots of homogenized bulk sediment at the University of Bordeaux 1 (UMR EPOC). Sampling resolution averages one sample every 20-30 cm (~10 ka). Precision of the isotopic analyses based on certified standards and in-house standards replicates is better than ± 0.2 ‰. Nitrogen isotopic values are reported in delta notation, where $\delta^{15}N = [(^{15}N/^{14}N\text{sample}/^{15}N/^{14}N\text{standard})-1)]*1000$ and the standard is atmospheric N_2. Some discrete samples were also selected all along the record and measured for their total organic carbon (C_{org}, wt %) contents using a LECO C-S 125 analyser after treatment of the sediment with HCL to remove $CaCO_3$. C/N ratios close to 10 and shipboard analyses during Leg 202 (Mix et al., 2003) exclude a significant input of terrestrial organic matter at site 1239. Opal was measured by an automated extraction method and wet chemical leaching (Müller et al., 1993).

X-Ray Fluorescence (XRF) core scanning is a non-destructive procedure which determines the chemical composition of measured sediments as element intensities in counts per second (cps), which are proportional to chemical proportions (Richter et al., 2006). XRF measurements of Fe intensities were carried out by using the Alfred Wegener Institute's Avaatech X-ray (XRF) core scanner at ~15 cm resolution (~3-7 ka), with generator settings of 10 kV. Fe data obtained by this method strikingly evolved in parallel to those performed by geochemical analyses characterizing the real Fe concentration contained within the sediment (Rincon et al., 2008). Fe MAR was obtained by the calibration of Fe measured by XRF with Fe concentration measured by ICP-OES.

5.4 Results and Discussion

Our SST record at Site 1239 reveals a warm Pliocene period with values ~4°C warmer than today, followed by a gradual cooling from ~2.8 to 1.7 Ma (Fig. 5.2A). From ~1.7 to 1.4 Ma, temperatures warmed up by ~4°C prior to a second pronounced cooling event until ~0.9 Ma corresponding to the Mid-Pleistocene transition. From ~0.9 Ma, long-term SST increased again until ~0.5 Ma with glacial/interglacial cycles of ~2°C. Contrary to the SST record, the trend shown by the productivity-related proxies (alk, TN, Corg and opal MARs) reveals two major high productivity phases between ~3.1-2.8 and ~1.9-1.4 Ma (Fig. 5.2B, C and D). These two periods of maximum biological production indifferently appeared during both warm and cold temperature conditions, thereby implying that long-term SST and productivity changes in the EEP were not coupled in the EEP over the Plio-Pleistocene period.

This lack of relationship between SST and productivity has already been reported in the Eastern Pacific (Lawrence et al., 2006; Dekens et al., 2007). Indeed, asynchronous changes in temperatures and productivity were used as an argument to suggest that SST variations in the EEP are not the result of changes in wind strength alone, but are also likely due to changes in the depth and/or temperatures of the ventilated thermocline (Dekens et al., 2007). In addition, Lawrence et al. (2006) showed that the maximum of productivity at the EEP Site 846 between ~3.0 and 1.5 Ma evolved independently of the monotonic SST cooling since ~5 Ma (Fig. 5.3). The authors argued that the EEP primary productivity was primarily dictated by changes in the source of nutrients rather than changes in the equatorial upwelling strength. However, the characteristics of the source waters and its nutrients content have not been evaluated yet to explain past productivity changes in the EEP since the Pliocene.

We therefore focus on the $\delta^{15}N$ record at Site 1239, commonly used as a proxy for nutrient (nitrate) cycling, in order to detect a potential link between nitrate supply and productivity changes in the EEP. Our $\delta^{15}N$ profile can be broadly divided into two distinctive parts. In the older part of the record until ~1.9 Ma, $\delta^{15}N$ values are low, around 2‰ (Fig. 5.2D). Thereafter, the profile shifts toward heavier values around 4‰, with large $\delta^{15}N$ amplitudes of ~2‰. The $\delta^{15}N$ records (1) the preformed $\delta^{15}N$ signature, (2) isotopic fractionation during nitrate uptake by phytoplankton (^{14}N being preferentially consumed over ^{15}N, resulting in low $\delta^{15}N$ under nitrate-replete conditions), and (3) water-column denitrification and N_2-fixation balance, which respectively account for the local sink and source of N in the ocean. The $\delta^{15}N$ ratio would have been unlikely affected by local water

column denitrification because our $\delta^{15}N$ values at Site 1239 are too low (1-4‰ lower than the mean oceanic nitrate (Sigman et al., 1997)) for being largely affected by such heavy nitrate associated to denitrification process, and too high for being influenced by strong regional N fixation. Thus the main mechanisms explaining variations of our $\delta^{15}N$ record at Site 1239 involve the relative nitrate utilization, changes of the nutrients source, and/or a change of the N isotopic composition of the nutrients within the nutricline.

The similar increasing $\delta^{15}N$ trend recorded in the Benguela (Etourneau et al., 2009) and California (Liu et al., 2008) sediments since ~3.5 Ma has been attributed to major changes in nutrient sources from the high to the low latitudes oceanic areas, from more Antarctic Intermediate water (AAIW) during the Pliocene to more Subantarctic Mode water (SAMW) over the Pleistocene. This may have resulted of the development of the polar frontal system in the Southern Ocean and the subsequent formation of SAMW around ~2.0 Ma (Etourneau et al., 2009; Liu et al., 2008). Whether such source changes occurred in the low-altitudes upwelling regions from ~2.0 Ma, we can expect a shift in our EEP Site 1239 $\delta^{15}N$, because both SAMW and AAIW are the main contributor of nutrient in the EEP surface waters (Toggweiler et al., 1991; Sarmiento et al., 2004). This should be mirrored in our EEP $\delta^{15}N$ record by values closer to the isotopic signature of preformed nitrate arising from either Subantarctic or Antarctic zones.

We examined the $\delta^{15}N$ signature at the Subantarctic Site 1090 and the Antarctic Site 1096 (Sigman et al., 2004), where SAMW and AAIW form, respectively. During the Pliocene, the $\delta^{15}N$ at Site 1090 was ~3‰ higher than at Site 1239 (Fig. 5.2D), while those at Site 1096 were relatively close (~1‰). In contrast, since ~1.9 Ma, $\delta^{15}N$ values at Site 1239 switched towards higher values than those at Site 1096, and closer to those found at Site 1090 (~1‰). This $\delta^{15}N$ shift around ~1.9 Ma implies that the changes of nutrients source affecting the coastal upwelling areas also controlled the nutrient supply to the EEP surface waters. We conclude that the $\delta^{15}N$ profile recorded in each coastal and open waters upwelling regions reflected changes in the ocean N budget driven by reorganizations of the Southern Ocean circulation since the Pliocene. However, it is important to mention that the $\delta^{15}N$ shift towards higher values did not synchronously increase perfectly (~2.4 Ma off Namibia (Etourneau et al., 2009), ~2.1 off California (Liu et al., 2008), and ~1.9 Ma in the EEP (this study)). This offset can be attributed to changes of the regional hydrological conditions and the N fractionation by the local primary productivity.

The formation and the diffusion to the low-latitudes of the poor-oxygenated SAMW associated to a shoaling of the thermocline around ~2.0 Ma would have favored the denitrification process in the eastern boundary currents such as off California (Liu et al., 2008), thus increasing the $\delta^{15}N$ signature of the nutrients circulating within the nutricline. As found for the last glacial/interglacial transition, the denitrification and N fixation inversely evolved, denitrification increasing (decreasing) and N fixation decreasing (increasing) during interglacials (glacials) (Altabet et al., 1995; Ren et al., 2009). Assuming a similar scenario across the Plio-Pleistocene, weaker denitrification during the Pliocene was probably accompanied by stronger N fixation, and inversely during the Pleistocene. Thus, the enhanced denitrification/N fixation ratio through the Plio-Pleistocene would have increased the isotopic composition of the nutrients pool.

The $\delta^{15}N$ trend towards higher values from a warm to a cold climate state over the past million years as reported off the Namibia (Etourneau et al., 2008), California (Liu et al., 2008), and EEP margins (this study), is inverse to that yielded for the last deglaciations. This implies that the biogeochemical, and physical, processes related to the marine N cycling between the high and low latitudes during the Pliocene revealed a different picture than that we might expect from glacial/interglacial studies. This major finding could therefore draw new perspectives of the marine N cycle evolution when considering climate under warmer conditions than today. However, further investigations are needed for improving our understanding of all the oceanic processes affecting the oceanic N budget through the Plio-Pleistocene.

At Site 1239, the $\delta^{15}N$ values remained overall below 4‰ since the Pliocene. According to Farrell et al. (1995), N isotopic signatures lower than 5-6‰ in the EEP, suggest that the phytoplankton productivity did not full utilize the nitrate pool. Despite variations in the source waters, the low $\delta^{15}N$ values found at Site 1239 implies that the nitrate was unlikely limiting in the EEP over the past 3 Ma. Besides, the lack of correlation between productivity-related proxies and $\delta^{15}N$ variations further lend support that changes in nitrate supply to the EEP alone did not regulate the biological production changes through the Plio-Pleistocene.

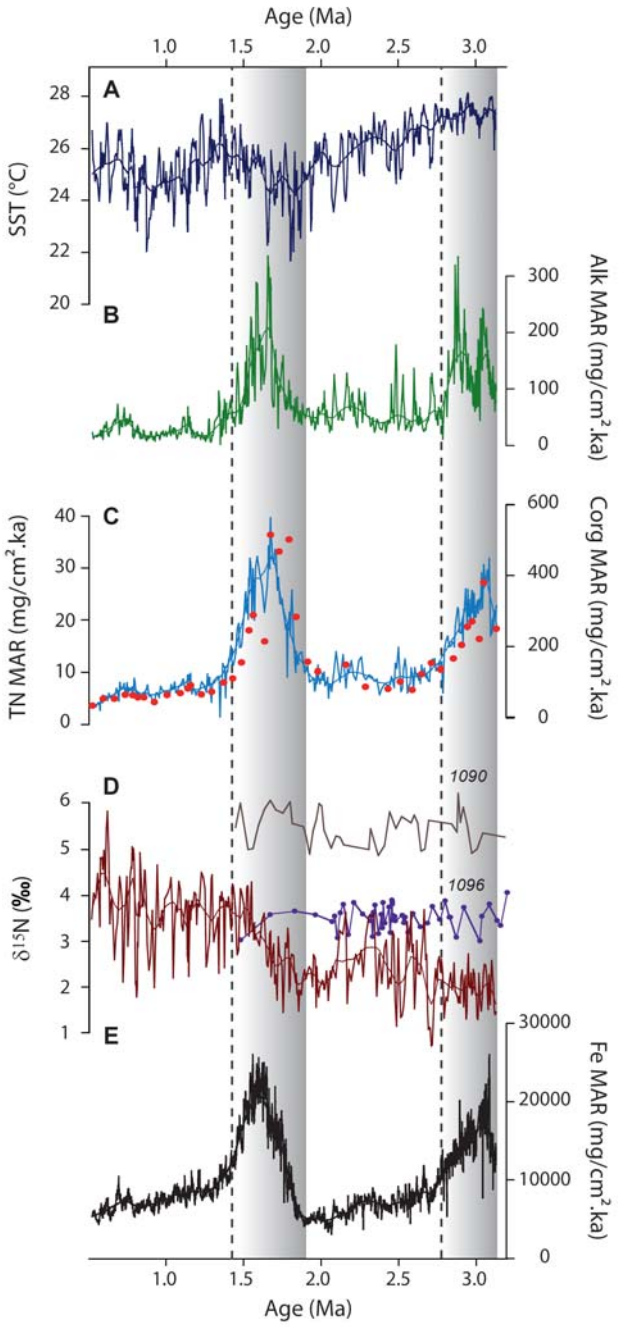

Figure 5.2 Paleorecords in the EEP at Site 1239. A: Alkenone-derived SST. B: Alkenone MAR. C: total nitrogen content (light blue curve) and organic carbon (red dots) MARs. D: $\delta^{15}N$ at Sites 1239 (brown), 1090 (grey) and 1096 (Sigman et al., 2004) (violet). E: Fe MAR. MAR ($mg/cm^2/ka$) = LSR (cm/ka) x DBD (mg/cm^3) x component percentage/100, where LSR, Linear Sedimentation Rate, is derived from our age model, and DBD, Dry Bulk Density, from Shipboard analyses (Mix et al., 2003).

In the modern EEP, Fe is the major factor limiting the primary productivity, while other nutrients such as nitrate or phosphate are available in high concentration (Bruland et al., 2005). Here, we compare our paleoproductivity estimates to a high resolution Fe MAR record from Site 1239 (Fig. 5.2E). Our Fe record strikingly shows the same profile as the productivity-related proxies records until ~0.5 Ma with a significant increase during the periods of maximum productivity between ~3.2-2.8 and 1.9-1.4 Ma. The outstanding resemblance between Fe and productivity markers thus suggests that changes in biological production were intimately tied to changes in iron concentration, and hence in iron fertilization since the warm Pliocene. As demonstrated above, nitrate supply was likely sufficient enough to fully feed phytoplankton. In counterpart, low Fe inputs into the EEP probably limited the primary productivity, and vice versa. Enhanced Fe supply at ~3.2 and 1.9 Ma could have thus triggered the most productive periods of the EEP history since 5 Ma (Lawrence et al., 2006; Fig. 5.3), and inversely limited the regional productivity between ~2.8-1.9 and ~1.4-0.5 Ma.

The iron entering into the EEP might have originated from two major sources: EUC, transporting Fe from the western equatorial Pacific, and terrestrial inputs from South America (or nearby islands such as Galapagos). A recent study stated that the Fe origin in the equatorial Pacific Ocean since the Pliocene was mainly linked to the EUC (Ziegler et al., 2008). This could be one plausible explanation as far as the change in local thermocline depth is concerned. The depth and nutrient content (i.e. Fe) of the thermocline may have been controlled by changes in regional oceanic circulation due to the closure of Panama, changes in the source of upwelled waters, oceanic heat distribution and/or wind-driven equatorial upwelling activity. The finale closure of the Panama Gateway might have affected the thermocline depth and/or properties only until its complete closure at ~2.8 Ma, while the other processes mentioned above may have continuously altered the thermocline depth and nutrient content through the Plio-Pleistocene cooling. However, the main factors controlling thermocline structure since the Pliocene are still not fully understood and need further investigations.

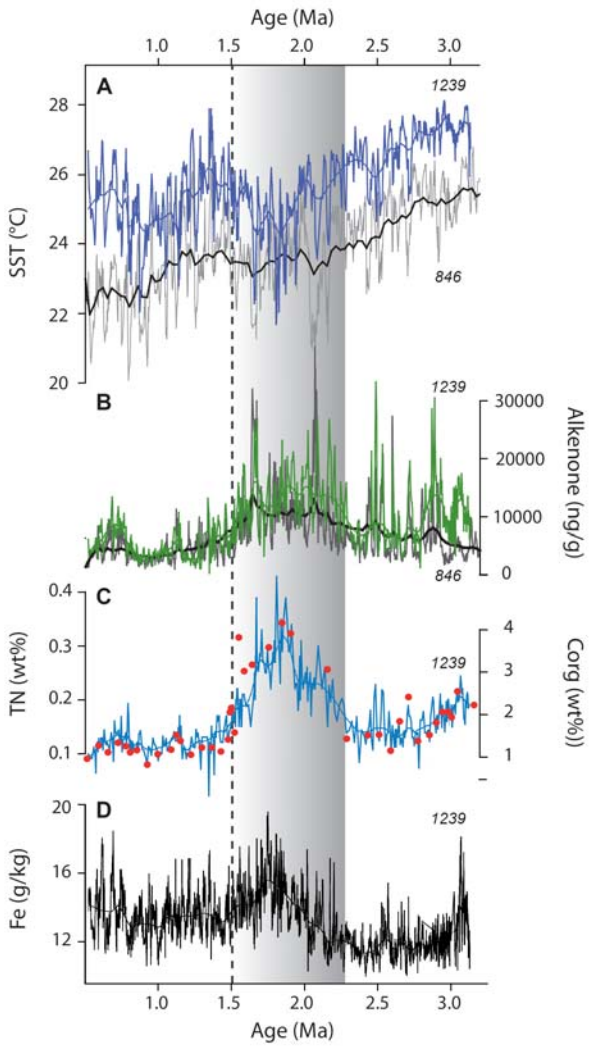

Figure 5.3 Comparison SSTs and productivity-related proxies at Sites 1239 and 846 (Lawrence et al., 2006). A: SSTs at Site 1239 (blue) and 846 (grey). B: Alkenone concentrations at Sites 1239 (green) and 846 (dark grey). C, Total nitrogen (light blue curve) and carbon organic (red dots) contents at Site 1239. D: Fe concentration at Site 1239. In this figure, we show the concentrations of alkenones, total nitrogen, and organic carbon contents for the comparison between both EEP sites 1239 and 846, and not the MARs as plotted in figure 1. Concentrations and elements contents show a longer maximum of productivity between ~2.4 and 1.5 Ma at both sites, while MARs indicate instead two shorter maximum periods between ~3.1-2.8 and ~1.9-1.4 Ma. This difference is explained by the conversion of the biogenic components into MARs. We however believe that the use of MARs (based on our well constrained age model) in this study is more relevant since the concentration or dilution effects may have affected both contents records. The overall similarity between trends of each paleoproductivity records (see figure below) suggest that biological production at Site 1239 and 846 (Lawrence et al., 2006) may have experienced a similar evolution as

well as in the entire Eastern Pacific (Dekens et al., 2007; Liu et al., 2008; Cortese et al., 2004). Our conclusion that primary productivity is primarily controlled by Fe fertilization could be therefore valid for the Eastern Pacific as whole, albeit further investigations on the impact of terrestrial micronutrients at more offshore sites in the EEP is required.

On the other hand, terrestrial inputs of Fe might also have played a significant role in iron fertilization (Rincon et al., 2008), driven by changes in wind strength (dust transport), precipitation rates (fluvial inputs) and/or tectonic activity (the final closure of Panama and the Andean uplift), the latter affecting in turn wind stress and continental rainfall. Some studies (Duce et al., 1991; Schroth et al., 2009) yielded that atmospheric Fe injected into the sea could be one the greatest iron supplier due its capacity of becoming bio-available. Over the Plio-Pleistocene, strengthening of the meridional circulation (Brierley et al., 2009), and hence trade winds, could have increased continental erosion and aeolian transport of Fe particles. In contrast, the contribution of major rivers is still unknown. The very low east-to-west SST gradient (Wara et al., 2005), related to permanent El Niño-like conditions during the warm Pliocene, could have enhanced rainfall over the EEP and rivers discharge. However, changes in the zonal and/or meridional atmospheric circulations could not fully explain the two main Fe pulses detected at Site 1239 between ~3.2-2.8 and ~1.9-1.4 Ma. Therefore, the main Fe supply into the EEP was probably the result of several mechanisms involving the modification of the land-ocean-atmosphere interactions which should be further explored in future researches.

5.5 Conclusions

Some periods of maximum biological production at Site 1239 have also been detected at several sites of the Eastern Pacific (Lawrence et al., 2006; Dekens et al., 2007; Liu et al., 2008; Cortese et al., 2004) (Fig. 5.3). We conclude that the addition of iron to the HNLC EEP has stimulated the most productive periods of this region since the Pliocene. However, we find no direct evidence between Plio-Pleistocene climate changes, supposed to be related to atmospheric CO_2 level variations (Lunt et al., 2008), and marine productivity changes in the EEP. It is therefore questionable the role played by the EEP regional biological pump on the global carbon cycle, and its impact on Pliocene climate change. Further investigations combining adequate geochemical analyses and model experiments are needed in order to improve our understanding on (1) the origins and variations of Fe entering into the EEP, as well as (2) the role played by both biological

pump efficiency and upwelling activity in the EEP on Plio-Pleistocene climate change, an interplay capable to act as a significant source or a sink of atmospheric CO_2.

5.6 Acknowledgements

We acknowledge G. Leduc, N. Khélifi, J. Xu for discussions, and objective criticism; and I. Billy, S. Koch, J. Heinze, and K. Charlier for technical assistance. This research was supported by the Deutsche Forschungsgemeinschaft as part of the Integrated Ocean Drilling Program (IODP/ODP) funding program through German projects SCHN 621/5-2 and SCHN 621/12-1 (University of Kiel), TI240/17-2 (AWI Bremerhaven), and the French program CNRS-ECLIPSE to PhM (University of Bordeaux I).

5.7 References

Altabet, M.A., Francois, R., Murray, D.W. & Prell, W.L. Climate related variations in denitrification in the Arabian Sea from sediment 15N/14N ratios. *Nature*, **373**, 506-509 (1995).

Bierley, C.M., Fedorov, A.V., Liu, Z., Herbert, T.D., Lawrence, K.T., & LaRiviere, J. Greatly expanded tropical warm pool and weakened Hadley circulation in the Early Pliocene. *Science* **323**, 1714-1718 (2009).

Bruland, K.W., Rue, E.L., Smith, G.J. & DiTullio, G.R. Iron, micronutrients and diatom blooms in the Peru upwelling regime: brown and blue waters off Peru. *Marine Chemistry*, **93**, 81-103 (2005).

Cortese, G., Gersonde, R., Hillenbrand, C.-L. & Kuhn, G. Opal sedimentation shifts in the world over the last 15 Myr. *Earth and Planetary Science Letters*, **224**, 509-527 (2004).

Dekens, P.S., Ravelo, A.C. & McCarthy, M.D. Warm upwelling regions in the Pliocene warm period. *Paleoceanography*, **22**, doi:10.1029/2006PA001394 (2007).

Duce, R.A. & Tindale, N.W. Atmospheric transport of iron and its deposition in the ocean. *Limnology and Oceanogaphy*, **36**, 1715-1726 (1991).

Farrell, J.W., Pedersen, T.F., Calvert, S.E. & Nielsen, B. Glacial-interglacial changes in nutrient utilization in the equatorial Pacific Ocean. *Nature*, **377**, 514-517 (1995).

Kessler, W.S. The circulation of the eastern tropical Pacific: A review. *Progress in Oceanography* **69**, 181-217 (2006).

Lawrence, K.T., Liu, Z. & Herbert, T.D. Evolution of the eastern tropical Pacific through Plio-Pleistocene glaciation. *Science*, **312**, 79-83 (2006).

Lisiecki, L.E. & Raymo, M.E. A Pliocene-Pleistocene stack of 57 globally distributed benthic $\delta^{18}O$ records. *Paleoceanography*, **20**, doi: 10.1029/2004PA001071 (2005).

Liu, Z., Altabet, M.A. & Herbert, T.D. Plio-Pleistocene denitrification in the eastern tropical North Pacific: Intensification at 2.1 Ma. *Geochemistry, Geophysics, Geosystems*, **9**, doi: 10.1029/2008GC002044 (2008).

Lunt, D.J., Foster, G.L., Haywood, A. & Stone, E.J. Late Pliocene Greenland glaciation controlled by a decline in atmospheric CO_2 levels. *Nature*, **454**, 1102-1106 (2008).

Mix, A.C., Tiedemann R. & Blum P. *Proceedings of the Ocean Drilling Program Initial Report*, **202,** College Station, Tex (2003).

Müller, P.J., Kirst, G., Ruhland, G., von Storch, I., & Rosell-Melé, A. Calibration of the alkenone paleotemperature index $U^{k'}_{37}$ based on core-tops from the eastern South Atlantic and the global ocean (60°N-60°S). *Geochimica et Cosmochimica Acta*, **62**, 1757-1772 (1998).

Müller, P. J., & Schneider, R. An automated leaching method for the determination of opal in sediments and particulate matter. *Deep-Sea Research I,* **40**, 425-444 (1993).

Murray, J.W., Barber, R.T., Roman, M.R., Bacon, C.R. & Feely, R.A. Physical and biological controls on carbon cycling in the equatorial Pacific. *Science*, **266**, 58-65 (1994).

Pennington, T.J., Mahoney, K.L., Kuhawara, V.S., Kolber, D.D., Calienes, & R., Chavez, F.P. Primary production in the eastern tropical Pacific: A review. *Progress in Oceanography*, **69**, 285-317 (2006).

Raymo, M.E., Grant, B., Horowitz, M. & Rau, G.H. Mid-Pliocene warmth: Stronger greenhouse and stronger conveyer. *Marine Micropaleontology*, **27**, 313-326 (1996).

Raymo, M.E., Lisiecki, L.E. & Nisancoglu, K.H. Plio-Pleistocene Ice Volume, Antarctic Climate, and the Global $\delta^{18}O$ Record. *Science*, **313**, 492-495 (2006).

Ren, H., Sigman, D.M., Meckler, A.N., Plessen, B., Robinson, R.S., Rosenthal, Y., & Haug, G. Foraminiferal isotope evidence of reduced nitrogen fixation in the Ice Age Atlantic Ocean. *Science*, **323**, 244-248 (2009).

Richter, T.O., Van der Gaast, S., Koster, B., Vaars, A., Gieles, R., De Stiger, H., De Haas, H., van Weering, T.C.E. The Avaatech XRF core scanner: technical description and applications to NE Atlantic sediments. In: Rothwell, R.G. (Ed.). *New Techniques in Sediment Core Analysis*, **267**, Geological Society, London, 39-50 (2006).

Rincon, D., Saukel, C., Lamy, F., Steph, S., Sturm, A. & Tiedemann, R. Plio-Pleistocene record of terrigenous sediment delivered into the eastern tropical and subtropical Pacific, ODP sites 1237 and 1239. Climate change : from the geologic past to the uncertain future : A tribute to André Berger - 26 to 29 May 2008 - Louvain-la-Neuve University – Belgium. Poster. Abstract Book.

Sarmiento, J.L., Gruber, N., Brzezinski, M.A. & Dunne, J.P. High-latitude controls of thermocline nutrients and low latitude biological productivity. *Nature*, **427**, 56-60 (2004).

Schroth, A.W., Crusius, J., Sholkovitz, E.R. & Bostick, B. Iron solubility driven by speciation in dust sources to the ocean. *Nature Geoscience,* **2**, 337-340 (2009).

Sigman, D.M., Altabet, M., Michener, R., McCorkle, D.C., Fry, B., & Holmes, R.M. Natural abundance-level measurement of the nitrogen isotopic composition of oceanic nitrate: An adaptation of the ammonia diffusion method. *Marine Chemistry*, **57**, 227–242 (1997).

Sigman, D.M., Jaccard, S.A., & Haug, G.H. Polar ocean stratification in a cold climate. *Nature*, **428**, 59-63 (2004).

Strub, P.T., Mesias, J.M., Montecinos-Banderet, V., Rutllant, J. & Salinas-Marchant, S. Coastal ocean circulation off western South America. *The Sea*, **11**, 273-313 (1998).

Takahashi, T., Feely, R.A., Weiss, R.F., Wanninkhof, R.H., Chipman, D.W., Sutherland, S.C., & Takahashi, T.T. Global air-sea flux of CO_2: An estimate based on measurements of sea-air pCO_2 difference. *Proceedings of the National Academy of Sciences*, **94**, 8292-8299 (1997).

Toggweiler, J.R., Dixon, K. & Broecker, W.S. The Peru Upwelling and the Ventilation of the South Pacific Thermocline. *Journal of Geophysical Research*, **96**, 20,467-20,497 (1991).

Ziegler, C.L., Murray, R.W., Plank, T. & Hemming, S.R. Sources of Fe to the equatorial Pacific Ocean from the Holocene to Miocene. *Earth and Planetary Science Letters*, **270**, 258-270 (2008).

Chapter VI

Plio-Pleistocene high-resolution sea surface temperature records from the Benguela Upwelling System and the Eastern Equatorial Pacific

---

Johan Etourneau[1], Ralph Schneider[1], Thomas Blanz[1], and Philippe Martinez[2]

[1]Institute for Geosciences, University of Kiel, D-24118 Kiel, Germany

[2]UMR CNRS 5805 EPOC, University of Bordeaux 1, 33405 Talence, France

6.1 Abstract

From a new sea surface temperature (SST) record in the Eastern Equatorial Pacific (EEP) we found that the west-to-east SST gradient across the equatorial Pacific irreversibly increased on average by 3°C over the past ~2.2 Ma, supposing a major transition in atmospheric circulation from weak to strong zonal, or Walker, circulation (WC) during the Plio-Pleistocene, thus corroborating previous studies. In comparison, the meridional SST gradient in the Benguela region increased on average by 4°C from 2.4-2.0 to 0.8 Ma in response to the intensification of the coastal upwelling. Increase in upwelling activity off Namibia, as well as probably in other coastal upwelling systems, was likely driven by stronger trade winds, associated to the intensification of meridional, or Hadley, circulation (HC). This implies that both atmospheric patterns were intimately coupled during the Plio-Pleistocene, and probably responded to the increase in pole to equator temperature gradient. This conclusion disqualifies the assumptions that weak atmospheric circulation in the tropics and subtropics precluded ice sheet formation at high latitudes, since the onset of significant Northern Hemisphere glaciation (NHG) occurred ~3.0 Ma ago, well before the development of both intense WC and HC.

6.2 Introduction

Current debate exists on Plio-Pleistocene changes in atmospheric circulation in tropical and subtropical regions, as well as their effects on global climate change. The study of such changes is particularly pertinent for the last 3.0 Ma during which Earth's climate transitioned from a warmer-than-today state (± 3-4 °C) (Ravelo et al., 2004) towards pronounced cold climatic conditions and widespread northern hemisphere ice sheets (Lisiecki & Raymo, 2005). In this context of global cooling, the timing of changes in zonal (Walker, WC) and meridional (Hadley, HC) circulations remains unclear, albeit of primary relevance for understanding better Pliocene-Pleistocene climate changes.

Most of the recent studies agreed on drastic changes in atmospheric circulation in tropical and subtropical regions since the Mid-Pliocene. Both WC and HC were likely weaker during the warm Pliocene period and strengthened during the Plio-Pleistocene cooling, as illustrated by a suite of sea surface temperature records revealing an increase in zonal or meridional temperature gradients (ΔSST) (Brierley et al., 2009; Jia et al., 2008; Lawrence et al., 2006; Ravelo et al., 2004; Wara et al., 2005). However, each ΔSST reconstructions commonly used to infer changes in WC and HC differ quite significantly on the exact timing of strongest intensification. For instance, some studies emphasized a strengthening of WC ~2.0 Ma ago (Ravelo et al., 2004; Wara et al., 2005), whereas other results suggested that it may have

occurred in concert with the onset of large ice sheets in the northern hemisphere ~3.0 Ma ago (Lawrence et al., 2006). Conversely, some paleorecords indicated that the development of strong HC appeared not before 2.3 Ma (Jia et al., 2008). A recent study proposed a strengthening of HC as early as 4.0 Ma (Brierley et al., 2009). Given the importance of changes in low-latitudes atmospheric circulation as an internal factor on high-latitude climatic conditions, it is fundamental to study the relationship between WC, HC, and Plio-Pleistocene climate change.

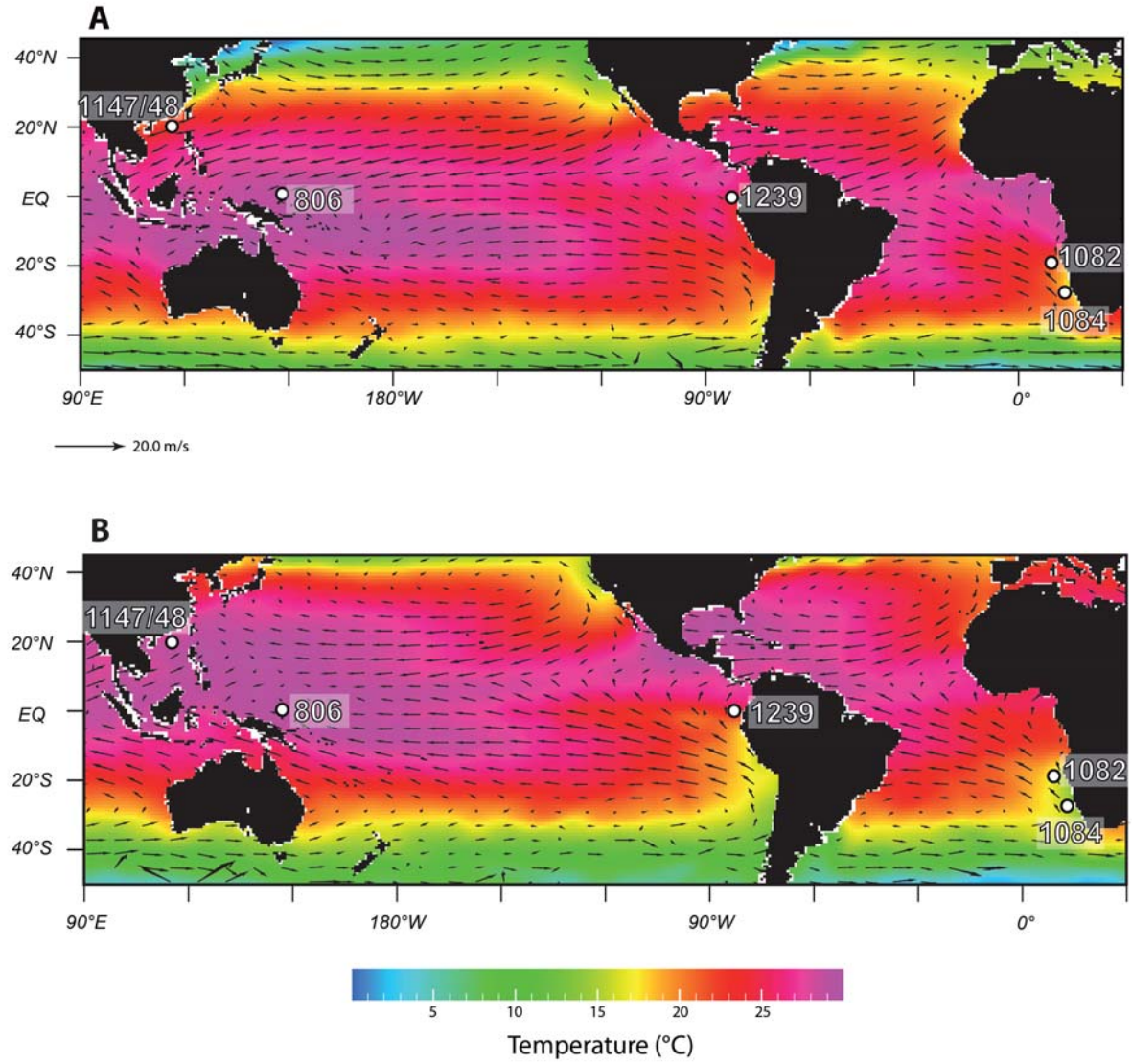

Figure 6.1 Modern SSTs (Levitus and Boyer, 1994) and wind speed (Woodruff et al., 1998) during the boreal winter (**A)** and boreal summer (**B**). Open circles indicate the location of the Ocean Drilling Program Sites considered in this study, in the EEP, 1239 (**Chapter V**), WEP, 806 (Wara et al., 2005), South China Sea, 1147/1148 (Jia et al., 2008), and the Benguela, 1082 (**Chapter IV**) and 1084 (Marlow et al., 2000).

In this study, we discuss changes in WC and HC strength over the last ~3.0 Ma by focusing on two new SST gradients: (1) a zonal SST between the Western Equatorial Pacific (WEP) Site 806 and the Eastern Equatorial Pacific (EEP) Site 1239 used here as a tracer of past changes in WC strength; and (2) a meridional SST across the Benguela region between Site 1082 and 1084 reflecting past changes in HC strength.

Today, Site 806 is permanently located in the WEP warm pool, while Site 1239 is situated in the cold EEP region, at the hinge point between the EEP cold tongue and the warmer easternmost equatorial surface waters of the Panama Basin. The SST asymmetry between the warm WEP and cold EEP mainly controls the modern Walker atmospheric circulation; the WC strength increases (decreases) as the west-to-east SST gradient increases (decreases). However, changes in the zonal SST gradient mainly respond to variations in EEP oceanic conditions because WEP SST remains relatively stable year-round. Thus, the reconstruction of the west-to-east SST gradient for the last ~3.0 Ma, in particularly by providing a new high resolution SST record in the EEP, might give a clearer picture of changes in WC strength since the Mid-Pliocene.

In comparison, to monitor past HC changes, we used a meridional SST gradient in the southeast Atlantic, within the Benguela Upwelling System (BUS). The BUS is mainly controlled by strong seasonal trade winds which foster the shoaling of cool waters from below the thermocline to the surface. The equatorward winds as part of HC are mostly influenced by the strength and position of the subtropical high-pressure system, which responds to changes in the pole to equator temperature gradient. When the later increases, HC and resultant trade winds strengthen, and vice versa. By reconstructing changes in upwelling activity off Namibia, we aim to scrutinize variations of trade wind intensity and HC. Combined with evidence from other coastal upwelling regions, also influenced by the same meridional atmospheric pattern, this should provide crucial information on HC strength changes for the past ~3.0 Ma.

6.3 Material and Methods

In this study, we generated high resolution SST records from two sites: Site 1239 (0°40.32'S, 82°4.86'W, 1414 m water depth) located at the northeastern reaches of EEP cold tongue; and Site 1082 (21°5'S, 11°49'E, 1280 m water depth) situated in the northern part of the modern Benguela upwelling system (BUS) close to the northernmost upwelling cell off Namibia (Fig. 6.1).

SSTs at both sites were derived from the alkenone unsaturation index ($U^{K'}_{37}$). Alkenones were extracted from freeze-dried samples at a 2-4 ka resolution by using an Accelerator Solvent Extraction (Dionex ASE) and then analyzed by double column Multi-dimensional Gas Chromatography (GC) 6890N at the CAU (Christian Albrecht University of Kiel). The two columns are directly connected to each other via a transfer line allowing the isolation of the C_{37} signal within the second GC. This technique improves the separation and individual integration of respective peaks in the chromatograms, even for low alkenone concentrations, less than 1 ng/g. We converted $U^{K'}_{37}$ into SSTs applying the core-top calibration of Müller et al. (1998) back to 3.2 Ma.

The high resolution SST record at Site 1239 enabled to improve the previous stratigraphy from the Shipboard Party (Mix et al., 2003) by correlating cold and warm period oscillations since the Pliocene with the SST record from the nearby and well-dated Site 846 (**Chatper III**). Besides, fine tuning of precession signal with the Barium content record for the Pleistocene and benthic $\delta^{18}O$ and $\delta^{13}C$ for the interval ~3.2-2.7 Ma has been performed, and corroborates the stratigraphy derived from SST correlations. The age model at Site 1082 is based on the direct correlation of oxygen isotope records from benthic and planktonic foraminifera species (Dupont et al., 2005) as well as the alkenone-SST record with the Plio-Pleistocene oxygen isotopes stack LR04 (Lisiecki and Raymo, 2005) (**Chatper III**).

Unlike the meridional SST gradient across the Benguela region, the zonal SST gradient across the equatorial Pacific is based on the comparison between two SST records using two different methods. At Site 1239, alkenone-derived SST reconstruction was applied, while SSTs at Site 806 were reconstructed using the Mg/Ca ratio (Wara et al., 2005). The application of two different SST proxies might however cause discrepancies based on the method rather than being paleoceanographic feature. After measuring some samples at Site 806 with the alkenone-SST method and applying the calibration of Sonzogni et al. (1997), commonly used for warm pool conditions, we found that the alkenone- and Mg/Ca-SSTs showed similar values over the last ~3.0 Ma (Fig. 6.2). This implies that the comparison of two SST records derived from different methods across the equatorial Pacific is sufficient enough to estimate changes in the zonal SST gradient since the Pliocene.

6.4 Results and Discussion

6.1.1 The Walker circulation

The Walker circulation can be represented by the zonal SST gradient between the west and east of the equatorial Pacific. We provided a new SST record in the EEP for the last ~3.0 Ma, at Site 1239. During the Pliocene warm period, SSTs at the EEP Site 1239 were on average ~3.5°C above modern annual mean (Fig. 6.2A). From ~2.8 Ma, SSTs started to cool in phase with the onset of major NHG, and then strongly declined from ~2.2 Ma to reach the coldest values of 22°C at ~1.6 Ma. Between ~1.6 and 1.4 Ma, surface waters at Site 1239 warmed up and became almost as warm as prior to 3.0 Ma (~27-28°C). From ~1.4 to 0.8 Ma, SSTs experienced a second cooling transition, before increasing again until 0.5 Ma, with temperatures solely 1°C colder on average than during the warm Pliocene period.

In the WEP warm pool, SSTs at Site 806 (Wara et al., 2005) did not reveal a long and continuous cooling trend but rather showed relative stable SSTs from ~3.0 to ~2.0 Ma prior to an increase of ~2°C until 0.5 Ma (Fig. 6.2A). The WEP-EEP SST gradient between Sites 806 and 1239 increased from ~2.2 Ma (Fig. 6.2C), thus reinforcing the Pacific SST asymmetry along the equator and contributing to the strengthening of WC, which confirms previous findings (Wara et al., 2005). This suggests that the development of WC appeared well after the onset of significant NHG, and probably had only a minor impact on high latitudes ice sheets formation as recently simulated by models (Haywood et al., 2007).

Around 2.2 Ma, WC intensification probably primarily responded to the EEP cooling, because WEP SSTs remained relatively stable and the WEP-EEP SST gradient increased. The EEP cooling may have been caused by (1) equatorial Pacific thermocline tilt changes, (2) EEP thermocline depth, (3) changes of source and/or temperatures of the upwelled waters, and (4) stronger convergent winds at the equator. Major tectonic events could have preconditioned both factors. Indeed, the complete Panama isthmus closure around ~3.0 Ma ceased the equatorial Pacific-Atlantic surface water exchanges, blocking the eastward flow of subsurface waters circulating below the thermocline from the western equatorial Atlantic (Coates and Obando, 1996). This may have affected the local oceanic circulation, the equatorial sea-level gradient across the Pacific and hence the thermocline depth in the EEP by causing the shoaling of the latter. However, the finale Panama closure may only have preconditioned and not continuously participated to the EEP cooling by shoaling the thermocline. On the other hand, a new study recently highlighted the role of the narrowing of the Indonesian Gateway during the Early Pliocene (Karas et al., 2009), which may have caused changes in subsurface water circulation

along the equatorial Pacific, influenced the west-to-east thermocline tilt and initiated the EEP cooling ~2.95 Ma ago (Karas et al., 2009). The Indonesian Gateway may have preconditioned the thermocline shoaling in the EEP but unlikely was the ultimate cause of the dramatic cooling in the EEP from ~2.2 to 1.6 Ma which led to strong WC intensification.

Previous studies emphasized that the thermocline depth in the low-latitude oceanic regions progressively shoaled around ~3.0 Ma in response to deep water cooling (e.g. Philander and Fedorov, 2003). This could also explain the concomitant EEP surface cooling, but probably not the strong SST decrease starting ~2.2 Ma ago. On the other hand, changes in upwelled waters temperature may also have influenced the SSTs at that time (Dekens et al., 2007). This assumption seems plausible for explaining the EEP cooling around ~2.2 Ma since it has been suggested that Subantarctic mode waters may have replaced Antarctic intermediate waters as the dominant water masses feeding the EEP equatorial upwelling from ~2.0 Ma onwards (**Chapter V**). In contrast, changes in meridional wind stress have been poorly considered, despite the fact that in the modern EEP system, convergent trade winds drive to equatorial divergence and open ocean upwelling. Changes in winds stress may have been caused by changes in the Hadley circulation, the meridional atmospheric pattern which results of pressure and SST difference between tropical and subtropical zones. However, only few studies focused on past Hadley circulation changes because of the scarcity of continuous paleo-SST records in the subtropical regions which would be needed to infer past changes in meridional atmospheric circulation.

6.1.2 The Hadley circulation

To study past changes of HC, we generated a meridional SST gradient across the Benguela upwelling system (BUS), an area particularly sensitive to HC and associated trade winds. Indeed, the northern part of the BUS, where Site 1082 is located, is seasonally cooled by strong trade winds, forcing the shoaling of the thermocline. In contrast, in the central part of the BUS, where Site 1084 is located, almost year-round strong winds cause a permanent upwelling activity and SST cooling. We may thus anticipate that both sites experienced similar oceanographic changes since at least the initiation of wind-driven coastal upwelling in the entire Benguela region. Precisely when the surface waters over the two sites underwent a cooling trend, the SST gradient between both sites sharply increased at ~2.4-2.0 Ma because the SST decrease at Site 1082 to the North was less pronounced compared to Site 1084, near the Lüderitz upwelling cell in the central BUS (Marlow et al., 2000) (Fig. 6.2B). We interpreted this difference between the two sites as a result of a transition from a short seasonal upwelling activity to a modern-like upwelling pattern controlled by trade winds (**Chapter IV**), in which surface waters in the central BUS are generally colder on mean annual basis than at Site 1082.

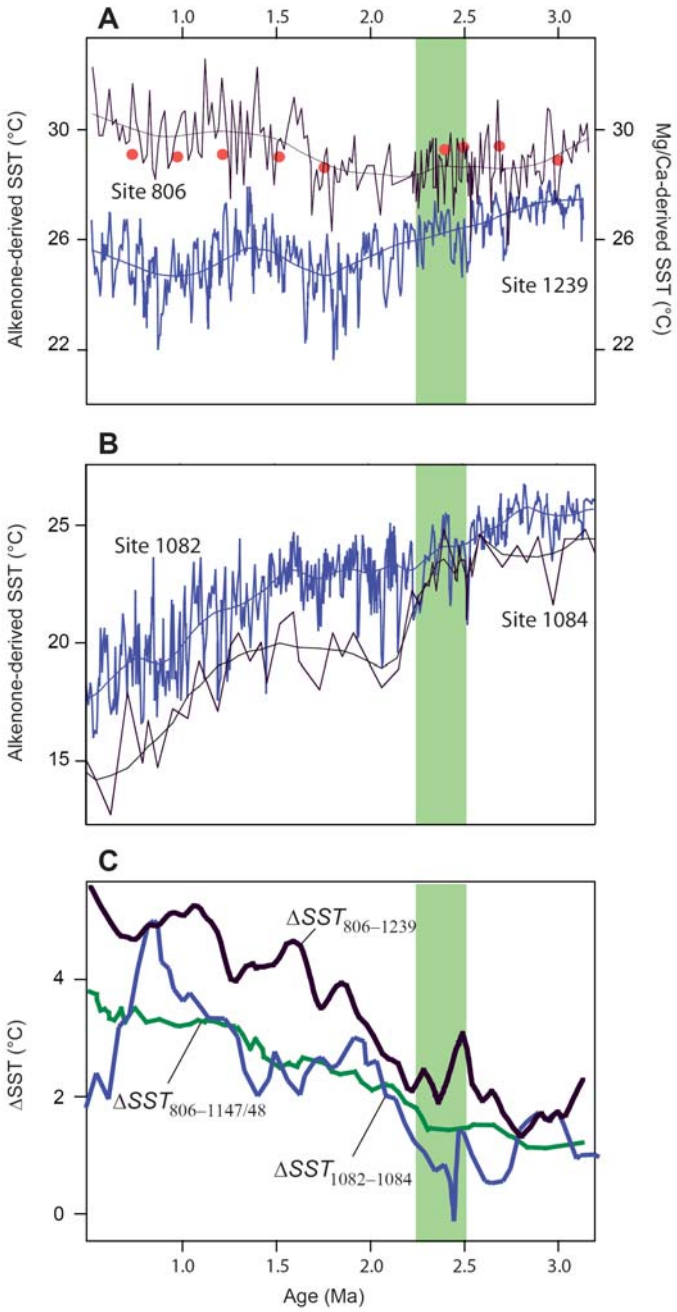

Figure 6.2 Plio-Pleistocene SST records and SST gradients. A: alkenone-SST at the EEP Site 1239 (**Chapter IV)** and the Mg/Ca-SST at the WEP Site 806 (Wara et al., 2005). Red dots indicate alkenone-SST at Site 806 (this study). B: alkenone-SST records at Sites 1082 and 1084 (**Chapter IV**; Marlow et al., 2000). C: SST gradients trends between Sites 1239 and 806 (black, $\Delta SST_{806\text{-}1239}$) as indicator of past WC changes, Sites 1082 and 1084 (blue, $\Delta SST_{1082\text{-}1084}$) and Sites 806 and 1147/48 (green, $\Delta SST_{806\text{-}1147/48}$) (Jia et al., 2008) for past HC changes. The green shaded area marks the concomitant development of WC and HC.

This assumption is supported by independent data. For instance, pollen-based analyses at Site 1082 indicated that this major transition in the Benguela upwelling activity corresponded to enhanced inland aridification (Dupont et al., 2006). Because upwelling intensified, less humidity was carried from the cool ocean to the continent, thus resulting in the Namib Desert extension. In addition, Lange et al. (1999) showed that mat-forming diatoms, typical of stratified water-column conditions, dominated surface waters prior to 2.0 Ma, and were replaced by diatom species, characteristic of ventilated waters and coastal upwelling conditions. This suggests that surface waters off Namibia were mainly stratified prior to ~2.4-2.0 Ma, and then vertically mixed through the Pleistocene. Because southeast trade wind intensification can be considered as the main factor conducive to strong upwelling of cold waters to the sea surface in the Benguela region, our observations suggest that trade winds have significantly intensified from ~2.4-2.0 Ma as a result of enhanced HC south of equator (**Chapter IV**).

If HC experienced a major transition from ~2.4-2.0 Ma at a global scale, this must be detected in other oceanic areas. Jia et al. (2008) were the first to report a substantial increase of the meridional SST gradient between the WEP and the South China Sea starting at ~2.3 Ma as a response to the intensification of HC (Fig. 6.2C). In the eastern tropical south Pacific, a net increase of terrestrial input into the Peru Basin from ~2.2 Ma onwards was attributed to a regional strengthening of the southeast trade winds (Lamy et al., 2009). Regional trade wind intensification off Peru may also explain the concomitant SST cooling found at Site 1237, in response to stronger upwelling off Peru. Correspondingly, off California, Liu et al. (2008) reported that the denitrification process characterizing this coastal upwelling region under modern conditions strengthened ~2.1 Ma ago. They ascribed this increase to the local shoaling of the thermocline and development of a modern-like frontal system in the Southern Ocean. While this assumption seems consistent with their findings, we could also suspect that HC, according to our assumption, may have significantly amplified denitrification in this region by participating to the strengthening of local upwelling and therefore to the thermocline shoaling. This would be particularly consistent with previous research led on land, which detected a concomitant aridification in California (Hsieh et al., 2001), probably tied to cooler surface waters due to enhanced upwelling, less evaporation and moisture export to the continent.

The pole to equator temperature gradient is the major driver of HC because it regulates subtropical high pressure systems and their latitudinal migration. With the ice sheet expansion in the northern and southern high latitudes (Jansen et al., 2000; Raymo et al., 2006), the temperatures at the poles probably strongly declined. In contrast, SST records reported in the tropics do not indicate such a profound cooling (Wara et al., 2005; Dekens et al., 2007; Karas et al., 2009; this study). SST in the tropical warm pools remained relatively similar to today or was

even colder. The increased temperature difference between high and low latitudes probably led to equatorward migration of the oceanic high pressure systems, closer to the continental low pressure cells. We propose that it may have reached a threshold from which the difference between high and low pressure systems was sufficiently high to promote strong trade winds, thus resulting in enhanced upwelling activity along the eastern boundary currents. In addition, stronger wind convergence may have fostered the cool waters from below the thermocline to shoal in the EEP, because changes in convergent winds are the dominant factor controlling the open ocean upwelling activity. Thus, it may have increased the west-to-east SST gradient across the equatorial Pacific and hence WC.

Recent model experiments showed that changes in HC may have had dramatic consequences on continental climatic conditions (Brierley et al., 2009). HC intensification may have substantially contributed to drier environmental conditions in regions close to the eastern boundary currents such as in Namibia, Peru, California and Mauritania (Fig. 6.3). The assumption of drier conditions with the establishment of HC is perfectly consistent with our findings and previous studies in these regions which suggested increasingly arid continental conditions from ~2.4-2.0 Ma in concert with HC intensification. Stronger HC may also have participated to strengthen winter Asian monsoon (Jia et al., 2008) and overall, to enhanced precipitation rate over Southeast Asia by affecting changes in zonal atmospheric conditions in the equatorial regions (Brierley et al., 2009). In contrast, the effects on high-latitudes from model simulations are rather mixed (Brierley et al., 2009) (Fig. 6.3). As argued, this may result of large error bars in the paleodata sets. Increased or reduced mean precipitation over northeast America and Greenland is not obvious. However, ice sheet extension in the Northern Hemisphere probably slows down between ~2.0 and ~1.5 Ma as shown by the benthic $\delta^{18}O$ stack (Lisiecki and Raymo, 2005). Was the ice sheets slowdown a climatic consequence of HC intensification and associated influences? To answer this question further studies are however needed.

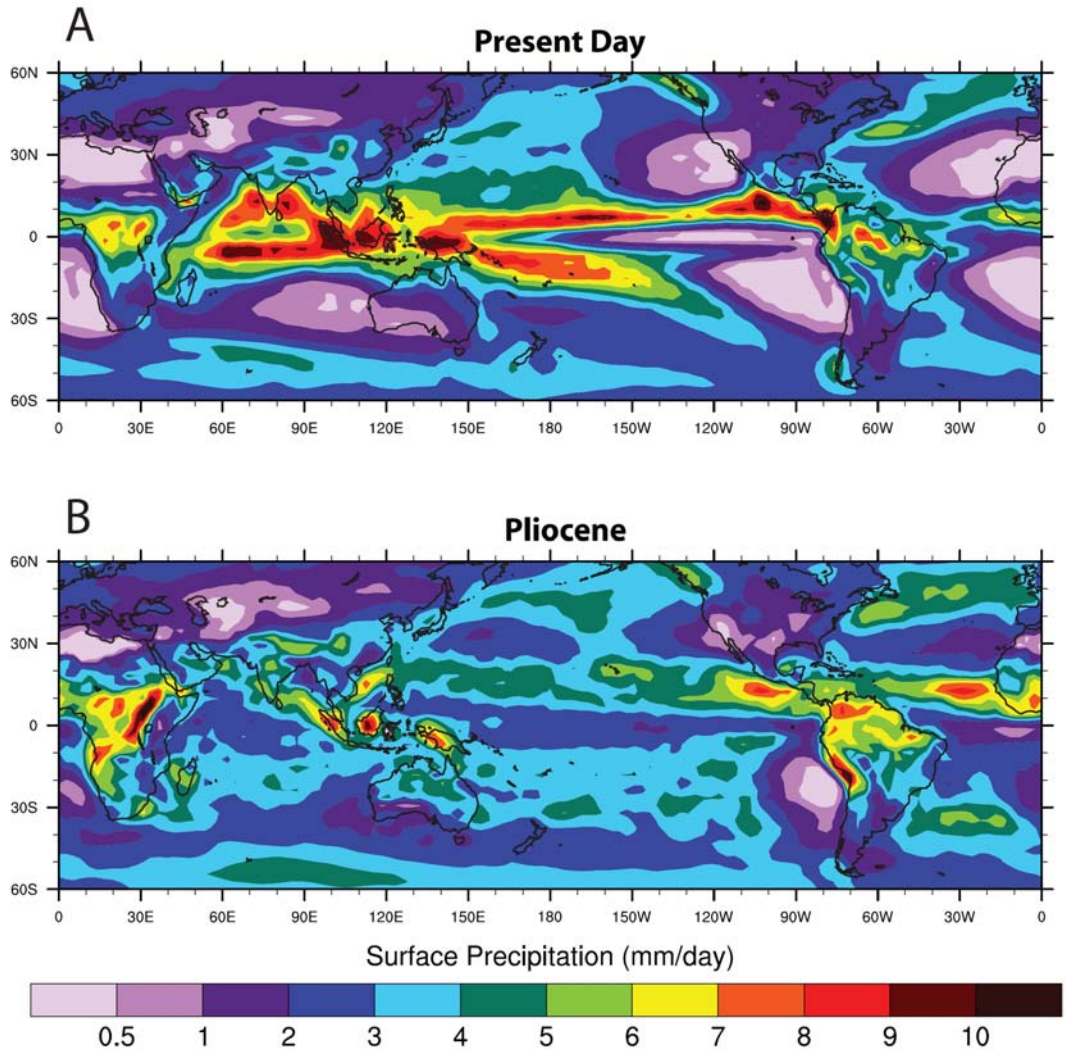

Figure 3. Surface precipitation during the present day (A) and the Pliocene (B) simulated with the atmospheric GCM (CAM3) (Brierley et al., 2009).

6.5 Summary and Conclusions

Overall, our results from two different ocean basins show that both WC and HC synchronously developed during the Plio-Pleistocene around about 2.4-2.0 Ma. The progressive intensification of HC, and associated trade winds, were likely caused by the gradual increase of temperature gradient between high and low latitudes. As the trade winds became stronger, the cool waters from below the shallow thermocline rose to the surface in both coastal and equatorial upwelling systems. The resulting EEP cooling likely augmented the SST asymmetry along the equator in the Pacific, which in turn conducted to the establishment of Walker circulation at the same time, strengthening in line with HC at ~2.0 Ma ago.

A number of uncertainties relates to hypotheses on the potential impact of such atmospheric changes on Plio-Pleistocene climate. While some studies argued that the intensification of WC may have actively participated to ice sheet expansion in the northern high-latitudes by increasing low-cloud cover and surface albedo, resulting in reduced heat release to the North Pacific and temperature decrease over North America (Barreiro et al., 2006), other emphasized that it had only a minor impact on northern high-latitude temperature evolution and ice sheet formation (Haywood et al., 2007). The latter assumption seems further supported by our results, because major changes in both zonal and meridional atmospheric circulation patterns probably occurred from ~2.4-2.0 Ma, which means well after the onset of major NHG around ~3.0 Ma.

6.6 References

Barreiro, M., Philander, G., Pacanowski, R., & Fedorov, A. Simulations of warm tropical conditions with application to middle Pliocene atmospheres. *Climate Dynamics*, **26**, 349-365 (2006).

Brierley, C.M., Fedorov, A.V., Liu, Z., Herbert, T.D., Lawrence, K.T. & LaRiviere, J.P. Greatly expanded tropical warm pool and weakened Hadley circulation in the Early Pliocene. *Science*, **323**, 1714-1718 (2009).

Coates, A.G., & Obando, J.A. The geologic evolution of the Central American Isthmus. In Jackson J.B.C., Budd, N., Coates, A.G. Evolution and Environment in Tropical America, U. Chicago Press, p. 21-56 (1996).

Dekens, P.S., Ravelo, A.C., & McCarthy, M.D. Warm upwelling regions in the Pliocene warm period. *Paleoceanography*, **22**, doi: 10.1029/2006PA001394 (2007).

Dupont, L.M., Donner, B., Vidal, L., Pérez, E.M., & Wefer, G. Linking desert evolution and coastal upwelling: Pliocene climate change in Namibia. *Geology*, **33**, 461-464 (2005).

Dupont, L.M. Late Pliocene vegetation and climate in Namibia (southern Africa) derived from palynology of ODP Site 1082. *Geochemistry, Geophysics, Geosystems*, **7**, doi: 10.1029/2005GC001208 (2006).

Haywood, A.M., Valdes, P.J., & Peck, V.L. A permanent El Niño-like state during the Pliocene?. *Paleoceanography,* **22**, doi: 10.1029/2006PA001323 (2007).

Hsieh, J.C., & Murray, B. A. ~24 000 year period climate signal in 1.7-2.0 million year old Death Valley strata. *Earth and Planetary Science Letters*, **141**, 11-19 (1996).

Jansen, E., Fronval, T., Rack, F., & Channell, J.E.T. Pliocene-Pleistocene ice rafting history and cyclicity in the Nordic Seas during the last 3.5 Myr. *Paleoceanography*, **15**, 709-721 (2000).

Jia, G., Chen, F., & Peng, P. Sea surface temperature differences between the western equatorial Pacific and northern South China Sea since the Pliocene and their paleoclimatic implications. *Geophysical Research Letters*, **35**, doi: 10.1029/2008GL034792 (2008).

Karas, C., Nürnberg, D., Gupta, A.K., Tiedemann, R., Mohan, K., & Bickert, T. Mid-Pliocene climate change amplified by a switch in Indonesian subsurface throughflow. *Nature Geoscience*, doi: 10.1038/ngeo520 (2009).

Lamy, F., Rincon-Martinez, D., Saukel, C., Steph, S., Sturm, A., Etourneau, J., & Tiedemann R., Plio-Pleistocene changes in SE trade wind strength and South American rainfall – Implications for ITCZ movements and long-term El Niño behavior, *Goldschmidt abstract book* (2009).

Lange, C.B., Berger, W.H., Lin, H.L., Wefer, G., & Shipboard Scientific Party Leg 175. The early Matuyama Diatom Maximum off SW Africa, Benguela current system (ODP leg 175). *Marine Geology*, **161**, 93-114 (1999).

Lawrence, K.T., Liu, Z. & Herbert, T.D. Evolution of the eastern tropical Pacific through Plio-Pleistocene glaciation. *Science*, **312**, 79-83 (2006).

Levitus, S., & Boyer, T.P. *World Ocean Atlas 1994*, Ocean Data View (1994).

Lisiecki, L.E. & Raymo, M.E. A Pliocene-Pleistocene stack of 57 globally distributed benthic $\delta^{18}O$ records. *Paleoceanography*, **20**, doi:10.1029/2004PA001071 (2005).

Liu, Z., Altabet, M.A. & Herbert, T.D. Plio-Pleistocene denitrification in the eastern tropical North Pacific: Intensification at 2.1 Ma. *Geochemistry, Geophysics, Geosystems*, **9**, doi: 10.1029/2008GC002044 (2008).

Marlow, J.R., Lange, C.L., Wefer, G., & Rosell-Melé, A. Upwelling intensification as part of the Pliocene-Pleistocene climate transition. *Science*, **290**, 2288-2291 (2000).

Mix, A.C., Tiedemann R. & Blum P. *Proceedings of the Ocean Drilling Program Initial Reports*, **202,** College Station, Tex (2003).

Müller, P.J., Kirst, G., Ruhland, G., von Storch, I., & Rosell-Melé, A. Calibration of the alkenone paleotemperature index U^{K}_{37} based on core-tops from the eastern South Atlantic and the global ocean (60°N-60°S). *Geochimica et Cosmochimica Acta*, **62**, 1757-1772 (1998).

Philander, S.G., & Fedorov, A. Role of tropics in changing the response to Milankovitch forcing some threee million years ago. *Paleoceanography*, **18**, doi: 10.1029/2002PA000837 (2003).

Ravelo, A.C., Andreasen, D.H., Lyle, M., Olivarez Lyle, A., & Wara, M. Regional climate shifts caused by gradual global cooling in the Pliocene epoch. *Nature*, **429**, 263-267 (2004).

Raymo, M.E., Lisiecki, L.E., & Nisancioglu, K.H. Plio-Pleistocene ice volume, Antarctic climate, and the global $\delta^{18}O$. *Scienc*e, **313**, 492-495 (2006).

Sonzogni, C., Bard, E., Rostek, F., Lafont, R., Rosell-Melé, A., & Eglinton, G. Core-top calibration of the alkenone index vs sea surface temperature in the Indian Ocean. *Deep-Sea Research II*, **44**, 1445-1460 (1997).

Wara, M., Ravelo, A.C., & Delaney, M.L. Permanent El Niño-like conditions during the Pliocene warm period. *Science*, **309**, 758-761 (2005).

Woodruff, S.D., Diaz, H.F., Elms, J.D., & Worley, S.J. COADS Release 2 data and metadata enhancements for improvements of marine surface flux fields. *Physics and Chemistry of the Earth*, **23**, 517-526 (1998).

Chapter VII

General Conclusions

The Pliocene-Pleistocene climate transition between ~3.5 and 0.5 Ma has been reconstructed from sedimentary records of two high productive low-latitudes upwelling regions, the Benguela Upwelling System (BUS) and the Eastern Equatorial Pacific (EEP). High resolution alkenone-sea surface temperature (SST), phytoplankton productivity-related proxies (alkenone concentration, total nitrogen, organic carbon and opal) and bulk nitrogen isotopes ($\delta^{15}N$) records were generated at the BUS Site 1082 and the EEP Site 1239 in order to monitor past changes in coastal and open waters upwelling activity, biological production and nutrient distribution.

8.1 The Plio-Pleistocene BUS

The new alkenone-derived SST record at Site 1082 indicated two periods of profound cooling between ~3.0-2.0 Ma and ~1.5-0.5 Ma, consistent with previous findings performed at the BUS Site 1084 (Marlow et al., 2000). However, the meridional SST gradient between both sites increased around ~2.4-2.0 Ma suggesting a major regional oceanic reorganization, a transition from a state dominated by stratified surface water conditions, with short periods of subsurface water upwelling, towards longer and stronger permanent upwelling activity. This assumption is supported (1) by diatom assemblages and (2) pollen data. On one hand, mat-forming diatom species, growing within stable and stratified water-column conditions, dominated the sedimentary record between ~3.0-2.0 Ma, while other taxa, typical of water-column mixing, appeared and progressively replaced diatom-mats from 2.0 Ma onwards (Lange et al., 1999). On the other hand, the Site 1082 pollen record revealed an enhancement of continental aridity starting at ~2.0 Ma (Dupont et al., 2006), interpreted as an indicator of stronger wind-driven upwelling activity, when cool waters limited evaporation over the ocean and hence rainfall over the continent.

Synchronous to the two cooling steps concurred two maximum of phytoplankton productivity. These two high productive periods have probably corresponded to two different oceanic regimes, and two different sources of nutrients. From ~3.0 to 2.4 Ma, stratified waters were likely accompanied of a shallow thermocline allowing the feeding of mat-forming diatoms and sporadically of coccolithophorids when the thermocline reached the surface through short upwelling intervals. In contrast, from ~2.4-2.0 Ma, intense coastal upwelling off Namibia became perennial, resulting in another type of nutrient-stimulated productivity.

In addition, the interval 2.4-2.0 Ma was also marked by a change of nutrient sources. Indeed, the low $\delta^{15}N$ values prior to ~2.4 Ma, close to those of the Antarctic Site 1096 (Sigman et al.,

2004), suggest that Antarctic intermediate waters (AAIW) probably fed the subsurface waters circulating under the thermocline in the Benguela region. In contrast, the development of a modern-like polar front system in the Southern Ocean at about 2.0 Ma led to Subantarctic mode water (SAMW) formation, lowering the equatorward circulation depth of AAIW, and replacing AAIW as the main source of nutrients entering the Benguela through nutrient-rich upwelled waters, as illustrated by the low $\delta^{15}N$ difference between Site 1082 and the Subantarctic Site 1096. This major finding is further supported by a similar study off California (Liu et al., 2008) and suggests that the Southern Ocean reorganization since 2.4 Ma probably regulated a significant part of the phytoplankton productivity through the nutrient distribution into the low-latitudes coastal upwelling areas.

8.2 The Plio-Pleistocene EEP

Contrary to the Benguela region, SST reconstruction at the EEP Site 1239 did not indicate a stepwise cooling during the Plio-Pleistocene climate transition, but instead two cooling periods between ~2.8-1.6 Ma and 1.4-0.8 Ma, interrupted by two intervals of warming between ~1.6-1.4 and 0.8-0.5 Ma. Around ~0.5 Ma, the EEP Site 1239 SST was only 2°C cooler than during the end of the warm Pliocene period (prior to 3.0 Ma) which draws a different picture than that at the previously studied Eastern Pacific sites (Lawrence et al., 2006; Dekens et al., 2007; Wara et al., 2005, Liu et al., 2008). This different pattern may have been tied to the location of Site 1239, influenced by both equatorial upwelling and warm pool conditions.

Also different to the Benguela region, alkenone-SST variations at EEP Site 1239 did not covary with the local primary productivity. Apparently, productivity-related proxies indicated a net increase during both warm (from ~3.2-2.8 Ma) and cold (~1.6-1.4 Ma) surface waters conditions. Thus, the regional oceanic circulation tied to upwelling activity or migration of the warm pool were unlikely the main driver of local productivity changes. Instead, the phytoplankton growth probably primarily responded to changes in the source of nutrients supply.

The $\delta^{15}N$ record at Site 1239, used here as an indicator of past changes in nutrient supply, indicated minimum values during the highest productive periods, and inversely, higher values during low productive periods. In addition, $\delta^{15}N$ values never exceeded 4-5‰ since the Pliocene which implies that the nitrate pool was not fully utilized over the last 3.0 Ma because nitrate was

probably largely supplied into the EEP, and hence, nitrate was unlikely a limiting factor for phytoplankton growth.

In contrast, the EEP biological production perfectly varied in concert with variations in supply of micronutrients as inferred by outstanding similarities between changes in high-resolution records of iron (Fe) content and productivity-related proxies. Two major pulses of Fe input occurred at ~3.2 and ~1.9 Ma and were accompanied by substantial increases of productivity as indicated by increased total nitrogen, organic carbon and alkenone MARs. These results suggest that enhanced Fe supply either from terrestrial (aeolian or fluvial) input and/or subsurface water mass transported by EUC have episodically fertilized the EEP surface waters and therefore triggered phytoplankton blooms. Certain studies asserted that the enhanced biological pump efficiency may have had an influence on the atmospheric CO_2 level, the atmospheric CO_2 drawdown being hypothesized as the most plausible cause for explaining the Pliocene cooling (Lunt et al., 2008). However, no clear evidence between climate changes and EEP productivity has been found; the two maxima of productivity never concurred with climatic events. It is therefore questionable if EEP productivity may have played, or not, a role on the Plio-Pleistocene climate changes, or had only a minor impact.

8.3 Tropical and subtropical atmospheric circulations

SST gradients across ocean basins were used to reconstruct Plio-Pleistocene changes in both zonal, or Walker (WC), and meridional, or Hadley (HC), atmospheric circulations because changes in latitudinal or longitudinal SST gradients can strengthen or weaken both atmospheric patterns. Across the equatorial Pacific Ocean, the east-to-west SST gradient between the EEP Site 1239 and the Western Equatorial Pacific Site 806 irreversibly increased by ~2°C over the past ~2.2 Ma, suggesting a strengthening of WC 600-800 kyr later than the onset of Northern Hemisphere glaciation. In comparison, the meridional SST gradient across the Benguela region, monitoring past changes in wind-driven upwelling activity, also increased by 4°C from ~2.4-2.0 to 0.8 Ma. This SST gradient shift has been interpreted as the result of HC intensification. This finding is further corroborated by studies implying a concomitant strengthening of HC in the Western Pacific (Jia et al., 2008), and in the Eastern Tropical South Pacific (Lamy et al., 2009), as well as by evidence for the shoaling of the thermocline reported off California around ~2.1 Ma (Liu et al., 2008) and the subsequent continental aridification (Hsieh et al., 1996), strongly suggesting enhanced trade winds in the Eastern Tropical North Pacific at about ~2.0 Ma.

Synchronous increase of both zonal and meridional SST gradients implies that the development of WC and HC was intimately coupled during the Plio-Pleistocene. The pole to equator temperature gradient probably increased through the Plio-Pleistocene cooling, and reinforced the atmospheric pressure gradient between oceanic and continental low pressure systems. The resulting increasing pressure gradient probably intensified trade winds, and hence HC, which led to the increase of the upwelling in coastal regions, but also in open ocean areas such as in the EEP, where strong wind convergence fostered the thermocline to shoal. As a result, the EEP cooling associated to relatively stable western equatorial Pacific SSTs increased together the zonal SST asymmetry and led to the development of WC.

The intensification of HC and WC probably had a strong influence on environmental conditions in tropical and subtropical regions. On one hand, the strengthening of HC may have, through enhanced coastal upwelling, increased arid conditions in the regions bordering the major eastern boundary currents, e.g. Namibia, California and Peru (Brierley et a., 2009; this study). On the other hand, changes in WC may have probably regulated the monsoon regime and precipitation rates throughout the tropics (Brierley et a., 2009). However, the effects of both HC and WC establishment on high latitudes climate remain uncertain, because the major expansion of ice sheets in the Northern Hemisphere occurred well before (~3.0 Ma ago) than the development of both atmospheric patterns (~2.4-2.0 Ma ago).

Chapter VIII

Perspectives

Over the last decade, the Pliocene-Pleistocene climatic transition has attracted many researchers to study the causes and the consequences of this global climate shift in a variety of high resolution settings for associated changes in continental ice sheet growth, ocean circulation, distribution of nutrients and atmospheric changes. This is of particular interest owing to the potential resemblance between the warm Pliocene climate conditions and those predicted for the near future. However, a strong lack of knowledge still exists with respect to the linkages between Plio-Pleistocene climate changes and low-to-high latitudes ocean-atmosphere interactions.

8.1 Sea surface temperature distribution

First, the cause-to-effect relationship between global SST reorganization and high latitudes ice accumulation during the Plio-Pleistocene cooling is not well understood. As illustrated in figure 8, SSTs were not homogeneously warmer during the end of the Pliocene warmth than today (according to the SST proxies and the different calibrations applied). For instance, SST values in the Pacific and Indian warm pools (Karas et al., 2009; Groenveld et al., 2006; Wara et al., 2005; **Chapter VI**) seem relatively similar to the modern ones, or even colder. In addition, zonal and meridional SST gradients were also different as previously demonstrated by recent studies (Brierley et al., 2009; Jia et al., 2008) as well as in **Chapter VI**, and confirmed by the SST mapping during the Pliocene warmth (Fig. 8). This observation suggests that the moisture and heat transfers between low and high latitudes probably had a great impact on global climate.

Model experiments simulated the impact that may have resulted from such a SST pattern on Pliocene climate and ice cover in the northern high latitudes (Barreiro et al., 2005; Philander and Fedorov, 2003; Haywood et al., 2007). However, the conclusions drawn from these experiments remain still controversial. This is partly due to the lack of high-resolution SST records in certain oceanic areas. While in the North Atlantic, the Pliocene SSTs are relatively well studied (Bartoli et al., 2005; 2006; Lawrence et al., 2006; Robinson et al., 2008), in contrast, Pliocene SST records are lacking in the North Pacific as well as in the Antarctic zone of the Southern Ocean. Yet, the long term SSTs variations in the western Atlantic and the Caribbean warm pool are still poorly known, especially for the end of the Pliocene warmth (~3.2-3.0 Ma). This is however of primary relevance when considering the close relationship between the western equatorial Atlantic warm pool conditions and the North Atlantic drift strength, modulating European climate. Thus, a first perspective would be to select Ocean Drilling Program Sites located in strategic areas, to generate SST records, at least for the end of the Pliocene warmth (~3.2-3.0 Ma), and to compare them to

the modern times. This would substantially improve our understanding of the low-to-high latitudes ocean-atmosphere interactions on the Pliocene climate, and subsequently improve predictions for the near future. This would also considerably help to scrutinize and better understand changes in atmospheric circulation in warmer-than-today climate, because SST variability is a direct driver of atmospheric circulation.

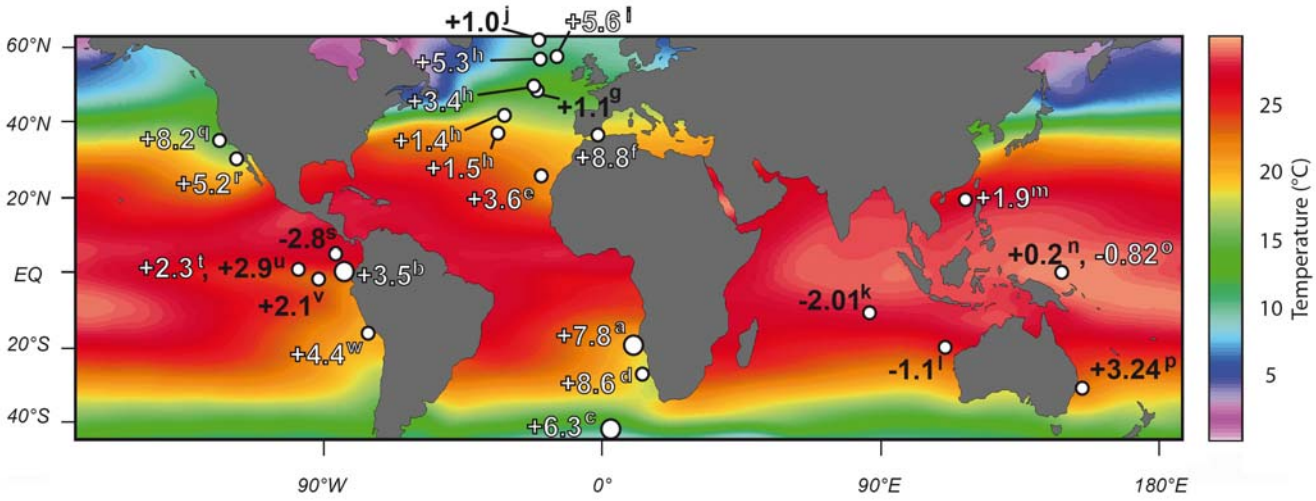

Figure 8. Mid-Pliocene (~3.2-3.0 Ma) alkenone- and Mg/Ca-based SST minus modern mean annual SST at 10 m water depth (in colour) (Levitus and Boyer, 1994) for Sites (a) 1082 (Etourneau et al., 2009, **Chapter IV**), (b) 1239 (Etourneau et al., in review, **Chapter V**), (c) 1090 (unpublished data), (d) 1084 (Marlow et al., 2000); (e) 658 (Herbert et al., 1998), (f) 978 (Khélifi et al., 2009), (g) 609 (Bartoli et al., 2006), (h) 552, 609, 607, and 606 (Robinson et al., 2008), (i) 982 (Lawrence et al., 982), (j) 984 (Bartoli et al., 2005), (k) 214 (Karas et al., 2009), (l) 763 (Karas et al., in prep), (m) 1147/48 (Jia et al., 2008), (n) 806 (Wara et al., 2005), (o) 806 (Etourneau et al., in prep., **Chapter VI**), (p) 590 (Karas et al., in prep), (q) 1014 (Dekens et al., 2007), (r) 1012 (Liu et al., 2008), (s) 1241 (Groenveld et al., 2006), (t) 847 (Dekens et al., 2007), (u) 847 (Wara et al., 2005), (v) 846 (Lawrence et al., 2006), and (w) 1237 (Dekens et al., 2007). White numbers indicate alkenone-SST and black numbers Mg/Ca-SST. Note that depending on the calibrations used for alkenone- or Mg/Ca-SST reconstructions, slight differences might appear (see Medina-Elizalde et al., 2008).

8.2 Biogeochemical cycles

Investigating the links between biogeochemical cycles and long-term climate change have been a long-standing objective of paleoclimate research, especially because the biogeochemical cycles may have significantly contributed to variations in greenhouse gases. As shown in the low-latitudes Benguela, EEP, and California upwelling systems, the denitrification/nitrogen fixation ratio was probably lower during the warm Pliocene and increased through the global climate cooling (Liu et al., 2008; **Chapters IV** and **V**). This implies that more fixed nitrogen was available for phytoplankton productivity during the Pliocene and less during the Pleistocene. However, due to more stratified water conditions during the Pliocene, the large fixed nitrogen pool was probably not fully utilized. The transition from more to less fixed nitrogen availability during the Plio-Pleistocene was reflected by the increasing trend in all nitrogen isotopes ($\delta^{15}N$) records between ~2.4-2.0 Ma, and was ascribed to the occurrence of a modern-like frontal system in the Southern Ocean which increased poor-oxygenated water export to low latitudes, denitrification in some coastal upwelling regions (e.g. California), and hence the reduction of available fixed nitrogen. However, it is still debatable if this was we the unique factor responsible of continuous reduction of fixed nitrogen in the surface oceans over the past 3.5 Ma since shifts of $\delta^{15}N$ did not occur perfectly synchronously. Was the global $\delta^{15}N$ trend recorded in upwelling regions only a response to a global ocean denitrification/nitrogen fixation ratio increase tied to changes in intermediate water circulation? Do similarities in the $\delta^{15}N$ patterns and absolute values exist over the last 5 Ma between the low-latitude upwelling system in the eastern Pacific, southeastern Atlantic, and western Indian Oceans? Can these similarities allow us to generalize about the intensity of denitrification expected during warm climate states? To what extent did the development of the denitrification zones affect the global climate since the Pliocene through increasing or decreasing the atmospheric CO_2 sequestration into the deep ocean?

To answer these questions, the biogeochemical processes have to be further explored, especially in high productive regions where denitrification processes are important. For instance, the Arabian Sea is one of the main loci for coastal and water column denitrification in the world's ocean, a process affecting greenhouse gases through the marine nitrogen inventory and the biological pump. Indeed, strong denitrification is known to reduce the effect of the biological pump on atmospheric CO_2 sequestration by reducing bioavailable fixed nitrogen (Ganeshram et al., 1995; Altabet et al., 1999, 2002). However, suboxic conditions likely alternated with oxic states over the last 60 Ka, as illustrated in the Arabian Sea for instance, which implies that water-column denitrification was

likely variable through warm and cold periods (Altabet et al., 2002). Although reduced denitrification may have been partially offset globally by reduced nitrogen fixation elsewhere (Ren et al., 2009), the close relationship reported between records of denitrification and atmospheric CO_2 recorded in the Antarctic ice cores suggest that on the whole, biological pump efficiency may have been greater during oxic phases (Altabet et al., 2002).

A recent study from the California margin showed that denitrification in the water-column may have been absent during the warm Pliocene and likely started to develop at 2.0 Ma (Liu et al., 2008). As also demonstrated in **Chapters IV** and **V**, the denitrification/nitrogen fixation ratio was likely lower during the Pliocene, thus resulting in a higher dissolved nitrate pool in the warm Pliocene ocean (**Chapters IV** and **V**). This is not what might be expected from glacial-interglacial studies indicating that warm interglacials are typically characterized by more, not less, denitrification possibly due to lower oxygen solubility in intermediate water formation areas (Galbraith et al., 2004; Meissner et al., 2005). The Plio-Pleistocene increase in denitrification as climate cooled has been attributed to a shoaling of the thermocline in the California margin as well as to a development of modern-like frontal system in the Southern Ocean. This could have altered the marine nitrogen inventory, and contributed to the slowdown of the Plio-Pleistocene cooling by limiting the biological pump efficiency (Liu et al., 2008).

Thus, long-term changes in both denitrification and nitrogen fixation in high productive regions may highlight the linkage between atmospheric CO_2 variations and nitrogen cycling, especially since a recent model study attributed the global Pliocene cooling to significant atmospheric CO_2 drawdown (Lunt et al., 2008). The cause of the CO_2 drawdown is unknown. Because of the importance of the Arabian Sea to the global oceanic nitrogen budget, it is urgent to explore variations in denitrification for the Plio-Pleistocene in the Arabian Sea and to extend previous records beyond 1.0 Ma (Altabet et al., 1999). Could a trend toward more denitrification and less nitrogen fixation with global cooling, as seen in the upwelling regions (Liu et al., 2008; **Chapters IV** and **V**), be a global characteristic and integral component of the Plio-Pleistocene climatic transition? If so, then this would suggest that the relationship between climate and denitrification during the cold Pleistocene glacial-interglacial transitions (i.e., more denitrification in warm periods) is reversed compared to the relationship between denitrification and climate in a warmer climate state. To explore whether pelagic denitrification evolved globally through the Plio-Pleistocene it is critical to obtain nitrogen isotopic records from marine sediments in the Arabian Sea.

8.3 Application of new proxies

8.3.1 Nitrogen and carbon isotopic composition of porphyrins

In this study as well as in most of the previous works aiming to reconstruct past nitrogen cycling, the nitrogen isotopic ($\delta^{15}N$) ratio was measured on bulk organic matter preserved in marine sediments. However, as illustrated in earlier studies, the bulk isotopic composition of the organic matter may be altered during its sinking through the water column by bacterial degradation and/or during its burial in the sediments by diagenesis effects (Altabet and Francois, 1994; Sachs and Repeta, 1999). In addition, it may have incorporated the $\delta^{15}N$ signal of the terrestrial organic matter (see **Chapter II**). In this study, diagenesis effects and terrestrial organic matter influence were not found to have affected the Plio-Pleistocene $\delta^{15}N$ in the Benguela and EEP. However, depending on the studied regions in the framework of future research, it is crucial to consider such effects when reconstructing the past nitrogen cycling with the bulk ^{15}N, especially because the effects can be as large as the primary signal (Altabet and Francois, 1994; Sachs and Repeta, 1999).

For circumventing such issue, another perspective would be to provide Plio-Pleistocene nitrogen isotopic records from the porphyrins, the degradation products of the chlorophyll, hypothesized to be an ideal biomarker of past nitrogen cycling (Higgins et al., 2009; Kashiyama et al., 2008), or from matrice-bound in foraminifera (Ren et al., 2009) and diatoms (Galbraith, 1997). While the later would be of particular interest for the period of maximum diatom productivity in the Benguela between ~3.0 and 2.0 Ma, the application of diatom- (or foraminifera-) bound $\delta^{15}N$ can also be altered by diagenesis effects. Contrary to the bulk $\delta^{15}N$ recording the isotopic signal of all the organic matter preserved in the sediments, the porphyrin $\delta^{15}N$ only reflect the isotopic signal of the phytoplankton primary producers, and therefore may record the isotopic fractionation occurring in the euphotic zone during the phytoplankton photosynthesis much better than that bulk organic matter. The nitrogen isotopic composition of the sedimentary porphyrins has been successfully applied from modern sediments as well as from Precambrian/Cambrian sediments, thus supporting the robustness of its preservation within the sediments for long time periods (Chicarelli et al., 1993; Sachs and Repeta, 1999). Furthermore, it is possible to measure the carbon isotopic compositions on the same sedimentary porphyrin fraction which could reveal a casual relationship between both nitrogen and carbon cycles variations. This would be of primary importance when considering that the variations of atmospheric CO_2 level over the past 3.0 Ma have never been explored yet, although it is thought to be one the main factor driving to the Pliocene cooling (Lunt

et al., 2008). Until now, one study attempted to assess the atmospheric CO_2 concentration but this estimation was restricted to the Pliocene warm period (Raymo et al., 1996). Thus, it appears critical to provide such long records for improving our understanding of the Plio-Pleistocene climate change.

8.3.2 Silicon isotopes

One of the main limiting nutrients which have not been fully considered in this study is the silicic acid supply. It has been hypothesized that the silica leakage from the Antarctic Ocean to the Benguela upwelling system may have triggered the Matuyama Diatom Maximum, the high-productive event mat-forming diatoms between ~3.0-2.0 Ma (**Chapter IV**). This silicic acid diffusion into the low latitudes coastal and open waters upwelling regions around ~3.0 Ma was also worldwide expressed as suggested by the synchronously enhanced opal burial in these regions (Cortese et al., 2005) and may have influenced global climate because the primary productivity related to this high opal sinks, mainly diatoms, in low latitudes upwelling systems could have been sufficiently efficient to have substantially enhanced atmospheric CO_2 sequestration to the deep ocean.

To scrutinize the past distribution of silicic acid into the high productive regions in low latitudes, the silicon isotopes ($\delta^{30}Si$) measured on diatoms can be used. The first studies applying this new proxy focused on the analyses of river waters (Georg et al. 2006b) and sea water (Reynolds et al., 2006). Recent work has also focused on the analyses and interpretation of the Si isotope composition of diatoms in the North Pacific Ocean, which showed a very distinct transition 2,73 million years ago marking a change from a Si-limited surface ocean to a Fe- and nitrate-limited situation thereafter (Reynolds et al., 2007). The $\delta^{30}Si$ and $\delta^{15}N$ records reveal a clear anticorrelation across this time which is explained by a change in iron supply to the surface waters of the North Pacific, the diatom productivity of which were iron-limited at that time (see also Brzezinski et al., 2002, for the Southern Ocean). These findings together with previous results for Si and N isotope fractionation from the Southern Ocean (e.g. Francois et al., 1997) could serve as a basis for the interpretation of the new record of the Benguela upwelling and may also reveal new information in the EEP once executed. In addition to the previously cited proxies, this may give a new overview of the marine productivity and nutrient cycling over the past 3.0 Ma and additionally, can give new insights on the role played by the biological production in the low-latitude oceanic regions on the Plio-Pleistocene climate.

References for chapters I-III and VII-VIII

Altabet, M.A., & Francois, R. Sedimentary nitrogen isotopic ratio as a recorder for surface ocean nitrate utilization. *Global Biogeochemical Cycles*, **8**, 103-116 (1994).

Altabet, M.A., Francois, R., Murray, D.W., & Prell, W.L. Climate related variations in denitrification in the Arabian Sea from sediment 15N/14N ratios. *Nature*, **373**, 506-509 (1995).

Altabet, M.A., Murray, D.W., & Prell, W.L. Climatically linked oscillations in Arabian Sea denitrification over the past 1 m.y.: Implications for the marine N cycle. *Paleoceanography*, **14**, 732-743 (1999).

Altabet, M.A., Higginson, M.J., & Murray, D.W. The effect of millennial-scale changes in Arabian Sea denitrification on atmospheric CO_2. *Nature*, **415**, 159-162 (2002).

Barreiro, M., Philander, G. Pacanowski, R., & Fedorov, A. Simulations of warm tropical conditions with application to middle Pliocene atmospheres. *Climate Dynamics.*, **26**, 349-365 (2006).

Bartoli, G., Sarnthein, M., Weinelt, M., Erlenkeuser, H., Garbe-Schönberg, D., & Lea, D.W. Finale closure of Panama and the onset of northern hemisphere glaciation. *Earth and Planetary Science Letters*, **237**, 33-44 (2005).

Bartoli, G., Sarnthein, M., & Weinelt, M. Late Pliocene millennial-scale climate variability in the northern North Atlantic prior to and after the onset of Northern Hemisphere glaciation. *Paleoceanography*, **21**, doi: 10.1029/2005PA001185 (2006).

Behl, R. J., & Kennett, J.P. Brief interstadial events in the Santa Barbara basin, NE Pacific, during the past 60 kyr. *Nature*, **379**, 243-246 (1996).

Brierley, C.M., Fedorov, A.V., Liu, Z., Herbert, T.D., Lawrence, K.T., & LaRiviere, J. Greatly expanded tropical warm pool and weakened Hadley circulation in the Early Pliocene. *Science*, **323**, 1714-1718 (2009).

Brandes, J. A., & Devol, A.H. A global marine-fixed nitrogen isotopic budget: Implications for Holocene nitrogen cycling. *Global Biogeochemical Cycles*, **16**, 1120 (2002).

Brassell, S.C., & Dumitrescu, M. Recognition of alkenones in a lower Aptian porcellanite from the west-central Pacific. *Organic Geochemistry*, **35**, 181-188 (2004).

Bruland, K.W., Rue, E.L., Smith, G.J., & DiTullio, G.R. Iron, micronutrients and diatom blooms in the Peru upwelling regime: brown and blue waters off Peru. *Marine Chemistry*, **93**, 81-103 (2005).

Brzezinski, M.A., Pride, C.J., Franck, V.M., Sigman, D.M., Sarmiento, J.L., Matsumoto, K., Gruber, N., Rau, G.H., & Coale, K.H. A switch from $Si(OH)_4$ to NO^{3-} depletion in the glacial Southern Ocean. *Geophysical Research Letters*, **29**, doi:10.1029/2001GL014349 (2002).

Cane, M.A. El Niño. *Annual Review of Earth and Planetary Sciences*, **14**, 43-70 (1986).

Carr, M.E. Estimation of potential productivity in Eastern Boundary Currents using remote sensing. *Deep-Sea Research II*, **49**, 59-80 (2002).

Chicarelli, M.I., Hayes, J.M., Popp, B.N., Eckardt, C.B., & Maxwell, J.R. Carbon and nitrogen isotopic compositions of alkyl porphyrins from the Triassic Serpiano oil shale. *Geochimica et Cosmochimica Acta*, **57**, 1307-1311 (1993).

Cline, J. D. & Kaplan, I. R. Isotopic fractionation of dissolved nitrate during denitrification in the eastern tropical North Pacific Ocean. *Marine Chemistry*, **3**, 271-299 (1975).

Conkright, M.E., Locarnini, R.A., Garcia, H.E., O´Brien, T.D., Boyer, T.P., Stephens, C., Antonov, J.I. World Ocean Atlas 2001: Objectives Analyses, Data Statistics, and Figures, CD-ROM Documentation. National Oceanography Data Center, Silver Spring, MD., 17 pp (2002).

Codispoti, L. A., & Christensen, J. P. Nitrification, Denitrification and Nitrous Oxide Cycling in the Eastern Tropical South Pacific Ocean, *Maine Chemistry* **16**, 277-300 (1985).

Codispoti, L. A., Brandes, J.A., Christensen, J.P., Devol, A.H., Naqvi, S.W.A., Paerl, H.W., & Yoshinari, T. The oceanic fixed nitrogen and nitrous oxide budgets: Moving targets as we enter the anthropocene?. *Scientia Marina*, **65**, 85-105 (2001).

Codispoti, L. A., Yoshinari, T., & Devol, A.H. Suboxic respiration in the oceanic water column, in *Respiration in Aquatic Ecosystems*, edited by del Giorgio, P. and P. J. LeB. Williams, 328, Oxford University Press, Cambridge, UK (2005).

Conte, M.H., Eglinton, G., & Madureira, L.A.S. Long-chain alkenones and alkyl alkenoates as paleotemperature indicators: their production, flux and early sedimentary diagenesis in the Eastern North Atlantic. *Organic Geochemistry*, **19**, 287-298 (1992).

Conte, M. H., & Eglinton, G. Alkenone and alkenoate distributions within the euphotic zone of the eastern North Atlantic: Correlation with production temperature. *Deep-Sea Research I*, **40**, 1935–1961 (1993).

Conte, M. H., Thompson, A., & Eglinton, G. Lipid biomarker diversity in the coccolithophorid Emiliania huxleyi (Prymnesiophyceae) and the related species Gephyrocapsa oceanica, *Journal of Phycology*, **31**, 272–282 (1995).

Conte, M.H., Weber, J.C., King, L.L., & Wakeham, S.G. The alkenone temperature signal in western North Atlantic surface waters. *Geochimica et Cosmochimica Acta*, **65**, 4275-4287 (2001).

Conte, M.H., Sicre, M-A., Rülhemann, C., Weber, J.C., Schulte, S., Schulz-Bull, D., & Blanz, T. Global temperature calibration of the alkenone unsaturation index ($U^{k'}_{37}$) in surface waters and comparison with surface sediments. *Geochemistry Geophysics Geosystems*, **7**, doi: 10.1029/2005GC001054 (2006).

Cortese, G., Gersonde, R., Hillenbrand, C.-L. & Kuhn, G. Opal sedimentation shifts in the world over the last 15 Myr. *Earth and Planetary Science Letters*, **224**, 509-527 (2004).

Dekens, P.S., Ravelo, A.C., & McCarthy, M.D. Warm upwelling regions in the Pliocene warm period. *Paleoceanography*, **22**, doi: 10.1029/2006PA001394 (2007).

Dekens, P.S., Ravelo, A.C., McCarthy, M.D. & Edwards, C.A. A 5 million year comparison of Mg/Ca and alkenone paleothermometers. *Geochemistry Geophysics Geosystems*, **9**, doi: 10.1029/2007GC001931 (2008).

Deutsch, C., Sigman, D.M., Thunell, R.C., Meckler, A.N., & Haug, G.H. Isotopic constraints on glacial/interglacial changes in the oceanic nitrogen budget. *Global Biogeochemical Cycles*, **18**, doi:10.1029/2003GB002189 (2004).

Driscoll, N.W., & Haug, G.H. A short circuit in thermohaline circulation: a cause for Northern Hemisphere Glaciation. *Science*, **282**, 436-438 (1998).

Dugdale, R.C., Lyle, M., Wilkerson, F.P. Chai, F., Barber, T., & Peng, T.H. Influence of equatorial diatom processes on Si deposition and atmospheric CO_2 cycles at glacial/interglacial timescales. *Paleoceanography*, **19**, doi: 10.1029/2003PA000929 (2004).

Dupont, L.M., Donner, B., Vidal, L., Pérez, E.M., & Wefer, G. Linking desert evolution and coastal upwelling: Pliocene climate change in Namibia. *Geology*, **33**, 461-464 (2005).

Dupont, L.M. Late Pliocene vegetation and climate in Namibia (southern Africa) derived from palynology of ODP Site 1082. *Geochemistry Geophysics Geosystems*, **7**, doi: 10.1029/2005GC001208 (2006).

Emeis, K.-C., Anderson, D.M., Doose, H., Kroon, D., & Schulz-Bull, D. Sea-surface temperatures and the history of monsoon upwelling in the northwest Arabian Sea during the last 500,000 years. *Quaternary Research,* **43**, 355-361 (1995).

Epstein, B.L., D´Hondt, S., & Hargraves, P.E. The possible metabolic role of C37 alkenones in Emiliania huxleyi. *Organic Geochemistry*, **32**, 867-875 (2001).

Ettwein, V.J., Stickley, C.E., Maslin, M.A., Laurie, E.R., Rosell-Melé, A., Vidal, L., & Brownless, M. Fluctuations in productivity and upwelling intensity at Site 1083 during the intensification of the Northern Hemisphere glaciation (2.40-2.65 Ma). *Proceedings of the Ocean Drilling Program Scientific Results*, **175**, 1-25 (2001).

Farrell, J.W., Pedersen, T.F., Calvert, S.E. & Nielsen, B. Glacial-interglacial changes in nutrient utilization in the equatorial Pacific Ocean. *Nature*, **377**, 514-517 (1995).

Fedorov, A.V., Dekens, P.S. McCarthy, M.D. Ravelo, A.C. deMenocal, P.B. Barreiro, M. Pacanowski, R.C., & Philander, S.G. The Pliocene Paradox (Mechanisms for a permanent El Niño). *Science*, **312**, 1485-1489 (2006).

Francois, R., Altabet, M.A., Yu, E-F., Sigman, D., Bacon, M.P., **Frank, M.**, Bohrmann, G., Bareille, G., & Labeyrie, L. Contribution of Southern Ocean surface-water stratification to low atmospheric CO_2 concentrations during the last glacial period. *Nature*, **389**, 929-935 (1997).

Galbraith, E.D. Interactions between climate and the marine nitrogen cycle on glacial-interglacial timescales, Thesis, University of British Columbia (1997).

Galbraith, E. D., Kienast, M., Pedersen, T.F. & Calvert, S.E. Glacial-interglacial modulation of the marine nitrogen cycle by high-latitude O_2 supply to the global thermocline. *Paleoceanography*, **19** (2004).

Ganeshram, R.S., Pedersen, T.F., Calvert, S.E., & Murray, J. Large changes in oceanic nutrient inventories from glacial to interglacial periods. *Nature*, **376**, 755-758 (1995).

Ganeshram, R.S., Pedersen, T.F., Calvert, S.E., & Francois, R. Reduced nitrogen fixation in the glacial ocean inferred from changes in marine nitrogen and phosphorus inventories. *Nature*, **415**, 156-159 (2002).

Georg, R.B., Reynolds, B.C., Frank, M., & Halliday, A.N. Mechanisms controlling the silicon isotopic compositions of river waters. *Earth and Planetary Science Letters*, **235**, 95-104 (2006b).

Gordon, A.L., Bosley, K.T., & Aikmann F. Tropical Atlantic water within the Benguela upwelling system at 27°S. *Deep-Sea Research I*, **42**, 1-12 (1995).

Gripp, A.E., & Gordon, R.G. Current plate velocities relative to the hotspots incorporating the NUVEL-1 global plate motion model. *Geophysical Research Letters*, **17**, 1109-1112 (1990).

Gruber, N. & Sarmiento, J. L. Global patterns of marine nitrogen fixation and denitrification, *Global Biogeochemical Cycles*, **11**, 235-266 (1997).

Gruber, N. The dynamics of the marine nitrogen cycle and its influence on atmospheric CO_2 variations, in *Carbon-climate interactions*, edited by Follows, M. J. and T. Oguz, 1-47, John Wiley & Sons, New York (2004).

Haug, G.H., & Tiedemann, R. Effect of the formation of the Isthmus of Panama on Atlantic Ocean thermohaline circulation. *Nature*, **393**, 673-676 (1998).

Haug, G.H., Sigman, D.M., Tiedemann, R., Pedersen, T.F., & Sarnthein, M. Onset of permanent stratification in the Subarctic Pacific Ocean. *Nature*, **401**, 779-782 (1999).

Haug, G.H., Ganoposlki, A., Sigman, D.M., Rosell-Melé, A., Swann, G.E.A., Tiedemann, R., Jaccard, S.L., Bollmann, J., Maslin, M., Leng, M.J., & Eglinton, G. North Pacific seasonality and the glaciation of North America 2.7 million years ago. *Nature*, 433, 821- 825 (2005).

Haywood, A.M., Valdes, P.J., & Peck, V.L. A permanent El Niño-like state during the Pliocene?. *Paleoceanography,* **22***,* doi:10.1029/2006PA001323 (2007).

Hebbeln, D., Marchant, M., Freudenthal, T., & Wefer, G. Surface sediment distribution along the Chilean continental slope related to upwelling and productivity. *Marine Geology*, **164**, 119-137 (2000a).

Herbert, T.D., & Schuffert, J.D. Alkenone unsaturation estimates of Late Miocene through Late Pliocene sea-surface temperatures at Site 958. *Proceedings of the Ocean Drilling Program Scientific Results*, **159**, College Station, Tex (1998).

Higgins, M.B., Robinson, R.S., Casciotti, K.L., McIlvin, M.R., & Pearson, A. A method for determining the nitrogen isotopic composition of porphyrins. *Analytical chemistry*, **81**, 184-192 (2009).

Holmes, M.E., Müller, P.J., Schneider, R.R., Segl, M., Pätzold, J., & Wefer, G. Stable nitrogen isotopes in Angola Basin surface sediments. *Marine Geology*, **134**, 1-12 (1996).

Hsieh, J.C., & Murray, B. A ~24 000 year period climate signal in 1.7-2.0 million year old Death Valley strata. *Earth and Planetary Science Letters*, **141**, 11-19 (1996).

Jahn, B., Donner, B., Müller, P.J., Röhl, U., Schneider, R., & Wefer, G. Pleistocene variations in dust input and marine productivity in the northern Benguela Current: Evidence of evolution of global glacial-interglacial cycles. *Palaeogeography, Palaeoclimatology, Palaeoecology*, **193**, 515-533 (2003).

Jansen, E., Fronval, T., Ranck, F., & Channell, J.E.T. Pliocene-Pleistocene ice rafting history and cyclicity in the Nordic Seas during the last 3.5 Myr. *Paleoceanography*, **15**, 709-721 (2000).

Jia, G., Chen, F., & Peng, P. Sea surface temperature differences between the western equatorial Pacific and northern South China Sea since the Pliocene and their paleoclimatic implications. *Geophysical Research Letters*, **35**, doi:10.1029/2008GL034792 (2008).

Karas, C., Nürnberg, D., Gupta, A.K., Tiedeamnn, R., Mohan, K., & Bickert, T. Mid-Pliocene climate change amplified by a switch in Indonesian subsurface throughflow. *Nature Geoscience*, doi: 10.1038/NGE520 (2009).

Karl, D., Letelier, R, Tupas, L., Dore, J., Christian, J., & Hebel, D. The role of nitrogen fixation in biogeochemical cycling in the subtropical North Pacific Ocean. *Nature*, **388**, 533-538 (1997).

Karl, D., Michales, A., Bergman, B., Capone, D., Carpentier, E., Letelier, R., Lipschultz, F., Paerl, H., Sigman, D., Stal, L. Dinitrogen fixation in the world's oceans. *Biogeochemistry*, **57/58**, 47-98 (2002).

Kashiyama, Y., Ogawa, N.O., Shiro, M., Tada, R., Kitazato, H., & Ohkouchi, N. Reconstruction of the biogeochemistry and ecology of photoautotrophs based on the nitrogen and carbon isotopic compositions of vandyl porphyrins from Miocene siliceous sediments. *Biogeosciences*, **5**, 797-816 (2008).

Keigwin, L. Isotopic Paleoceanography of the Caribbean and East Pacific: Role of Panama uplift in late Neogene time. *Science*, **217**, 350-352 (1982).

Kessler, W.S. The circulation of the eastern tropical Pacific: A review. *Progress in Oceanography*, **69**, 181-217 (2006).

Khelifi, N., Sarnthein, M., Andersen, N., Blanz T., Frank, M., Garbe-Schönberg, D., Haley, B.A., Stumpf, R., & Weinelt, M. A major and long-term Pliocene intensification of the Mediterranean outflow, 3.5 – 3.3 Ma ago, *accepted in Geology*.

Lamy, F., Rincon-Martinez, D., Saukel, C., Steph, S., Sturm, A., Etourneau, J., & R. Tiedemann, R. Plio-Pleistocene changes in SE trade wind strength and South American rainfall – Implications for ITCZ movements and long-term El Niño behavior, *Goldschmidt abstract book* (2009).

Lange, C.B., Berger, W.H., Lin, H.-L., & Wefer, G. Shipboard Scientific Party leg 175, The early Matuyama Diatom Maximum off SW Africa, Benguela current system (ODP leg 175). *Marine Geology*, **161**, 93-114 (1999).

Lawrence, K.T., Herbert, T.D., Brown, C.M., Raymo, M.E., & Haywood, A.M. High-amplitude variations in the North Atlantic sea surface temperature during the early Pliocene warm period. *Paleoceanography*, in press (2009).

Lawrence, K.T., Liu, Z., & Herbert, T.D. Evolution of the eastern tropical Pacific through Plio-Pleistocene glaciation. *Science*, **312**, 79-83 (2006).

Levitus, S., & Boyer, T.P. *World Ocean Atlas 1994*, Ocean Data View (1994).

Lisiecki, L.E., & Raymo, M.E. A Pliocene-Pleistocene stack of 57 globally distributed benthic ^{18}O records. *Paleoceanography*, **20**, doi:10.1029/2004PA001071 (2005).

Liu, K.-K., & Kaplan, I.R. The eastern tropical Pacific as a source of ^{15}N-enriched nitrate in seawater off southern California. *Limnology and Oceanography*, **34**, 820-830 (1989).

Liu, Z., Altabet, M.A., & Herbert, T.D. Plio-Pleistocene denitrification in the eastern tropical North Pacific: Intensification at 2.1 Ma. *Geochemistry, Geophysics, Geosystems*, **9**, doi: 10.1029/2008GC002044 (2008).

Lunt, D.J., Foster, G.L., Haywood, A., & Stone, E.J. Late Pliocene Greenland glaciation controlled by a decline in atmospheric CO_2 levels. *Nature*, **454**, 1102-1106 (2008).

Mariotti, A. Atmospheric nitrogen is a reliable standard for natural N-15 abundance measurements. *Nature*, **303**, 685-687.

Marlow, J.R., Lange, C.L., Wefer, G., & Rosell-Melé, A. Upwelling intensification as part of the Pliocene-Pleistocene climate transition. *Science*, **290**, 2288-2291 (2000).

Marlowe, I. T., Brassell, S. C., Eglinton, G., & Green, J.C. Long-chain alkenones and alkyl alkenoates and the fossil coccolith record of marine sediments. *Chemical Geology*, **88**, 349–375 (1990).

Martinez, P., Bertrand, P., Calvert, S.E., Pedersen, T.F., Shimmield, G.B., Lallier-Vergès, E., & Fontugne, M.R. Spatial variations in nutrient utilization, production and diagenesis in the sediments of a coastal upwelling regime (NW Africa): Implications for the paleoceanographic record. *Journal of Marine Research*, **58**, 809–835 (2000).

Martinez, P., Lamy, F., Robinson, R.R., Pichevin, L., & Billy, I. Atypical d15N variations at the southern boundary of the East Pacific oxygen minimum zone over the last 50 ka. *Quaternary Science Reviews*, **25**, 3017-3028 (2006).

McKay, J. L., Pedersen, T.F., & Kienast, S.S. Organic carbon accumulation over the last 16 kyr off Vancouver Island, Canada: evidence for increased marine productivity during the deglacial. *Quaternary Science Reviews*, **23**, 261-281 (2004).

Medina-Elizalde, M., Lea, D., & Fantle, M.S. Implications of seawater Mg/Ca variability for Plio-Pleistocene tropical climate reconstruction. *Earth and Planetary Science Letters*, **269**, 585-595 (2008).

Meissner, K., Galbraith, E.D., & Voelker, C. Denitrification under glacial and interglacial conditions: a physical approach. *Paleoceanography*, **20**, doi: 10.1029/2004PA001083 (2005).

Meyers, P. A. Organic geochemical proxies of paleoceanographic, paleolimnologic, and paleoclimatic processes. *Organic Geochemistry*, **27**, 213-250 (1997).

Mix, A.C., Tiedemann, R., & Blum, P. Site 1239. *Proceedings of the Ocean Drilling Program Initial Report,* **202,** College Station, Tex (2003).

Müller, P. J., & Schneider, R. An automated leaching method for the determination of opal in sediments and particulate matter. *Deep-Sea Research I*, **40**, 425-444 (1993).

Müller, P.J., Kirst, G., Ruhland, G., von Storch, I., & Rosell-Melé, A. Calibration of the alkenone paleotemperature index $U^{k'}_{37}$ based on core-tops from the eastern South Atlantic and the global ocean (60°N-60°S), *Geochimica et Cosmochimica Acta*, **62**, 1757-1772 (1998).

Murray, J.W., Barber, R.T., Roman, M.R., Bacon, C.R., & Feely, R.A. Physical and biological controls on carbon cycling in the equatorial Pacific. *Science*, **266**, 58-65 (1994).

Paillard, D., Labeyrie, L., & Yiou, P. Macintosh program performs time-series analysis. *EOS Trans. AGU*, **77**, 379 (1996).

Pelejero, C., & Grimalt, J.O. The correlation between the $U^{k'}_{37}$ index and sea surface temperatures in the warm boundary: The South China Sea. *Geochimica et Cosmochimica Acta*, **61**, 4789–4797 (1997).

Pennington, T.J., Mahoney, K.L., Kuhawara, V.S., Kolber, D.D., Calienes, & R., Chavez, F.P. Primary production in the eastern tropical Pacific: A review. *Progress in Oceanography*, **69**, 285-317 (2006).

Pérez, M.E., Lin, H-L., Lange, C.B., & Schneider, R. Pliocene-Pleistocene opal records off southwest Africa, Sites 1082 and 1084: a comparison of analytical techniques. *Proceedings of the Ocean Drilling Program Scientific Results*, **175**, College Station, Tex (2001).

Philander, S.G., & Fedorov, A. Role of tropics in changing the response to Milankovitch forcing some threee million years ago. *Paleoceanography*, **18**, doi: 10.1029/2002PA000837 (2003).

Pichevin, L., Martinez, P., Bertrand, P., Schneider, R., & Giraudeau, J. Nitrogen cycling on the Namibian shelf and slope over the last two climatic cycles: Local and global forcings. *Paleoceanography*, **20**, doi:10.1029/2004PA001001 (2005).

Pisias, N.G., Mayer, L.A., & Mix, A.C. Paleoceanography of the eastern equatorial Pacific during the Neogene: synthesis of Leg 138 drilling results. *Proceedings of the Ocean Drilling Program Scientific Results,* **138**, College Station, Tex (1995).

Prahl, F.G., & Wakehahm, S.G. Calibration of unsaturation patterns in long-chain ketone compositions for paleotemperature assessment. *Nature*, **330**, 367-369 (1987).

Prahl, F.G., Muehlhausen, L.A., & Zahnle, D.L. Further evaluation of long-chain alkenones as indicators of paleoceanographic conditions. *Geochimica et Cosmochimica Acta*, **52**, 2303-2310 (1988).

Prahl, F.G., Dymond, J., & Sparrow, M.A. Annual biomarker record for export production in the central Arabian Sea. *Deep-Sea Research I*, **47**, 1581-1604 (2000).

Prahl, F.G., Popp, B.N., Karl, D.M., & Sparrow, M.A. Ecology and biogeochemistry of alkenone production at Station ALOHA. *Deep-Sea Research I*, **52**, 699-719 (2005).

Raffi, I., Backman, J., Fornaciari, E., Pälike, H., Rio, D., Lourens, L., & Hilgen, F. A review of calcareous nannofossil astrobiochronology encompassing the past 25 million years. *Quaternary Science Review*, **25**, 3113–3137 (2006).

Ravelo, A.C., Andreasen, D.H., Lyle, M., Olivarez Lyle, A., & Wara, M. Regional climate shifts caused by gradual cooling in the Pliocene epoch. *Nature*, **429**, 263-267 (2004).

Raymo, M.E., Grant, B., Horowitz, M., & Rau, G.H. Mid-Pliocene warmth: Stronger greenhouse and stronger conveyer. *Marine Micropaleontology*, **27**, 313-326 (1996).

Raymo, M.E., Lisiecki, L.E., & Nisancoglu, K.H. Plio-Pleistocene Ice Volume, Antarctic Climate, and the Global $\delta^{18}O$ Record. *Science*, **313**, 492-495 (2006).

Ren, H., Sigman, D.M., Meckler, A.N., Plessen, B., Robinson, R.S., Rosenthal, Y., & Haug, G. Foraminiferal isotope evidence of reduced nitrogen fixation in the Ice Age Atlantic Ocean. *Science*, **323**, 244-248 (2009).

Reynolds, B.C., Frank, M., & Halliday, A.N. Silicon isotope fractionation during nutrient utilization in the North Pacific. *Earth and Planetary Science Letters*, **244**, 431-443 (2006).

Reynolds, B.C., Frank, M., & Halliday, A.N. Evidence for a major change in silicon cycling in the subarctic North Pacific at 2.73 Ma. *Paleoceanography*, **23**, doi: 10.1029/2007PA001563 (2008).

Robinson, M.M., Dowsett, H.J., Dwyer, G.S., & Lawrence, K.T. Reevaluation of mid-Pliocene North Atlantic sea surface temperatures. *Paleoceanography*, **23**, doi: 10.1029/2008PA001608 (2008).

Robinson, R.S., & Meyers, P. Biogeochemical changes within the Benguela Current upwelling system during the Matuyama Diatom Maximum: Nitrogen isotope evidence from Ocean Drilling Program Sites 1082 and 1084. *Paleoceanography*, **17**, doi:10.1029/2001PA000659 (2002).

Rodgers, K.B., Blanke, B., Madec, G., Aumont, O., Ciais, P., & Dutay, J. Extratropical sources of Equatorial Pacific upwelling in an OGCM. *Geophysical Research Letters*, **30**, doi: 10.1029/2002GL016003 (2003).

Sachs, J., & Repeta, D.J. Oligotrophy and nitrogen fixation during eastern Mediterranean sapropels events. *Science*, **286**, 2485-2488 (1999).

Sawada, K., & Shiraiwa, Y. Alkenone and alkenoic acid compositions of the membrane fractions of Emiliana huxleyi. *Phytochemistry*, **65**, 1299-1307 (2004).

Schroth, A.W., Crusius, J., Sholkovitz, E.R. & Bostick, B. Iron solubility driven by speciation in dust sources to the ocean. *Nature Geosciences* **2**, 337-340 (2009).

Schlitzer, R. Ocean Data View, http://www.awi-bremerhaven.de/GEO/ODV (2005).

Shackleton, N.J., Backman, J., Zimmerman, H., Kent, D.V., Hallm M.A., Roberts, D.G., Schnitker, D., Baldauf, J.G., Desprairies, A., Homrighausen, R., Huddlestun, P., Keene, J.B., Kaltenback, A.J., Krumsiek, K.A.O., Morton, A.C., Murray, J.W., & Westberg-Smith, J. Oxygen isotope calibration of the onset of ice-rafting and history of glaciation in the North Atlantic region. *Nature*, **307**, 620-623 (1984).

Shannon, L.V. The Benguela ecosystem, I, Evolution of the Benguela physical features and processes. *Oceanography And Marine Biology: An Annual Review*, edited by M. Barnes, 105-182 (1985).

Sicre, M., Bard, E., Ezat, U., & Rostek, F. Alkenone distributions in the North Atlantic and Nordic sea surface waters. *Geochemistry, Geophysics, Geosystems*, **3**, doi: 10.1029/2001GC000159 (2002).

Sigman, D. M., Altabet, M.A., McCorkle, D.C., Francois, R., & Fischer, G. The ^{15}N of nitrate in the Southern Ocean: Nitrogen cycling and circulation in the ocean interior. *Journal of Geophysical Research*, **105**, 19599-19614 (2000).

Sigman, D.M., & Boyle, E.A. Glacial/interglacial variations in atmospheric carbon dioxide. *Nature*, **407**, 859-869 (2000).

Sigman, D.M., Jaccard, S.A., & Haug, G.H. Polar ocean stratification in a cold climate. *Nature*, **428**, 59-63 (2004).

Sikes, E. L., Farrington, J.W., & Keigwin, L.D. Use of the alkenone unsaturation ratio $U^{k'}_{37}$ to determine past sea surface temperatures: Core top SST calibrations and methodology considerations. *Earth and Planetary Science Letters*, **104**, 36–47 (1991).

Sonzogni, C., Bard, E., & Eglinton, G. Core-top calibration of the alkenone index vs. sea surface temperature in the Indian Ocean. *Deep-Sea Research II*, **44**, 1445–1460 (1997).

Strub, P.T., Mesias, J.M., Montecinos-Banderet, V., Rutllant, J., & Salinas-Marchant, S. Coastal ocean circulation off western South America. *The Sea*, **11**, 273-313 (1998).

Summerhayes, C.P., Kroon, D., Rosell, M.A., Jordan, R.W., Schrader, H.J., Hearn, R., Villanueva, J., Grimalt, J.O., & Eglinton, G. Variability in the Benguela Current upwelling system. *Progress in Oceanography*, **35**, 207-251 (1995).

Ternois, Y., Sicre, M.-A., Boireau, A., Conte, M.H., & Eglinton, G. Evaluation of long-chain alkenones as paleo-temperature indicators in the Mediterranean Sea. *Deep-Sea Research I*, **44**, 271–286 (1997).

Thierstein, H. R., Geitzenauer, K.R., Molfino, B., & Shackleton, N.J. Global synchronicity of late Quaternary coccolith datum levels: Validation by oxygen isotopes. *Geology*, **5**, 400– 404 (1977).

Tiedemann, R., Sarnthein, M., & Shackleton, N.J. Astronomic timescale fort he Pliocene Atlantic ^{18}O and dust flux records of Ocean Drilling Program Site 659. *Paleoceanography*, **9**, 619-638 (1994).

Twichell, S.C., Meyers, P.A., & Diester-Haass, L. Significance of high C/N ratios in organic-carbon-rich Neogene sediments under the Benguela Current upwelling system. *Organic Geochemistry*, **33**, 715-722 (2002).

Tyrrell, T. The relative influences of nitrogen and phosphorus on oceanic primary production. *Nature*, **400**, 525-531 (1999).

Volkman, J. K., Barrett, S.M., Blackburn, S.I., & Sikes, E. L. Alkenones in Gephyrocapsa oceanica: Implications for studies of paleoclimate. *Geochimica et Cosmochimica Acta*, **59**, 513–520 (1995).

Wada, E. & Hattori, A. Nitrogen in the Sea: Forms, Abundances, and Rate Processes. CRC Press (1990).

Wakeham, S.G., Hedges, J.I., Lee, C., Peterson, M.L., & Hernes, P.J. Compositions and transport of lipid biomarkers through the water column and sufficial sediments of the equatorial Pacific Ocean. *Deep-Sea Research II*, **44**, 2131-2162 (1997).

Wara, M., Ravelo, A.C., & Delaney, M.L. Permanent El Niño-like conditions during the Pliocene warm period. *Science*, **309**, 758-761 (2005).

Wefer, G., Berger, W.H., Richter, C. et Shipboard Party. Site 1082. *Proceeding of the Ocean Drilling Program Initial Reports*, **159**, College Station, Tex (1998).

Ziegler, C.L., Murray, R.W., Plank, T. & Hemming, S.R. Sources of Fe to the equatorial Pacific Ocean from the Holocene to Miocene. *Earth and Planetary Science Letters*, **270**, 258-270 (2008).

Appendix 1: Site 1082 data

* Leg –Site – Core- Type-Section

LegSitHolCorTypSec*	Depth (mbsf)	Depth (mcd)	Age (Ma)	SST (°C)	Alk conc (mmol/g)	$\delta^{15}N$ (‰)	TN (%)	Opal (%)
175-1082-A-1-H-1	0.17	0.17	0.002	19.60	4676			
175-1082-A-1-H-1	0.67	0.67	0.005	19.80	3380			
175-1082-A-1-H-1	1.17	1.17	0.007	18.40	3194			
175-1082-A-1-H-2	1.67	1.67	0.010	17.40	2866			
175-1082-A-1-H-2	2.17	2.17	0.013	16.20	5126			
175-1082-A-1-H-2	2.67	2.67	0.016	16.10	5973			
175-1082-A-1-H-3	3.17	3.17	0.019	16.00	6908			
175-1082-A-1-H-3	3.67	3.67	0.026	16.30	6243			
175-1082-A-1-H-3	4.17	4.17	0.032	15.90	6489			
175-1082-A-1-H-4	4.67	4.67	0.039	16.20	5603			
175-1082-A-1-H-4	5.17	5.17	0.045	16.00	7644			
175-1082-A-1-H-4	5.67	5.67	0.052	16.60	6268			
175-1082-A-1-H-5	6.17	6.17	0.058	16.80	6164			
175-1082-A-1-H-5	6.67	6.67	0.063	16.60	6526			
175-1082-A-1-H-5	7.17	7.17	0.067	17.60	7851			
175-1082-A-2-H-1	7.97	9.16	0.083	19.90	6945			
175-1082-A-2-H-1	8.47	9.66	0.087	19.80	11534			
175-1082-A-2-H-1	8.97	10.16	0.091	20.30	13605			
175-1082-A-2-H-2	9.47	10.66	0.095	20.70	10242			
175-1082-A-2-H-2	9.97	11.16	0.102	19.70	7601			
175-1082-A-2-H-2	10.47	11.66	0.108	19.50	8265			
175-1082-A-2-H-3	10.97	12.16	0.115	20.00	11768			
175-1082-A-2-H-3	11.47	12.66	0.122	21.70	5821			
175-1082-A-2-H-3	11.97	13.16	0.128	20.10	9540			
175-1082-A-2-H-4	12.37	13.56	0.134	18.40	9735			
175-1082-A-2-H-4	12.87	14.06	0.140	16.50	11625			
175-1082-A-2-H-4	13.37	14.56	0.146	16.80	16004			
175-1082-A-2-H-5	13.77	14.96	0.151	16.90	9232			
175-1082-A-2-H-5	14.27	15.46	0.158	17.20	6506			
175-1082-A-2-H-5	14.77	15.96	0.164	16.40	7790			
175-1082-A-2-H-6	15.17	16.36	0.167	16.80	10450			
175-1082-A-2-H-6	15.67	16.86	0.171	17.00	16788			
175-1082-A-2-H-6	16.17	17.36	0.175	17.50	10650			
175-1082-A-2-H-7	16.57	17.76	0.186	17.20	11532			

LegSitHolCorTypSec	Depth (mbsf)	Depth (mcd)	Age (Ma)	SST (°C)	Alk conc (mmol/g)	$\delta^{15}N$ (‰)	TN (%)	Opal (%)
175-1082-A-2-H-7	17.07	18.26	0.190	18.20	13976			
175-1082-A-3-H-1	17.47	19.84	0.202	19.70	17911			
175-1082-A-3-H-1	17.97	20.34	0.205	19.90	20947			
175-1082-A-3-H-2	18.87	21.24	0.212	20.50	18694			
175-1082-A-3-H-2	19.37	21.74	0.216	21.30	13691			
175-1082-A-3-H-2	19.87	22.24	0.218	20.10	8886			
175-1082-A-3-H-3	20.27	22.64	0.220	19.30	9999			
175-1082-A-3-H-3	20.77	23.14	0.222	17.80	16505			
175-1082-A-3-H-3	21.27	23.64	0.232	18.70	39480			
175-1082-A-3-H-4	21.67	24.04	0.240	20.80	18304			
175-1082-A-3-H-4	22.17	24.54	0.243	19.90	15436			
175-1082-A-3-H-4	22.67	25.04	0.246	18.00	17596			
175-1082-A-3-H-5	23.07	25.44	0.249	15.50	31256			
175-1082-A-3-H-5	23.57	25.94	0.252	15.40	28074			
175-1082-A-3-H-5	24.07	26.44	0.259	15.50	17772			
175-1082-A-3-H-6	24.47	26.84	0.265	16.70	16108			
175-1082-A-3-H-6	24.97	27.34	0.270	16.10	12923			
175-1082-A-3-H-6	25.47	27.84	0.276	17.40	12677			
175-1082-A-3-H-7	25.87	28.24	0.280	17.70	17983			
175-1082-A-3-H-7	26.37	28.74	0.285	18.20	15609			
175-1082-A-4-H-1	26.97	29.61	0.291	17.50	8254			
175-1082-A-4-H-1	27.47	30.11	0.294	17.60	16276			
175-1082-A-4-H-1	27.97	30.61	0.302	17.50	23161			
175-1082-A-4-H-2	28.37	31.01	0.308	18.10	19626			
175-1082-A-4-H-2	28.87	31.51	0.316	19.00	14539			
175-1082-A-4-H-2	29.37	32.01	0.317	18.80	11359			
175-1082-A-4-H-3	29.77	32.41	0.317	18.50	16222			
175-1082-A-4-H-3	30.27	32.91	0.328	21.00	6897			
175-1082-A-4-H-3	30.77	33.41	0.331	20.60	10679			
175-1082-A-4-H-4	31.17	33.81	0.334	18.60	9832			
175-1082-A-4-H-4	31.67	34.31	0.338	17.30	15485			
175-1082-A-4-H-4	32.17	34.81	0.341	15.60	22243			
175-1082-A-4-H-5	32.57	35.21	0.354	16.50	16866			
175-1082-A-4-H-5	33.07	35.71	0.358	15.90	10101			
175-1082-A-4-H-5	33.57	36.21	0.362	16.20	14431			
175-1082-A-4-H-6	33.97	36.61	0.365	16.30	16493			
175-1082-A-4-H-6	34.47	37.11	0.368	17.20	18482			
175-1082-A-4-H-6	34.97	37.61	0.372	17.50	15006			

LegSitHolCorTypSec	Depth (mbsf)	Depth (mcd)	Age (Ma)	SST (°C)	Alk conc (mmol/g)	$\delta^{15}N$ (‰)	TN (%)	Opal (%)
175-1082-A-4-H-7	35.37	38.01	0.376	17.50	17146	3.45	0.349	
175-1082-A-4-H-7	35.87	38.51	0.381	18.90	14638	2.91	0.146	
175-1082-A-5-H-1	36.51	40.25	0.399	20.50	9296	2.98	0.107	
175-1082-A-5-H-1	36.97	40.71	0.404	20.80	6225	3.03	0.095	
175-1082-A-5-H-1	37.47	41.21	0.406	19.80	5987	4.11	0.226	
175-1082-A-5-H-2	37.91	41.65	0.407	20.30	5489	3.93	0.105	
175-1082-A-5-H-2	38.37	42.11	0.408	19.50	3958	4.28	0.089	
175-1082-A-5-H-2	38.87	42.61	0.410	19.70	3439	5.00	0.111	
175-1082-A-5-H-3	39.31	43.05	0.416	17.90	4131	5.94	0.108	
175-1082-A-5-H-3	39.77	43.51	0.421	15.40	3366	3.36	0.164	
175-1082-A-5-H-3	40.27	44.01	0.428	14.50	3070	4.74	0.126	
175-1082-A-5-H-4	40.71	44.45	0.433	14.40	4145	4.54	0.145	
175-1082-A-5-H-4	41.17	44.91	0.436	15.30	5853	3.79	0.150	
175-1082-A-5-H-4	41.67	45.41	0.440	16.00	5752	3.61	0.132	
175-1082-A-5-H-5	42.11	45.85	0.445	15.80	5680	3.43	0.125	
175-1082-A-5-H-5	42.57	46.31	0.451	15.00	6473	3.95	0.168	
175-1082-A-5-H-5	43.07	46.81	0.457	15.30	5504	3.63	0.106	
175-1082-A-5-H-6	43.47	47.21	0.462	14.90	6943	3.83	0.135	
175-1082-A-5-H-6	43.97	47.71	0.467	16.20	5944	3.64	0.137	
175-1082-A-5-H-6	44.47	48.21	0.471	17.80	15187	2.83	0.473	
175-1082-A-5-H-7	44.91	48.65	0.474	17.50	10951	3.38	0.159	
175-1082-A-5-H-7	45.37	49.11	0.478	18.20	11444	3.40	0.174	
175-1082-A-6-H-1	45.9	50.91	0.491	19.20	11753	2.39	0.207	
175-1082-A-6-H-1	46.4	51.41	0.502	18.10	10598	2.84	0.207	
175-1082-A-6-H-1	46.9	51.91	0.512	17.40	12378	2.88	0.474	
175-1082-A-6-H-2	47.3	52.31	0.522	18.30	10637	2.51	0.198	
175-1082-A-6-H-2	47.8	52.81	0.526	18.10	7607	3.41	0.153	
175-1082-A-6-H-2	48.3	53.31	0.530	17.50	6892	3.57	0.270	
175-1082-A-6-H-3	49.2	54.21	0.538	16.00	12019	3.62	0.423	
175-1082-A-6-H-3	49.7	54.71	0.545	16.30	9594	3.70	0.392	
175-1082-A-6-H-4	50.2	55.21	0.552	16.20	11945	3.73	0.462	
175-1082-A-6-H-4	50.7	55.71	0.556	16.20	13842	3.30	0.494	
175-1082-A-6-H-4	51.2	56.21	0.560	16.80	12845	3.60	0.445	
175-1082-A-6-H-5	51.6	56.61	0.563	18.00	18617	3.77	0.598	
175-1082-A-6-H-5	52.1	57.11	0.567	18.50	17954	3.53	0.627	
175-1082-A-6-H-5	52.6	57.61	0.572	18.20	28094	3.07	0.905	
175-1082-A-6-H-6	53	58.01	0.576	20.60	10700	4.46	0.359	
175-1082-A-6-H-6	53.5	58.51	0.585	18.80	12544	3.94	0.470	

LegSitHolCorTypSec	Depth (mbsf)	Depth (mcd)	Age (Ma)	SST (°C)	Alk conc (mmol/g)	$\delta^{15}N$ (‰)	TN (%)	Opal (%)
175-1082-A-6-H-6	54	59.01	0.592	20.00	34190	4.13	0.762	
175-1082-A-6-H-7	54.4	59.41	0.597	20.60	24131	3.47	0.694	
175-1082-A-6-H-7	54.9	59.91	0.602	19.60	29754	2.79	0.740	
175-1082-A-7-H-1	55.39	61.3	0.612	20.30	61953	4.16	0.554	
175-1082-A-7-H-1	55.9	61.81	0.622	17.70	7535	3.23	0.977	
175-1082-A-7-H-1	56.41	62.32	0.632	17.00	8910	3.71	0.434	
175-1082-A-7-H-2	56.9	62.81	0.639	17.20	11596	3.96	0.515	
175-1082-A-7-H-2	57.4	63.31	0.646	17.60	11665	3.77	0.526	
175-1082-A-7-H-2	57.92	63.83	0.649	17.20	20447	3.43	0.520	
175-1082-A-7-H-3	58.4	64.31	0.651	17.40	21976	3.23	0.272	
175-1082-A-7-H-3	58.9	64.81	0.654	18.80	25893	3.25	0.273	
175-1082-A-7-H-3	59.37	65.28	0.656	19.80	15261	2.98	0.239	
175-1082-A-7-H-4	59.9	65.81	0.662	17.00	23619	2.83	0.210	
175-1082-A-7-H-4	60.4	66.31	0.673	18.00	28149	3.46	0.247	
175-1082-A-7-H-4	60.89	66.8	0.684	19.90	38328	3.28	0.264	
175-1082-A-7-H-5	61.4	67.31	0.688	19.50	58169	4.11	0.309	
175-1082-A-7-H-5	61.9	67.81	0.692	20.40	37406	3.26	0.411	
175-1082-A-7-H-5	62.37	68.28	0.696	21.20	27962	3.35	0.329	
175-1082-A-7-H-6	62.9	68.81	0.704	20.50	32418	3.65	0.247	
175-1082-A-7-H-6	63.4	69.31	0.711	19.50	16349	3.64	0.220	
175-1082-A-7-H-6	63.9	69.81	0.718	17.70	21454	3.11	0.143	
175-1082-A-7-H-7	64.4	70.31	0.722	19.10	22028	2.71	0.243	
175-1082-A-8-H-1	64.9	71.34	0.730	19.60	18798	2.47	0.236	
175-1082-A-8-H-2	65.11	71.55	0.732	19.80	20889	2.91	0.225	
175-1082-A-8-H-2	65.69	72.13	0.737	19.20	21930	2.90	0.213	
175-1082-A-8-H-2	66.11	72.55	0.740	19.70	21145	2.80	0.217	
175-1082-A-8-H-3	66.61	73.05	0.748	18.20	13299	3.31	0.231	
175-1082-A-8-H-3	67.11	73.55	0.750	19.10	11861	3.77	0.225	
175-1082-A-8-H-3	67.61	74.05	0.753	19.50	15947	3.23	0.235	
175-1082-A-8-H-4	68.11	74.55	0.755	20.20	21762	3.26	0.253	
175-1082-A-8-H-4	68.61	75.05	0.757	19.50	21042	2.93	0.284	
175-1082-A-8-H-4	69.11	75.55	0.760	19.50	27165	3.10	0.305	
175-1082-A-8-H-5	69.61	76.05	0.762	22.20	17944	3.11	0.335	
175-1082-A-8-H-5	70.11	76.55	0.763	20.50	23106	3.28	0.290	
175-1082-A-8-H-5	70.6	77.04	0.763	20.20	16594	3.80	0.196	
175-1082-A-8-H-6	71.11	77.55	0.764	18.30	17895	3.88	0.288	
175-1082-A-8-H-6	71.61	78.05	0.768	19.20	16472	3.69	0.217	
175-1082-A-8-H-6	72.11	78.55	0.772	19.90	8283	3.83	0.278	

LegSitHolCorTypSec	Depth (mbsf)	Depth (mcd)	Age (Ma)	SST (°C)	Alk conc (mmol/g)	$\delta^{15}N$ (‰)	TN (%)	Opal (%)
175-1082-A-8-H-7	72.61	79.05	0.776	20.70	8335	4.06	0.257	
175-1082-A-8-H-7	73.13	79.57	0.777	18.80	5247	4.70	0.194	
175-1082-A-8-H-7	73.61	80.05	0.779	18.30	4551	5.08	0.120	
175-1082-A-8-H-8	74.11	80.55	0.780	20.80	3412	5.75	0.191	
175-1082-A-8-H-8	74.4	83.03	0.794	16.60	15060	5.08	0.200	
175-1082-A-9-H-1	74.61	81.05	0.802	16.70	4950	4.75	0.102	
175-1082-A-9-H-1	74.9	83.53	0.805	16.90	13454	4.14	0.107	
175-1082-A-9-H-1	75.42	84.05	0.807	17.70	19401	3.48	0.185	
175-1082-A-9-H-2	75.9	84.53	0.810	19.20	17522	3.75	0.238	
175-1082-A-9-H-2	76.4	85.03	0.813	19.70	11951	3.70	0.273	
175-1082-A-9-H-2	76.92	85.55	0.815	19.50	7410	4.04	0.229	
175-1082-A-9-H-3	77.4	86.03	0.818	20.30	7034	4.26	0.162	
175-1082-A-9-H-3	77.9	86.53	0.826	19.20	7679	4.12	0.138	
175-1082-A-9-H-4	78.6	87.23	0.832	20.10	12219	4.29	0.183	
175-1082-A-9-H-4	79.09	87.72	0.836	20.30	8092	3.53	0.270	
175-1082-A-9-H-4	79.59	88.22	0.840	18.70	13499	3.85	0.189	
175-1082-A-9-H-5	80.1	88.73	0.846	20.80	9556	4.65	0.226	
175-1082-A-9-H-5	80.59	89.22	0.847	20.60	12338	3.56	0.201	
175-1082-A-9-H-5	81.09	89.72	0.849	21.20	9216	4.00	0.176	
175-1082-A-9-H-6	81.6	90.23	0.850	21.90	6757	4.46	0.149	
175-1082-A-9-H-6	82.1	90.73	0.854	21.40	10224	4.90	0.131	
175-1082-A-9-H-6	82.6	91.23	0.858	23.60	5123	4.54	0.210	
175-1082-A-9-H-7	83.1	91.73	0.861	20.20	5760	5.62	0.302	
175-1082-A-9-H-7	83.6	92.23	0.865	17.60	8153	4.69	0.163	
175-1082-A-9-H-7	83.9	93.51	0.868	17.60	9039	4.35	0.169	
175-1082-A-10-H-1	84.1	92.73	0.873	19.20	2931	3.55	0.161	
175-1082-A-10-H-2	84.34	93.95	0.876	16.90	12173	5.00	0.123	
175-1082-A-10-H-2	84.84	94.45	0.878	17.50	16438	3.50	0.160	
175-1082-A-10-H-2	85.34	94.95	0.880	17.70	16803	2.90	0.238	
175-1082-A-10-H-3	85.84	95.45	0.882	18.80	12448	3.07	0.258	
175-1082-A-10-H-3	86.35	95.96	0.887	18.30	12246	3.91	0.181	
175-1082-A-10-H-3	86.87	96.48	0.892	19.30	10659	4.88	0.326	
175-1082-A-10-H-4	87.34	96.95	0.897	19.30	11110	2.99	0.279	
175-1082-A-10-H-4	87.83	97.44	0.902	18.80	12608	4.12	0.191	
175-1082-A-10-H-4	88.3	97.91	0.907	18.20	11735	3.57	0.240	
175-1082-A-10-H-5	88.64	98.25	0.910	21.00	7027	4.58	0.179	
175-1082-A-10-H-5	89.14	98.75	0.913	18.60	8242	5.12	0.169	
175-1082-A-10-H-5	89.64	99.25	0.916	18.50	6870	4.38	0.170	

LegSitHolCorTypSec	Depth (mbsf)	Depth (mcd)	Age (Ma)	SST (°C)	Alk conc (mmol/g)	$\delta^{15}N$ (‰)	TN (%)	Opal (%)
175-1082-A-10-H-6	90.14	99.75	0.919	18.20	3948	4.47	0.151	
175-1082-A-10-H-6	90.64	100.25	0.922	17.80	3672	4.34	0.139	
175-1082-A-10-H-6	91.15	100.76	0.929	18.80	5320	4.17	0.170	
175-1082-A-10-H-7	91.64	101.25	0.936	18.80	6718	4.16	0.183	
175-1082-A-10-H-7	92.14	101.75	0.942	18.00	14057	3.72	0.217	
175-1082-A-10-H-7	92.64	102.25	0.949	20.50	13200	3.55	0.235	
175-1082-A-10-H-8	93.14	102.75	0.956	21.80	15635	3.35	0.262	
175-1082-A-10-H-8	93.4	105.55	0.957	18.50	4077	4.32	0.176	
175-1082-A-11-H-1	93.64	103.25	0.964	21.60	6551	4.45	0.171	
175-1082-A-11-H-1	93.9	106.05	0.971	18.50	14693	4.06	0.254	
175-1082-A-11-H-1	94.4	106.55	0.978	18.80	24675	3.62	0.353	
175-1082-A-11-H-2	94.9	107.05	0.986	17.70	6832	4.17	0.235	
175-1082-A-11-H-2	95.4	107.55	0.992	20.40	8720	3.93	0.203	
175-1082-A-11-H-2	95.9	108.05	0.998	21.30	6650	4.38	0.160	
175-1082-A-11-H-3	96.4	108.55	1.004	17.60	11075	3.10	0.169	
175-1082-A-11-H-3	96.9	109.05	1.008	18.20	13820	3.26	0.212	
175-1082-A-11-H-3	97.4	109.55	1.013	19.00	19351	3.34	0.264	
175-1082-A-11-H-4	97.75	109.9	1.015	20.20	8681	4.26	0.246	
175-1082-A-11-H-4	98.25	110.4	1.020	21.70	15442	4.60	0.310	
175-1082-A-11-H-4	98.75	110.9	1.024	22.40	7860	3.99	0.292	
175-1082-A-11-H-5	99.25	111.4	1.026	21.20	7342	4.11	0.285	
175-1082-A-11-H-5	99.75	111.9	1.028	20.70	7279	4.09	0.225	
175-1082-A-11-H-5	100.25	112.4	1.030	20.80	10643	3.89	0.293	
175-1082-A-11-H-6	100.75	112.9	1.032	19.30	6480	4.21	0.279	
175-1082-A-11-H-6	101.25	113.4	1.034	19.10	5857	4.13	0.234	
175-1082-A-11-H-6	101.75	113.9	1.036	19.10	5954	4.43	0.209	
175-1082-A-11-H-7	102.25	114.4	1.038	17.70	7676	4.05	0.160	
175-1082-A-11-H-7	102.75	114.9	1.044	19.10	13929	4.00	0.214	
175-1082-A-12-H-1	102.9	117.37	1.072	23.40	6419	3.99	0.181	
175-1082-A-12-H-2	103.24	117.71	1.077	21.70	6411	4.36	0.185	
175-1082-A-12-H-2	103.74	118.21	1.085	21.70	4567	3.83	0.185	
175-1082-A-12-H-2	104.24	118.71	1.092	22.40	4942	3.39	0.208	
175-1082-A-12-H-3	104.61	119.08	1.098	20.80	11840	3.37	0.260	
175-1082-A-12-H-3	105.11	119.58	1.103	22.60	10048	3.25	0.322	
175-1082-A-12-H-3	105.69	120.16	1.108	23.60	6613	4.03	0.197	
175-1082-A-12-H-4	105.94	120.41	1.110	23.20	6275	4.01	0.189	
175-1082-A-12-H-4	106.44	120.91	1.114	21.80	5666	4.46	0.186	
175-1082-A-12-H-4	106.92	121.39	1.117	20.40	9220	4.12	0.207	

LegSitHolCorTypSec	Depth (mbsf)	Depth (mcd)	Age (Ma)	SST (°C)	Alk conc (mmol/g)	$\delta^{15}N$ (‰)	TN (%)	Opal (%)
175-1082-A-12-H-5	107.29	121.76	1.120	20.90	12146	3.94	0.235	
175-1082-A-12-H-5	107.79	122.26	1.123	20.10	7506	4.13	0.194	
175-1082-A-12-H-5	108.29	122.76	1.126	18.50	4876	3.85	0.217	
175-1082-A-12-H-6	108.79	123.26	1.131	19.60	10310	3.51	0.324	
175-1082-A-12-H-6	109.29	123.76	1.135	19.90	16382	3.73	0.365	
175-1082-A-12-H-6	109.79	124.26	1.140	20.40	26770	3.54	0.339	
175-1082-A-12-H-7	110.29	124.76	1.145	21.50	33752	3.75	0.369	
175-1082-A-12-H-7	110.79	125.26	1.149	21.80	26280	3.84	0.298	
175-1082-A-12-H-7	111.29	125.76	1.154	22.10	26302	4.24	0.330	
175-1082-A-12-H-8	111.79	126.26	1.161	21.50	24706	4.02	0.346	
175-1082-A-12-H-8	112.3	126.77	1.168	22.40	20596	3.76	0.338	
175-1082-A-13-H-1	112.4	128.06	1.178	22.10	18858	4.24	0.280	
175-1082-A-13-H-1	112.9	128.56	1.188	23.10	12423	4.64	0.232	
175-1082-A-13-H-1	113.4	129.06	1.192	21.60	9280	4.35	0.201	
175-1082-A-13-H-2	113.9	129.56	1.195	21.20	5836	4.90	0.180	
175-1082-A-13-H-2	114.4	130.06	1.199	20.00	9627	4.09	0.212	
175-1082-A-13-H-3	114.52	130.18	1.200	17.60	10221	3.93	0.217	
175-1082-A-13-H-3	115.02	130.68	1.207	18.30	7750	4.24	0.222	
175-1082-A-13-H-3	115.52	131.18	1.215	18.50	6626	4.34	0.212	
175-1082-A-13-H-4	115.73	131.39	1.218	21.80	10153	3.79	0.187	
175-1082-A-13-H-4	116.23	131.89	1.219	21.70	11479	3.78	0.200	
175-1082-A-13-H-4	116.73	132.39	1.219	21.00	13334	3.79	0.217	
175-1082-A-13-H-5	117.23	132.89	1.220	20.40	7469	5.31	0.137	
175-1082-A-13-H-5	117.73	133.39	1.240	23.20	4644	5.36	0.143	
175-1082-A-13-H-5	118.21	133.87	1.245	19.00	4751	4.18	0.153	
175-1082-A-13-H-6	118.76	134.42	1.250	18.40	4994	3.58	0.208	
175-1082-A-13-H-6	119.26	134.92	1.260	19.70	8659	3.69	0.202	
175-1082-A-13-H-6	119.76	135.42	1.262	18.90	16306	3.38	0.268	
175-1082-A-14-H-1	121.9	137.56	1.271	20.80	5814	3.06	0.174	
175-1082-A-14-H-1	122.4	138.06	1.273	21.10	5636	3.31	0.168	
175-1082-A-14-H-1	122.88	138.54	1.276	22.10	3454	4.08	0.134	
175-1082-A-14-H-2	123.4	139.06	1.278	22.70	4005	3.92	0.123	
175-1082-A-14-H-2	123.90	139.56	1.280	23.00	2724	4.12	0.126	
175-1082-A-14-H-2	124.45	140.11	1.284	22.50	3378	3.46	0.144	
175-1082-A-14-H-3	124.90	140.56	1.287	22.10	3797	3.07	0.172	
175-1082-A-14-H-3	125.40	141.06	1.290	21.80	2894	3.41	0.157	
175-1082-A-14-H-3	125.90	141.56	1.294	22.00	3666	3.38	0.160	
175-1082-A-14-H-4	126.40	142.06	1.296	21.20	3609	2.92	0.154	

LegSitHolCorTypSec	Depth (mbsf)	Depth(mcd)	Age (Ma)	SST (°C)	Alk conc (mmol/g)	$\delta^{15}N$ (‰)	TN (%)	Opal (%)
175-1082-A-14-H-4	126.91	142.57	1.298	21.20	4798	3.25	0.183	
175-1082-A-14-H-4	127.40	143.06	1.303	22.30	6764	3.40	0.179	
175-1082-A-14-H-5	127.90	143.56	1.308	22.80	19836	2.79	0.264	
175-1082-A-14-H-5	128.32	143.98	1.312	23.10	8123	3.10	0.145	
175-1082-A-15-X-1	128.70	144.36	1.316	24.40	881	4.06	0.040	
175-1082-A-15-X-1	129.20	144.86	1.321	21.00	5272	3.41	0.168	
175-1082-A-15-X-1	129.70	145.36	1.326	20.80	5485	3.16	0.181	
175-1082-A-15-X-2	129.82	145.48	1.327	20.60	6330	3.06	0.188	
175-1082-A-15-X-2	130.32	145.98	1.332	21.50	11138	2.53	0.243	
175-1082-A-15-X-2	130.82	146.48	1.340	20.70	10498	2.73	0.274	
175-1082-A-15-X-3	131.32	146.98	1.345	21.50	9914			
175-1082-A-15-X-3	131.82	147.48	1.349	21.80	6832	3.39	0.211	
175-1082-A-15-X-3	132.30	147.96	1.354	22.50	7129	3.46	0.207	
175-1082-A-15-X-4	132.42	148.08	1.355	22.10	8189	3.58	0.212	
175-1082-A-15-X-4	132.92	148.58	1.359	21.80	6651	4.12	0.237	
175-1082-A-15-X-4	133.42	149.08	1.362	21.50	5923	3.60	0.237	
175-1082-A-15-X-5	133.92	149.58	1.366	20.80	6311	3.36	0.274	
175-1082-A-15-X-6	134.25	149.91	1.368	20.60	6107	3.33	0.285	
175-1082-A-15-X-6	134.73	150.39	1.372	19.80	6394	3.52	0.265	
175-1082-A-16-X-1	138.40	154.06	1.396	23.30	3637	4.10	0.135	
175-1082-A-16-X-1	138.90	154.56	1.404	21.80	4238	2.93	0.200	
175-1082-A-16-X-1	139.40	155.06	1.412	21.00	5897	3.23	0.279	
175-1082-A-16-X-2	139.90	155.56	1.416	21.20	6363	2.50	0.273	
175-1082-A-16-X-2	140.41	156.07	1.420	21.70	7178			
175-1082-A-16-X-2	140.90	156.56	1.424	21.90	6096	3.07	0.214	
175-1082-A-16-X-3	141.40	157.06	1.436	22.80	3858			
175-1082-A-16-X-3	141.90	157.56	1.440	22.80	3059	3.61	0.153	
175-1082-A-16-X-3	142.39	158.05	1.444	22.80	1822	3.18	0.25	
175-1082-A-16-X-4	142.90	158.56	1.448	22.40	1456	2.85	0.23	
1751082-C-17-H-7	143.34	161.97	1.451	23.27	6136			
175-1082-A-16-X-4	143.39	159.05	1.453	21.00	1930	2.13	0.31	
1751082-C-17-H-8	143.84	162.47	1.456	23.73	5016			
175-1082-A-16-X-4	143.90	159.56	1.459	19.20	4686	2.47	0.43	
1751082-C-18-H-1	144.1	162.73	1.472	22.00	9839			
1751082-C-17-H-8	144.34	162.97	1.476	23.79	4544			
175-1082-A-16-X-5	144.40	160.06	1.481	17.90	7044	2.27	0.61	
1751082-C-18-H-2	144.63	163.26	1.486	23.45	5043			
175-1082-A-16-X-5	144.80	160.46	1.493	20.20	11223	2.29	0.73	

LegSitHolCorTypSec	Depth (mbsf)	Depth(mcd)	Age (Ma)	SST (°C)	Alk conc (mmol/g)	$\delta^{15}N$ (‰)	TN (%)	Opal (%)
1751082-C-17-H-CC	144.84	163.47	1.498	23.30	5244			
1751082-C-18-H-2	145.33	163.96	1.505	22.36	12453			9.82
1751082-C-18-H-2	145.73	164.36	1.511	22.73	9970			
1751082-C-18-H-3	146.25	164.88	1.515	23.97	9398			
1751082-C-18-H-3	146.64	165.27	1.519	23.55	11000			
1751082-C-18-H-3	147.13	165.76	1.525	23.18	14940			
1751082-C-18-H-4	147.63	166.26	1.529	23.39	11572			7.47
175-1082-A-17-X-1	148.00	163.66	1.535	22.40	8990	1.65	0.40	
1751082-C-18-H-4	148.13	166.76	1.553	22.94	9318			
175-1082-A-17-X-1	148.50	164.16	1.562	22.40	10308	2.18	0.41	
1751082-C-18-H-4	148.63	167.26	1.565	23.33	7615			
175-1082-A-17-X-1	149.00	164.66	1.570	22.50	8689	2.16	0.39	
1751082-C-18-H-5	149.13	167.76	1.571	24.27	3584			
175-1082-A-17-X-2	149.50	165.16	1.575	22.10	7353	2.47	0.38	
1751082-C-18-H-5	149.63	168.26	1.576	24.00	4119			
175-1082-A-17-X-2	150.00	165.66	1.581	22.20	7294	2.39	0.44	
175-1082-A-17-X-2	150.50	166.16	1.582	22.50	5721	2.24	0.42	
1751082-C-18-H-6	150.63	169.26	1.582	24.48	5334			
175-1082-A-17-X-3	151.00	166.66	1.588	22.60	4374	2.24	0.34	
1751082-C-18-H-6	151.13	169.76	1.593	24.48	3715			
175-1082-A-17-X-3	151.50	167.16	1.594	23.50	4167	3.01	0.35	
175-1082-A-17-X-4	151.61	167.27	1.598	22.80	5243	2.25	0.34	
1751082-C-18-H-6	151.63	170.26	1.600	24.67	2848			
175-1082-A-17-X-4	152.11	167.77	1.603	22.50	6572	2.00	0.37	
1751082-C-18-H-7	152.13	170.76	1.608	23.76	2388			
1751082-C-18-H-7	152.63	171.26	1.613	23.27	2660			
1751082-C-18-H-7	153.13	171.76	1.618	23.27	3133			
1751082-C-19-H-1	153.6	172.23	1.623	24.52	9269			
1751082-C-18-H-8	153.63	172.26	1.623	23.15	3467			
1751082-C-19-H-2	153.77	172.4	1.624	23.85	5061			
1751082-C-18-H-8	154.13	172.76	1.628	22.82	4709			
1751082-C-19-H-2	154.27	172.9	1.630	23.97	3509			
1751082-C-18-H-CC	154.63	173.26	1.638	24.03	4914			
1751082-C-19-H-2	154.77	173.4	1.640	23.45	4093			
1751082-C-19-H-3	155.27	173.9	1.642	23.33	3609			18.33
1751082-C-19-H-3	155.77	174.4	1.655	23.45	3596			
1751082-C-19-H-3	156.27	174.9	1.670	22.33	2126			
1751082-C-19-H-4	156.77	175.4	1.675	22.48	3673			

LegSitHolCorTypSec	Depth (mbsf)	Depth(mcd)	Age (Ma)	SST (°C)	Alk conc (mmol/g)	$\delta^{15}N$ (‰)	TN (%)	Opal (%)
1751082-C-19-H-4	157.27	175.9	1.675	22.27	3396			
175-1082-A-18-X-1	157.70	173.36	1.676	21.80	4110	2.84	0.54	
1751082-C-19-H-4	157.77	176.4	1.680	23.27	2844			
175-1082-A-18-X-1	158.20	173.86	1.682	21.40	2891	2.91	0.42	
1751082-C-19-H-5	158.27	176.9	1.686	22.45	6417			
175-1082-A-18-X-1	158.71	174.37	1.687	21.80	3489	2.84	0.50	
1751082-C-19-H-5	158.77	177.4	1.691	22.73	5689			
175-1082-A-18-X-2	158.85	174.51	1.692	22.20	2969	2.47	0.51	
1751082-C-19-H-5	159.27	177.9	1.696	22.55	5364			
175-1082-A-18-X-2	159.38	175.04	1.697	22.30	4731	2.78	0.58	
175-1082-A-18-X-2	159.86	175.52	1.701	22.30	4818	2.68	0.51	
175-1082-A-18-X-3	160.35	176.01	1.703	22.50	4353	2.53	0.44	
175-1082-A-18-X-3	160.85	176.51	1.704	22.60	3331	2.89	0.44	
1751082-C-19-H-7	161.27	179.9	1.704	22.03	11673			
175-1082-A-18-X-3	161.35	177.01	1.705	21.90	8211	2.88	0.76	
1751082-C-19-H-7	161.77	180.4	1.705	23.00	7315			
175-1082-A-18-X-4	161.85	177.51	1.707	22.20	7871	2.54	0.75	
1751082-C-19-H-7	162.27	180.9	1.711	23.27	7466			
175-1082-A-18-X-4	162.33	177.99	1.713	22.40	6095	2.75	0.60	
1751082-C-19-H-8	162.77	181.4	1.715	23.33	6646			
175-1082-A-18-X-4	162.81	178.47	1.720	22.80	3320	2.74	0.43	
1751082-C-20-H-1	163.1	181.73	1.733	20.52	8732			
1751082-C-19-H-8	163.27	181.9	1.738	23.55	12071			
1751082-C-20-H-1	163.6	182.23	1.741	20.76	11288			
1751082-C-20-H-1	164.1	182.73	1.748	20.70	12460			9.91
1751082-C-20-H-2	164.6	183.23	1.751	22.52	9609			
1751082-C-20-H-2	165.1	183.73	1.754	22.94	6545			
1751082-C-20-H-2	165.6	184.23	1.755	23.33	5246			
1751082-C-20-H-3	166.1	184.73	1.758	23.79	4761			14.84
1751082-C-20-H-3	166.6	185.23	1.758	23.12	14597			
1751082-C-20-H-3	167.1	185.73	1.760	23.97	9758			
175-1082-A-19-X-1	167.30	182.96	1.760	22.00	8615	2.86	0.53	
1751082-C-20-H-4	167.6	186.23	1.765	23.76	4315			
175-1082-A-19-X-2	167.61	183.27	1.765	22.80	7364	2.82	0.45	
175-1082-A-19-X-2	168.09	183.75	1.769	22.40	6229	2.45	0.38	
1751082-C-20-H-4	168.1	186.73	1.769	22.97	5093			
1751082-C-20-H-4	168.6	187.23	1.772	21.97	7739			
175-1082-A-19-X-2	168.61	184.27	1.773	21.70	6827	2.71	0.41	

LegSitHolCorTypSec	Depth (mbsf)	Depth(mcd)	Age (Ma)	SST (°C)	Alk conc (mmol/g)	$\delta^{15}N$ (‰)	TN (%)	Opal (%)
175-1082-A-19-X-3	169.11	184.77	1.780	22.20	5435	2.33	0.36	
175-1082-A-19-X-3	169.61	185.27	1.783	22.80	5094	3.40	0.36	
175-1082-A-19-X-4	169.95	185.61	1.787	22.90	8006	2.95	0.44	
175-1082-A-19-X-4	170.45	186.11	1.789	22.70	14298	2.39	0.72	
175-1082-A-19-X-4	170.95	186.61	1.794	23.20	10220	2.87	0.52	
1751082-C-20-H-6	171.1	189.73	1.795	23.61	5965			
175-1082-A-19-X-5	171.45	187.11	1.797	23.40	9087	3.17	0.47	
1751082-C-20-H-6	171.6	190.23	1.800	22.82	10092			
175-1082-A-19-X-5	171.95	187.61	1.810	22.90		3.02	0.37	
1751082-C-20-H-7	172.1	190.73	1.818	23.15	6777			
175-1082-A-19-X-5	172.40	188.06	1.830	22.70	4197	3.52	0.35	
1751082-C-20-H-7	172.6	191.23	1.843	24.12	3739			
1751082-C-21-H-1	172.6	191.23	1.843	24.15	2247			
1751082-C-21-H-2	173.06	191.69	1.852	22.03	2796			24.76
1751082-C-21-H-2	173.56	192.19	1.863	21.94	2310			
1751082-C-21-H-2	174.05	192.68	1.864	23.27	3021			
1751082-C-21-H-3	174.56	193.19	1.864	23.33	3684			
1751082-C-21-H-3	175.06	193.69	1.865	23.64	4981			
1751082-C-21-H-3	175.56	194.19	1.865	23.88	3575			
1751082-C-21-H-4	176.06	194.69	1.876	24.00	2887			20.36
1751082-C-21-H-4	176.53	195.16	1.877	23.97	2998			
1751082-C-21-H-4	176.98	195.61	1.888	24.24	5495			
175-1082-A-20-X-1	177.00	192.66	1.893	22.00	5867	2.79	0.46	
1751082-C-21-H-5	177.56	196.19	1.898	24.55	3774			
175-1082-A-20-X-2	177.59	193.25	1.899	22.30	5554	2.92	0.45	
175-1082-A-20-X-2	178.09	193.75	1.905	22.80	5713	3.05	0.41	
1751082-C-21-H-5	178.11	196.74	1.905	23.85	1785			
175-1082-A-20-X-2	178.56	194.22	1.918	22.70	6006	2.83	0.36	
1751082-C-21-H-5	178.56	197.19	1.919	21.52	2114			
175-1082-A-20-X-3	179.02	194.68	1.928	23.10	4324	3.23	0.34	
175-1082-A-20-X-3	179.52	195.18	1.933	22.70	5908	3.02	0.35	
175-1082-A-20-X-3	180.02	195.68	1.937	23.20	6832	2.61	0.40	
175-1082-A-20-X-4	180.34	196	1.940	23.50	5607	2.96	0.34	
1751082-C-21-H-7	180.56	199.19	1.941	22.88	1955			
175-1082-A-20-X-4	180.84	196.5	1.942	23.70	3036	2.92	0.27	
1751082-C-21-H-7	181.06	199.69	1.943	23.09	2012			
175-1082-A-20-X-4	181.34	197	1.946	20.20	3350	2.93	0.37	
1751082-C-21-H-7	181.56	200.19	1.948	24.55	788			

LegSitHolCorTypSec	Depth (mbsf)	Depth (mcd)	Age (Ma)	SST (°C)	Alk conc (mmol/g)	$\delta^{15}N$ (‰)	TN (%)	Opal (%)
175-1082-A-20-X-5	181.84	197.5	1.956	20.70	2535	3.39	0.46	
1751082-C-21-H-8	182.06	200.69	1.962	24.15	1383			
175-1082-A-20-X-5	182.32	197.98	1.968	20.80	3792	3.10	0.45	
1751082-C-22-H-1	182.32	200.95	1.974	23.15	2864			
1751082-C-21-H-8	182.56	201.19	1.977	23.94	1572			
1751082-C-22-H-1	182.6	201.23	1.980	23.12	3230			
175-1082-A-20-X-5	182.84	198.5	1.980	20.30	5386	2.89	0.49	
1751082-C-22-H-1	183.1	201.73	1.986	23.00	2548			
1751082-C-22-H-2	183.6	202.23	1.991	23.09	5256			
1751082-C-22-H-2	184.1	202.73	1.992	23.97	4967			11.71
1751082-C-22-H-2	184.54	203.17	1.996	24.03	6287			
1751082-C-22-H-3	185.1	203.73	1.997	24.00	3907			
1751082-C-22-H-3	185.6	204.23	2.002	23.45	4294			
1751082-C-22-H-3	186.1	204.73	2.002	23.48	3806			
175-1082-A-21-X-1	186.60	202.26	2.008	23.30	4268	2.75	0.39	
1751082-C-22-H-4	186.6	205.23	2.013	22.58	4249			
175-1082-A-21-X-2	187.02	202.68	2.015	22.60	5911	2.78	0.40	
1751082-C-22-H-4	187.1	205.73	2.025	22.73	3991			
1751082-C-22-H-5	187.3	205.93	2.032	22.97	3617			
175-1082-A-21-X-2	187.52	203.18	2.033	22.50	6067	3.17	0.37	
1751082-C-22-H-5	187.8	206.43	2.038	23.06	3962			
175-1082-A-21-X-2	188.02	203.68	2.039	21.70	5120	3.36	0.38	
1751082-C-22-H-5	188.3	206.93	2.045	21.70	2535			
175-1082-A-21-X-3	188.52	204.18	2.047	21.20	6140	3.03	0.43	
175-1082-A-21-X-3	189.02	204.68	2.055	21.30	7112	2.83	0.47	
175-1082-A-21-X-3	189.50	205.16	2.057	21.80	6161	2.86	0.47	
175-1082-A-21-X-4	190.02	205.68	2.060	21.30	6147	3.07	0.49	
175-1082-A-21-X-4	190.52	206.18	2.061	22.10	5191	3.36	0.49	
175-1082-A-21-X-4	190.93	206.59	2.063	21.50	5246	3.48	0.49	
175-1082-A-21-X-5	191.07	206.73	2.065	21.80	6253	3.17	0.50	
175-1082-A-21-X-5	191.57	207.23	2.067	19.50	6767	3.17	0.60	
1751082-C-23-H-1	191.6	210.23	2.071	23.67	9118			
175-1082-A-21-X-5	191.97	207.63	2.073	19.20	6611	2.84	0.61	
175-1082-A-21-X-6	192.10	207.76	2.076	19.00	8621	2.84	0.66	
1751082-C-23-H-1	192.13	210.76	2.079	23.97	2799			
175-1082-A-21-X-6	192.60	208.26	2.090	19.20	12601	1.84	0.67	
1751082-C-23-H-1	192.6	211.23	2.093	24.00	2014			
175-1082-A-21-X-6	193.10	208.76	2.097	20.70	10423	1.96	0.56	

LegSitHolCorTypSec	Depth (mbsf)	Depth(mcd)	Age (Ma)	SST (°C)	Alk conc (mmol/g)	$\delta^{15}N$ (‰)	TN (%)	Opal (%)
1751082-C-23-H-2	193.1	211.73	2.100	24.39	1251			
1751082-C-23-H-2	193.6	212.23	2.101	23.67	2237			
1751082-C-23-H-2	194.1	212.73	2.103	22.33	5287			
1751082-C-23-H-3	194.6	213.23	2.104	23.45	5800			
1751082-C-23-H-3	195.1	213.73	2.105	24.58	11034			
1751082-C-23-H-3	195.6	214.23	2.107	25.06	8404			
1751082-C-24-H-1	195.7	214.33	2.108	22.24	5300			
1751082-C-23-H-4	196.08	214.71	2.110	24.70	8123			
1751082-C-24-H-1	196.2	214.83	2.112	22.39	12635			
175-1082-A-22-X-1	196.30	211.96	2.113	22.80	14223	1.92	0.42	
1751082-C-23-H-4	196.6	215.23	2.115	24.91	3637			
1751082-C-24-H-1	196.7	215.33	2.116	22.94	11220			
175-1082-A-22-X-1	196.80	212.46	2.118	23.20	13726	2.40	0.41	
1751082-C-23-H-4	197	215.63	2.120	24.52	2846			
1751082-C-24-H-2	197.23	215.86	2.123	23.21	12612			
175-1082-A-22-X-1	197.30	212.96	2.126	24.30	13142	2.07	0.38	
1751082-C-24-H-2	197.7	216.33	2.132	23.33	17582			
175-1082-A-22-X-2	197.80	213.46	2.135	24.40	11463	2.32	0.36	
175-1082-A-22-X-2	198.30	213.96	2.136	24.30	11690	1.99	0.35	
175-1082-A-22-X-2	198.80	214.46	2.139	23.80	10892	2.45	0.38	
175-1082-A-22-X-3	198.92	214.58	2.140	23.90	10298	2.36	0.35	
175-1082-A-22-X-3	199.42	215.08	2.144	23.90	7733	2.50	0.30	
175-1082-A-22-X-3	199.85	215.51	2.147	24.00	4922	2.56	0.22	
175-1082-A-22-X-4	200.42	216.08	2.151	22.60	6462	2.88	0.30	
175-1082-A-22-X-4	200.92	216.58	2.155	19.60	7612	2.32	0.42	
175-1082-A-23-X-1	206.00	221.66	2.185	23.80	6989	2.95	0.28	
175-1082-A-23-X-1	206.50	222.16	2.188	23.50	6030	3.07	0.28	
175-1082-A-23-X-1	207.00	222.66	2.191	23.30	4404	2.11	0.26	
175-1082-A-23-X-2	207.50	223.16	2.193	23.10	5320	3.31	0.28	
175-1082-A-23-X-2	208.00	223.66	2.196	23.00	10011	2.46	0.40	
175-1082-A-23-X-3	208.16	223.82	2.197	22.40	12661	2.14	0.49	
175-1082-A-23-X-3	208.66	224.32	2.200	22.30	13862	2.21	0.55	
175-1082-A-23-X-3	209.16	224.82	2.202	22.50	9619	2.05	0.45	
175-1082-A-23-X-4	209.66	225.32	2.203	22.80	13608	2.68	0.43	
175-1082-A-23-X-4	210.16	225.82	2.205	22.60	15570	2.33	0.46	
175-1082-A-23-X-4	210.66	226.32	2.207	22.80	11577	2.44	0.36	
175-1082-A-23-X-5	211.16	226.82	2.208	23.00	9659	2.59	0.35	
175-1082-A-23-X-6	211.31	226.97	2.209	23.20	7696	2.58	0.35	

LegSitHolCorTypSec	Depth (mbsf)	Depth (mcd)	Age (Ma)	SST (°C)	Alk conc (mmol/g)	$\delta^{15}N$ (‰)	TN (%)	Opal (%)
175-1082-A-23-X-6	211.82	227.48	2.211	23.10	8200	2.83	0.37	
175-1082-A-23-X-6	212.31	227.97	2.212	23.30	5275	3.00	0.30	
175-1082-A-24-X-1	215.60	231.26	2.223	24.20	4049	3.57	0.26	
175-1082-A-24-X-1	216.10	231.76	2.225	24.30	5791	3.44	0.28	
175-1082-A-24-X-1	216.60	232.26	2.227	24.20	5208	3.03	0.28	
175-1082-A-24-X-2	217.11	232.77	2.229	24.20	5643	3.16	0.29	
175-1082-A-24-X-2	217.61	233.27	2.231	23.40	6500	2.78	0.32	
175-1082-A-24-X-2	218.11	233.77	2.233	23.10	6379	2.92	0.33	
175-1082-A-24-X-3	218.36	234.02	2.234	22.30	4493	3.01	0.32	
175-1082-A-24-X-3	218.86	234.52	2.236	21.90	4430	2.89	0.31	
175-1082-A-24-X-3	219.36	235.02	2.238	21.30	3181	2.98	0.27	
175-1082-A-24-X-4	219.86	235.52	2.240	21.00	3325	2.97	0.30	
175-1082-A-24-X-4	220.36	236.02	2.250	21.40	3305	3.17	0.29	
175-1082-A-24-X-4	220.86	236.52	2.261	22.00	2707	2.90	0.27	
175-1082-A-24-X-5	221.39	237.05	2.272	21.30	6086	2.24	0.51	
175-1082-A-24-X-5	221.89	237.55	2.283	21.80	4833	2.44	0.37	
175-1082-A-24-X-5	222.39	238.05	2.298	23.50	8286	2.55	0.42	
175-1082-A-25-X-1	225.30	240.96	2.300	23.40	6109	2.68	0.41	
175-1082-A-25-X-1	225.80	241.46	2.300	23.70	6061	2.76	0.39	
175-1082-A-25-X-1	226.28	241.94	2.320	23.50	13572	2.03	0.56	
175-1082-A-25-X-2	226.78	242.44	2.327	23.70	11758	2.00	0.49	
175-1082-A-25-X-2	227.28	242.94	2.333	24.30	12310	1.39	0.42	
175-1082-A-25-X-2	227.78	243.44	2.340	25.00	5706	1.77	0.32	
175-1082-A-25-X-3	228.28	243.94	2.344	24.70	8404	1.91	0.39	
175-1082-A-25-X-3	228.78	244.44	2.347	24.70	6936	1.82	0.37	
175-1082-A-25-X-3	229.28	244.94	2.351	24.40	7254	2.23	0.43	
175-1082-A-25-X-4	229.78	245.44	2.354	23.50	11578	1.60	0.50	
175-1082-A-25-X-4	230.28	245.94	2.358	22.90	13506	1.24	0.46	
175-1082-A-25-X-4	230.76	246.42	2.359	23.10	13262	1.32	0.44	
175-1082-A-26-X-1	234.90	250.56	2.374	24.10	4607	1.85	0.25	
175-1082-A-26-X-1	235.40	251.06	2.376	24.20	5770	1.63	0.29	
175-1082-A-26-X-1	235.90	251.56	2.378	24.10	5407	2.02	0.29	
175-1082-A-26-X-2	236.40	252.06	2.380	24.10	6152	1.43	0.29	
175-1082-A-26-X-2	236.90	252.56	2.382	24.20	6578	1.70	0.33	
175-1082-A-26-X-2	237.40	253.06	2.384	24.10	10413	1.08	0.44	
175-1082-A-26-X-3	237.90	253.56	2.386	24.40	5349	1.46	0.26	
175-1082-A-26-X-3	238.40	254.06	2.388	24.40	10300	2.44	0.36	
175-1082-A-26-X-3	238.90	254.56	2.389	24.40	9992	2.45	0.32	

LegSitHolCorTypSec	Depth (mbsf)	Depth (mcd)	Age (Ma)	SST (°C)	Alk conc (mmol/g)	$\delta^{15}N$ (‰)	TN (%)	Opal (%)
175-1082-A-26-X-4	239.40	255.06	2.391	24.80	5704	2.90	0.24	
175-1082-A-26-X-4	239.90	255.56	2.393	25.00	2708	2.89	0.21	
175-1082-A-26-X-4	240.40	256.06	2.395	25.40	3854	2.42	0.22	
175-1082-A-26-X-4	240.68	256.34	2.405	24.40	9165	1.05	0.26	
175-1082-A-26-X-5	240.90	256.56	2.410	25.50	4038	1.95	0.25	
175-1082-A-26-X-5	241.40	257.06	2.412	25.30	5185	2.38	0.27	
175-1082-A-26-X-5	241.90	257.56	2.414	25.30	4666	2.89	0.23	
175-1082-A-26-X-6	242.40	258.06	2.416	25.30	3921	2.68	0.21	
175-1082-A-26-X-6	242.91	258.57	2.418	25.40	3522	2.54	0.21	
175-1082-A-26-X-6	243.40	259.06	2.421	25.10	4908	2.89	0.29	
175-1082-A-26-X-7	243.90	259.56	2.425	25.40	4815	2.03	0.30	
175-1082-A-27-X-1	244.50	260.16	2.429	22.40	5863	0.92	0.32	
175-1082-A-27-X-1	245.00	260.66	2.433	22.00	14019	1.65	0.53	
175-1082-A-27-X-1	245.50	261.16	2.435	21.60	6885	1.51	0.32	
175-1082-A-27-X-2	246.00	261.66	2.438	21.90	13210	1.35	0.51	
175-1082-A-27-X-2	246.50	262.16	2.441	23.00	16148	1.30	0.63	
175-1082-A-27-X-2	247.00	262.66	2.444	23.50	13132	0.90	0.51	
175-1082-A-27-X-3	247.50	263.16	2.447	23.20	17941	1.80	0.64	
175-1082-A-27-X-3	248.00	263.66	2.450	23.30	13408	0.54	0.70	
175-1082-A-27-X-3	248.50	264.16	2.453	23.60	13515	1.88	0.61	
175-1082-A-27-X-4	249.00	264.66	2.456	23.90	13422	1.66	0.50	
175-1082-A-27-X-4	249.70	265.36	2.460	24.40	11616	2.03	0.43	
175-1082-A-27-X-4	250.00	265.66	2.467	24.40	12289	2.03	0.49	
175-1082-A-27-X-5	250.54	266.2	2.480	23.70	10322	1.79	0.47	
175-1082-A-27-X-5	250.84	266.5	2.488	23.80	10095	1.89	0.47	
175-1082-A-27-X-5	251.14	266.8	2.491	24.10	8612	1.69	0.40	
175-1082-A-27-X-5	251.45	267.11	2.495	24.30	7925	2.19	0.36	
175-1082-A-27-X-CC	252.04	267.7	2.503	24.30	6812	2.10	0.35	
175-1082-A-28-X-1	254.17	269.83	2.514	23.70	7706	1.96	0.39	
175-1082-A-28-X-1	254.47	270.13	2.516	23.60	8341	2.64	0.42	
175-1082-A-28-X-1	254.77	270.43	2.518	23.20	7175	2.90	0.41	
175-1082-A-28-X-1	255.08	270.74	2.519	22.90	9121	2.82	0.53	
175-1082-A-28-X-2	255.60	271.26	2.522	21.50	2663	2.10	0.28	
175-1082-A-28-X-2	256.10	271.76	2.525	20.80	5951	2.11	0.37	
175-1082-A-28-X-2	256.60	272.26	2.530	21.50	7510	2.05	0.42	
175-1082-A-28-X-3	257.10	272.76	2.534	22.70	13278	1.55	0.61	
175-1082-A-28-X-3	257.60	273.26	2.539	24.10	6771	2.25	0.31	
175-1082-A-28-X-3	258.10	273.76	2.543	24.80	4653	2.00	0.27	

LegSitHolCorTypSec	Depth (mbsf)	Depth (mcd)	Age (Ma)	SST (°C)	Alk conc (mmol/g)	$\delta^{15}N$ (‰)	TN (%)	Opal (%)
175-1082-A-28-X-4	258.60	274.26	2.548	25.00	3337	2.46	0.23	
175-1082-A-28-X-4	259.11	274.77	2.550	25.10	5421	1.60	0.28	
175-1082-A-28-X-4	259.60	275.26	2.553	25.00	4868	2.54	0.23	
175-1082-A-28-X-5	260.00	275.66	2.555	25.00	6142	1.74	0.26	
175-1082-A-28-X-5	260.50	276.16	2.557	25.10	5653	2.39	0.25	
175-1082-A-28-X-5	261.00	276.66	2.560	25.20	7202	1.66	0.29	
175-1082-A-28-X-6	261.50	277.16	2.563	24.30	11820	1.22	0.37	
175-1082-A-28-X-6	261.98	277.64	2.565	24.20	9621	0.71	0.31	
175-1082-A-29-X-1	263.70	279.36	2.573	24.40	9484	1.44	0.33	20.28
175-1082-A-29-X-1	264.20	279.86	2.575	24.70	9044	1.68	0.34	26.54
175-1082-A-29-X-1	264.70	280.36	2.578	25.40	6893	2.21	0.31	
175-1082-A-29-X-2	265.20	280.86	2.580	25.20	6511	0.90	0.26	18.81
175-1082-A-29-X-2	265.70	281.36	2.585	25.80	6250	0.75	0.25	11.30
175-1082-A-29-X-2	266.20	281.86	2.587	25.50	6581	0.91	0.24	11.18
175-1082-A-29-X-3	266.70	282.36	2.589	25.40	4581	1.24	0.24	12.20
175-1082-A-29-X-3	267.20	282.86	2.592	25.20	6747	0.51	0.28	12.57
175-1082-A-29-X-3	267.70	283.36	2.594	25.30	4498	0.87	0.26	15.72
175-1082-A-29-X-4	268.20	283.86	2.596	25.00	6574	1.11	0.29	11.50
175-1082-A-29-X-4	268.70	284.36	2.598	24.80	8062	1.61	0.36	18.90
175-1082-A-29-X-4	269.20	284.86	2.600	24.60	9956	1.54	0.37	18.90
175-1082-A-29-X-5	269.70	285.36	2.603	24.00	10088	1.67	0.37	5.83
175-1082-A-29-X-5	270.20	285.86	2.604	24.10	11641	0.79	0.37	8.88
175-1082-A-29-X-5	270.70	286.36	2.605	24.10	15307	1.12	0.43	7.03
175-1082-A-29-X-6	271.20	286.86	2.606	24.40	8158	0.12	0.28	16.99
175-1082-A-29-X-6	271.70	287.36	2.607	24.50	7306	0.67	0.28	16.68
175-1082-A-29-X-6	272.20	287.86	2.608	24.00	7586	0.57	0.29	25.55
175-1082-A-29-X-7	272.69	288.36	2.614	24.00	9209	0.07	0.28	18.20
175-1082-A-30-X-1	273.40	289.06	2.623	25.30	6750	1.84	0.27	14.19
175-1082-A-30-X-1	273.90	289.56	2.628	25.20	8315	0.38	0.27	16.83
175-1082-A-30-X-1	274.40	290.06	2.634	24.50	9183	1.03	0.29	19.46
175-1082-A-30-X-2	274.90	290.56	2.639	25.00	4443	0.13	0.24	20.35
175-1082-A-30-X-2	275.40	291.06	2.645	24.20	4570	1.34	0.27	27.97
175-1082-A-30-X-2	275.90	291.56	2.649	24.40	5222	0.39	0.27	
175-1082-A-30-X-3	276.40	292.06	2.654	24.70	4258	0.67	0.29	15.10
175-1082-A-30-X-3	276.90	292.56	2.658	24.60	5323	0.86	0.32	14.50
175-1082-A-30-X-3	277.40	293.06	2.663	25.30	6764	1.66	0.32	17.00
175-1082-A-30-X-4	277.90	293.56	2.669	24.70	3865	1.57	0.30	29.00
175-1082-A-30-X-4	278.40	294.06	2.675	24.10	6286	1.60	0.35	25.80

LegSitHolCorTypSec	Depth (mbsf)	Depth(mcd)	Age (Ma)	SST (°C)	Alk conc (mmol/g)	$\delta^{15}N$ (‰)	TN (%)	Opal (%)
175-1082-A-30-X-4	278.90	294.56	2.681	24.20	7551	0.81	0.39	14.90
175-1082-A-30-X-5	279.40	295.06	2.688	24.20	9537	0.91	0.44	15.10
175-1082-A-30-X-5	279.87	295.53	2.688	25.00	4982	0.97	0.29	18.40
175-1082-A-30-X-CC	280.16	295.82	2.689	24.50	12262	1.27	0.29	
175-1082-A-31-X-1	283.00	298.66	2.693	25.70	4589	2.44	0.32	27.27
175-1082-A-31-X-1	283.51	299.07	2.695	25.20	6834	2.06	0.36	
175-1082-A-31-X-2	283.90	299.56	2.697	25.90	5691	2.45	0.39	15.88
175-1082-A-31-X-2	284.40	300.06	2.700	26.00	4563	1.98	0.31	
175-1082-A-31-X-2	284.88	300.54	2.703	26.30	4637	1.73	0.28	29.54
175-1082-A-31-X-3	285.02	300.68	2.703	26.10	4819	2.23	0.32	
175-1082-A-31-X-3	285.52	301.18	2.703	25.50	7811	1.88	0.36	17.73
175-1082-A-31-X-3	286.02	301.68	2.704	25.10	7777	1.25	0.38	
175-1082-A-31-X-4	286.49	302.15	2.704	25.20	8416	1.56	0.31	17.27
175-1082-A-31-X-4	286.99	302.65	2.705	24.50	10416	1.28	0.29	
175-1082-A-31-X-4	287.49	303.15	2.706	25.00	4645	0.35	0.31	23.78
175-1082-A-31-X-5	287.66	303.32	2.707	25.36	4327	0.10	0.29	
175-1082-A-31-X-5	288.16	303.82	2.708	24.40	5233	0.93	0.34	19.53
175-1082-A-31-X-5	288.66	304.32	2.709	24.70	4361	0.70	0.41	15.37
175-1082-A-32-X-1	292.60	308.26	2.720	24.60	5622	0.36	0.44	
175-1082-A-32-X-1	293.10	308.76	2.721	24.70	3880	1.37	0.58	24.15
175-1082-A-32-X-1	293.60	309.26	2.723	24.10	6361	0.64	0.22	
175-1082-A-32-X-2	294.10	309.76	2.725	24.20	7902	1.02	0.34	11.32
175-1082-A-32-X-2	294.60	310.26	2.728	24.20	9632	0.82	0.36	
175-1082-A-32-X-2	295.07	310.73	2.731	25.00	4857	1.63	0.25	20.40
175-1082-A-32-X-3	295.60	311.26	2.734	24.50	12545	0.58	0.23	
175-1082-A-32-X-3	296.10	311.76	2.737	25.70	5171	2.27	0.21	14.81
175-1082-A-32-X-3	296.60	312.26	2.740	25.20	7406	0.98	0.19	
175-1082-A-32-X-4	297.10	312.76	2.743	26.10	2853	0.63	0.19	8.94
175-1082-A-32-X-4	297.60	313.26	2.747	25.50	2864	1.57	0.19	
175-1082-A-32-X-4	298.10	313.76	2.752	25.70	3092	1.45	0.21	
175-1082-A-32-X-5	298.60	314.26	2.756	25.70	8828	1.25	0.29	
175-1082-A-32-X-5	299.08	314.64	2.760	25.50	6566	1.03	0.29	
175-1082-A-33-X-1	302.20	317.86	2.785	26.30	10834	2.31	0.30	
175-1082-A-33-X-1	302.70	318.36	2.788	26.10	9581	2.29	0.30	
175-1082-A-33-X-1	303.20	318.86	2.791	25.90	8693	1.80	0.28	
175-1082-A-33-X-2	303.70	319.36	2.794	25.97	8946	1.49	0.29	
175-1082-A-33-X-2	304.20	319.86	2.796	25.85	8727	1.47	0.28	
175-1082-A-33-X-2	304.70	320.36	2.799	25.76	9841	1.90	0.34	

LegSitHolCorTypSec	Depth (mbsf)	Depth (mcd)	Age (Ma)	SST (°C)	Alk conc (mmol/g)	$\delta^{15}N$ (‰)	TN (%)	Opal (%)
175-1082-A-33-X-3	305.20	320.86	2.802	25.55	8075	1.58	0.36	
175-1082-A-33-X-3	305.70	321.36	2.805	25.03	13741	1.59	0.44	
175-1082-A-33-X-3	306.21	321.87	2.807	25.36	8186	1.39	0.29	
175-1082-A-33-X-4	306.74	322.4	2.808	25.61	13650	1.32	0.38	
175-1082-A-33-X-4	307.24	322.9	2.810	25.55	16878	1.12	0.44	
175-1082-A-33-X-4	307.74	323.4	2.812	25.39	14564	1.44	0.43	
175-1082-A-33-X-5	308.24	323.9	2.813	25.42	10588	1.34	0.31	
175-1082-A-33-X-5	308.74	324.4	2.815	25.12	14393	1.64	0.43	
175-1082-A-33-X-5	309.24	324.9	2.817	25.30	8542	1.57	0.28	
175-1082-A-34-X-1	311.80	327.46	2.825	26.73	6496	0.73	0.21	
175-1082-A-34-X-1	312.30	327.96	2.829	26.70	10931	1.67	0.24	
175-1082-A-34-X-1	312.80	328.46	2.833	26.67	7800	0.80	0.23	
175-1082-A-34-X-2	313.30	328.96	2.834	26.36	10616	1.31	0.26	
175-1082-A-34-X-2	313.80	329.46	2.836	26.18	9688	1.89	0.31	
175-1082-A-34-X-2	314.30	329.96	2.837	26.15	12577	2.01	0.31	
175-1082-A-34-X-3	314.82	330.48	2.839	25.94	8099	1.43	0.26	
175-1082-A-34-X-3	315.32	330.98	2.841	25.79	8317	1.93	0.25	
175-1082-A-34-X-3	315.82	331.48	2.842	25.73	5467	1.96	0.21	
175-1082-A-34-X-4	316.28	331.94	2.844	25.48	9031	1.53	0.28	
175-1082-A-34-X-4	316.78	332.44	2.845	25.48	9325	1.35	0.26	
175-1082-A-34-X-CC	317.52	333.18	2.848	24.64	16456	1.56	0.26	
175-1082-A-35-X-1	321.50	337.16	2.887	26.00	6028	0.98	0.27	
175-1082-A-35-X-1	322.00	337.66	2.892	25.91	7233	1.25	0.23	
175-1082-A-35-X-1	322.50	338.16	2.898	26.42	4132	1.30	0.21	
175-1082-A-35-X-2	323.00	338.66	2.900	26.03	5326	1.87	0.22	
175-1082-A-35-X-2	323.50	339.16	2.903	26.15	3251	1.84	0.22	
175-1082-A-35-X-2	324.00	339.66	2.905	26.18	3948	2.56	0.23	
175-1082-A-35-X-3	324.50	340.16	2.908	26.03	5292	1.81	0.25	
175-1082-A-35-X-3	325.00	340.66	2.910	26.06	4915	1.66	0.25	
175-1082-A-35-X-3	325.50	341.16	2.914	25.88	3547	1.60	0.22	
175-1082-A-35-X-4	326.00	341.66	2.918	25.48	4041	1.43	0.25	
175-1082-A-35-X-4	326.50	342.16	2.921	24.94	5710	1.76	0.28	
175-1082-A-35-X-4	327.00	342.66	2.925	24.50	6256	2.31	0.33	
175-1082-A-35-X-5	327.50	343.16	2.935	25.76	7209	1.52	0.36	
175-1082-A-36-X-1	327.77	343.43	2.941	25.80	3248	1.63	0.22	
175-1082-A-35-X-5	328.00	343.66	2.945	25.90	5791	1.32	0.27	
175-1082-A-35-X-5	328.10	343.76	2.948	26.30	2734	2.00	0.23	
175-1082-A-36-X-1	328.17	343.83	2.948	26.00	3434	2.18	0.22	

LegSitHolCorTypSec	Depth (mbsf)	Depth (mcd)	Age (Ma)	SST (°C)	Alk conc (mmol/g)	$\delta^{15}N$ (‰)	TN (%)	Opal (%)
175-1082-A-37-X-2	331.27	346.93	2.975	23.50	5277	2.41	0.31	
175-1082-A-37-X-2	331.66	347.32	2.980	24.00	5658	2.13	0.32	
175-1082-A-37-X-2	332.46	348.12	2.983	24.20	7260	2.66	0.37	
175-1082-A-37-X-3	332.86	348.52	2.984	24.90	8570	2.41	0.39	
175-1082-A-37-X-3	333.26	348.92	2.985	25.20	9083	2.63	0.38	
175-1082-A-37-X-3	333.66	349.32	2.989	25.10	7483	2.62	0.36	
175-1082-A-37-X-4	334.29	349.95	2.995	25.50	7506	2.52	0.47	
175-1082-A-37-X-4	334.44	350.1	2.995	24.80	8670	2.87	0.45	
175-1082-A-37-X-4	334.86	350.52	2.996	24.90	8641	2.89	0.49	
175-1082-A-37-X-4	335.26	350.92	2.996	24.90	7967	2.48	0.40	
175-1082-A-37-X-4	335.66	351.32	2.997	24.80	8094	2.86	0.41	
175-1082-A-37-X-5	336.29	351.95	2.998	25.40	5525	2.99	0.40	
175-1082-A-37-X-5	336.46	352.12	3.010	24.50	7969	3.11	0.42	
175-1082-A-37-X-CC	336.88	352.54	3.011	24.40	11642	3.12	0.52	
175-1082-A-38-X-1	340.70	356.36	3.025	25.80	6612	2.75	0.31	
175-1082-A-38-X-1	341.20	356.86	3.035	25.80	3420	2.45	0.28	
175-1082-A-38-X-1	341.37	357.03	3.038	25.30	3662	1.96	0.27	
175-1082-A-38-X-1	341.77	357.43	3.045	25.10	2631	2.21	0.23	
175-1082-A-38-X-2	342.17	357.83	3.049	25.60	2974	2.24	0.26	
175-1082-A-38-X-2	342.57	358.23	3.053	25.70	4636	2.90	0.31	
175-1082-A-38-X-2	343.37	359.03	3.060	26.40	4762	2.08	0.23	
175-1082-A-38-X-3	343.77	359.43	3.068	25.80	6208	2.53	0.29	
175-1082-A-38-X-3	344.17	359.83	3.075	25.60	3098	0.95	0.19	
175-1082-A-38-X-3	344.57	360.23	3.083	25.50	6494	1.96	0.28	
175-1082-A-38-X-3	344.70	360.36	3.085	25.90	4465	2.42	0.29	
175-1082-A-38-X-4	345.37	361.03	3.090	25.10	5065	2.01	0.25	
175-1082-A-38-X-4	345.75	361.41	3.094	25.30	5948	2.13	0.26	
175-1082-A-38-X-4	346.17	361.83	3.099	25.60	5459	2.30	0.25	
175-1082-A-38-X-4	346.58	362.24	3.104	25.60	6716	1.41	0.30	
175-1082-A-38-X-5	346.70	362.36	3.105	26.10	5045	2.18	0.30	
175-1082-A-38-X-5	347.37	363.03	3.109	25.70	6953	2.46	0.30	
175-1082-A-38-X-5	347.77	363.43	3.112	25.50	6156	2.16	0.28	
175-1082-A-38-X-6	348.17	363.83	3.114	25.50	5513	2.17	0.28	
175-1082-A-38-X-6	348.57	364.23	3.117	25.20	6857	2.45	0.31	
175-1082-A-38-X-CC	349.20	364.86	3.121	25.20	5822	1.55	0.27	
175-1082-A-39-X-1	350.90	366.56	3.131	25.10	4291	2.25	0.35	
175-1082-A-39-X-1	351.07	366.73	3.132	24.50	4298	1.73	0.27	
175-1082-A-39-X-1	351.47	367.13	3.135	24.40	5667	1.53	0.30	

LegSitHolCorTypSec	Depth (mbsf)	Depth (mcd)	Age (Ma)	SST (°C)	Alk conc (mmol/g)	$\delta^{15}N$ (‰)	TN (%)	Opal (%)
175-1082-A-39-X-2	351.84	367.5	3.140	24.70	9779	1.66	0.40	
175-1082-A-39-X-2	352.27	367.93	3.145	26.00	12560	2.06	0.51	
175-1082-A-39-X-2	353.06	368.72	3.155	26.10	13526	1.25	0.28	
175-1082-A-39-X-3	353.24	368.9	3.159	26.10	12446	1.82	0.26	
175-1082-A-39-X-4	353.89	369.55	3.175	26.00	16405	2.11	0.30	
175-1082-A-39-X-4	354.29	369.95	3.183	25.90	17514	2.36	0.29	
175-1082-A-39-X-4	354.69	370.35	3.192	26.10	13346	1.63	0.29	
175-1082-A-39-X-5	355.31	370.97	3.205	26.00	12111	2.15	0.30	
175-1082-A-39-X-5	355.71	371.37	3.208	26.20	7442	1.39	0.29	
175-1082-A-39-X-CC	356.11	371.77	3.212	25.70	14499	1.92	0.32	
175-1082-A-39-X-CC	356.46	372.12	3.215	25.40	12174	1.80	0.33	
175-1082-A-40-X-1	360.07	375.73	3.240	26.10	11669	1.37	0.29	
175-1082-A-40-X-2	360.49	376.15	3.245	25.90	19048	1.57	0.34	
175-1082-A-40-X-2	360.79	376.45	3.249	26.00	16214	1.82	0.30	
175-1082-A-40-X-2	361.09	376.75	3.253	25.90	16195	1.95	0.31	
175-1082-A-40-X-2	361.39	377.05	3.256	26.20	13853	0.91	0.28	
175-1082-A-40-X-2	361.69	377.35	3.260	25.90	13442	0.59	0.29	
175-1082-A-40-X-3	361.99	377.65	3.264	25.90	13328	1.17	0.30	
175-1082-A-40-X-4	362.36	378.02	3.270	25.60	15504	1.07	0.29	
175-1082-A-40-X-4	362.66	378.32	3.274	25.60	15604	1.44	0.31	
175-1082-A-40-X-4	362.96	378.62	3.278	25.60	14752	1.62	0.34	
175-1082-A-40-X-4	363.26	378.92	3.282	25.60	7729	1.73	0.41	
175-1082-A-40-X-5	363.79	379.45	3.290	26.20	8994	1.54	0.37	
175-1082-A-40-X-5	363.86	379.52	3.292	25.70	28234	1.87	0.38	
175-1082-A-40-X-5	364.16	379.82	3.299	25.80	25674	1.26	0.35	
175-1082-A-40-X-5	364.46	380.12	3.307	25.80	17312	1.42	0.28	
175-1082-A-40-X-5	364.76	380.42	3.314	25.80	8474	1.28	0.31	
175-1082-A-40-X-5	365.00	380.66	3.320	25.50	11542	2.23	0.33	
175-1082-A-40-X-6	365.36	381.02	3.321	25.50	9537	1.57	0.32	
175-1082-A-40-X-6	365.66	381.32	3.322	25.70	8264	1.67	0.31	
175-1082-A-40-X-6	365.96	381.62	3.323	25.80	7561	1.70	0.30	
175-1082-A-40-X-CC	366.21	381.87	3.324	25.70	8722	1.65	0.28	
175-1082-A-40-X-CC	366.44	382.1	3.324	25.80	8885	1.48	0.30	
175-1082-A-41-X-1	369.67	385.33	3.334	25.80	4535	1.86	0.24	
175-1082-A-41-X-1	369.98	385.64	3.335	25.90	5818	1.81	0.26	
175-1082-A-41-X-1	370.28	385.94	3.336	25.80	7365	1.96	0.28	
175-1082-A-41-X-1	370.57	386.23	3.337	25.60	5732	0.98	0.26	
175-1082-A-41-X-1	370.60	386.26	3.337	26.10	3934	0.84	0.27	

LegSitHolCorTypSec	Depth (mbsf)	Depth (mcd)	Age (Ma)	SST (°C)	Alk conc (mmol/g)	$\delta^{15}N$ (‰)	TN (%)	Opal (%)
175-1082-A-41-X-2	371.17	386.83	3.339	25.50	5590	1.41	0.27	
175-1082-A-41-X-2	371.47	387.13	3.340	25.80	5102	1.25	0.24	
175-1082-A-41-X-2	371.77	387.43	3.345	25.90	5613	1.35	0.24	
175-1082-A-41-X-2	372.07	387.73	3.350	26.20	4819	0.78	0.19	
175-1082-A-41-X-3	372.60	388.26	3.365	26.30	7390	1.34	0.23	
175-1082-A-41-X-3	372.67	388.33	3.366	25.80	6165	0.95	0.23	
175-1082-A-41-X-3	372.97	388.63	3.371	25.50	6880	1.66	0.30	
175-1082-A-41-X-3	373.27	388.93	3.375	25.30	5604	1.54	0.29	
175-1082-A-41-X-3	373.57	389.23	3.380	24.70	12790	2.82	0.53	
175-1082-A-41-X-3	373.60	389.26	3.381	25.20	8515	2.53	0.60	
175-1082-A-41-X-4	374.17	389.83	3.390	25.80	7008	2.07	0.29	
175-1082-A-41-X-4	374.47	390.13	3.395	25.80	15760	2.80	0.47	
175-1082-A-41-X-4	374.77	390.43	3.400	26.60	7441	2.23	0.30	
175-1082-A-41-X-4	375.07	390.73	3.402	26.50	9663	1.92	0.22	
175-1082-A-41-X-5	375.60	391.26	3.405	25.60	2902	2.28	0.22	
175-1082-A-41-X-5	375.67	391.33	3.406	26.30	6777	2.08	0.23	
175-1082-A-41-X-5	375.95	391.61	3.412	26.60	10729	2.34	0.24	
175-1082-A-41-X-5	376.27	391.93	3.419	26.60	18856	3.69	0.31	
175-1082-A-41-X-5	376.57	392.23	3.425	26.50	19533	3.14	0.34	
175-1082-A-41-X-6	377.18	392.84	3.440	26.50	5772	1.77	0.24	
175-1082-A-41-X-6	377.47	393.13	3.443	26.60	4942	1.79	0.23	
175-1082-A-41-X-6	377.77	393.43	3.447	26.20	4606	1.90	0.21	
175-1082-A-41-X-6	378.07	393.73	3.450	26.80	4016	1.76	0.20	
175-1082-A-42-X-1	379.37	395.03	3.465	26.50	4700	1.20	0.20	
175-1082-A-42-X-1	379.67	395.33	3.468	26.50	3031	1.01	0.19	
175-1082-A-42-X-1	379.98	395.64	3.471	26.70	4168	0.99	0.19	
175-1082-A-42-X-1	380.27	395.93	3.474	26.70	4553	0.27	0.21	
175-1082-A-42-X-2	380.80	396.46	3.480	27.18	3324	1.71	0.23	

Appendix 2: Site 1239 data

* Leg –Site – Core- Type-Section

LegSitHolCorTypSec*	Depth (mbsf)	Depth (mcd)	Age (Ma)	SST (°C)	Alk conc (mmol/g)	$\delta^{15}N$ (‰)	TN (%)	Corg (%)
202-1239-A-3-H-3	15.93	17.32	0.519	26.67	6157.91	3.46	0.10	0.95
202-1239-A-3-H-3	16.11	17.54	0.525	25.58	3073.04			
202-1239-A-3-H-3	16.31	17.76	0.532	25.33	4062.34	4.03	0.09	
202-1239-A-3-H-3	16.51	17.97	0.539	24.73	4147.65			
202-1239-A-3-H-3	16.71	18.19	0.545	25.00	4097.74	3.92	0.09	
202-1239-A-3-H-3	16.91	18.40	0.552	24.82	4035.18			
202-1239-A-3-H-3	17.11	18.60	0.558	24.48	5079.72	4.45	0.11	
202-1239-A-3-H-3	17.31	18.80	0.564	23.97	4632.08			
202-1239-A-3-H-4	17.49	18.96	0.567	24.21	5683.59	3.78	0.09	
202-1239-A-3-H-4	17.72	19.16	0.570	24.61	6359.11			
202-1239-A-3-H-4	17.95	19.36	0.572	25.18	4619.97	3.30	0.06	
202-1239-A-3-H-4	18.12	19.51	0.574	25.58	3779.68			
202-1239-A-3-H-4	18.28	19.67	0.576	26.21	5106.60	4.80	0.11	
202-1239-A-3-H-4	18.52	19.91	0.578	25.21	6010.38			
202-1239-A-3-H-4	18.76	20.15	0.581	25.48	6268.81	4.79	0.12	
202-1239-A-3-H-5	18.93	20.31	0.583	25.70	4688.80			
202-1239-A-3-H-5	19.13	20.51	0.586	25.82	2733.47	4.80	0.10	
202-1239-A-3-H-5	19.33	20.71	0.588	25.30	3102.62			
202-1239-A-3-H-5	19.53	20.91	0.591	25.27	6817.17	4.55	0.13	1.26
202-1239-A-3-H-5	19.73	21.10	0.595	25.70	8422.30			
202-1239-A-3-H-5	19.93	21.29	0.599	25.79	7298.26	4.96	0.11	
202-1239-A-3-H-5	20.13	21.48	0.603	25.42	7244.37			
202-1239-A-3-H-5	20.33	21.67	0.607	26.09	8533.31	4.18	0.13	
202-1239-A-3-H-6	20.54	21.85	0.610	26.30	9546.85			
202-1239-A-3-H-6	20.74	22.03	0.614	26.97	7071.24	5.45	0.13	
202-1239-A-3-H-6	20.94	22.20	0.618	26.91	4674.09			
202-1239-A-3-H-6	21.14	22.38	0.622	26.39	4080.10	5.81	0.11	
202-1239-A-3-H-6	21.34	22.56	0.625	25.88	3853.61			
202-1239-A-3-H-6	21.54	22.74	0.629	24.73	5757.70	4.98	0.14	
202-1239-A-3-H-6	21.74	22.92	0.633	23.91	5723.48			
202-1239-A-3-H-7	21.97	23.13	0.637	24.18	6488.83	3.36	0.12	
202-1239-A-3-H-7	22.15	23.29	0.640	24.33	6059.09			
202-1239-A-3-H-7	22.35	23.47	0.643	24.45	6173.36	3.81	0.12	
202-1239-A-3-H-7	22.55	23.65	0.647	24.91	6968.13			

LegSitHolCorTypSec	Depth (mbsf)	Depth (mcd)	Age (Ma)	SST (°C)	Alk conc (mmol/g)	$\delta^{15}N$ (‰)	TN (%)	Corg (%)
202-1239-A-3-H-CC	22.80	23.87	0.651	24.94	8571.67	3.93	0.12	
202-1239-A-4-H-1	22.50	24.61	0.665	25.33	9383.54			
202-1239-A-4-H-1	22.60	24.73	0.667	25.67	8302.59	2.58	0.11	1.11
202-1239-A-4-H-1	22.90	25.09	0.674	25.79	8864.92			
202-1239-A-4-H-1	23.10	25.30	0.678	25.76	11127.87	3.20	0.14	
202-1239-A-4-H-1	23.30	25.51	0.682	25.61	13350.62			
202-1239-A-4-H-1	23.50	25.70	0.685	25.94	12314.81	3.37	0.13	
202-1239-A-4-H-1	23.70	25.89	0.689	26.48	8127.57			
202-1239-A-4-H-2	23.93	26.11	0.693	26.70	3703.17	3.91	0.09	
202-1239-A-4-H-2	24.11	26.28	0.696	26.30	7116.04			
202-1239-A-4-H-2	24.31	26.47	0.700	26.55	8630.69	4.39	0.16	
202-1239-A-4-H-2	24.51	26.69	0.704	26.58	7687.21			
202-1239-A-4-H-2	24.71	26.91	0.708	26.70	6757.14	4.19	0.14	
202-1239-A-4-H-2	24.91	27.13	0.712	26.18	6307.26			
202-1239-A-4-H-2	25.11	27.34	0.715	25.88	7806.50	3.81	0.14	
202-1239-A-4-H-2	25.31	27.54	0.718	24.67	10238.68			
202-1239-A-4-H-3	25.52	27.75	0.722	24.42	10608.75	2.09	0.14	
202-1239-A-4-H-3	25.72	27.95	0.725	24.52	11697.63			
202-1239-A-4-H-3	25.92	28.15	0.728	24.36	10404.73	2.60	0.14	
202-1239-A-4-H-3	26.12	28.36	0.731	24.73	7011.52			
202-1239-A-4-H-3	26.32	28.60	0.734	24.85	7079.04	3.54	0.13	1.33
202-1239-A-4-H-3	26.52	28.80	0.737	24.42	9574.95			
202-1239-A-4-H-3	26.72	28.99	0.740	24.61	8421.48	3.98	0.12	
202-1239-A-4-H-4	26.93	29.20	0.743	24.52	7992.74			
202-1239-A-4-H-4	27.13	29.39	0.746	24.61	7864.05	4.39	0.17	
202-1239-A-4-H-4	27.33	29.58	0.749	23.64	9007.15			
202-1239-A-4-H-4	27.53	29.78	0.753	24.03	7105.64	2.88	0.10	
202-1239-A-4-H-4	27.73	29.97	0.756	24.88	7109.26			
202-1239-A-4-H-4	27.93	30.16	0.759	25.82	8579.82	3.32	0.12	
202-1239-A-4-H-4	28.13	30.36	0.763	25.70	10490.46			
202-1239-A-4-H-4	28.33	30.56	0.767	25.70	8035.90	4.37	0.13	
202-1239-A-4-H-5	28.54	30.79	0.771	25.48	8147.66			
202-1239-A-4-H-5	28.74	31.01	0.775	26.33	7645.29	4.60	0.14	
202-1239-A-4-H-5	28.84	31.11	0.776	26.15	7111.50			
202-1239-A-4-H-5	28.94	31.22	0.778	26.73	8214.71	4.57	0.14	
202-1239-A-4-H-5	29.04	31.32	0.780	26.00	5146.72			
202-1239-A-4-H-5	29.14	31.41	0.782	25.88	3190.11	5.04	0.12	
202-1239-A-4-H-5	29.24	31.51	0.784	25.79	3682.76			

LegSitHolCorTypSec	Depth (mbsf)	Depth (mcd)	Age (Ma)	SST (°C)	Alk conc (mmol/g)	$\delta^{15}N$ (‰)	TN (%)	Corg (%)
202-1239-A-4-H-5	29.34	31.61	0.785	26.03	2609.50	4.74	0.13	1.25
202-1239-A-4-H-5	29.44	31.71	0.787	25.88	3701.73			
202-1239-A-4-H-5	29.54	31.80	0.789	25.70	3223.59	4.99	0.15	
202-1239-A-4-H-5	29.64	31.90	0.791	24.48	3942.18			
202-1239-A-4-H-5	29.74	32.00	0.792	25.36	3665.86	4.86	0.19	
202-1239-A-4-H-5	29.84	32.10	0.794	24.00	5014.14			
202-1239-A-4-H-6	29.96	32.21	0.796	24.48	4177.02	4.33	0.17	
202-1239-A-4-H-6	30.04	32.29	0.798	23.21	4649.71			
202-1239-A-4-H-6	30.14	32.39	0.799	23.79	4422.52	2.84	0.14	
202-1239-A-4-H-6	30.24	32.49	0.801	23.21	5391.98			
202-1239-A-4-H-6	30.34	32.58	0.803	23.52	4522.07	2.04	0.12	
202-1239-A-4-H-6	30.44	32.68	0.805	23.24	5010.40			
202-1239-A-4-H-6	30.54	32.78	0.806	24.00	4282.93	2.11	0.10	
202-1239-A-4-H-6	30.64	32.88	0.808	23.45	6290.78			
202-1239-A-4-H-6	30.74	32.97	0.810	24.09	5060.13	1.77	0.11	
202-1239-A-4-H-6	30.84	33.08	0.812	22.82	6805.74			
202-1239-A-4-H-6	30.94	33.19	0.814	23.76	5259.83	1.98	0.12	
202-1239-A-4-H-6	31.04	33.30	0.815	23.70	5825.24			
202-1239-A-4-H-6	31.14	33.41	0.817	24.67	3993.45	2.95	0.11	1.11
202-1239-A-4-H-6	31.24	33.51	0.818	24.27	5833.54			
202-1239-A-4-H-6	31.34	33.62	0.819	24.36	5140.06	2.86	0.12	
202-1239-A-4-H-7	31.44	33.73	0.820	24.42	5476.92			
202-1239-A-4-H-7	31.54	33.84	0.822	24.45	4501.25	3.80	0.12	
202-1239-A-4-H-7	31.64	33.95	0.823	24.70	4335.17			
202-1239-A-4-H-7	31.74	34.06	0.824	24.42	3866.28	3.80	0.12	
202-1239-A-4-H-7	31.84	34.17	0.826	25.24	3509.35			
202-1239-A-4-H-7	31.94	34.28	0.827	24.73	2855.86	3.84	0.11	
202-1239-A-4-H-7	32.04	34.38	0.828	24.82	3570.87			
202-1239-A-4-H-CC	32.15	34.51	0.830	24.27	4410.66	3.53	0.12	
202-1239-A-4-H-CC	32.23	34.60	0.831	24.58	3886.00			
202-1239-A-4-H-CC	32.33	34.71	0.832	25.15	2506.19	4.91	0.10	
202-1239-A-5-H-1	31.90	35.65	0.844	25.33	3033.51			
202-1239-A-5-H-1	32.00	35.75	0.847	24.82	2546.74	3.75	0.11	
202-1239-A-5-H-1	32.10	35.85	0.849	25.24	5340.54			
202-1239-A-5-H-1	32.20	35.95	0.851	25.36	3747.78	3.75	0.12	
202-1239-A-5-H-1	32.30	36.05	0.854	24.61	4831.06			
202-1239-A-5-H-1	32.40	36.14	0.856	25.70	3817.41	4.14	0.12	1.16
202-1239-A-5-H-1	32.50	36.24	0.858	25.55	3542.89			

LegSitHolCorTypSec	Depth (mbsf)	Depth (mcd)	Age (Ma)	SST (°C)	Alk conc (mmol/g)	$\delta^{15}N$ (‰)	TN (%)	Corg (%)
202-1239-A-5-H-1	32.60	36.34	0.860	25.64	3168.34	4.53	0.12	
202-1239-A-5-H-1	32.70	36.44	0.863	25.70	2616.74			
202-1239-A-5-H-1	32.80	36.54	0.865	25.64	2449.51	4.51	0.11	
202-1239-A-5-H-1	32.90	36.63	0.866	25.09	1998.01			
202-1239-A-5-H-1	33.00	36.73	0.868	24.91	2067.77	4.27	0.14	
202-1239-A-5-H-1	33.10	36.83	0.870	24.21	1789.57			
202-1239-A-5-H-1	33.20	36.93	0.871	22.03	3117.16	3.93	0.14	
202-1239-A-5-H-1	33.30	37.03	0.873	22.15	3260.97			
202-1239-A-5-H-2	33.60	37.33	0.879	22.52	2114.93	2.92	0.14	
202-1239-A-5-H-2	33.90	37.64	0.884	22.55	3252.11			
202-1239-A-5-H-2	34.20	37.94	0.889	23.30	2615.58	2.35	0.11	
202-1239-A-5-H-2	34.50	38.26	0.895	23.27	4468.76			
202-1239-A-5-H-2	34.80	38.57	0.901	23.42	4662.79	2.64	0.10	
202-1239-A-5-H-3	35.11	38.89	0.906	24.09	2699.19			
202-1239-A-5-H-3	35.41	39.21	0.912	24.55	2067.43	3.65	0.09	
202-1239-A-5-H-3	35.71	39.52	0.917	23.64	2924.13			
202-1239-A-5-H-3	36.01	39.83	0.923	24.52	1458.60	1.97	0.08	0.81
202-1239-A-5-H-3	36.31	40.13	0.928	24.27	3289.77			
202-1239-A-5-H-4	36.61	40.39	0.933	24.09	4430.42	3.13	0.11	
202-1239-A-5-H-4	36.91	40.66	0.938	24.52	3230.56			
202-1239-A-5-H-4	37.21	40.93	0.943	24.91	3411.11	4.64	0.11	
202-1239-A-5-H-4	37.51	41.23	0.948	25.55	3208.59			
202-1239-A-5-H-4	37.81	41.54	0.954	26.00	1897.99	3.34	0.10	
202-1239-A-5-H-5	38.12	41.84	0.959	25.64	2768.57			
202-1239-A-5-H-5	38.42	42.12	0.963	24.76	3960.33	3.28	0.13	
202-1239-A-5-H-5	38.72	42.40	0.968	24.48	3985.77			
202-1239-A-5-H-5	39.02	42.69	0.973	24.67	3512.11	3.65	0.12	
202-1239-A-5-H-5	39.32	42.97	0.977	24.67	4513.25			
202-1239-A-5-H-6	39.63	43.26	0.982	25.48	2902.82	3.21	0.11	
202-1239-A-5-H-6	39.93	43.56	0.987	24.67	3278.78			
202-1239-A-5-H-6	40.23	43.87	0.991	24.82	3291.00	3.90	0.10	
202-1239-A-5-H-6	40.53	44.17	0.996	24.24	4086.53			
202-1239-A-5-H-6	40.83	44.47	1.000	25.09	2640.30	3.95	0.09	
202-1239-A-5-H-7	41.14	44.78	1.005	24.48	3254.04			
202-1239-A-5-H-7	41.44	45.06	1.009	24.27	3627.50	4.01	0.10	1.06
202-1239-A-5-H-CC	41.79	45.41	1.014	23.94	3683.60			
202-1239-A-6-H-1	41.40	45.96	1.022	24.88	6000.45	4.16	0.10	
202-1239-A-6-H-1	41.50	46.04	1.023	24.39	3287.51			

LegSitHolCorTypSec	Depth (mbsf)	Depth (mcd)	Age (Ma)	SST (°C)	Alk conc (mmol/g)	$\delta^{15}N$ (‰)	TN (%)	Corg (%)
202-1239-A-6-H-1	41.80	46.36	1.028	25.09	3033.17	4.36	0.13	
202-1239-A-6-H-1	42.10	46.69	1.031	25.45	4066.82			
202-1239-A-6-H-1	42.70	47.36	1.039	24.97	4960.10	3.75	0.11	
202-1239-A-6-H-2	43.01	47.67	1.043	24.30	5212.80			
202-1239-A-6-H-2	43.31	47.94	1.046	23.91	3319.14	2.18	0.12	
202-1239-A-6-H-2	43.61	48.22	1.049	23.00	4794.78			
202-1239-A-6-H-2	43.91	48.50	1.053	23.52	4498.91	3.21	0.13	
202-1239-A-6-H-2	44.21	48.78	1.058	24.18	4741.50			
202-1239-A-6-H-3	44.51	49.06	1.063	25.79	2717.59	3.74	0.10	
202-1239-A-6-H-3	44.81	49.36	1.067	25.91	1893.56			
202-1239-A-6-H-3	45.11	49.68	1.073	25.67	3145.74	3.62	0.11	
202-1239-A-6-H-3	45.41	49.99	1.077	25.73	3804.05			
202-1239-A-6-H-3	45.71	50.31	1.082	26.03	3790.28	4.29	0.12	
202-1239-A-6-H-4	46.02	50.64	1.087	24.88	3892.44			
202-1239-A-6-H-4	46.32	50.96	1.092	24.76	3295.37	4.10	0.13	1.17
202-1239-A-6-H-4	46.62	51.25	1.096	24.24	4259.48			
202-1239-A-6-H-4	46.92	51.55	1.101	24.58	6420.77	3.33	0.13	
202-1239-A-6-H-4	47.22	51.84	1.105	24.27	8089.25			
202-1239-A-6-H-5	47.52	52.13	1.110	25.12	7767.73	3.21	0.14	
202-1239-A-6-H-5	47.82	52.42	1.114	25.21	8072.79			
202-1239-A-6-H-5	48.12	52.72	1.118	25.94	6636.30	3.55	0.12	
202-1239-A-6-H-5	48.42	53.02	1.123	24.70	4224.03			
202-1239-A-6-H-5	48.72	53.32	1.127	24.45	4630.03	3.88	0.12	
202-1239-A-6-H-6	48.92	53.52	1.130	24.09	4154.31			
202-1239-A-6-H-6	49.02	53.62	1.132	24.30	4444.47	3.83	0.13	
202-1239-A-6-H-6	49.12	53.72	1.133	23.97	5248.67			
202-1239-A-6-H-6	49.22	53.82	1.135	23.88	5846.14	3.62	0.13	
202-1239-A-6-H-6	49.32	53.92	1.136	23.03	7241.76			
202-1239-A-6-H-6	49.42	54.02	1.137	23.27	10696.45	2.67	0.15	
202-1239-A-6-H-6	49.52	54.12	1.138	22.79	7726.41			
202-1239-A-6-H-6	49.62	54.21	1.139	23.82	8088.52	2.65	0.15	
202-1239-A-6-H-6	49.72	54.31	1.140	23.64	7404.79			
202-1239-A-6-H-6	49.82	54.41	1.141	24.12	7440.30	2.54	0.14	1.52
202-1239-A-6-H-6	49.92	54.51	1.142	24.09	5921.49			
202-1239-A-6-H-6	50.02	54.61	1.143	24.33	6916.41	2.98	0.14	
202-1239-A-6-H-6	50.12	54.71	1.144	24.64	5560.72			
202-1239-A-6-H-6	50.22	54.81	1.145	25.21	7078.85	3.86	0.15	
202-1239-A-6-H-6	50.32	54.91	1.146	24.27	6163.22			

LegSitHolCorTypSec	Depth (mbsf)	Depth (mcd)	Age (Ma)	SST (°C)	Alk conc (mmol/g)	$\delta^{15}N$ (‰)	TN (%)	Corg (%)
202-1239-A-6-H-7	50.42	55.01	1.147	24.09	7905.83	2.22	0.17	
202-1239-A-6-H-7	50.52	55.11	1.148	23.88	8692.14			
202-1239-A-6-H-7	50.62	55.21	1.149	24.30	6479.16	2.70	0.14	
202-1239-A-6-H-7	50.72	55.32	1.150	24.33	5885.89			
202-1239-A-6-H-7	50.82	55.46	1.151	24.97	4830.84	3.20	0.13	
202-1239-A-6-H-7	50.92	55.56	1.152	24.42	5416.68			
202-1239-A-6-H-7	51.02	55.64	1.153	25.09	4598.73	3.36	0.12	
202-1239-A-6-H-7	51.12	55.73	1.154	25.27	4767.71			
202-1239-A-6-H-CC	51.15	55.76	1.154	25.52	5257.51	3.76	0.13	
202-1239-A-6-H-CC	51.25	55.85	1.155	24.27	6015.77			
202-1239-A-6-H-CC	51.35	55.94	1.156	24.67	6185.89	3.50	0.15	
202-1239-A-6-H-CC	51.45	56.02	1.156	24.94	4186.86			
202-1239-A-7-H-1	51.00	56.22	1.158	24.67	4765.69	3.60	0.14	1.38
202-1239-A-7-H-1	51.00	56.22	1.158	25.76	4584.45			
202-1239-A-7-H-1	51.10	56.33	1.159	25.61	3263.85	3.45	0.12	
202-1239-A-7-H-1	51.20	56.48	1.161	25.64	3784.18			
202-1239-A-7-H-1	51.50	56.90	1.165	26.18	2147.00	3.85	0.09	
202-1239-A-7-H-1	51.80	57.15	1.168	26.12	4175.98			
202-1239-A-7-H-1	52.10	57.41	1.173	26.36	3619.33	3.74	0.11	
202-1239-A-7-H-2	52.40	57.67	1.178	26.06	3472.68			
202-1239-A-7-H-2	52.70	57.93	1.183	26.21	2271.32	4.05	0.11	
202-1239-A-7-H-2	53.00	58.22	1.188	25.97	2309.60			
202-1239-A-7-H-2	53.30	58.58	1.192	26.27	2640.90	4.01	0.09	
202-1239-A-7-H-2	53.60	58.91	1.196	25.42	3799.82			
202-1239-A-7-H-3	53.90	59.14	1.198	24.45	3896.18	3.35	0.10	
202-1239-A-7-H-3	54.20	59.38	1.201	24.36	3543.33			
202-1239-A-7-H-3	54.50	59.65	1.204	25.58	2597.31	3.80	0.10	
202-1239-A-7-H-3	54.80	59.91	1.209	24.64	2807.52			
202-1239-A-7-H-3	55.10	60.18	1.214	24.85	2784.32	3.73	0.10	
202-1239-A-7-H-4	55.40	60.48	1.221	26.85	1660.63			
202-1239-A-7-H-4	55.70	60.82	1.228	27.24	3590.51	4.48	0.13	1.05
202-1239-A-7-H-4	56.00	61.13	1.234	27.30	2360.36			
202-1239-A-7-H-4	56.30	61.43	1.241	26.55	1763.16	4.37	0.11	
202-1239-A-7-H-4	56.60	61.72	1.247	25.00	2584.68			
202-1239-A-7-H-5	56.90	61.95	1.252	24.24	1206.16	4.13	0.11	
202-1239-A-7-H-5	57.10	62.11	1.256	24.24	1689.65			
202-1239-A-7-H-5	57.30	62.27	1.259	23.79	2579.22	2.43	0.14	
202-1239-A-7-H-5	57.50	62.42	1.262	24.39	2076.46			

LegSitHolCorTypSec	Depth (mbsf)	Depth (mcd)	Age (Ma)	SST (°C)	Alk conc (mmol/g)	$\delta^{15}N$ (‰)	TN (%)	Corg (%)
202-1239-A-7-H-5	57.70	62.58	1.266	24.33	2198.59	2.57	0.13	
202-1239-A-7-H-5	57.90	62.74	1.269	24.82	4168.21			
202-1239-A-7-H-5	58.10	62.90	1.273	25.03	7198.18	2.79	0.14	
202-1239-A-7-H-5	58.30	63.06	1.276	25.64	7442.92			
202-1239-A-7-H-6	58.51	63.24	1.280	26.42	1930.12	2.99	0.12	
202-1239-A-7-H-6	58.71	63.41	1.284	26.24	1107.18			
202-1239-A-7-H-6	58.91	63.58	1.286	27.09	1033.49	3.62	0.10	
202-1239-A-7-H-6	59.11	63.75	1.289	26.00	1233.28			
202-1239-A-7-H-6	59.31	63.92	1.292	25.24	2193.59	4.34	0.07	
202-1239-A-7-H-6	59.51	64.09	1.294	25.79	2958.56			
202-1239-A-7-H-6	59.71	64.26	1.297	26.33	2762.44	4.43	0.12	1.22
202-1239-A-7-H-7	59.92	64.43	1.300	25.94	3231.88			
202-1239-A-7-H-7	60.12	64.60	1.302	25.97	3790.38	3.41	0.13	
202-1239-A-7-H-7	60.32	64.76	1.305	25.45	4482.55			
202-1239-A-7-H-7	60.52	64.93	1.308	26.12	5338.98	2.97	0.13	
202-1239-A-7-H-CC	60.77	65.14	1.311	26.30	6916.72			
202-1239-A-8-H-1	60.70	66.63	1.334	25.45	7451.02	3.50	0.13	
202-1239-A-8-H-1	60.90	66.83	1.338	25.64	13136.21			
202-1239-A-8-H-1	61.10	67.04	1.341	25.70	11210.06	2.28	0.12	
202-1239-A-8-H-1	61.30	67.25	1.344	25.58	10385.08			
202-1239-A-8-H-1	61.50	67.46	1.347	27.88	265.59	3.96	0.02	
202-1239-A-8-H-1	61.70	67.65	1.350	26.24	6670.35			
202-1239-A-8-H-2	61.91	67.84	1.353	27.24	3658.05	3.86	0.12	
202-1239-A-8-H-2	62.11	68.03	1.356	26.48	2186.09			
202-1239-A-8-H-2	62.31	68.21	1.359	27.88	2590.25	4.05	0.10	
202-1239-A-8-H-2	62.51	68.39	1.362	26.97	3477.42			
202-1239-A-8-H-2	62.71	68.58	1.365	27.67	7964.87	3.87	0.15	
202-1239-A-8-H-2	62.91	68.76	1.368	27.06	3698.36			
202-1239-A-8-H-2	63.11	68.96	1.371	27.24	6290.08	3.92	0.13	1.22
202-1239-A-8-H-2	63.31	69.16	1.374	24.70	9776.60			
202-1239-A-8-H-3	63.52	69.37	1.378	25.18	6486.48	2.41	0.13	
202-1239-A-8-H-3	63.72	69.56	1.381	24.06	7409.46			
202-1239-A-8-H-3	63.92	69.76	1.384	26.52	2571.61	3.86	0.06	
202-1239-A-8-H-3	64.12	69.96	1.387	24.94	8746.25			
202-1239-A-8-H-3	64.32	70.16	1.390	26.33	6330.76	3.84	0.14	
202-1239-A-8-H-3	64.52	70.39	1.394	25.67	6138.57			
202-1239-A-8-H-3	64.72	70.61	1.397	25.73	6139.40	3.73	0.13	
202-1239-A-8-H-4	64.94	70.86	1.401	25.48	7721.92			

LegSitHolCorTypSec	Depth (mbsf)	Depth (mcd)	Age (Ma)	SST (°C)	Alk conc (mmol/g)	$\delta^{15}N$ (‰)	TN (%)	Corg (%)
202-1239-A-8-H-4	65.14	71.09	1.405	25.30	8329.74	3.94	0.17	
202-1239-A-8-H-4	65.34	71.30	1.408	24.97	10150.94			
202-1239-A-8-H-4	65.54	71.50	1.411	25.27	8477.82	3.75	0.16	
202-1239-A-8-H-4	65.74	71.70	1.414	25.21	9149.37			
202-1239-A-8-H-4	65.94	71.90	1.417	25.24	8324.74	3.29	0.17	
202-1239-A-8-H-4	66.14	72.10	1.421	25.45	8046.14			
202-1239-A-8-H-4	66.34	72.30	1.424	25.42	5271.95	3.23	0.13	
202-1239-A-8-H-5	66.55	72.51	1.427	25.64	5380.10			
202-1239-A-8-H-5	66.75	72.71	1.430	26.03	4342.09	4.22	0.12	1.13
202-1239-A-8-H-5	66.95	72.91	1.433	26.52	5035.47			
202-1239-A-8-H-5	67.15	73.11	1.436	26.36	4387.40	4.16	0.12	
202-1239-A-8-H-5	67.35	73.31	1.440	26.39	4199.13			
202-1239-A-8-H-5	67.55	73.51	1.443	26.52	3223.40	3.90	0.12	
202-1239-A-8-H-5	67.75	73.71	1.446	26.76	5110.58			
202-1239-A-8-H-6	67.96	73.91	1.449	26.15	5522.78	3.61	0.14	
202-1239-A-8-H-6	68.16	74.11	1.452	25.39	8668.38			
202-1239-A-8-H-6	68.36	74.31	1.455	25.15	11880.39	2.87	0.15	
202-1239-A-8-H-6	68.56	74.51	1.458	24.82	12156.62			
202-1239-A-8-H-6	68.76	74.71	1.462	25.09	11440.72	2.69	0.16	
202-1239-A-8-H-6	68.96	74.91	1.465	25.18	9895.99			
202-1239-A-8-H-6	69.16	75.11	1.468	24.85	7049.88	2.79	0.17	
202-1239-A-8-H-6	69.36	75.31	1.471	24.67	3402.58			
202-1239-A-8-H-7	69.57	75.53	1.475	25.91	3845.70	3.53	0.13	
202-1239-A-8-H-7	69.77	75.73	1.478	26.27	5081.46			
202-1239-A-8-H-7	69.97	75.94	1.481	26.91	5811.83	4.13	0.13	
202-1239-A-8-H-CC	70.15	76.11	1.484	26.27	3642.09			
202-1239-A-8-H-CC	70.35	76.28	1.487	26.33	4497.64	4.06	0.14	1.41
202-1239-A-9-H-1	69.90	77.02	1.500	25.09	6630.70			
202-1239-A-9-H-1	70.00	77.15	1.502	25.79	6348.41	3.78	0.16	
202-1239-A-9-H-1	70.10	77.28	1.504	26.03	7649.87			
202-1239-A-9-H-1	70.20	77.41	1.507	25.52	5521.83	3.41	0.17	
202-1239-A-9-H-1	70.30	77.54	1.509	25.36	10942.16			
202-1239-A-9-H-1	70.40	77.67	1.511	25.03	10663.61	3.31	0.18	
202-1239-A-9-H-1	70.50	77.80	1.514	24.45	8494.58			
202-1239-A-9-H-1	70.60	77.91	1.515	25.27	9303.04	3.14	0.19	
202-1239-A-9-H-1	70.70	78.01	1.517	24.64	5118.79			
202-1239-A-9-H-1	70.80	78.11	1.519	25.76	12887.69	3.75	0.16	
202-1239-A-9-H-1	70.90	78.22	1.521	25.91	10149.22			

LegSitHolCorTypSec	Depth (mbsf)	Depth (mcd)	Age (Ma)	SST (°C)	Alk conc (mmol/g)	$\delta^{15}N$ (‰)	TN (%)	Corg (%)
202-1239-A-9-H-1	71.00	78.32	1.523	26.09	7572.87	4.13	0.16	
202-1239-A-9-H-1	71.10	78.42	1.524	25.58	7496.65			
202-1239-A-9-H-1	71.20	78.52	1.526	25.27	6737.41	4.19	0.17	
202-1239-A-9-H-1	71.30	78.62	1.528	25.21	5376.29			
202-1239-A-9-H-2	71.41	78.73	1.530	25.27	5958.52	4.14	0.15	
202-1239-A-9-H-2	71.51	78.83	1.532	24.97	5726.68			
202-1239-A-9-H-2	71.61	78.93	1.533	24.88	8472.90	3.56	0.20	2.05
202-1239-A-9-H-2	71.71	79.03	1.535	24.09	10470.48			
202-1239-A-9-H-2	71.81	79.13	1.537	24.39	11006.11	3.10	0.19	
202-1239-A-9-H-2	71.91	79.23	1.539	24.67	11333.70			
202-1239-A-9-H-2	72.01	79.33	1.540	24.73	12063.57	3.23	0.22	
202-1239-A-9-H-2	72.11	79.43	1.542	24.33	13049.92			
202-1239-A-9-H-2	72.21	79.53	1.544	24.48	14317.12	3.35	0.22	
202-1239-A-9-H-2	72.31	79.63	1.545	24.12	15741.87			
202-1239-A-9-H-2	72.41	79.73	1.547	24.85	14100.07	3.92	0.20	
202-1239-A-9-H-2	72.51	79.83	1.549	25.12	14972.69			
202-1239-A-9-H-2	72.61	79.93	1.551	25.42	13118.56	4.22	0.17	
202-1239-A-9-H-2	72.71	80.02	1.552	25.61	9482.24			
202-1239-A-9-H-2	72.81	80.11	1.554	25.52	7967.64	4.27	0.15	
202-1239-A-9-H-3	72.93	80.23	1.556	25.55	7524.26			
202-1239-A-9-H-3	73.03	80.32	1.558	25.91	8968.15	3.19	0.17	
202-1239-A-9-H-3	73.13	80.41	1.559	25.91	12307.13			
202-1239-A-9-H-3	73.23	80.51	1.561	26.12	12357.18	3.31	0.20	
202-1239-A-9-H-3	73.33	80.60	1.562	26.12	13147.81			
202-1239-A-9-H-3	73.43	80.69	1.564	25.79	11856.65	3.31	0.20	2.15
202-1239-A-9-H-3	73.53	80.79	1.565	25.82	10848.53			
202-1239-A-9-H-3	73.63	80.88	1.567	25.88	10128.70	3.02	0.19	
202-1239-A-9-H-3	73.73	80.97	1.568	25.91	7302.85			
202-1239-A-9-H-3	73.83	81.07	1.570	25.85	7689.94	3.13	0.15	
202-1239-A-9-H-3	73.93	81.16	1.571	25.76	5795.11			
202-1239-A-9-H-3	74.03	81.26	1.573	25.73	5558.23	3.38	0.15	
202-1239-A-9-H-3	74.13	81.35	1.574	25.45	9090.22			
202-1239-A-9-H-3	74.23	81.45	1.576	25.45	10556.01	3.02	0.18	
202-1239-A-9-H-3	74.33	81.55	1.577	25.24	12675.21			
202-1239-A-9-H-4	74.43	81.65	1.579	25.24	15381.32	3.10	0.21	
202-1239-A-9-H-4	74.53	81.75	1.581	25.36	19032.78			
202-1239-A-9-H-4	75.03	82.24	1.588	25.48	18599.73	3.04	0.21	
202-1239-A-9-H-4	75.53	82.73	1.596	26.12	10589.73			

LegSitHolCorTypSec	Depth (mbsf)	Depth (mcd)	Age (Ma)	SST (°C)	Alk conc (mmol/g)	$\delta^{15}N$ (‰)	TN (%)	Corg (%)
202-1239-A-9-H-5	76.05	83.25	1.604	25.33	12819.67	2.89	0.19	
202-1239-A-9-H-5	76.55	83.74	1.612	25.73	6154.18			
202-1239-A-9-H-5	77.05	84.25	1.620	25.03	12666.79	3.42	0.19	
202-1239-A-9-H-6	77.55	84.75	1.628	25.48	7410.12			
202-1239-A-9-H-6	78.05	85.20	1.635	25.64	8646.25	3.59	0.15	1.57
202-1239-A-9-H-6	78.55	85.62	1.641	25.18	9630.62			
202-1239-A-9-H-7	79.56	86.56	1.652	23.12	19411.00	2.49	0.20	
202-1239-A-9-H-CC	79.75	86.87	1.656	22.27	25357.80			
202-1239-A-9-H-CC	79.85	87.05	1.658	22.52	22671.13	2.43	0.22	
202-1239-A-9-H-CC	79.95	87.11	1.659	22.61	22729.87			
202-1239-A-10-H-1	79.40	87.16	1.660	22.76	22874.91	2.50	0.25	
202-1239-A-10-H-1	79.50	87.35	1.662	22.39	20193.17			
202-1239-A-10-H-1	79.60	87.54	1.665	22.88	16733.97	2.62	0.20	
202-1239-A-10-H-1	79.70	87.65	1.666	23.36	19388.74			
202-1239-A-10-H-1	79.80	87.75	1.667	23.64	20981.75	2.94	0.28	
202-1239-A-10-H-1	79.90	87.83	1.668	23.73	19677.35			
202-1239-A-10-H-1	80.00	87.92	1.669	24.03	16657.56	3.15	0.26	
202-1239-A-10-H-1	80.10	88.00	1.670	23.88	21514.22			
202-1239-A-10-H-1	80.20	88.08	1.671	24.39	23282.02	2.79	0.33	
202-1239-A-10-H-1	80.30	88.17	1.673	24.39	26428.23			
202-1239-A-10-H-1	80.40	88.25	1.674	24.33	26791.32	2.84	0.39	
202-1239-A-10-H-1	80.50	88.34	1.675	24.45	25000.03			
202-1239-A-10-H-1	80.60	88.43	1.676	24.45	18200.20	3.20	0.31	3.81
202-1239-A-10-H-1	80.70	88.52	1.677	24.52	16062.19			
202-1239-A-10-H-1	80.80	88.61	1.678	25.18	14623.54	2.22	0.27	
202-1239-A-10-H-2	80.91	88.70	1.679	25.91	11841.68			
202-1239-A-10-H-2	81.11	88.88	1.682	25.61	6836.17	2.32	0.27	
202-1239-A-10-H-2	81.31	89.06	1.685	25.36	6358.89			
202-1239-A-10-H-2	81.51	89.24	1.689	25.12	6034.29	2.71	0.25	
202-1239-A-10-H-2	81.71	89.42	1.692	25.06	6103.51			
202-1239-A-10-H-2	81.91	89.60	1.695	24.88	6438.16	2.92	0.29	
202-1239-A-10-H-2	82.11	89.78	1.698	24.03	11009.12			
202-1239-A-10-H-2	82.31	89.96	1.702	23.82	12139.86	2.06	0.28	
202-1239-A-10-H-3	82.51	90.15	1.705	23.91	13925.85			
202-1239-A-10-H-3	82.71	90.38	1.709	24.42	10902.83	2.25	0.33	
202-1239-A-10-H-3	82.91	90.61	1.714	24.09	12423.32			
202-1239-A-10-H-3	83.11	90.83	1.718	24.12	9731.10	1.71	0.27	
202-1239-A-10-H-3	83.31	91.05	1.722	25.09	3206.09			

LegSitHolCorTypSec	Depth (mbsf)	Depth (mcd)	Age (Ma)	SST (°C)	Alk conc (mmol/g)	$\delta^{15}N$ (‰)	TN (%)	Corg (%)
202-1239-A-10-H-3	83.51	91.27	1.726	24.91	9726.50	3.08	0.27	
202-1239-A-10-H-3	83.71	91.48	1.729	25.12	9975.25			
202-1239-A-10-H-4	83.93	91.73	1.734	25.09	10253.58	2.67	0.25	3.02
202-1239-A-10-H-4	84.13	91.95	1.738	25.45	12106.50			
202-1239-A-10-H-4	84.33	92.16	1.742	25.06	13708.52	2.63	0.25	
202-1239-A-10-H-4	84.53	92.38	1.746	24.70	15082.24			
202-1239-A-10-H-4	84.73	92.60	1.750	24.67	16477.87	2.43	0.29	
202-1239-A-10-H-4	84.93	92.82	1.754	23.39	17385.83			
202-1239-A-10-H-4	85.13	93.04	1.758	24.06	13563.32	1.43	0.26	
202-1239-A-10-H-4	85.33	93.25	1.761	25.03	11991.24			
202-1239-A-10-H-5	85.54	93.45	1.765	25.55	9194.33	2.31	0.25	
202-1239-A-10-H-5	85.74	93.65	1.769	25.88	7878.02			
202-1239-A-10-H-5	85.94	93.85	1.772	26.18	7686.07	2.94	0.22	
202-1239-A-10-H-5	86.14	94.05	1.775	25.85	9954.09			
202-1239-A-10-H-5	86.34	94.25	1.778	25.67	9642.28	2.91	0.25	
202-1239-A-10-H-5	86.54	94.44	1.780	25.39	9365.67			
202-1239-A-10-H-5	86.74	94.64	1.782	25.09	11911.25	2.84	0.26	
202-1239-A-10-H-6	86.96	94.85	1.785	24.91	12925.44			
202-1239-A-10-H-6	87.16	95.05	1.787	24.97	11670.36	3.26	0.29	
202-1239-A-10-H-6	87.36	95.24	1.789	24.48	13238.49			
202-1239-A-10-H-6	87.56	95.45	1.792	24.55	15827.65	3.06	0.27	3.17
202-1239-A-10-H-6	87.76	95.65	1.794	23.82	13469.96			
202-1239-A-10-H-6	87.96	95.86	1.797	23.61	12680.89	1.89	0.31	
202-1239-A-10-H-6	88.16	96.07	1.799	23.42	10964.57			
202-1239-A-10-H-6	88.36	96.29	1.802	24.18	15361.62	2.01	0.27	
202-1239-A-10-H-7	88.57	96.49	1.804	21.70	10154.89			
202-1239-A-10-H-7	88.77	96.69	1.807	21.67	10102.14	2.60	0.34	
202-1239-A-10-H-7	88.97	96.88	1.809	22.03	10580.13			
202-1239-A-10-H-CC	89.23	97.09	1.812	22.91	11258.82	2.70	0.43	
202-1239-A-11-H-1	88.90	97.97	1.822	23.61	11701.27			
202-1239-A-11-H-1	89.10	98.16	1.825	22.03	9030.31	2.67	0.31	
202-1239-A-11-H-1	89.30	98.33	1.827	22.88	10717.24			
202-1239-A-11-H-1	89.50	98.50	1.829	25.18	15312.39	2.31	0.29	
202-1239-A-11-H-1	89.70	98.67	1.831	25.33	18456.39			
202-1239-A-11-H-1	89.90	98.84	1.833	25.85	12203.15	2.21	0.27	
202-1239-A-11-H-1	90.10	99.01	1.835	25.45	13809.57			
202-1239-A-11-H-1	90.30	99.21	1.837	24.73	14947.68	2.09	0.23	
202-1239-A-11-H-2	90.51	99.42	1.840	24.18	14146.36			

LegSitHolCorTypSec	Depth (mbsf)	Depth (mcd)	Age (Ma)	SST (°C)	Alk conc (mmol/g)	$\delta^{15}N$ (‰)	TN (%)	Corg (%)
202-1239-A-11-H-2	90.71	99.62	1.842	24.94	16625.13	2.28	0.35	3.58
202-1239-A-11-H-2	90.91	99.82	1.844	24.70	23069.03			
202-1239-A-11-H-2	91.11	100.02	1.847	25.12	15044.36	1.84	0.31	
202-1239-A-11-H-2	91.31	100.21	1.849	24.30	16238.75			
202-1239-A-11-H-2	91.51	100.41	1.852	24.09	14280.36	1.91	0.29	
202-1239-A-11-H-2	91.71	100.61	1.854	23.88	11609.49			
202-1239-A-11-H-3	92.02	100.92	1.858	22.85	12703.76	1.46	0.34	
202-1239-A-11-H-3	92.22	101.12	1.860	23.64	11406.20			
202-1239-A-11-H-3	92.42	101.32	1.865	23.97	16088.23	1.92	0.36	
202-1239-A-11-H-3	92.62	101.51	1.870	22.55	10745.74			
202-1239-A-11-H-3	92.82	101.71	1.875	23.61	10518.80	1.82	0.39	
202-1239-A-11-H-3	93.02	101.91	1.880	25.45	20241.10			
202-1239-A-11-H-3	93.22	102.11	1.885	25.39	17334.34	2.17	0.35	
202-1239-A-11-H-4	93.43	102.32	1.890	25.06	16938.40			
202-1239-A-11-H-4	93.63	102.52	1.895	24.79	15135.77	2.36	0.29	
202-1239-A-11-H-4	93.83	102.71	1.900	25.06	14031.58			
202-1239-A-11-H-4	94.03	102.91	1.905	24.97	15409.72	2.16	0.29	
202-1239-A-11-H-4	94.23	103.11	1.910	24.85	19532.39			
202-1239-A-11-H-4	94.43	103.31	1.915	24.79	19521.77	2.30	0.34	4.16
202-1239-A-11-H-4	94.63	103.51	1.920	24.97	21075.49			
202-1239-A-11-H-4	94.83	103.72	1.925	25.06	19137.58	2.43	0.28	
202-1239-A-11-H-5	95.04	103.96	1.931	25.48	14705.99			
202-1239-A-11-H-5	95.24	104.20	1.937	22.82	9305.70	2.36	0.22	
202-1239-A-11-H-5	95.44	104.39	1.942	23.30	11652.44			
202-1239-A-11-H-5	95.64	104.58	1.947	24.94	15830.21	2.00	0.23	
202-1239-A-11-H-5	95.84	104.77	1.950	24.55	12609.23			
202-1239-A-11-H-5	96.04	104.96	1.953	24.64	10580.08	2.69	0.23	
202-1239-A-11-H-5	96.24	105.15	1.956	25.55	10525.17			
202-1239-A-11-H-6	96.45	105.34	1.959	25.70	7886.17	2.64	0.18	
202-1239-A-11-H-6	96.65	105.53	1.962	25.76	9962.27			
202-1239-A-11-H-6	96.85	105.72	1.965	26.18	8784.35	2.59	0.20	
202-1239-A-11-H-6	97.05	105.89	1.968	26.24	10947.22			
202-1239-A-11-H-6	97.25	106.05	1.970	25.42	12331.73	1.54	0.28	
202-1239-A-11-H-6	97.45	106.21	1.973	25.52	12344.59			
202-1239-A-11-H-6	97.65	106.37	1.975	25.85	10279.79	2.42	0.20	
202-1239-A-11-H-6	97.85	106.54	1.978	25.79	16636.34			
202-1239-A-11-H-7	98.06	106.73	1.981	26.15	10323.58	1.92	0.31	3.91
202-1239-A-11-H-7	98.26	106.92	1.984	25.52	18596.21			

LegSitHolCorTypSec	Depth (mbsf)	Depth (mcd)	Age (Ma)	SST (°C)	Alk conc (mmol/g)	$\delta^{15}N$ (‰)	TN (%)	Corg (%)
202-1239-A-11-H-7	98.46	107.11	1.987	25.64	15873.16	1.77	0.25	
202-1239-A-11-H-CC	98.62	107.30	1.990	25.79	16556.69			
202-1239-A-11-H-CC	98.82	107.57	1.994	26.21	16579.38	1.98	0.22	
202-1239-A-12-H-1	98.50	108.34	2.006	25.03	16646.55			
202-1239-A-12-H-1	98.70	108.57	2.010	25.48	18870.32	2.13	0.25	
202-1239-A-12-H-1	98.90	108.80	2.013	25.85	18657.84			
202-1239-A-12-H-1	99.10	108.99	2.016	26.03	18287.90	2.10	0.23	
202-1239-A-12-H-1	99.30	109.18	2.019	26.36	20636.19			
202-1239-A-12-H-1	99.50	109.33	2.021	25.97	24732.85	1.94	0.26	
202-1239-A-12-H-1	99.70	109.46	2.023	26.09	22130.37			
202-1239-A-12-H-2	99.91	109.59	2.025	26.55	18315.92	1.93	0.20	
202-1239-A-12-H-2	100.11	109.75	2.028	26.55	10523.35			
202-1239-A-12-H-2	100.31	109.95	2.031	26.30	13484.22	2.02	0.22	
202-1239-A-12-H-2	100.71	110.35	2.037	26.33	16951.19	2.34	0.23	
202-1239-A-12-H-2	101.11	110.75	2.043	25.64	12275.70	2.16	0.25	
202-1239-A-12-H-2	101.31	110.95	2.046	25.21	11825.91			
202-1239-A-12-H-3	101.52	111.16	2.049	24.94	14516.32	1.69	0.17	
202-1239-A-12-H-3	101.72	111.36	2.052	25.45	10796.37			
202-1239-A-12-H-3	101.92	111.56	2.055	25.45	7173.47	2.06	0.23	
202-1239-A-12-H-3	102.12	111.77	2.059	25.58	10638.19			
202-1239-A-12-H-3	102.32	112.00	2.062	25.70	9736.89	2.33	0.22	
202-1239-A-12-H-3	102.52	112.23	2.066	25.64	10575.64			
202-1239-A-12-H-3	102.72	112.46	2.069	25.21	10480.41	2.18	0.24	
202-1239-A-12-H-4	102.93	112.70	2.073	24.12	16743.03			
202-1239-A-12-H-4	103.13	112.93	2.076	23.97	17102.64	2.43	0.22	
202-1239-A-12-H-4	103.63	113.48	2.085	23.55	27064.24			
202-1239-A-12-H-4	104.13	114.03	2.099	24.33	15465.82	2.18	0.30	
202-1239-A-12-H-5	104.65	114.57	2.112	25.33	11104.71			
202-1239-A-12-H-5	105.15	115.07	2.124	25.30	16258.44	3.21	0.22	
202-1239-A-12-H-5	105.65	115.53	2.133	26.55	10849.70			
202-1239-A-12-H-6	106.17	116.08	2.143	26.33	8708.68	3.13	0.26	
202-1239-A-12-H-6	106.67	116.65	2.154	24.33	15712.87			
202-1239-A-12-H-6	107.17	117.22	2.163	23.97	21339.05	3.61	0.15	3.06
202-1239-A-12-H-7	107.67	117.71	2.167	24.15	26677.86			
202-1239-A-12-H-7	108.07	118.11	2.171	24.88	22673.98	1.63	0.23	
202-1239-A-13-H-1	108.10	119.01	2.179	26.30	20676.09			
202-1239-A-13-H-1	108.60	119.46	2.184	26.67	12968.56	2.37	0.20	
202-1239-A-13-H-1	109.10	119.91	2.190	26.42	12056.88			

LegSitHolCorTypSec	Depth (mbsf)	Depth (mcd)	Age (Ma)	SST (°C)	Alk conc (mmol/g)	$\delta^{15}N$ (‰)	TN (%)	Corg (%)
202-1239-A-13-H-2	109.62	120.41	2.197	26.58	17236.13	2.11	0.24	
202-1239-A-13-H-2	110.12	120.90	2.204	25.67	22120.73			
202-1239-A-13-H-2	110.62	121.37	2.211	26.06	9815.10	2.42	0.18	
202-1239-A-13-H-3	111.14	121.86	2.218	26.55	12996.20			
202-1239-A-13-H-3	111.64	122.33	2.227	26.36	7385.48	2.70	0.16	
202-1239-A-13-H-3	112.14	122.81	2.236	26.33	5395.48			
202-1239-A-13-H-4	112.65	123.30	2.245	25.85	15838.25	2.49	0.19	
202-1239-A-13-H-4	113.15	123.79	2.253	25.03	12071.20			
202-1239-A-13-H-4	113.65	124.28	2.261	26.85	12285.40	2.79	0.20	
202-1239-A-13-H-5	114.15	124.76	2.268	26.61	6413.16			
202-1239-A-13-H-5	114.65	125.25	2.275	25.18	12991.02	2.21	0.19	
202-1239-A-13-H-5	115.15	125.74	2.282	24.94	15796.51			
202-1239-A-13-H-6	115.66	126.23	2.291	26.61	8662.80	3.08	0.14	1.43
202-1239-A-13-H-6	116.16	126.72	2.302	26.27	8387.11			
202-1239-A-13-H-6	116.66	127.18	2.311	26.67	7699.54	3.53	0.14	
202-1239-A-13-H-7	117.17	127.66	2.321	26.55	5504.55			
202-1239-A-13-H-7	117.57	128.02	2.329	26.58	6521.30	3.52	0.16	
202-1239-A-13-H-CC	117.85	128.31	2.335	25.79	6837.20			
202-1239-A-14-H-1	117.60	128.92	2.346	27.36	3411.80	3.57	0.12	
202-1239-A-14-H-1	118.10	129.42	2.354	26.64	4978.81			
202-1239-A-14-H-1	118.60	129.93	2.362	26.42	9002.26	1.79	0.17	
202-1239-A-14-H-2	119.12	130.45	2.370	26.18	9392.11			
202-1239-A-14-H-2	119.62	130.96	2.379	27.00	4468.58	2.71	0.08	
202-1239-A-14-H-2	120.12	131.47	2.387	26.82	4281.97			
202-1239-A-14-H-3	120.63	131.98	2.395	26.12	5793.83	2.06	0.14	
202-1239-A-14-H-3	121.13	132.48	2.404	26.82	6855.76			
202-1239-A-14-H-3	121.63	132.97	2.413	27.06	6768.28	2.87	0.13	
202-1239-A-14-H-4	121.95	133.28	2.419	27.06	3593.97			
202-1239-A-14-H-4	122.25	133.58	2.425	26.73	4302.74	3.01	0.12	
202-1239-A-14-H-4	122.55	133.89	2.430	25.33	7341.78			
202-1239-A-14-H-4	122.85	134.19	2.436	25.24	7016.82	1.95	0.14	1.51
202-1239-A-14-H-4	123.15	134.49	2.441	25.15	8223.90			
202-1239-A-14-H-5	123.47	134.82	2.447	25.12	7941.58	2.19	0.15	
202-1239-A-14-H-5	123.77	135.12	2.452	25.85	10844.42			
202-1239-A-14-H-5	124.07	135.42	2.456	25.55	21218.89	2.05	0.18	
202-1239-A-14-H-5	124.37	135.73	2.460	26.12	9127.44			
202-1239-A-14-H-5	124.67	136.02	2.464	26.39	9154.61	3.20	0.12	
202-1239-A-14-H-6	125.00	136.33	2.469	26.61	6887.45			

LegSitHolCorTypSec	Depth (mbsf)	Depth (mcd)	Age (Ma)	SST (°C)	Alk conc (mmol/g)	$\delta^{15}N$ (‰)	TN (%)	Corg (%)
202-1239-A-14-H-6	125.30	136.62	2.473	26.39	5889.39	3.11	0.11	
202-1239-A-14-H-6	125.60	136.90	2.477	26.24	13042.26			
202-1239-A-14-H-6	125.90	137.18	2.481	25.88	22905.63	1.72	0.20	
202-1239-A-14-H-6	126.20	137.46	2.486	25.15	33158.50			
202-1239-A-14-H-7	126.53	137.76	2.490	24.64	27402.72	1.13	0.23	
202-1239-A-14-H-7	126.83	138.02	2.494	25.64	9958.64			
202-1239-A-14-H-7	127.13	138.29	2.501	26.73	3594.51	3.04	0.14	
202-1239-A-15-H-1	126.90	138.98	2.516	24.82	7772.40	1.32	0.12	1.52
202-1239-A-15-H-1	127.20	139.42	2.523	25.18	13865.20			
202-1239-A-15-H-1	127.50	139.73	2.527	25.12	15787.51	1.37	0.16	
202-1239-A-15-H-1	127.80	140.01	2.531	25.21	22390.77			
202-1239-A-15-H-1	128.10	140.29	2.535	25.97	16313.43	1.53	0.22	
202-1239-A-15-H-2	128.42	140.59	2.539	26.42	13255.17			
202-1239-A-15-H-2	128.72	140.88	2.543	26.94	7668.08	1.92	0.21	
202-1239-A-15-H-2	129.02	141.18	2.547	27.39	4090.01			
202-1239-A-15-H-2	129.32	141.47	2.552	26.85	4397.01	2.45	0.15	
202-1239-A-15-H-2	129.62	141.77	2.556	26.67	6114.85			
202-1239-A-15-H-3	129.93	142.08	2.560	26.39	6034.54	3.41	0.11	
202-1239-A-15-H-3	130.23	142.38	2.564	26.21	7675.36			
202-1239-A-15-H-3	130.53	142.68	2.568	26.42	7444.48	2.77	0.13	
202-1239-A-15-H-3	130.83	142.98	2.572	26.97	6786.04			
202-1239-A-15-H-3	131.13	143.28	2.576	27.15	6629.58	2.93	0.14	
202-1239-A-15-H-4	131.44	143.58	2.580	27.27	5660.23			
202-1239-A-15-H-4	131.74	143.87	2.583	27.55	4568.94	3.62	0.18	
202-1239-A-15-H-4	132.04	144.16	2.587	27.27	4575.03			
202-1239-A-15-H-4	132.34	144.45	2.591	27.24	5079.26	2.75	0.15	1.14
202-1239-A-15-H-4	132.64	144.74	2.594	27.30	5280.50			
202-1239-A-15-H-5	132.95	145.04	2.598	26.85	11937.19	2.91	0.10	
202-1239-A-15-H-5	133.25	145.33	2.602	25.70	20610.99			
202-1239-A-15-H-5	133.55	145.66	2.606	25.79	13369.22	1.51	0.15	
202-1239-A-15-H-5	133.85	146.02	2.610	26.45	8192.91			
202-1239-A-15-H-5	134.15	146.30	2.614	26.64	10425.44	2.06	0.13	
202-1239-A-15-H-6	134.47	146.60	2.618	26.52	8435.49			
202-1239-A-15-H-6	134.77	146.88	2.621	26.45	4617.62	3.00	0.11	
202-1239-A-15-H-6	135.07	147.17	2.624	26.76	6038.19			
202-1239-A-15-H-6	135.37	147.46	2.626	26.91	6669.27	2.35	0.14	
202-1239-A-15-H-6	135.67	147.75	2.629	26.88	6865.89			
202-1239-A-15-H-7	135.99	148.06	2.632	26.61	4722.82	2.27	0.11	

LegSitHolCorTypSec	Depth (mbsf)	Depth (mcd)	Age (Ma)	SST (°C)	Alk conc (mmol/g)	$\delta^{15}N$ (‰)	TN (%)	Corg (%)
202-1239-A-15-H-7	136.29	148.37	2.634	26.21	5159.40			
202-1239-A-15-H-7	136.59	148.70	2.637	26.61	5826.79	2.29	0.14	
202-1239-A-15-H-CC	136.89	149.03	2.640	26.15	10154.58			
202-1239-A-16-H-1	136.40	149.21	2.642	26.82	6427.54	2.26	0.13	
202-1239-A-16-H-1	136.70	149.54	2.646	26.18	10056.23			
202-1239-A-16-H-1	137.00	149.85	2.651	26.85	6770.81	2.65	0.16	1.84
202-1239-A-16-H-1	137.30	150.15	2.656	27.36	5069.37			
202-1239-A-16-H-1	137.60	150.45	2.661	27.27	3502.66	3.02	0.12	
202-1239-A-16-H-2	137.91	150.75	2.665	27.52	3052.70			
202-1239-A-16-H-2	138.21	151.05	2.670	27.67	3112.55	3.67	0.13	
202-1239-A-16-H-2	138.51	151.34	2.675	27.36	3953.99			
202-1239-A-16-H-2	138.81	151.63	2.679	27.30	3477.90	2.58	0.11	
202-1239-A-16-H-2	139.11	151.92	2.682	27.24	4784.85			
202-1239-A-16-H-3	139.43	152.25	2.685	27.15	5644.74	2.70	0.14	
202-1239-A-16-H-3	139.73	152.55	2.688	27.06	6558.73			
202-1239-A-16-H-3	140.03	152.85	2.691	26.97	6569.36	1.47	0.13	
202-1239-A-16-H-3	140.33	153.15	2.694	27.06	5978.28			
202-1239-A-16-H-3	140.63	153.44	2.697	26.61	7732.01	1.06	0.14	
202-1239-A-16-H-4	140.94	153.74	2.700	26.21	9965.84			
202-1239-A-16-H-4	141.24	154.04	2.703	26.15	10181.88	1.11	0.14	
202-1239-A-16-H-4	141.54	154.33	2.705	26.27	11463.17			
202-1239-A-16-H-4	141.84	154.62	2.708	26.42	11891.26	1.09	0.17	
202-1239-A-16-H-4	142.14	154.91	2.711	25.24	16596.27			
202-1239-A-16-H-5	142.45	155.22	2.714	25.64	18024.54	0.70	0.19	2.41
202-1239-A-16-H-5	142.75	155.53	2.718	25.45	19539.63			
202-1239-A-16-H-5	143.05	155.85	2.722	25.45	15988.26	0.73	0.17	
202-1239-A-16-H-5	143.35	156.16	2.725	25.58	13716.54			
202-1239-A-16-H-5	143.65	156.44	2.729	26.18	12600.71	1.31	0.17	
202-1239-A-16-H-6	143.97	156.73	2.732	26.64	12361.80			
202-1239-A-16-H-6	144.27	157.01	2.736	26.85	11102.23	2.06	0.16	
202-1239-A-16-H-6	144.57	157.30	2.739	27.24	7056.22			
202-1239-A-16-H-6	144.87	157.65	2.742	27.64	6411.60	2.38	0.13	
202-1239-A-16-H-6	145.17	157.99	2.746	27.70	5504.19			
202-1239-A-16-H-7	145.48	158.31	2.749	27.64	5693.47	2.19	0.13	
202-1239-A-16-H-7	145.78	158.58	2.752	27.58	6922.40			
202-1239-A-16-H-7	146.08	158.85	2.754	27.48	4555.43	2.11	0.12	
202-1239-A-16-H-CC	146.34	159.08	2.757	27.27	5693.33			
202-1239-A-17-H-1	145.90	159.19	2.758	27.48	3960.09	2.53	0.11	

LegSitHolCorTypSec	Depth (mbsf)	Depth (mcd)	Age (Ma)	SST (°C)	Alk conc (mmol/g)	$\delta^{15}N$ (‰)	TN (%)	Corg (%)
202-1239-A-17-H-1	146.20	159.52	2.762	27.06	8054.06			
202-1239-A-17-H-1	146.50	159.84	2.766	27.06	7042.44	2.64	0.14	
202-1239-A-17-H-1	146.80	160.17	2.771	26.97	6868.07			
202-1239-A-17-H-1	147.10	160.42	2.774	27.15	5555.16	2.32	0.13	1.37
202-1239-A-17-H-2	147.41	160.67	2.778	27.27	6697.25			
202-1239-A-17-H-2	147.71	160.91	2.781	27.52	5551.55	2.59	0.14	
202-1239-A-17-H-2	148.01	161.16	2.785	27.52	5055.47			
202-1239-A-17-H-2	148.31	161.40	2.788	27.52	1292.54	2.29	0.07	
202-1239-A-17-H-2	148.61	161.65	2.792	27.33	4244.89			
202-1239-A-17-H-3	149.12	162.16	2.798	26.73	7982.61	1.31	0.16	
202-1239-A-17-H-3	149.52	162.57	2.804	26.85	9742.12			
202-1239-A-17-H-3	149.92	162.97	2.809	27.03	8865.85	1.76	0.16	
202-1239-A-17-H-3	150.32	163.37	2.814	27.24	11096.27			
202-1239-A-17-H-4	150.74	163.49	2.816	27.48	9471.55	1.68	0.18	
202-1239-A-17-H-4	151.14	163.79	2.820	27.52	9327.41			
202-1239-A-17-H-4	150.44	164.18	2.825	27.12	15583.87	2.06	0.14	
202-1239-A-17-H-4	151.54	164.57	2.830	27.48	11351.34			
202-1239-A-17-H-5	152.36	165.37	2.840	27.03	11389.06	2.29	0.14	
202-1239-A-17-H-5	152.76	165.76	2.845	26.82	12468.56			
202-1239-A-17-H-5	153.16	166.15	2.850	26.73	12820.39	1.93	0.14	
202-1239-A-17-H-6	153.58	166.57	2.853	26.64	14521.46			
202-1239-A-17-H-6	153.98	166.96	2.856	27.15	13377.33	2.07	0.14	1.52
202-1239-A-17-H-6	154.38	167.35	2.859	27.21	15012.78			
202-1239-A-17-H-6	154.78	167.74	2.862	27.33	9034.37	2.51	0.12	
202-1239-A-17-H-7	155.30	168.23	2.865	27.30	15090.49			
202-1239-A-17-H-CC	155.73	168.64	2.868	27.21	28536.93	1.90	0.17	
202-1239-A-18-H-1	155.50	170.37	2.881	27.36	13257.29			
202-1239-A-18-H-1	155.90	170.77	2.884	26.76	20652.09	1.77	0.20	
202-1239-A-18-H-1	156.30	171.17	2.887	26.52	30383.66			
202-1239-A-18-H-1	156.70	171.57	2.889	26.91	23846.24	1.65	0.20	
202-1239-A-18-H-2	157.11	171.99	2.892	27.06	21058.70			
202-1239-A-18-H-2	157.51	172.44	2.896	27.33	16281.78	1.78	0.15	
202-1239-A-18-H-2	157.91	172.89	2.899	27.27	16933.33			
202-1239-A-18-H-2	158.31	173.32	2.902	27.36	14092.46	1.64	0.15	
202-1239-A-18-H-3	158.72	173.72	2.904	27.82	11175.58			
202-1239-A-18-H-3	159.12	174.13	2.906	27.91	9156.02	2.18	0.14	
202-1239-A-18-H-3	159.52	174.54	2.908	27.85	12451.65			
202-1239-A-18-H-4	159.93	174.95	2.911	27.48	10792.43	2.26	0.17	

LegSitHolCorTypSec	Depth (mbsf)	Depth (mcd)	Age (Ma)	SST (°C)	Alk conc (mmol/g)	$\delta^{15}N$ (‰)	TN (%)	Corg (%)
202-1239-A-18-H-4	160.33	175.34	2.913	27.58	10112.68			
202-1239-A-18-H-4	160.73	175.74	2.915	27.76	7924.44	2.36	0.17	1.8
202-1239-A-18-H-4	161.13	176.15	2.917	27.55	11507.13			
202-1239-A-18-H-5	161.55	176.57	2.919	27.33	10501.36	2.11	0.15	
202-1239-A-18-H-5	161.95	176.95	2.921	27.00	13125.89			
202-1239-A-18-H-5	162.35	177.31	2.923	27.00	14120.89	1.55	0.16	
202-1239-A-18-H-5	162.75	177.66	2.925	26.58	16085.03			
202-1239-A-18-H-6	163.17	178.03	2.927	26.64	15361.18	1.73	0.17	
202-1239-A-18-H-6	163.57	178.38	2.929	26.73	19978.32			
202-1239-A-18-H-6	163.97	178.74	2.931	27.15	15765.97	2.13	0.19	
202-1239-A-18-H-7	164.29	179.10	2.933	27.06	15173.82			
202-1239-A-18-H-CC	164.75	179.23	2.934	27.21	15600.41	2.24	0.21	
202-1239-A-19-H-1	165.10	179.63	2.936	27.18	16125.75			
202-1239-A-19-H-1	165.50	179.69	2.936	27.45	13821.97	1.76	0.20	
202-1239-A-19-H-1	165.90	180.14	2.939	27.45	13796.30			
202-1239-A-19-H-1	166.30	180.60	2.941	27.70	12149.40	1.29	0.18	
202-1239-A-19-H-2	166.71	181.01	2.944	27.70	11975.90			
202-1239-A-19-H-2	167.11	181.41	2.946	27.82	8103.57	1.47	0.15	
202-1239-A-19-H-2	167.51	181.80	2.948	27.91	11634.50			
202-1239-A-19-H-3	167.93	182.22	2.950	28.00	10484.09	2.39	0.19	2.06
202-1239-A-19-H-3	168.33	182.61	2.952	28.09	11657.36			
202-1239-A-19-H-3	168.73	183.01	2.955	28.12	8227.52	2.70	0.17	
202-1239-A-19-H-3	169.13	183.34	2.956	28.09	9087.74			
202-1239-A-19-H-4	169.55	183.64	2.958	28.03	10010.86	2.06	0.18	
202-1239-A-19-H-4	169.65	183.74	2.959	27.73	9939.71	2.00	0.16	
202-1239-A-19-H-4	169.95	184.20	2.961	27.67	9055.94			
202-1239-A-19-H-4	170.35	184.64	2.964	27.61	7534.98	1.97	0.14	
202-1239-A-19-H-4	170.75	185.03	2.966	27.61	7231.47			
202-1239-A-19-H-5	171.56	185.85	2.970	27.24	9960.92			
202-1239-A-19-H-5	171.96	186.26	2.973	27.33	8554.65	2.29	0.17	
202-1239-A-19-H-5	172.36	186.66	2.975	27.30	9375.04			
202-1239-A-19-H-6	172.78	187.08	2.977	27.45	8455.44	1.82	0.20	
202-1239-A-19-H-6	173.18	187.22	2.978	27.48	9149.79	1.94	0.17	2.06
202-1239-A-19-H-6	173.58	187.48	2.979	27.67	7214.49			
202-1239-A-19-H-7	174.00	187.48	2.979	27.67	9205.58			
202-1239-A-19-H-7	174.40	187.70	2.981	27.73	8610.32	1.93	0.16	
202-1239-A-19-H-CC	174.81	187.88	2.982	27.55	8462.37	2.03	0.16	
202-1239-A-20-X-1	174.60	187.92	2.982	27.52	7290.61			

LegSitHolCorTypSec	Depth (mbsf)	Depth (mcd)	Age (Ma)	SST (°C)	Alk conc (mmol/g)	$\delta^{15}N$ (‰)	TN (%)	Corg (%)
202-1239-A-20-X-1	175.00	188.10	2.983	27.27	7935.58	1.86	0.17	
202-1239-A-20-X-1	175.40	188.26	2.984	27.55	5711.17			
202-1239-A-20-X-1	175.80	188.29	2.984	27.48	7343.79			
202-1239-A-20-X-2	176.21	188.48	2.985	27.70	6274.57	2.11	0.19	
202-1239-A-20-X-2	176.61	188.69	2.986	27.64	8322.93	2.37	0.18	
202-1239-A-20-X-2	177.01	188.88	2.987	27.73	7612.60			
202-1239-A-20-X-3	177.42	189.08	2.988	27.39	6888.86	2.34	0.20	
202-1239-A-20-X-3	177.82	189.10	2.988	27.73	7356.56			
202-1239-A-20-X-3	178.22	189.31	2.989	27.64	9164.96			
202-1239-A-20-X-3	178.62	189.54	2.991	27.48	6761.60	2.29	0.20	
202-1239-A-20-X-4	179.02	189.80	2.992	27.33	7572.58			
202-1239-A-20-X-4	179.42	190.24	2.995	27.39	5955.55	2.28	0.19	
202-1239-A-20-X-4	179.82	190.55	2.996	27.42	7055.42			
202-1239-A-20-X-4	180.22	190.89	2.998	27.48	5345.72	2.07	0.18	
202-1239-A-21-X-1	179.60	191.25	3.000	27.27	11627.48			
202-1239-A-20-X-5	180.63	191.61	3.002	27.36	6122.07	1.82	0.18	
202-1239-A-21-X-1	180.00	192.02	3.004	27.27	9877.37			
202-1239-A-20-X-5	181.03	192.50	3.007	27.24	5352.54	1.80	0.17	
202-1239-A-21-X-1	180.40	192.91	3.009	27.45	10611.40			
202-1239-A-20-X-5	181.43	193.31	3.012	27.12	5762.28	1.33	0.19	
202-1239-A-21-X-2	180.82	193.71	3.014	27.36	12437.81			
202-1239-A-20-X-5	181.83	194.13	3.016	26.94	5586.60	1.28	0.15	
202-1239-A-21-X-2	181.22	194.53	3.018	27.27	14922.80			
202-1239-A-20-X-6	182.24	194.79	3.020	26.91	6467.36	1.50	0.16	
202-1239-A-21-X-2	181.62	194.90	3.020	27.27	14582.41			
202-1239-A-20-X-6	182.64	195.30	3.023	27.18	5531.40	2.28	0.18	1.93
202-1239-A-21-X-2	182.02	195.70	3.025	27.27	14390.97			
202-1239-A-20-X-6	183.04	196.12	3.027	26.85	4783.77	1.98	0.19	
202-1239-A-20-X-7	183.46	196.52	3.029	26.39	3321.66			
202-1239-A-21-X-3	182.83	196.92	3.032	27.15	15214.27	1.65	0.19	
202-1239-A-20-X-7	183.86	197.32	3.034	26.79	9895.45			
202-1239-A-21-X-3	183.23	198.13	3.041	27.12	14683.84			
202-1239-A-20-X-CC	184.24	198.53	3.044	26.94	9527.98	1.73	0.20	
202-1239-A-21-X-3	183.63	198.93	3.048	27.12	16621.49			
202-1239-A-21-X-4	184.04	199.34	3.052	27.15	16939.90	2.29	0.22	2.54
202-1239-A-21-X-4	184.44	199.74	3.055	27.18	16428.98			
202-1239-A-21-X-4	184.84	200.14	3.059	27.48	13670.23	2.48	0.20	
202-1239-A-21-X-5	185.26	200.56	3.063	27.55	14086.74			

LegSitHolCorTypSec	Depth (mbsf)	Depth (mcd)	Age (Ma)	SST (°C)	Alk conc (mmol/g)	$\delta^{15}N$ (‰)	TN (%)	Corg (%)
202-1239-A-21-X-5	185.66	200.96	3.067	27.55	13072.57	2.46	0.20	
202-1239-A-21-X-5	186.06	201.36	3.070	27.45	17364.87			
202-1239-A-21-X-5	186.46	201.76	3.074	27.39	15533.98	2.15	0.24	
202-1239-A-21-X-6	186.87	202.17	3.078	27.21	11970.81			
202-1239-A-21-X-6	187.27	202.57	3.080	27.24	13818.95	1.62	0.22	
202-1239-A-21-X-6	187.67	202.97	3.082	27.24	12873.42			
202-1239-A-21-X-7	188.08	203.38	3.084	27.36	11364.73	1.50	0.21	
202-1239-A-21-X-7	188.48	203.78	3.086	27.52	7493.07			
202-1239-A-21-X-CC	188.94	204.24	3.088	27.39	10508.88	2.25	0.22	
202-1239-A-22-X-1	189.20	205.58	3.095	27.79	9930.80			
202-1239-A-22-X-1	189.60	205.98	3.097	27.94	8736.98	1.60	0.16	
202-1239-A-22-X-1	190.00	206.38	3.099	27.85	11618.63			
202-1239-A-22-X-2	190.41	206.79	3.101	27.94	9076.67	2.17	0.16	
202-1239-A-22-X-2	190.81	207.19	3.103	27.91	9463.37			
202-1239-A-22-X-2	191.21	207.59	3.105	27.88	7373.03	2.57	0.15	
202-1239-A-22-X-2	191.61	207.99	3.107	27.91	8921.74			
202-1239-A-22-X-3	192.02	208.40	3.109	27.97	10153.22	2.39	0.19	
202-1239-A-22-X-3	192.42	208.80	3.111	27.97	10504.01			
202-1239-A-22-X-3	192.82	209.20	3.113	27.91	8593.41	2.15	0.19	
202-1239-A-22-X-3	193.22	209.60	3.114	27.85	13394.01			
202-1239-A-22-X-4	193.63	210.01	3.116	27.58	10807.30	2.04	0.21	
202-1239-A-22-X-4	194.03	210.41	3.118	27.45	10868.74			
202-1239-A-22-X-4	194.43	210.81	3.120	27.12	10157.41	1.57	0.21	
202-1239-A-22-X-4	194.83	211.21	3.122	27.24	9484.32			
202-1239-A-22-X-5	195.24	211.62	3.124	26.97	8136.48	1.42	0.21	
202-1239-A-22-X-5	195.64	212.02	3.126	25.94	6131.48			
202-1239-A-22-X-5	196.04	212.42	3.128	26.64	7384.44	1.39	0.18	
202-1239-A-22-X-6	196.45	212.83	3.131	27.48	9810.93			
202-1239-A-22-X-6	196.85	213.23	3.133	26.73	8162.24	1.44	0.19	2.22